UNIVERSITY OF SOUTHAMPTON

THE COMPUTER SIMULATION OF ANISOTROPIC SYSTEMS

- by -

Paul Simpson, B.Sc.

-

A dissertation submitted in partial fulfilment of
the requirements for the degree of
Doctor Philosophy at the University of Southampton

-

Department of Chemistry October, 1982.

ACKNOWLEDGEMENTS

My greatest debt is to my supervisor, Professor G.R. Luckhurst for his never ending source of inspiration, encouragement and advice during my last three years at Southampton for which I am extremely grateful.

I would also like to thank Dr. C. Zannoni, Dr. S. Romano and Dr. R.L. Humphries for helpful advice and access to versions of their computer programs which were subseqently modified and used throughout this thesis. The assistance, advice? and friendship of various members of the Liquid Crystal group is also acknowledged, in particular, Dr. B. Timimi, Dr. C. Stockley, Dr. F. Viloria, Mrs. R. Hashim, Mr. C. Counsell, Mr. G. Attard and Dr. A. Bagmet together with Mr. G. Faisal. Also I would like to thank Dr. G. Harburn for the preparation of the optical diffraction patterns used in Chapter 7.

Assistance from the following bodies is also acknowledged:-

The University of Southampton Computing Service for generous allocations of computer resources.
The Science and Engineering Research Council for a three year studentship and a grant of computer time.
NATO for funding a visit to the University of Bologna, Italy.

Finally, I would like to thank my wife and my parents for their patience, encouragement and support during the last three years, and especially Heather for her devoted assistance with the labourious task of proof reading this thesis.

TABLE OF CONTENTS

CHAPTER 1 PAGE

INTRODUCTION

CHAPTER 2

COMPUTER SIMULATIONS

CHAPTER 3

THE LEBWOHL-LASHER MODEL AND THE MOLECULAR FIELD APPROXIMATION.

UNIVERSITY OF SOUTHAMPTON

ABSTRACT

FACULTY OF SCIENCE

CHEMISTRY

Doctor of Philosophy

THE COMPUTER SIMULATION OF ANISOTROPIC SYSTEMS

by Paul Simpson

This thesis is concerned with the study of the properties of anisotropic systems using the Monte-Carlo computer simulation technique.

Following a brief introduction to liquid crystals, Chapter 1 discusses the effect of external forces on liquid crystals, intermolecular pair potentials, distribution functions and molecular field theory, leading to a chapter describing techniques and problems associated with the computer simulation of anisotropic systems. In Chapter 3, properties of the nematic-isotropic phase transition using the Lebwohl-Lasher model, together with various modifications are investigated. Chapter 4 then discusses the simulation with anisotropic particles interacting via nearest neighbour dispersion forces together with full ranged dipolar forces. The next two chapters give details of simulations of the effect of external forces on anisotropic systems. In particular, in Chapter 5 where an external magnetic field interaction is applied to investigate the pinning of the director and to study the transition properties in a high magnetic field and in Chapter 6 where surface forces are applied, which together with orthogonal external fields are used to simulate the Freedericksz transition. Finally in Chapter 7, the orientational properties associated with the smectic-E to smectic-B phase transition are studied.

Throughout this thesis, wherever possible, results are compared with the predictions of molecular field theory.

To my wife, Heather.

Chapter 1

Introduction

1.1 Liquid Crystals

The phrase 'Liquid Crystal' was first used by Lehmann (1900) to describe a state of matter which had been observed between the crystalline and liquid phases of various cholesteryl esters and 4-4'-dimethoxyazoxybenzene. Much uncertainty existed up until this date as to the nature of this phase, first reported by Planar (1861) and later by Lobisch (1872), where on cooling melts of some cholesteryl esters a striking colour phenomenon was observed. In 1888 however, Reinitzer made a detailed study of this behaviour and observed that the state was actually liquid-like, yet it possessed optical properties usually associated with crystalline solids. From this early period until about 20 years ago a relatively consistant effort was devoted to the classification, and understanding of liquid crystals with three notable symposia taking place in 1931, 1933 and 1952. However, in the last 20 years with the realisation of the importance of liquid crystals in electronic display devices, (see for example Goodman, 1973; Shanks, 1982), an enormous effort has been made to fully comprehend their chemical, optical, physical and mechanical properties. A comprehensive and interesting account of the history of liquid crystals has been written by Kelker (1973).

The liquid crystalline phase is a very loose description of what in reality is normally a complex series of phases or mesophases (from middle phases) which occur between the crystalline state at low temperatures and the liquid state at high temperatures. The crystalline phase is characterised by the molecules having perfect long range translational and orientational order, and therefore exhibiting anisotropic properties whereas in the liquid

state at high temperatures no long range correlations exist.

Generally the mesophases can be classified into two types, those forming plastic crystals and those forming liquid crystals. (Gray and Winsor, 1974). In the case of plastic crystals the constituent molecules exhibit long range translational order although they are rotationally disordered. Whereas liquid crystals have a high degree of orientational order and often some spatial order. However, since this thesis is only concerned with the anisotropic properties of liquid crystals, nothing more will be said of plastic crystals.

In order for a molecular system to form a liquid crystalline mesophase the molecules must interact via some anisotropic intermolecular potential. The principle requisite for this is that the molecules themselves are anisotropic. Thus the molecules forming such systems are generally quite complex and are either disc-like in shape, or more usually rod-like with a relatively high length to breadth ratio. Actually about 2% of all known organic compounds have the necessary anisotropy to form liquid crystalline phases.

It is the long range order, always present in liquid crystal mesophases, that gives rise to their characteristic orientational physical properties. (de Gennes 1974, de Jeu, 1980). This long range order extends over several thousand Angstroms, where the molecules tend to align on average parallel with some preferred direction in space, called the director. Thermal fluctuations dictate that the molecules actually reorient about this director axis. However, within different regions of the bulk sample, the director is aligned in different directions, and on a macroscopic scale these regions of high order vary continuously throughout the sample and appear isotropically distributed.

The liquid crystal phases can be broadly subdivided into two types, those which are formed as a function of temperature from crystalline phases called thermotropics and

those that are induced by the presence of various concentrations of solvents, called lyotropics. The latter are very important in biological membrane systems and in lipid solutions but will not be discussed further.

1.2 Description and classification of the liquid crystal mesophases

The mesophases forming the liquid crystalline state can be classified into three broad classes: nematics (from the Greek word νημα meaning thread-like); cholesterics, and smectics (from the Greek word σμημα, meaning soap-like). The smectic mesophase has further subdivisions according to the various degrees of order and symmetry present, (smectic A, smectic B etc) and together with the nematic and cholesteric mesophase will now be described in detail.

The Nematic mesophase

This is by far the most commonly occuring liquid crystalline mesophase and has the lowest degree of order of all the presently known mesophases. It has a low viscosity and its appearance is generally cloudy, becoming clear when heated to the isotropic phase. The nematic phase is strongly affected by external fields because each molecule normally has a large anisotropic magnetic susceptibility, and fields in excess of about 0.1T (Luckhurst, 1972) will align the director to give monodomain samples which are optically uniaxial about the director axis. The nematic phase has a high degree of orientational order and short range translational order. A schematic representation of this phase is shown in Figure 1.1 where the elipses represent the elongated molecules.

The Cholesteric mesophase

The name cholesteric stems from the fact that all the early cholesteric materials were derivatives of cholesterol. Like the nematic mesophase, the cholesteric mesophase has little translational order. The constituent molecules are chiral giving rise to a non-uniform director being present. Going through the sample the director actually twists in a helical fashion, forming a type of twisted nematic. This can be seen in Figure 1.2. The periodicity of the twist, called the pitch, is comparible with the wavelength of light; and in thin films of cholesteric mesophases the pitch satisfies the basic scattering requirement for Bragg reflection to occur, resulting in the phase appearing highly coloured. The pitch is often strongly affected by external influences, for example, temperature, pressure and external magnetic or electric fields, thus thin films of cholesterics are extremely useful in detecting changes in these external stimuli.

Nematics can be made to form cholesterics by the addition of a suitable optically active material. In actual fact, the nematic phases can be thought as being a cholesteric, but with an infinitely large pitch. This observation is confirmed experimentally as no known compound has a cholesteric and a nematic mesophase, it is always a case of either or none.

The Smectic-A mesophase

As well as having orientational order, all the smectic mesophases (with the exception of the smectic D mesophase) have an additional degree of order because the molecules are spatially ordered into layers. (Gray, 1979).

In the smectic-A (S_A) mesophase, the molecules tend to align parallel with respect to a director, but in addition they form into layers with the director parallel to the

layer normal; a diagramatic representation is shown in Figure 1.3a. Within each layer the molecules are almost totally translationally disordered. Thus they possess orientational and one degree of spatial order only. Experimentally it has been observed that the molecules can rotate about their long axis and can move from one layer to another. Furthermore the layers are free to slide over one another, and like the nematic phase, a monodomain S_A phase is optically uniaxial.

The Smectic-B mesophase

In addition to the features described for the S_A mesophase this phase displays long range spatial order within each layer. The centres of mass of the molecules are ordered to form a hexagonal close packed network. Again the director is orthogonal to the layer planes and the molecules are free to rotate about their long axes. A representation of this phase is depicted in Figure 1.3b. The extra order in this phase makes it almost crystalline and there has been much discussion about and its difference with crystalline and plastic crystalline phases (de Vries et al, 1979).

The Smectic-C mesophase

This mesophase is very similar to the S_A phase except that the molecules are tilted with respect to the layer normal. (See Figure 1.3c). The additional degree of order means that the S_C phase is optically biaxial.

Two types of S_C mesophases have been observed, one in which the tilt angle varies with temperature (Taylor et al 1970) (for example TBBA (see Table 1.1)) and the other in which it remains constant (for example HOAB) (Diele et al, 1972).

The Smectic - D, E, F, G, H, mesophases

Relatively few compounds form the remaining smectic mesophases and consequently much uncertainty exists as to their exact structures. Firstly the S_E phase: X-ray and neutron scattering work (Leadbetter et al, 1976; Leadbetter et al, 1979; Leadbetter et al, 1980; Richardson et al, 1978,

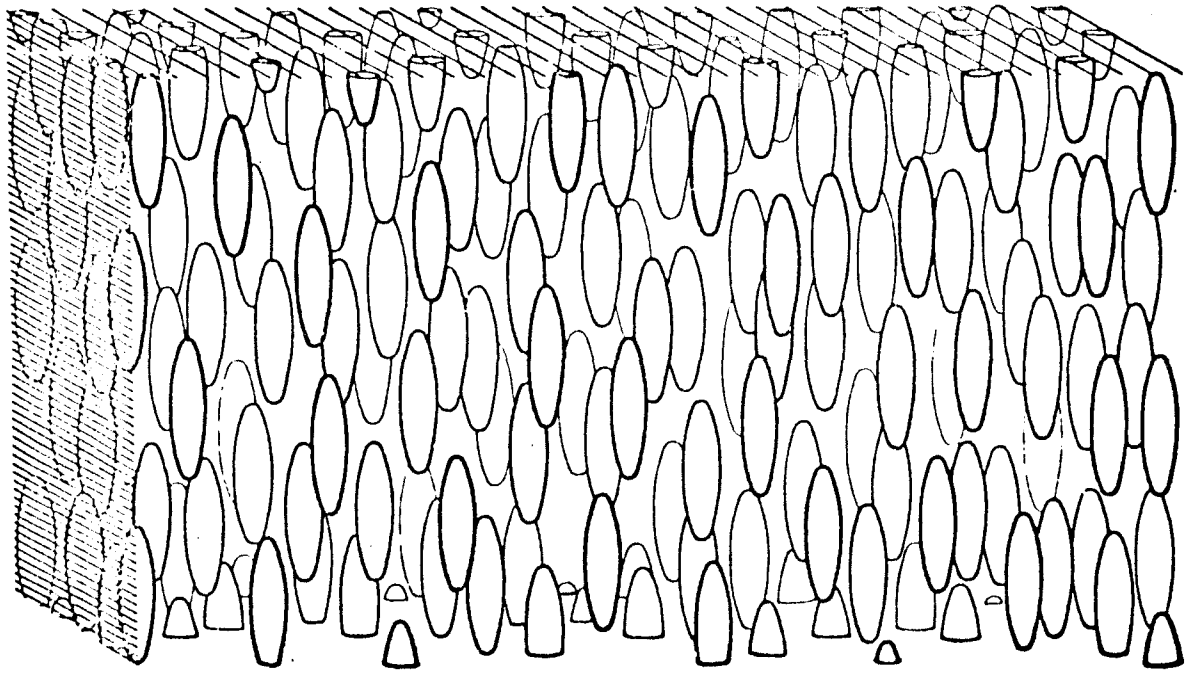

Fig 1.1 A schematic representation of the nematic mesophase

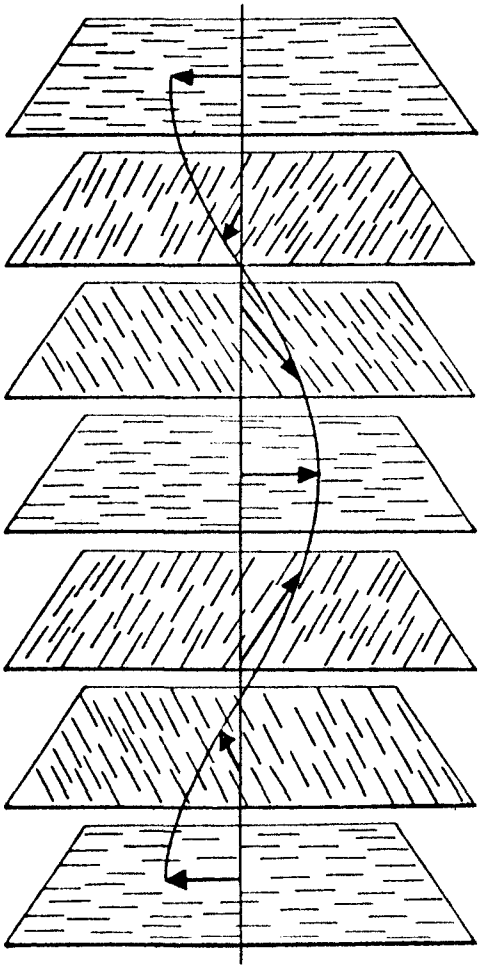

Fig 1.2 The molecular organisation of the cholesteric phase.

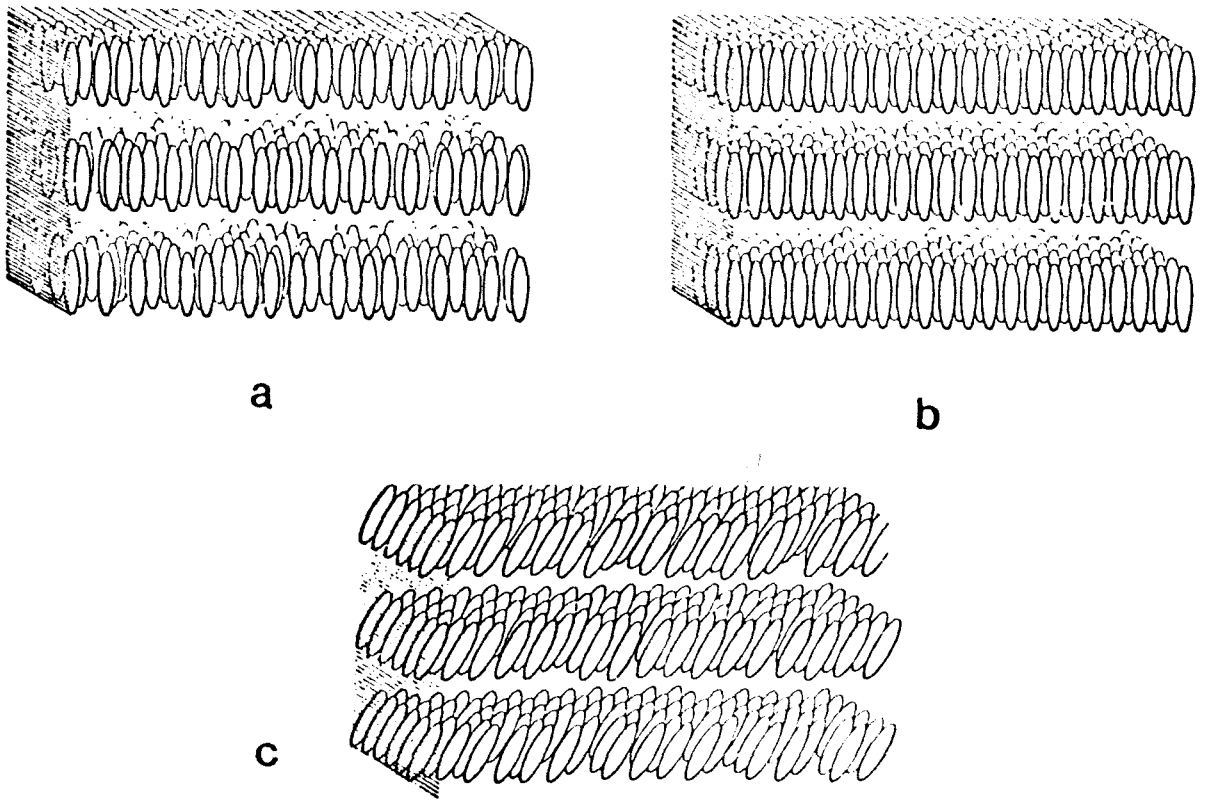

Fig 1.3 Schematic representation of a) the S_A, b) S_B, c) the S_C mesophases.

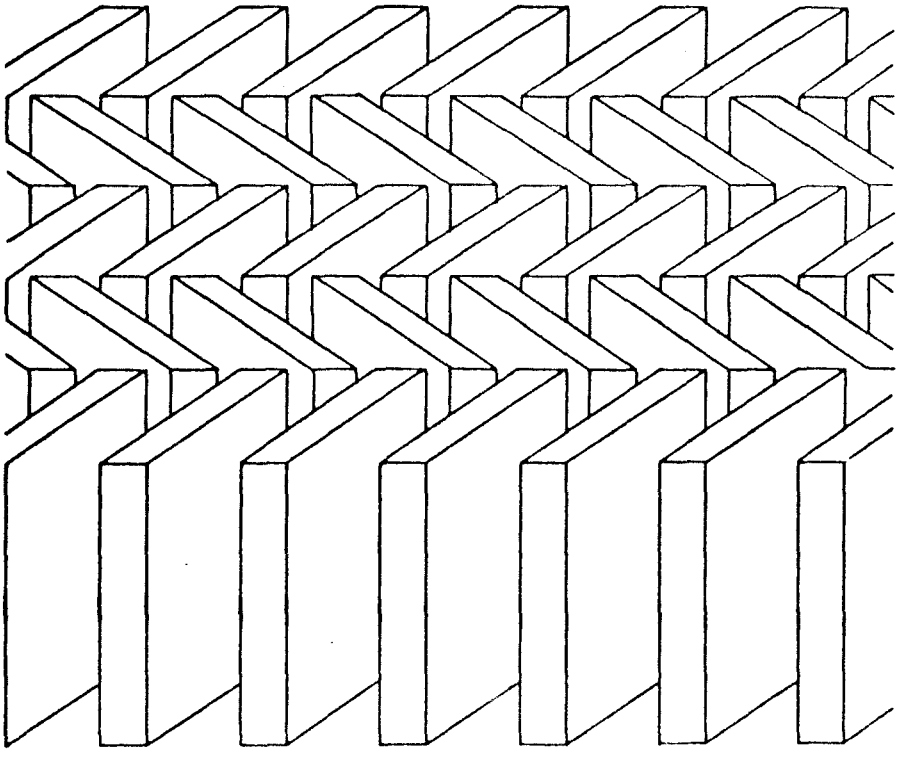

Fig 1.4 A schematic representation of one layer in the S_E mesophase.

Pindak et al 1981; Doucet et al 1975) has shown that the molecules forming the S_E mesophase lie parallel with the layer normal and are hexagonally close packed. This phase is also optically birefringent and biaxial, although, the biaxiality does not arise from tilting within layers. Instead the additional degree of long range order occurs with respect to the short molecular axis, in this case the short axis in the plane of the aromatic rings. Looking down on the layer the short molecular axis forms a long range 'herring bone' structure. A representation of one layer is shown in Figure 1.4.

The S_G phase is very similar to the S_E phase, except that the molecules are tilted with respect to the layers, and the S_H has been reported to be the tilted analogue of the S_B mesophase. (Hervet et al, 1975).

Finally the S_D and S_F mesophases. To date the exact nature of the structure of these phases has not been determined although the S_F is probably very similar to the S_C phase and the S_D phase has cubic symmetry, and should probably not be classified in the smectic scheme.

A list of typical molecules forming these various mesophases, together with their transition temperatures is given in Table 1.1.

1.3 The Effect of External forces

When a liquid crystalline material is cooled from an isotropic liquid, regions form in the sample in which the molecules tend to align, on average parallel with a director. Throughout the entire sample the orientation of the director changes continuously, and on average appears isotropically distributed. Thus the overall order of the entire system is zero, although at a molecular level, a high degree of orientational order exists. It is therefore advantageous in order to study the macroscopic properties of liquid crystals, to produce a monodomain sample with a

unique director axis. Fortunately there are a number of ways in which this can be achieved, although always by exposing the mesophase to an external force, either by means of an external field or by some physical constraint.

The simplest method for producing monodomain samples is to apply a magnetic field to the mesophase. When a static field interacts with a molecule, assuming it to be cylindrically symmetric, then the free energy density of the system increases by an amount defined by (Emsley and Lindon, 1975):-

$$A_{mag} = -1/3\,\Delta\chi B^2 P_2(\cos\beta) \qquad 1.1$$

Here $\Delta\chi$ is the total anisotropy in the bulk diamagnetic susceptibility $(\chi_{11}-\chi_{\perp})$, B is the magnetic field strength and $P_2(\cos\beta)$ is the second Legendre polymonial with β being the angle between the director and the field. For nematics a magnetic flux density of about 0.1 Tesla is all that is required to align the director, either parallel or perpendicular to the field, depending on the sign of $\Delta\chi$.

In cholesterics however, for the case where $\Delta\chi$ is positive, the molecules experience two competing forces, firstly that caused by the external field, and secondly that from the intermolecular potential causing the director to twist (Pincus, 1970). At low fields the helical twist remains until at some critical field this is destroyed and a nematic is formed (Planar and Phillips, 1968). This critical field is normally of the order of 10 Tesla although it can be significantly less for cholesterics with large pitchs.

In principle, magnetic fields should also align the director in smectic phases. However, the magnetic free energy is not large enough to overcome the barrier caused by reorientating the layers within a sample. None-the-less, uniform smectics can be produced by allowing them to form whilst cooling from their isotropic (or nematic) phases in an external field, or in the presence of suitably treated

surfaces. In the case of tilted smectics where the monodomain mesophase is biaxial, an external field is only sufficient to align one of the symmetry axes, and a second orthogonal force has to be applied, normally by means of treatment of the container walls. This surface effect will be discussed later.

In addition to magnetic fields, electric fields will also produce alignment. In this case it is produced by the anisotropy in the dielectric constant. However, complications arise, since the anisotropy in the dielectric constant is a function of the frequency of the field.

The most common method for producing uniformity of the director axis is with the aid of surface forces, and, the director in a nematic can be aligned by sandwiching the material between two suitably prepared glass plates. Depending on the surface preparation different effects can occur. For example, rubbing a glass surface repeatedly in one direction with a material like paper or cotton wool will induce microscopic scratchs which cause the nematic molecules in contact with it to align parallel with the direction of rubbing. Thus, a monodomain nematic will be formed when it is sandwiched between two glass plates, providing the surface 'scratching' is in the same direction. This phenomena can lead to some very interesting effects, e.g. if one plate is rotated through 90° a twisted nematic results with a pitch equal to four times the separation of the glass plates. It is this principle that is responsible for the rotation of planes of polarised light in electronic display devices.

Alignment perpendicular to the glass surfaces can also be achieved, in this case by coating the surfaces with, for example, the compound DMOAP (Priestly, Wojtowicz and Sheng, 1974).

It should be noted that although these external fields or forces produce monodomain mesophases, they are normally not large enough to quench thermal fluctuations of the

director. Thus in a macroscopic sample the mean director can be aligned with magnetic flux densities of about 0.1T, microscopically it will fluctuate about this mean direction. In order to quench these fluctuations extremely large external forces would have to be applied (Poggi and Fillippini, 1977).

1.4 The Freedericksz Transition and Elastic Constants

Interesting effects occur when the mesophases are subjected to more than one external force. For example, if we take a nematic sandwiched between two glass plates with the surface treated such that the director is uniform throughout the sample, what happens when a field is applied orthogonal to the director? (assuming the diamagnetic susceptibility to be positive). For low fields the director remains fixed by the surface alignment, but on increasing the field a point is reached when the director begins to orientate parallel with the field. This effect was first observed by Freedericksz and Tsvetkov (1933, 1934) and from the value of the field at which the deformation starts to occur, and from the way the director orientates as a function of the field, information about the elasticity in the sample can be evaluated.

An orientated nematic liquid crystal can undergo an infinite number of different deformations. However, these can be resolved into three fundamental deformations each characterised by three elastic constants, usually denoted K_{11}, K_{22} and K_{33} (Frank, 1958) to describe the splay, twist and bend modes respectively. These deformations, are depicted in Figure 1.5a and their existence is a consequence of the long range orientational order that exists in such a phase. As in solids, the ease with which these deformations occur will be functions of the intermolecular interactions present. Applying continuum theory (Oseen 1933; Zocher 1933; Frank 1958; Ericksen 1960, 1961; Leslie 1966,

1968) to such a system, where it is assumed that in a deformed sample the director varies continuously from one point to another, the free energy density, f, can be written in terms of the elastic constants as (Zocher, 1933; Frank, 1958):-

$$f = K_{11}(\mathrm{div}\underline{n})^2 + K_{22}(\underline{n}.\mathrm{curl}\underline{n})^2 + K_{33}(\underline{n}\times\mathrm{curl}\underline{n})^2 \qquad 1.2$$

Here $\underline{n}$ is the orientation of the director in an x, y, z coordinate system. This equation can be used to describe the Freedericksz transition, and Figure 1.5b depicts the three experimental arrangements required to evaluate directly the three Frank elastic constants by this technique. Figure 1.5b(1) shows the geometry of surface alignment and field direction required to obtain the splay elastic constant directly. In this case, we define the surfaces to be in the yz plane with the surface alignment parallel with the z direction, and the orthogonal field to be in the x direction. Thus the deformation at a point, induced by the field in the sample can be defined by the vector ($\sin\theta$, 0, $\cos\theta$), where θ is as defined in Figure 1.5b(1) and the field by the vector (B_x,0,0). The free energy density contribution from the external field can therefore be written as (de Gennes, 1974):-

$$f_m = -\frac{1}{2}\Delta\chi B^2\sin^2\theta \qquad 1.3$$

The equilibrium state can be found by minimising the total free energy, F, with respect to variations in the director pattern, hence, the total free energy is:-

$$F_{tot} = \int_0^{d/2}\left[(K_{11}\cos^2\theta + K_{33}\sin^2\theta)\left(\frac{d\theta}{dz}\right)^2 - \Delta\chi B^2\sin^2\theta\right] dz \qquad 1.4$$

Here d is the distance between the plates and B is the magnetic flux density. In this situation there is no deformation in the y direction and so the twist elastic

constant does not contribute to the free energy. This equation can be minimised using the Euler-Lagrange relationship with the knowledge that F is a minimum for θ = 0 with z = 0 or d, and has a maximum, θ_m, in the centre of the cell at z=d/2. In this case we assume there is strong anchoring at the surfaces. Thus we find (Zocher, 1933; Saupe 1960; Pincus, 1970; Deuling, 1972; Gruler et al, 1972; Priest 1972; Gruler 1974; Ben-Abraham, 1976):-

$$(\Delta X)^{1/2} B dz = \left[K_{11} + \frac{(K_{33} - K_{11})\sin^2\theta}{\sin^2\theta_m - \sin^2\theta} \right]^{\frac{1}{2}} d\theta \qquad 1.5$$

Integrating and making the substitution $\sin\lambda = \sin\theta/\sin\theta_m$ gives:-

$$(\Delta X)^{\frac{1}{2}} \frac{Bd}{2} = \int_0^{\pi/2} \left[\frac{K_{11} + (K_{33} - K_{11})\sin^2\theta_m \sin^2\lambda}{1 - \sin^2\theta_m \sin^2\lambda} \right]^{\frac{1}{2}} d\lambda \qquad 1.6$$

Clearly at the critical field B_c, $\theta_m = 0^+$ and we find:-

$$K_{11} = \Delta X \left[\frac{d}{\pi} B_c\right]^2. \qquad 1.7$$

The same procedure can now be used for the two other starting geometries, shown in Figure 1.5b(2) and 1.5b(3). For perpendicular surface alignment with an orthogonal field (Figure 1.5b(3)) exactly the same equations occur except that K_{11} must be replaced by K_{33} and vice-versa, thus at the critical field we now have:-

$$K_{33} = \Delta X \left[\frac{d}{\pi} B_c\right]^2 \qquad 1.8$$

However for the geometry in Figure 1.5b(2), the free energy density depends only on the twist elastic constant, K_{22} and the field as a function of the deformation in the centre of the sample is given in this case by (Gruler et al, 1972):-

$$(\Delta\chi)^{1/2} B dx = \left[\frac{K_{22}}{\sin^2\theta_m - \sin^2\lambda}\right]^{\frac{1}{2}} d\theta \qquad 1.9$$

or as before:-

$$(\Delta\chi)^{1/2} B\frac{d}{2} = \int_0^{\pi/2}\left[\frac{K_{22}}{1 - \sin^2\theta_m \sin^2\lambda}\right]^{1/2} d\lambda \qquad 1.10$$

so again at the critical field

$$K_{22} = \Delta\chi\left[\frac{d}{\pi} B_c\right]^2. \qquad 1.11$$

From this discussion the three elastic constants of a particular nematic can be obtained directly by measuring the critical fields for the three appropriate geometries or indirectly by measuring the director deformation as a function of external field. In principle any anisotropic property such as the dielectric permittivitity or the electric or thermal conductivity can be used to probe the average state of alignment although the most common and most accurate method is to utilise the anisotropy in the refractive index, and to measure the difference in optical path length (de Jeu, 1980). Also the Freedericksz transition can be induced by electric fields (Gruler et al, 1972; Deuling, 1972; Roa et al, 1976; Ben-Abraham, 1976; Deuling, 1974a,b; Deuling et al 1975; Deuling et al 1976; Aneva et al, 1980) and measured in the same way as previously described or by measuring the capacitance. (Maze, 1978; Schad et al, 1978; 1979; Tough and Raynes, 1979). In addition the theory for the transition has been generalised for fields in any direction (Dafermos, 1968; Deuling et al, 1975; Motooka and Fukuhara, 1979; Motooka et al, 1979) and for geometries in which the surfaces are not parallel (Fraser, 1978).

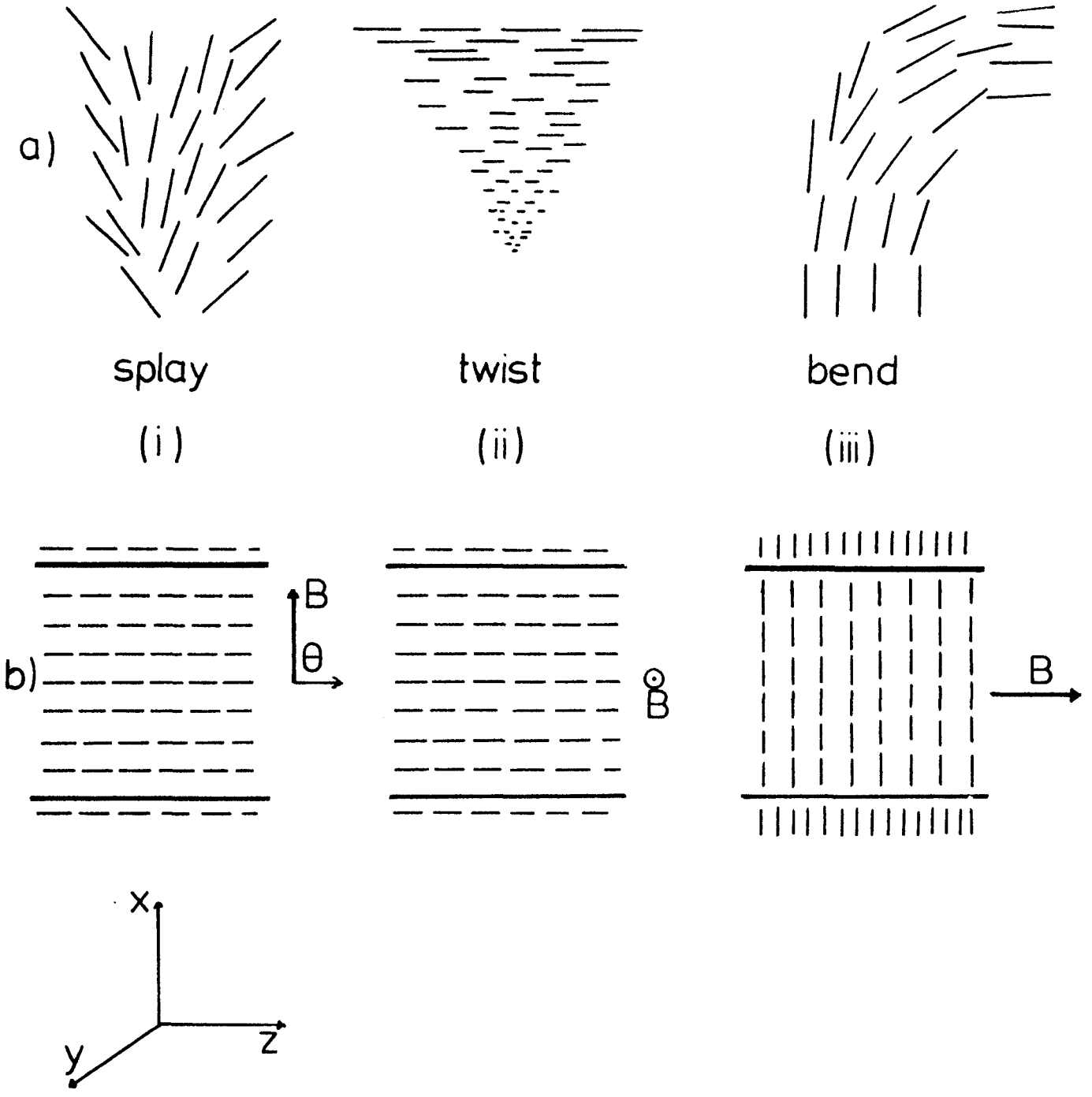

Fig 1.5 a) Diagram showing the three fundamental deformations possible, ie splay, twist and bend in a nematic.
b) Gives the geometric arrangements required in the Freedericksz transition experiment for surface alignment and field direction to obtain the three elastic constants K_{11}, K_{22} and K_{33}.

To date numerous papers have been published giving experimental values of the three elastic constants (See for example Saupe, 1960; Durand et al, 1969; Priest, 1972; Haller, 1972; Gruler, 1973; Gruler and Meier, 1973; Léger, 1973; de Gennes, 1974; Gruler, 1975; de Jeu et al, 1976; Maze and Johnson, 1975, 1976; Karat and Madhusudana, 1976, 1977a, 1977b, 1979; de Jeu and Claassen, 1977; Bunning et al, 1981; Flapper et al, 1981; Uchida and Takahashi, 1981) and depending on the precise method, results for the same constant and compound often differ by up to 100%. Typical values for K_{11}, K_{22} and K_{33} for PAA at 120°C are 5.0×10^{-7}, 3.8×10^{-7} and 10.0×10^{-7} dynes respectively (de Gennes 1974). Normally the bend constant (K_{33}) is found to be larger than the other two, and in general $K_{22} < K_{11} < K_{33}$ although substituent hydrocarbon chains or other groups can reverse the order of K_{22} and K_{11}. Furthermore, to a good approximation the ratio of $K_{11}:K_{22}:K_{33}$ for a specific compound is almost constant over a mesophase temperature range (de Jeu, 1980).

To date various attempts have been made to predict the ratio of $K_{11}:K_{22}:K_{33}$. The crudest approach gives all three elastic constants equal, although other theories have been postulated and, depending on what approximations are made, a wide range of ratios are found. For example, Saupe (1960) predicted it to be -7:11:17, whereas Nehring and Saupe (1971) found it to be 5:11:5. Further work in this area has been published by Gruler (1973;1975), Priest (1972), Poniewierski, and Stecki (1979), Faber (1977;1980), and Dunmur and Miller (1982).

1.5 Order Parameters

One of the most significant characteristics of liquid crystals is the presence of long range orientational order. To define the degree of order in a system it is usual to introduce an order parameter that changes value when transforming from one phase to another.

Starting from first principles we define a quantity which gives the probability of finding a single molecule at a specific position and orientation in a phase. This probability is (Zannoni, 1979):-

$$\rho^{(1)}(\underline{r}_1,\Omega_1) = \frac{N}{Z_N} \int d\underline{r}_2^N \, d\Omega_2^N \exp\left(\frac{-1}{kT} U(\underline{r}^N,\Omega^N)\right) \qquad 1.12$$

Here as in the rest of this section, integration variables with sub and super-scripts will imply integration over the range of variables, so in this case, over $\underline{r}_2$, $\underline{r}_3 \ldots\ldots \underline{r}_N$ and Ω_2, $\Omega_3 \ldots\ldots\ldots \Omega_N$.

The integrations over $d\Omega$, actually refer to the three Euler angles in this case $d\Omega = d\alpha \sin\beta d\beta d\gamma$ over the limits $0<\alpha<2\pi$, $0<\beta<\pi$ and $0<\gamma<2\pi$. $U(\underline{r}^N,\Omega^N)$ is the potential energy of the whole system. k is the Boltzmann constant and T is temperature. Z_N is the partition function:-

$$Z_N = \int d\underline{r}_1^N \, d\Omega_1^N \exp\left(\frac{-1}{kT} U(\underline{r}^N,\Omega^N)\right) \qquad 1.13$$

For a homogeneous system, the physical properties are unchanged with translation and the interaction energy will depend only on the relative separation, thus for an isotropic fluid or a nematic we can write:-

$$\rho^{(1)}(\underline{r}_1\Omega_1) = \rho f(\Omega_1) \qquad 1.14$$

Where the singlet orientational distribution function, $f(\Omega_1)$ is

$$f(\Omega_1) = \frac{V}{Z_N} \int d\underline{r}_2^N d\Omega_2^N \exp\left(\frac{-1}{kT} U(\underline{r},^N\Omega^N)\right) \qquad 1.15$$

and ρ is the number density.
For an isotropic fluid we have simply:-

$$\rho^{(1)}(\underline{r}_1,\Omega_1) = \rho/8\pi^2 \qquad 1.16$$

The average of any single particle orientational function, $A(\Omega)$, can be written in terms of $f(\Omega)$ as:-

$$\bar{A} = \int d\Omega f(\Omega) A(\Omega). \qquad 1.17$$

where the upper bar denotes a purely orientational average. Since $f(\Omega)$ is a function of the Euler angles it can be expanded in a Wigner series (Rose, 1957) which form a complete set of orthogonal functions spanning all orientational space, therefore:-

$$f(\Omega) = \sum_{Lmn} f_{Lmn} D^{L}_{m\,n}(\Omega) \qquad 1.18$$

Here f_{Lmn} is an expansion coefficient and $D^{L}_{mn}(\Omega)$ is a Wigner rotation matrix (see Appendix 1). Multiplying both sides of this equation by $D^{L*}_{mn}(\Omega)$ and integrating over all Ω gives:-

$$\int d\Omega f(\Omega)\, D^{L*}_{mn}(\Omega) = \int \sum_{Lmn} f_{Lm\,n}\, D^{L}_{mn}(\Omega) D^{L*}_{mn}(\Omega) d\Omega \qquad 1.19$$

The first term is simply the definition of the average of $D^{L*}_{mn}(\Omega)$, while the second term simplifies because of the orthogonality relationship of Wigner rotation matrices, giving:-

$$\overline{D^{L*}_{mn}} = f_{Lmn} \left[\frac{8\pi^2}{2L+1} \right] \qquad 1.20$$

Thus the singlet orientational distribution function is:-

$$f(\Omega) = \frac{1}{8\pi^2} \sum_{Lmn} (2L+1)\, \overline{D^{L*}_{mn}}\, D^{L}_{mn}(\Omega) \qquad 1.21$$

The averages $\overline{D^{L*}_{mn}}$ are the infinite number of orientational order parameters which completely define $f(\Omega)$. Assuming we know the exact form of the singlet distribution

function, then we are able to calculate all the order parameters, and conversely, knowing more and more order parameters gives extra information about $f(\Omega)$.

For a particular rank L, since the subscripts m and n can have values, L,L-1.....-L, there can be up to $(2L+1)^2$ order parameters, although this number can be reduced if the symmetries of the mesophase and its molecules are taken into account. For example, in an uniaxial nematic mesophase, the distribution function must be invariant to any rotation about the axis of symmetry or director. If we define this to be along the z axis direction then the subscript m has to be zero, since the singlet distribution function must be independent of the Euler angle α. Furthermore, if we assume that the molecules are cylindrically symmetric and the system has a mirror plane perpendicular to the director then n=o and L adopts even values only. Thus, making these approximations reduces the singlet orientational distribution function to:-

$$f(\beta) = \sum_{L_{even}} f_L D^L_{oo}(\beta) \qquad 1.22$$

As $f(\beta)=f(\Omega)/4\pi^2$, it follows that the expansion coefficients f_L are:-

$$f_L = \frac{(2L+1)}{2} P_L \qquad 1.23$$

and now the order parameters are just the averages of the Legendre polynomials, of which the first six even ranked are given in Appendix 7. The singlet orientational distribution function for cylind-rically symmetric particles is therefore:-

$$f(\beta) = \sum_{L} \frac{(2L+1)}{2} \bar{P}_L P_L(\cos\beta) \qquad 1.24$$

At this point it is worth considering whether the expansion is convergent. Clearly for a totally ordered

system all the $\overline{P}_L$'s will be unity and therefore the expansion will diverge. However, for lower orientational order, $f(\beta)$ could converge since $\overline{P}_0 > \overline{P}_2 > \overline{P}_4$.....,although the factor ((2L+1)/2) would have to be taken into account.

For systems of lower symmetry, further order parameters are required to define the singlet orientational distribution function, a full account of which has been given by Zannoni (1979).

1.6 Pair distribution functions

In the previous section we have seen how the single particle distribution function could be used to calculate the orientational order parameters. However, the pair distribution function can yield more information, although it is more difficult to calculate. The probability of simultaneously finding a particle at $\underline{r}_1$ with orientation Ω_1, and a second molecule at $\underline{r}_2$ and Ω_2 can be written as (Hansen and McDonald, 1976; Zannoni, 1979; Tildesley, 1982):-

$$P^{(2)}(\underline{r}_1,\Omega_1;\underline{r}_2,\Omega_2) = \left[\frac{N(N-1)}{Z_N}\right]\int d\underline{r}_3^N d\Omega_3^N \exp\left(\frac{-1}{kT}U(r^N,\Omega^N)\right) \qquad 1.25$$

Where the integration is now over variables $d\underline{r}_3$, $d\underline{r}_4$.....$d\underline{r}_N$ and $d\Omega_3$, $d\Omega_4$.....$d\Omega_N$. As the separation of the two molecules becomes infinitely large, then assuming there are no infintely long range translational or orientational correlations (c.f crystalline solids), the pair distribution probability will just become the product of two single particle probabilities. So:-

$$P^{(2)}(\underline{r}_1,\Omega_1;\underline{r}_2,\Omega_2)_{r_1-r_2\to\infty} = P^{(1)}(\underline{r}_1,\Omega_1)P^{(1)}(\underline{r}_2,\Omega_2) \qquad 1.26$$

This property can be used to define a reduced two particle distribution or correlation function such that it tends to one as $r_1-r_2\to\infty$, ie:-

$$g^{(2)}(\Omega_1,\Omega_2,\underline{r}_{12}) = \frac{P^{(2)}(\underline{r}_1,\Omega_1;\underline{r}_2,\Omega_2)}{P^{(1)}(\underline{r}_1,\Omega_1)P^{(1)}(\underline{r}_2,\Omega_2)} \qquad 1.27$$

In very dilute systems where simultaneous interactions involving three or more particles can be neglected we find:-

$$\lim_{\rho\to 0} g^{(1)}(\Omega_1,\Omega_2,\underline{r}_{12}) = \exp\left(-\frac{1}{kT}\, U(\Omega_1,\underline{r}_1,\Omega_2\underline{r}_2)\right) \qquad 1.28$$

From equation 1.14 we have seen for an homogeneous fluid or nematic that:-

$$P^{(1)}(\Omega) = \rho f(\Omega) \qquad 1.29$$

thus substitution into equation 1.27 gives:-

$$P^{(2)}(\underline{r}_1\Omega_1;\underline{r}_2,\Omega_2) = \rho^2 f(\Omega_1)f(\Omega_2)g^{(2)}(\Omega_1,\Omega_2\underline{r}_{12}) \qquad 1.30$$

For spherical molecules this becomes totally independent of relative orientation and reduces to the radial distribution function, g(r), measured in atomic liquids.

For convenience we shall introduce a scaled pair correlation function defined as:-

$$G(\underline{r}_{12},\Omega_1,\Omega_2) = f(\Omega_1)f(\Omega_2)g^{(2)}(\Omega_1,\Omega_2,\underline{r}_{12}) \qquad 1.31$$

This also has limiting properties as $r_1 - r_2 \to \infty$

$$\lim_{\underline{r}_{12}\to\infty} G(\underline{r}_{12},\Omega_1,\Omega_2) = f(\Omega_1)f(\Omega_2) \qquad 1.32$$

and as $\rho \to 0$

$$\lim_{\rho \to 0} G(\underline{r}_{12},\Omega_1,\Omega_2) = f(\Omega_1)f(\Omega_2)\exp(-\frac{1}{kT}(\underline{r}_{12},\Omega_1,\Omega_2)) \qquad 1.33$$

When $G(\underline{r}_{12},\Omega_1,\Omega_2)$ is defined in a laboratory axis system, it will not only depend on the separation of molecules 1 and 2, but also on the orientation of the intermolecular vector, Ω_r, so it can be expanded as (Rose 1957):-

$$G(\underline{r}_{12},\Omega_1,\Omega_2) = \sum G^{m_1 m_2 n_1 n_2}_{L L_1 L_2}(r_{12}) D^{L_1}_{m_1 n_1}(\Omega_1)$$

$$\times D^{L_2}_{m_2 n_2}(\Omega_2) D^{L}_{mo}(\Omega_r) \qquad 1.34$$

If we now exploit the symmetry of an idealised system, in this case if we assume that the distribution of the intermolecular vector is spherically symmetric, the system is rotationally invariant and the molecules are cylindrically symmetric it can be shown that this expression reduces to (Zannoni, 1979):-

$$G(\underline{r}_{12},\Omega_1,\Omega_2) = G(\underline{r}_{12},\Omega_{12}) \qquad 1.35$$

$$= \sum \frac{(2L+1)}{64\pi^4} G^{oo}_{L}(r_{12}) D^{L}_{oo}(\Omega_{12})$$

So the reduced pair distribution function depends only on the relative orientations of the two molecules. Multiplying both sides of equation 1.35 by $D^{L*}_{oo}(\Omega_{12})$ and integrating gives:-

$$G^{oo}_{L}(r_{12}) = \int d\Omega_1 d\Omega_2 G(\underline{r}_{12},\Omega_{12}) D^{L}_{oo}(\Omega_{12}) \qquad 1.36$$

$$= \overline{D^{L}_{oo}(\Omega_{12})} G^{oo}_{o}(r_{12})$$

Here $G^{oo}\delta(r_{12})$ is the probability of finding two molecules separated by a distance r_{12}. We can now define a normalised reduced pair correlation function as:-

$$G_L(r_{12}) = \frac{G_L^{oo}(r_{12})}{G_o^{oo}(r_{12})} = \overline{D_{oo}^L(\Omega_{12})(r_{12})} \qquad 1.37$$

$$= \overline{P_L(\cos\beta_{12})(r_{12})} \qquad 1.38$$

This pair correlation function is extremely important in systems composed of cylindrically symmetric molecules and has some interesting properties. For example , if r_{12} is taken to equal the average nearest neighbour separation then $G_L(r_{\text{nearest neighbour}})$, $(L\neq 0)$ will define a short range order parameter. It also provides a rigorous test to molecular field theory (see later) as this predicts $G_L(r)$ to be independent of r. Furthermore, with certain interaction potentials, it also provides a route to the total internal energy (see Chapter 3). Also, using the closure relationship for Wigner rotation matrices (see Appendix 1) equation 1.37 can be re-written as:-

$$G_L(r_{12}) = \overline{\sum_n D_{no}^L(\Omega_1)\sum_n D_{on}^L(\Omega_2)}$$

or, in terms of modified spherical harmonics as:-

$$G_L(r_{12}) = \sum_n C_{Ln}(\beta_1,\alpha_1)C_{Ln}(\beta_2\alpha_2) \qquad 1.39$$

Therefore assuming local unaxial symmetry, in the limit that $r_{12}\to\infty$ the average of the above expression can be written as:-

$$\lim_{r_{12}\to\infty} G_L(r_{12}) = \bar{P}_L^{\,2} \qquad 1.40$$

Thus these pair correlations functions also provide a route to the set of orientational order parameters for our idealised nematic composed of cylindrically symmetric molecules.

1.7 Intermolecular pair potentials

To investigate the molecular properties of liquid crystalline systems a precise knowledge of the form of the intermolecular pair potential should be known. Generally molecules which form liquid crystal phases are extremely complex, often being composed of two or more aromatic rings and often having long flexible alkyl chains. Clearly it would be impossible to take into account the myriad of interactions involved, and, therefore to study such systems theoretically severe approximations have to be imposed.

However, before considering these approximations it is instructive to consider the evaluation of the interactions which exist in these molecular systems. One way would be to simply calculate the number of atom-atom interactions that exist in large molecules, or another to identify and evaluate the major contributions arising from electronic effects. For example, any fluctuation in the charge distribution will produce an instantaneous electropole moment, which in turn will induce an effect in neighbouring species. These forces are known as London dispersion forces (London, 1930 Margenau and Kestner, 1969 Hirschfelder *et al*, 1964) and can be extremely important. Also some molecules possess dipole moments, for example, in the cyanobiphenyls where the CN group is largely responsible for the dipole moment (Dunmur and Miller, 1980), where dipole-dipole, dipole-induced dipole and higher ranked interactions will occur. Of course these interactions will have different magnitudes depending on the intermolecular separation and orientation of the molecular axes, and they will be either attractive or repulsive. Dipole-dipole

interactions, for example, are attractive and diminish as r^{-3} (here r is the intermolecular separation), while dispersion forces vary as r^{-6}.

An alternative approach to obtaining the form of the intermolecular potential is by introducing a mathematical formalism based on some assumed molecular interaction. At the most crudest level, the molecules can be regarded as hard spheres, so that the potential energy is infinite when the spheres overlap but otherwise zero. A softer interaction can be used, for example the Lennard-Jones potential. In this case the spherical molecules experience a strong repulsive force when the molecular separation is less some pre-defined equilibrium distance, and relatively strong long range attractive forces. However, in general molecules are not spherical, and even assuming them rigid the intermolecular potential will depend on as many as 5 independent coordinates. In this case a true representation of the pair potential, provided the molecules do not overlap, can be written as the infinite series (Stone 1978, 1979):-

$$U_{12} = \sum u^{k_1k_2}_{L_1L_2J}(r_{12}) S^{k_1k_2}_{L_1L_2J}(\Omega_{12}) \qquad 1.41$$

Here the summation is over all sub and super scripts, the coefficient u depends only on the intermolecular separation, and:-

$$S^{k_1k_2}_{L_1L_2J}(\Omega_{12}) = i^{(L_1-L_2-J)} \sum_{m_1m_2M} (^{L_1L_1J}_{m_1m_2M}) D^{L_1}_{m_1k_1}(\Omega_1)$$

$$\times D^{L_2}_{m_2k_2}(\Omega_2) C_{Jm}(\theta\phi). \qquad 1.42$$

The term in parenthesis is the Wigner 3-j symbol (Rose, 1957), the $D^L_{mk}(\Omega)$ are the Wigner rotation matrices (Rose, 1957), a few properties of which are listed in Appendix 1, and $C_{JM}(\theta\,\phi)$ is a modified spherical harmonic with arguments θ and ϕ, the spherical polar angles of the

intermolecular vector in some space fixed coordinate system as defined in Figure 1.6. Throughout this thesis the symbol, Ω, will refer to the three Euler angles, α,β,γ as defined by Rose (1957).

This expression has the distinct advantage that it factors out the distance dependence of the potential, the orientations of molecules 1 and 2, and the orientation of the intermolecular vector into individual terms, which allows relatively easy mathematical manipulation. A few of the S-functions with $k_1=k_2=0$ are listed in Appendix 2 in terms of the unit vectors describing the orientations of each molecule , $\underline{z}_1$, and $\underline{z}_2$ and the intermolecular vector $\underline{r}_{12}$ (Stone, 1978). Furthermore, various terms from equation 1.41 can be identified with more classical interactions. For example, dipole-dipole interactions occur as the S_{112} term. Thus:-

$$U_{dip\text{-}dip} = u^{oo}_{112}(r)\, S^{oo}_{112}(\Omega) \qquad 1.43$$

$$= u^{oo}_{112}(r)\left[\underline{z}_1\cdot\underline{z}_2 - 3(\underline{z}_1\underline{r})(\underline{z}_2\cdot\underline{r})\right]$$

where

$$u^{oo}_{112}(r) = (30)^{1/2}\mu_1\mu_2/4\pi\varepsilon_0 r^3 \qquad 1.44$$

and similarly anisotropic london dispersion forces are contained in the terms, S^{oo}_{022}, S^{oo}_{202}, S^{oo}_{222}, and S^{oo}_{224}. This results in the dispersion potential between a pair of linear molecules:-

$$U_{disp} = \gamma\varepsilon_o\left[1 - \frac{3}{2}(\underline{z}_1\cdot\underline{r})^2 - \frac{3}{2}(\underline{z}_2\cdot\underline{r})^2\right] + \frac{3}{2}\gamma^2\varepsilon_o\left[(\underline{z}_1\cdot\underline{r})^2 + (\underline{z}_2\cdot r)^2 - 9(\underline{z}_1\cdot\underline{r})^2(\underline{z}_2\cdot\underline{r})^2 + 6(\underline{z}_1\cdot\underline{r})(\underline{z}_1\cdot\underline{r})(\underline{z}_1\cdot\underline{z}_2) - (\underline{z}_1\cdot\underline{z}_2)^2\right]$$

1.45

where $U_{202} = U_{022} = -\gamma\varepsilon_o\sqrt{5}$ 1.46

$U_{220} = -\gamma^2\varepsilon_o/\sqrt{5}$ 1.47

$U_{222} = -\gamma^2\varepsilon_o\sqrt{10/7}$ 1.48

$U_{224} = -\gamma^2\varepsilon_o 54\sqrt{2/35}$ 1.49

This is in accord with the expression quoted by Kohin (1960) and the earlier derivation given by de Boer (1942).

In general any type of interaction can be identified with terms from equation 1.41 to represent any type of molecular interaction, for example dipole-induced dipole, quadrupole-quadrupole etc, and so it has extreme importance in the investigation of the molecular properties of liquids.

1.8 The molecular field approximation and Maier-Saupe theory

The aim of this section is to give a derivation of the highly successful Maier-Saupe theory with the aid of the statistical mechanics developed in section 1.5. Simply it involves using the molecular field approximation to obtain a suitable potential of mean torque from which various thermodynamic relations can be obtained.

The total potential energy of a liquid or gaseous system to a good approximation can be written as the sum of all the effective pair interactions (Hansen and McDonald,

1976)i.e.:-

$$U(X^N) = \sum_{i<j}^{N} U(X_i, X_j) \qquad 1.50$$

Here X is an abbreviation for the spatial and orientational coordinates $\underline{r}$ and Ω. If we differentiate equation 1.12 with respect to all the coordinates of molecule 1 we find:-

$$\nabla_1 P^{(1)}(X_1) = -\frac{1}{kT} \int dX_2 \nabla_1 U(X_1, X_2) P^{(2)}(X_1, X_2) \qquad 1.51$$

This equation is the first is a series of the Yvon-Born -Green hierarchy (Hansen and McDonald, 1976; Luckhurst, 1979) and expresses the gradient of one distribution function as the integral of the next. Substituting equations 1.14 and 1.30 and dividing by $f(\Omega_1)$ gives:-

$$\nabla_1 \ln f(\Omega_1) = -\frac{\rho}{kT} d\underline{r}_2 d\Omega_2 \nabla_1 U(\underline{r}_{12}, \Omega_1, \Omega_2) f(\Omega_2) g(\underline{r}_{12}, \Omega_1, \Omega_2) \qquad 1.52$$

At this stage we invoke the molecular field approximation and assume that the reduced pair correlation function is independent of the orientation of the two molecules, and so $g(\underline{r}_{12}, \Omega_1, \Omega_2)$ can be replaced by $g(\underline{r}_{12})$.

This allows equation 1.52 to be integrated, giving:-

$$f(\Omega_1) = \frac{1}{Z} \exp\left(-\frac{1}{kT} U(\Omega_1)\right) \qquad 1.53$$

Here Z can be obtained from the normalising condition i.e.:-

$$\int d\Omega f(\Omega) = 1 \qquad 1.54$$

$U(\Omega_1)$ is the potential of mean torque or the pseudo potential for molecule 1 placed in a field created by the interaction with all other molecules in the system. It is

related to the pair potential by

$$U(\Omega_1) = \rho \int dr_{12} d\Omega_2 \; U(r_{12},\Omega_1,\Omega_2) f(\Omega_1) g(r_{12}) \qquad 1.55$$

In otherwords, the potential of mean torque can be obtained by averaging a pair potential over all orientations of the second molecule and intermolecular vector, and over all intermolecular separations.

Certain thermodynamic results can now be written down. For example the total configurational internal energy is:-

$$U = \frac{\rho^2 V}{2} \int dr_{12} d\Omega_1 d\Omega_2 U(r_{12},\Omega_1,\Omega_2) f(\Omega_1) f(\Omega_2) g(r_{12}) \qquad 1.56$$

The entropy in terms of the N-body distribution function is (Luckhurst, 1979):-

$$S = \left(\frac{-k}{N!}\right) \int dX^N P^{(N)}(X^N) \ln(P^{(N)}(X^N)/N!) \qquad 1.57$$

thus in the limit of the molecular field approximation, this can be written as:-

$$S = -Nk \int d\Omega_1 f(\Omega_1) \ln(f(\Omega_1)) - Nk \ln\rho + k \ln N!$$
$$- (k\rho^N/N!) \int dr^N g^N(r^N) \ln(g^{(N)}(r^N)). \qquad 1.58$$

and the Helmholtz free energy can be evaluated since

$$\Delta A = \Delta U - T\Delta S \qquad 1.59$$

In order to obtain a pseudo potential, we must start from a suitable pair potential, a suitable starting point being the equation given earlier. (Equation 1.41)

Averaging this equation over all intermolecular separations, all orientations of molecule 2 and all orientations of the intermolecular vector, assuming cylindrically symmetric molecules forming a uniaxial

mesophase with the director along the z-laboratory axis gives the potential of mean torque as (Humphries et al, 1972 Luckhurst, 1979):-

$$U(\beta) = \sum_L \bar{u}_L \bar{P}_L P_L(\cos\beta) \qquad 1.60$$

where $\bar{u}_L$ is the average of the L^{th} ranked interaction parameter, $\bar{P}_L$ are the averages of the Legendre polynomials which, as we have seen are the the orientational order parameters, and β is the angle between the molecular symmetry axis and the director.

Maier and Saupe (1958, 1959, 1960) obtained just the second rank term in this summation since they used as a starting point an expression for second rank intermolecular dispersion forces. Prior to this, Kreiger and James (1954) used a similar pseudo potential to describe molecular orientational order in crystalline systems.

The orientational contribution to the internal energy can now be evaluated since:-

$$f(\beta) = \frac{1}{Z} \exp\left(\frac{1}{kT} \sum_L \bar{u}_L \bar{P}_L P_L(\cos\beta)\right) \qquad 1.61$$

where the orientational partition function is:-

$$Z = \int d\beta \sin\beta \exp\left(\frac{1}{kT} \sum_L \bar{u}_L \bar{P}_2 P_2(\cos\beta)\right) \qquad 1.62$$

Using equation 1.56 the total internal energy can be written as:-

$$U = \frac{N}{2} \sum \bar{u}_L \bar{P}_L^2 \qquad 1.63$$

and the entropy from equation 1.58 as:-

$$S = \frac{N}{T} \sum_L \bar{u}_L \bar{P}_L^2 + Nk \ln Z \qquad 1.64$$

Combining these two expressions gives the Helmholtz free energy, A,

$$A = -\frac{N}{2} \sum_L \bar{u}_L \bar{P}_L^2 - NkT\ln Z$$

or $$\frac{A}{NkT} = \frac{1}{2kT} \sum_L \bar{u}_L \bar{P}_L^2 - \ln Z \qquad 1.65$$

The orientational order parameters can now be calculated since

$$\bar{P}_L = \frac{1}{Z} \int d\beta \sin\beta P_L(\cos\beta) f(\beta)$$

$$= \frac{1}{Z} \int d\beta \sin\beta P_L(\cos\beta) \exp\left(\frac{1}{kT} \sum u_L \bar{P}_L P_L(\cos\beta)\right)$$

1.66

which is consistant with the constraint that for equilibrium the free energy is a minimum with respect to variations in the order parameters. Restricting the pseudo potential to second rank terms as in Maier and Saupe's derivation gives the self consistant equations for the order parameters:-

$$\bar{P}_2 = \frac{1}{Z} \int d\beta \sin\beta P_2(\cos\beta) \exp\left(\frac{\varepsilon}{kT} \bar{P}_2 P_2(\cos\beta)\right) \qquad 1.67$$

and

$$\bar{P}_4 = \frac{1}{Z} \int d\beta \sin\beta P_4(\cos\beta) \exp\left(\frac{\varepsilon}{kT} \bar{P}_2 P_2(\cos\beta)\right) \qquad 1.68$$

where $\varepsilon = \bar{u}_2$. Figure 1.7 shows the temperature dependance of $\bar{P}_2$ calculated using equation 1.67. A solution exists for all values of kT/ε with $\bar{P}_2$ equal to zero, corresponding to the isotropic phase. In addition in the range of kT/ε between 0 and 0.2228 two other solutions for $\bar{P}_2$ exist. To determine which of these various solutions constitute a stable phase, the orientational free energy must be calculated. It turns out that between $kT/\varepsilon = 0$ and

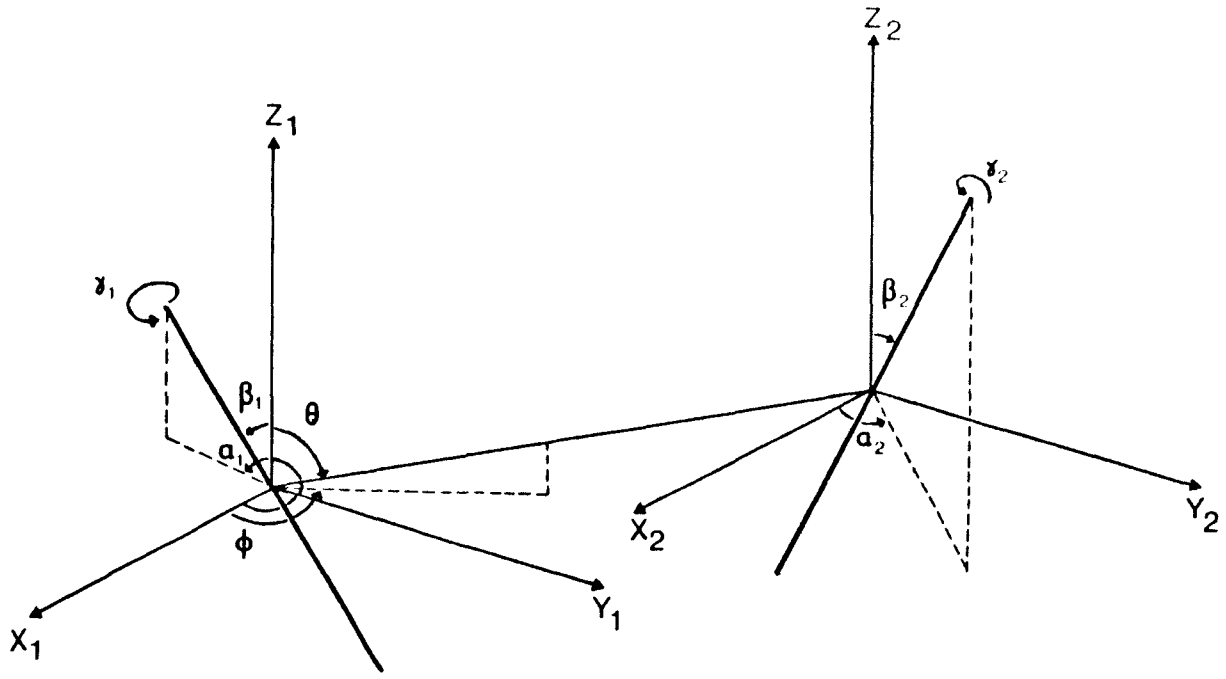

Fig 1.6 Axis coordinate system for a pair of molecules of arbitrary shape.

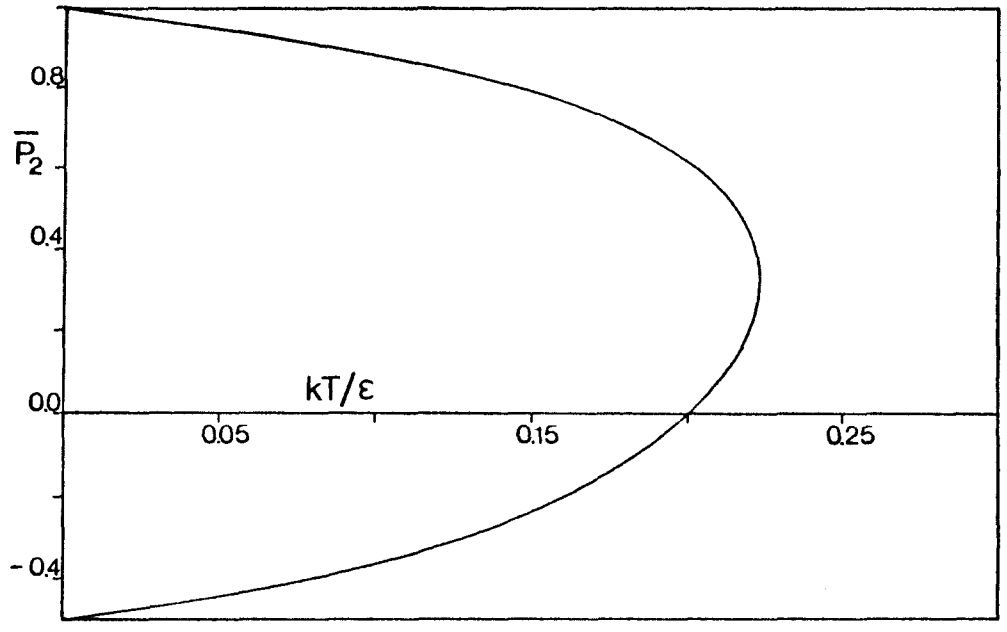

Fig 1.7 The Maier-Saupe molecular field prediction for the temperature dependence of the orientational order parameter $\bar{P}_2$.

kT/ϵ = 0.2202 the phase of highest order is stable, while at higher temperatures the isotropic state is more stable. At kT/ϵ = 0.2202 the gradient of the free energy $(\partial A/\partial T)_V$ is discontinuous with an entropy change of $\Delta S/Nk$ = 0.417. Therefore, at this temperature, a first order transition occurs between the nematic and isotropic phases. $\bar{P}_2$ at the transition is 0.429 while $\bar{P}_4$ is predicted to be 0.120.

Although this theory is unable to predict the transition temperatures of real nematic phases, because the interaction parameter, ϵ, will depend on various parameters arising from various interactions present, (eg dipolar, dispersion, etc) it does give relatively good agreement with the order parameter when plotted on a reduced temperature scale (eg T/T_{NI}, where T_{NI} is the nematic-isotropic phase transition temperature) (See for example Humphries *et al*, 1972, Humphries and Luckhurst, 1972).

Further modifications have been made to the simple theory, for example, by retaining fourth rank terms in the pseudo potential (Humphries *et al*, 1972), it is possible to fit almost exactly any experimental data (with the exception of the change in entropy at the transition, pair correlations and related quantities) simply by varying the ratio of ϵ_2 to ϵ_4. However, nothing more will be said of this theory. Other modification have been made by Horn and Faber, (1979) who investigated the inclusion of other higher ranked terms in the pseudo potential, for example terms dependant on $(\bar{P}_2\bar{P}_4)$, $\bar{P}_2^3$, and terms which depend on these order parameters which themselves are functions of the reduced temperature. These modifications are, however, difficult to justify since they do not occur in the rigorous derivation of the potential of the mean torque. However, like the Humphries-James-Luckhurst theory they do provide better agreement with experimental trends than the simple theory. A similar although more complete discussion has been given by Kventzel and Katriel (1982).

The simple Maier-Saupe derivation assumes nothing of

the volume dependence on the pseudo potential, and various people have investigated ways of including this, for example Humphries and Luckhurst, (1972); Humphries et al (1972). However, the overall effect of including volume changes only produces slight improvements to the predicted results, (Cotter, 1977).

Furthermore, the molecular field theory has been applied to non-cylindrically symmetric molecules (Luckhurst et al, 1975; Straley, 1974) to yield a reasonable account of the temperature dependance of the order paramter at constant volume for the molecule PAA.

However, the largest and perhaps most severe approximation in all the theoretical works is the use of the molecular field approximation and one of the aims, therefore, of this thesis is to test its validity.

A theory of the next highest order has been developed by Sheng and Wojtowicz (1976), which instead of looking at one molecule in a field of others, investigates the properties of two in the molecular field created by their neighbours. This is known as the constant coupling or two site cluster theory and has also been used with varying degrees of success to describe some of the properties in ferro and antiferromagnetism, in particular the determination of critical points, the temperature dependance of magnetism and susceptibility, and the short range order. In the mean field approximation, orientation is independent of separation, so with short range effects taken into account an improvement oven mean field theory would be envisaged. Indeed when compared with experimental data this is the case.

The theory is very similar to that in the Maier-Saupe derivation, except the pseudo potential is now:-

$$V_{cc} = (z-1)\left[V_{MF}(\cos\beta_1) + V_{MF}(\cos\beta_2)\right] + V_{12}(\cos\beta_{12}) \qquad 1.69$$

In otherwords the average constant coupling potential, V_{cc}, is composed of two types of term, V_{MF} which is the molecular field pseudo potential experienced by molecules 1 and 2, and a term arising from the direct interaction of molecules 1 and 2, V_{12}. The coefficient z is simply the coordination number. The V_{12} term will clearly depend on the difference in orientation between molecules 1 and 2, as

$$\cos\beta_{12} = \cos\beta_1\cos\beta_2 + \sin\beta_1\sin\beta_2\cos(\phi_1-\phi_2) \qquad 1.70$$

where β_1, β_2 and ϕ_1 and ϕ_2 are defined in Figure 1.6. Thus V_{cc} can be expanded generally as:-

$$V_{cc} = \sum_{\substack{L \\ \text{even}}} u_L \left[(z-1)\bar{P}_L\left[P_L(\cos\beta_1) + P_L(\cos\beta_2)\right] + P_L(\cos\beta_{12})\right] \qquad 1.71$$

Here $\bar{P}_L$ are the long range order parameters defined as:-

$$\bar{P}_L = \frac{1}{Z}\int_0^{\pi}\int_0^{\pi}\int_0^{2\pi} P_L(\cos\beta_1)\exp(-1/kT\ V_{cc})\sin\beta_1\sin\beta_2 d\beta_1 d\beta_2 d\phi \qquad 1.72$$

and short range order parameters σ_L can also be evaluated as:-

$$\sigma_L = \frac{1}{Z}\int_0^{\pi}\int_0^{\pi}\int_0^{\pi} P_L(\cos\beta_{12})\exp(1/kTV_{cc})\sin\beta_1\sin\beta_2 d\beta_1 d\beta_2 d\phi \qquad 1.73$$

We know that the potential of mean torque felt by molecule 1 can be expanded as:-

$$\bar{V}_{mF} = \sum_{L,\text{even}} \gamma_L P_L(\cos\beta_1) \qquad 1.74$$

where γ_L is a function of temperature and the order

parameters. This reduces to V_{MF} in the case $\gamma_L = \bar{u}_L \bar{P}_L$.

We now have two routes to the calculation of a $\bar{P}_L$ and two unknown variables, γ_L and the parameter scaling the potential, $\bar{u}_L$, thus assuming both routes give the same $\bar{P}_L$ then:-

$$\frac{1}{Z}\int_0^{\pi} P_L(\cos\beta_1)\exp\left(\frac{1}{kT}\bar{V}_{mF}\right) \qquad 1.75$$

$$= \frac{1}{Z}\int\int\int P_L(\cos\beta_1)\exp\left(\frac{1}{kT}V_{cc}\right)\sin\beta_1\sin\beta_2\sin\beta_{12}\,d\beta_1 d\beta_2$$

where $\bar{V}_{cc} = -\sum_Z (z-1)\gamma_L P_L(\cos\beta_1) P_L(\cos\beta_2) + \bar{U}_L P_L(\cos\beta_1)$

1.76

In solving these equations, Sheng and Wojtowicz have allowed terms in $\bar{u}_L$ for L>2 to be zero, and terms in γ_L with L>4 also to be zero, thus allowing the equations to be solved iteratively for γ_L. Substitution of these values into equations 1.72 and 1.73 will then yield the long and short range order parameters.

In a similar manner, as described earlier, various thermodynamic properties can be evaluated, for example, the free energy, from which the transition temperature can be found, and the average internal energy per particle.

The results from this theory will be compared with the predictions of the Maier-Saupe theory in Chapter 3.

As an extension to this theory, a three site expansion (Lekkerkerker *et al*, 1978) and the four site expansion (Van der Haegen, 1980) have recently been proposed which will also be discussed briefly in Chapter 3.

Chapter 2

Computer Simulations

2.1 Introduction

Over the last two decades, modern silicon technology has resulted in the production of faster, larger and more powerful computers. Every year, newer and faster machines appear, with the present trend going from conventional serial Von Neumann processors to much faster parallel computers. Computations which may have taken several hours in the early sixties now take only a few seconds. This recent dramatic upsurge in computer power has therefore allowed physical scientists to apply the technique of computer simulation to the study of physical systems.

Before discussing computer sumulations in detail however, we must first of all ask, why is the technique of computer simulation so important? From a theoretician's point of view, this technique has extreme value in that it provides a tool to perform 'exact experiments' on well defined model systems thus enabling these computer experiments to be compared directly with both real experimental data and predictions from theories. With the aid of mathematical techniques and analytic relationships the properties of dilute atomic gas es can be calculated directly since the system can be regarded as consisting of totally independent entities, for example, particles or oscillators. However, for more condensed systems this analytic mathematical approach is not possible, since for compressed gas-es or liquids the atoms or molecules interact with each other giving a many bodied, multi-interaction problem. To a certain extent this problem can be overcome by resorting to computer simulation techniques, at least for relatively simple systems, where the interaction potential can be regarded as adopting a simple form, and consisting of pairwise interactions only. In the case of the simulation of atomic liquids, for example liquid argon, a high degree of

agreement can be obtained between data measured experimentally and that calculated from computer simulations, thus providing a fairly rigorous test to the derived pair potentials. The same is true, although to a lesser extent, in the simulation of the properties of molecular liquids, for example, liquid nitrogen, hydrogen chloride and even for simple triatomic molecules, for example carbon disulphide and water. However, for more condensed systems, or dilute systems or large complex molecules, approximations have to be made to formulate the pair potential before the simulation can be attempted. For systems consisting of large molecules, it would be a computational impossibility to account for all interactions and so assumptions related to the symmetry of the molecules and to the form of the interaction potential have to be enforced. Even so, the simulation of such systems does provide a very important probe into the understanding of the properties of such molecular systems.

Computer simulations provide a rigorous test, not only of pair potentials but also provides a test of properties calculated via other routes. In addition, and often more important, computer simulations allow the assumptions used in various approximate theories, for example, the molecular field approximation, to be fully tested.

Clearly computer simulations allow not only laboratory obtainable data to be calculated, but also other very important properties, for example, an infinite number of distribution and correlation functions together with properties at extreme temperatures or pressures can be extracted from simulations which would otherwise be totally inaccessable.

2.2 Techniques involved

There are two principle techniques used in computer simulation studies, the Monte-Carlo technique, and the method of molecular dynamics. However, before discussing

both methods in any detail, we shall look at some problems which are always encountered and are common to both techniques.

Firstly and perhaps the biggest problem is associated with the size of systems studied. In a real experiment one deals normally with the order of 10^{23} atoms or molecules, but unfortunately computers are limited in size, and so only a small fraction of this number can be studied. Indeed early computer simulation studies used as few as 32 molecules (Rosenbluth and Rosenbluth, 1954), and even today, few simulations are performed on systems with more than 1000 interacting atoms or molecules (particles). This therefore means that in order to predict the properties of essentially infinite systems from our small finite system, a careful extrapolation has to be performed. However, broadly speaking bulk properties are only weakly dependent on N, where N is the number of particles, for N greater than 100 (Hansen and McDonald, 1976) except for properties calculated close to a phase transition, where, statistically a true phase transition cannot occur except in infinite systems.

The fact that small systems have to be used, gives rise a further problem, that of surface effects. Clearly for a system of say 1000 particles a relatively high proportion will exist at or close to a surface, which, will produce adverse properties. To remove these surface abnormalities, periodic boundary conditions are imposed. This device involves surrounding the isolated system of N particles by an infinite number of exact replicas of itself. Thus a particle at a position (x, y, z) in the cell will see exact replicas of itself at positions $(x\pm n_a a, y\pm n_b b, z\pm n_c c)$, where n_a, n_b, n_c each adopt all integer values between 0 and infinity, and in this case the cell is defined to be rectangular with dimensions (a,b,c). Also, when a particle is moved out through one face of the cell it automatically reenters at the opposite face in order to preserve N. This effect is depicted in Figure 2.1 for a two dimensional

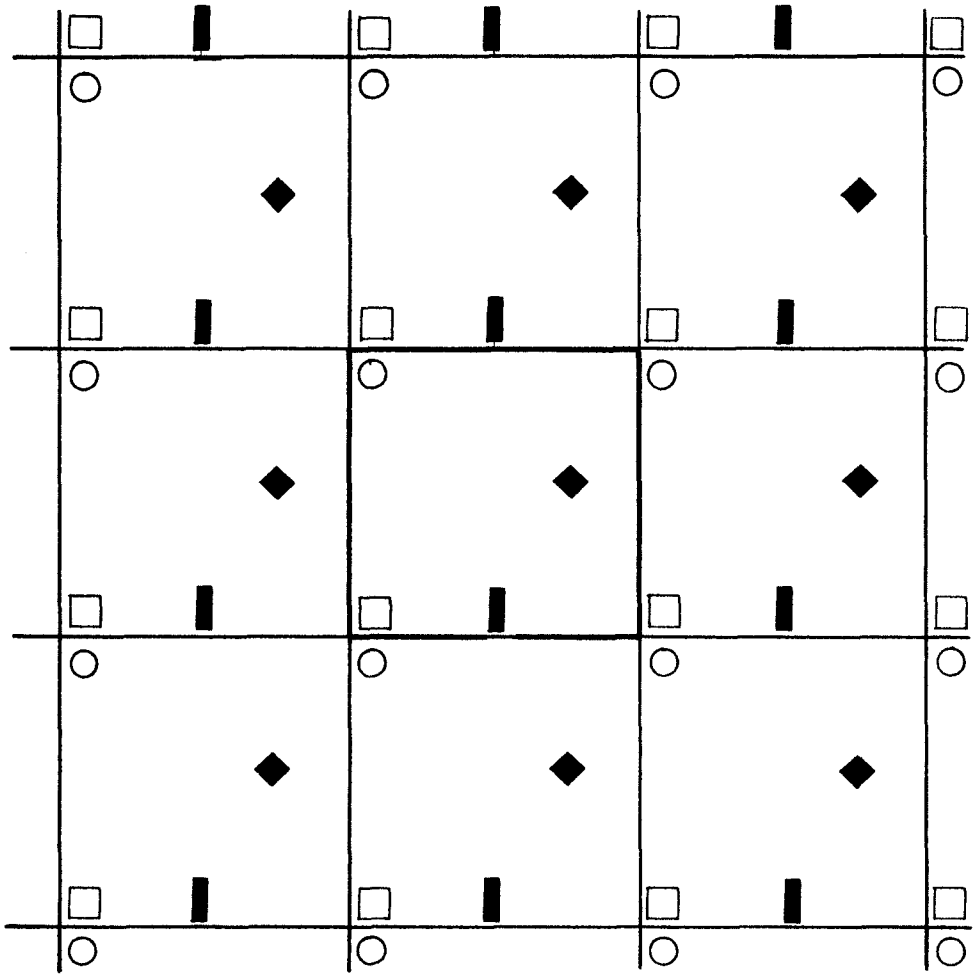

Fig 2.1 Two dimensional periodic boundary conditions.

square system. In general any shaped cell can be used provided that on replication it fills all space. Thus in two dimensions the cell could either be triangular, square, rectangular or hexagonal. In three dimensions it is usual to use a cubic cell giving cubic periodic boundary conditions, although other more complex cells have been used, for example, truncated octahedra (D.J. Adams 1982). Actually any space filling polyhedra can be used although it is usual to chose a cell representative of the chemical structure of the system. The major disadvantage with periodic boundary conditions is that it introduces spurious periodic correlations with a regularity equal to the cell dimensions, and so, in calculating distance dependent correlation and distribution functions one must always be aware of this effect.

Another problem encountered in computer simulations, although not as severe as the difficulty encountered using a finite number of particles, is the choice of a starting configuration. By this we refer to the positions and orientations of the N particles in our cell at the start of the calculation. Generally at a specific set of external conditions (for example, temperature, pressure) the system will exist in equilibrium, therefore unless the starting configuration for a specific simulation is an equilibrated one, then a stage during which time the particles equilibrate will have to be undertaken. This equilibrium process can be minimised with a judicious choice of starting configuration, since it is unlikely that a fully equilibrated state will always exist. For example, at low temperatures it is sensible to take a configuration representative of the degree of order which would exist at low temperatures, in otherwords an ordered state, and similarly at high temperatures where a totally random state would represent the high degree of disorder present.

2.2.1 The Monte-Carlo technique

The Monte-Carlo method is a technique which involves random or probabilistic events. Basically it involves the generation of a sequence of configurations in phase space by random displacements. Not all of the configurations are counted, and the decision as to accept or reject the random move is made in a way as to ensure that configurational space is sampled with a probability proportional to the Boltzmann distribution, during which stage, various thermodynamic ensemble averages and other properties of interest are evaluated.

At this point it is worth defining what is meant by 'ensemble'. Statistically there are many types of ensemble, the most commonly used of which is the canonical ensemble. In this case the number of particles, the volume and the temperature are held constant allowing the internal energy to fluctuate. Examples of other less common ensembles are the grand canonical ensemble in which energy, volume and temperature are constant (N fluctuates) and the isothermal-isobaric ensemble where, as its name partially suggests, the pressure, temperature and N are held constant. However, throughout this thesis, although the word ensemble will be used loosely, it will actually always refer to the canonical ensemble, as in all the simulations, temperature, volume and temperature are held constant.

Any ensemble average can be defined by the relation:-

$$\langle M \rangle = \int M(X_1^N) p(X_1^N) dX / \int p(X_1^N) dX_1^N \qquad 2.1$$

Here the angular brackets denote an ensemble average of some function, M, which is dependent on the phase space variables X_1^N where, as in Chapter 1 variables with sub and superscripts denote the set between 1 and N, and $p(X_1^N)$ is the probability density function. For example, the average configurational internal energy of an ensemble of N

particles can be written as:-

$$\langle U \rangle = \int U(q_1^N)p(q_1^N)dq_1^N / \int p(q_1^N)dq_1^N \qquad 2.2$$

where again q_1^N denotes the N configurational variables q_1, $q_2 \ldots\ldots\ldots q_N$, where the q_i represent the variables spanning space and orientation $(x_i, y_i, z_i, \alpha_i, \beta_i, \gamma_i)$. For a molecular or atomic system $p(q_1^N)$ is simply the Boltzmann distribution:-

$$p(q_1^N) = \exp(-U(q_1^N)/kT)/Q \qquad 2.3$$

where Q is the partition function:-

$$Q = \int \exp(-U(q_1^N)/kT)dq_1^N \qquad 2.4$$

Here $U(q_1^N)$ will usually be the sum of all pair interactions although strictly speaking many bodied interactions should be included.

A very crude approach to a Monte Carlo simulation would be to simply generate random configurations. For each configuration the internal energy, $U(q^N)$ and the Boltzmann factor would be calculated and using equation 2.2, replacing the integrals by summations, $\langle U \rangle$ could, in principle be calculated. However, this method would be impractical for two reasons. Firstly, the probability density function is proportional to the Boltzmann factor, which varies very rapidly with changes in $U(q^N)$. Therefore only configurations with relatively low internal energy will contribute significantly to the probability density, and so prohibitively large numbers of configurations would have to be sampled in order to obtain any form of average. The solution to this problem is to sample the region of phase

space of low internal energy and therefore of high probability density. This technique is known as importance sampling and involves the selection of configurations according to a defined probability density function, and in this case according to the Boltzmann distribution.

The second failure, of this simple Monte Carlo scheme and perhaps more serious is that the partition function, Q, in equation 2.3 is very difficult to evaluate. However, this problem can be solved by not choosing a series of unconnected random configurations, but to choose it such that the sequence forms a Markov chain, in which the memory of a particular step (configuration) extends back to the previous step only, and not beyond. This leads to the important consequence in that it is now only the ratios of the probability density functions that are important, and the partition functions cancel. A detailed account and proof of this has been written by Hansen and McDonald (1976) and Valleau and Whittington (1980).

The method normally used to circumscribe these two fundamental problems in the Monte Carlo simulation of atomic and molecular systems is that originally proposed by Metropolis et al (1953). A flow chart of the scheme is given in Figure 2.2. As a starting point, some initial configuration is taken, which in general will contain N particles, each with some position and orientation. The total energy is then evaluated as a typical guide to the rate of convergence to equilibrium. The system then advances through one move by initially selecting a particle. This selection can either be random (see Appendix 3), or can be performed sequentially by taking the i^{th} particle for this move and the $(i+1)^{th}$ for the next, and so on. The selected particle is then given a random displacement after which the change in internal energy, ΔU is evaluated from which a decision is made whether to accept the move or reject it. If the new configuration has a lower potential energy, in

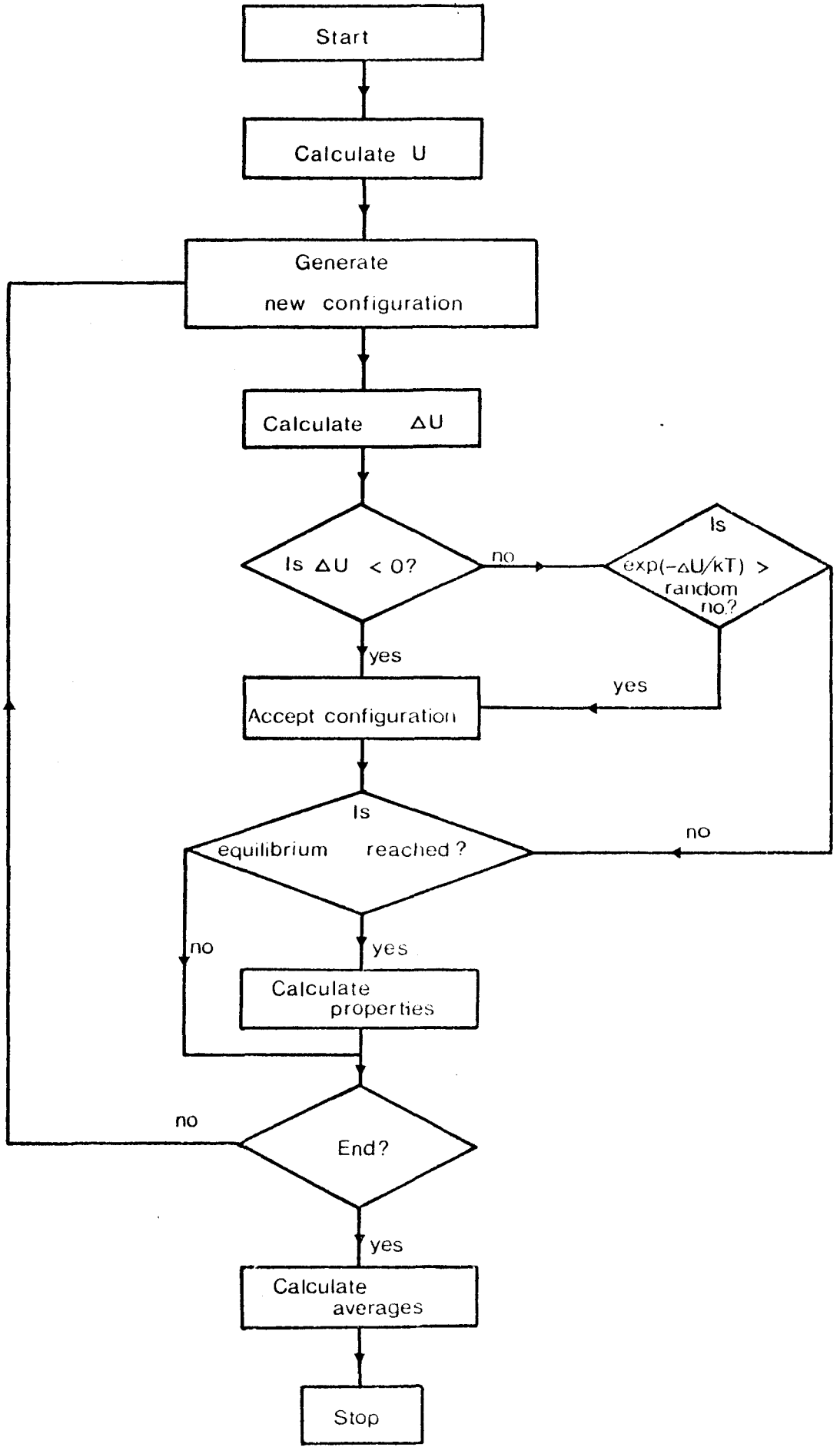

Fig 2.2 A schematic representation of the Monte Carlo algorithm.

otherwords if the move takes the system to a more stable state, then the move is accepted, otherwise it is rejected with a probability proportional to the Boltzmann distribution. This probability is obtained by comparing the quantity $\exp(-\Delta U/kT)$, (it is at this stage that temperature enters the calculation) with a number chosen at random in the range 0 to +1 (See Appendix 3). If the Boltzmann factor is greater than the random number then the move is accepted, else the move is rejected and the old configuration recounted in the averaging process. Usually the way in which the new move is generated is controlled such that approximately half of the total number of configurations generated are rejected. This is achieved by restricting the way in which the move is evaluated, usually by constraining it some way, such that it has to occur within certain limits. The factor of a half is rather arbitrary, and chosen as a compromise between on one hand, a total rejection of all configurations, and on the other, a situation in which all configurations are accepted because the change in internal energy is very small. This procedure is then repeated until the internal energy of the system reaches an equilibrium value at which point a stage known as the production phase is entered where all the requisite averages and properties are calculated. Typically, the equilibrium and production stages can consist of anything up to, and often in excess of 1000 cycles, where a cycle is defined as N attempted moves.

Generally throughout both equilibration and production stages the average internal energy of a particular configuration, is calculated directly. Another, equally important quantity, the heat capacity can be evaluated, from which the exact location and order of phase transitions can be obtained. In the canonical ensemble, this is the heat capacity at constant volume defined as:-

$$C_V = (\partial \langle U \rangle / \partial T)_V . \qquad 2.5$$

However, we have seen that the ensemble average of the internal energy can be written in the form given by equation 2.2 which on differentiation with respect to $1/kT$ and rearrangement gives:-

$$\frac{\partial \langle U \rangle}{\partial 1/kT} = -\langle U^2 \rangle + \langle U \rangle^2 \qquad 2.6$$

Thus the heat capacity is simply

$$C_v = \frac{1}{kT^2}\left(\langle U^2 \rangle - \langle U \rangle^2 \right) \qquad 2.7$$

$$\text{or } C_v/k = \left(\langle U^2 \rangle - \langle U \rangle^2 \right)/k^2T^2 \qquad 2.8$$

Therefore given the mean square fluctuations and the square of the average internal energy, C_v can be computed. However, since C_v calculated in this manner is actually obtained as a fluctuation quantity it is often prone to large errors and uncertainty.

However, C_v can be calculated, although now indirectly, but to a much higher accuracy, simply by the numerical differentiation of the curve obtained for the internal energy as a function of temperature. The usual procedure in this case is to fit the simulated data to a known algebraic function and to differentiate it. Usually the function is a continuous set of cubic polynomials, called a cubic spline. Therefore this process can only be applied at the end of a series of simulations when several values of the average internal energy have been evaluated at many temperatures (usually at least 10).

Other thermodynamic properties of extreme value in atomic and molecular systems are the free energy and entropy. In the canonical ensemble the free energy is actually the Helmholtz free energy. However, their calculation using Monte-Carlo techniques presents a severe

problem, since neither can be written as ensemble averages in the form of equation 2.1. Instead they have to be calculated using integration and extrapolation techniques from the state of interest, to a state in which the free energy is known. This process however is very laborious and prone to large errors, and together with other methods based on interpolation procedures and virial expansions are discussed further by Zannoni (1979).

2.2.2 The method of molecular dynamics

As the content of this thesis is based on simulations using the Monte-Carlo technique, relatively little will be said of the method of molecular dynamics. Like the Monto-Carlo method, molecular dynamics also suffers from the problems associated with finite size and boundary effects. In fact, with molecular dynamics one is often restricted to employ even smaller ensembles than used in Monte-Carlo methods since larger, more complex computational calculations are required.

The method of molecular dynamics is based on a very simple concept and involves setting up and solving the equations of motion of a collection of interacting particles. It has the distinct advantage over the Monte-Carlo technique in the ability to calculate not only equilibrium averages but also important time dependent properties.

Very good reviews and detailed descriptions of this technique have been written by Alder and Wainwrite (1959, 1960), Rahman (1964), Berne and Harp (1970) and Zannoni (1979).

2.3 Computer Simulations and Anisotropic systems

To date very little work has been published on the computer simulations of anisotropic systems, as compared with the enormous amount of effort that has been applied to the study of atomic and simple molecular systems. The

principle reason for this is probably due to the fact that computer simulators know little or nothing of the physics associated with liquid crystals, and conversely many liquid crystal researchers are unfamiliar with concepts in computer simulation. Furthermore, some of the approximations which have to be made in the study of anisotropic systems, would at first conceal the extreme importance of this field of work.

In the study of anisotropic systems, one is usually interested in the physical properties close to a phase transition (e.g. nematic-isotropic). This necessitates the use of large systems and therefore usually the Monte-Carlo method. In addition real nematogenic molecules are extremely complex and so approximations have to be imposed to make the calculations computationally possible. The earliest simulation on such an anisotropic system calculated properties of two dimensional elipses (Vieillard-Baron, 1972). At first sight, two dimensional simulations would appear pointless, but even simulations of linear systems provides valuable information, since one dimensional systems can be solved exactly using analytic techniques, thus providing an accurate test to computer simulations. For two and three dimensional systems however, analytic methods normally employ the molecular field approximation, thus simulation of these systems provides a good test to this approximation. (Denham et al, 1977; 1980)

The earliest three dimensional simulation of an anisotropic system, imposed the approximation that the molecules consisted of cylindrically symmetric rods and could only orientate in twelve discrete orientations. (Lasher, 1972). Furthermore, the molecules were restricted to lie at the sites of a cubic lattice, thus removing all translational degrees of freedom. This later approximation seems severe, although it has since been shown that the effect of translation has very little effect on the important anisotropic properties calculated (Luckhurst and

Romano, 1980). Futher work by Lebwohl and Lasher (1972) removed the quantisation of the orientation of the molecules and this model system, in which the anisotropic particles were fixed to the points of a cubic lattice and interacting via the potential:-

$$U_{ij} = - \varepsilon_{ij}(r)P_2(\cos\beta_{ij}) \qquad 2.9$$

has provided the foundations for virtually all subsequent calculations on anisotropic systems. This pair potential has the important feature that it can be compared directly with that used in the Maier-Saupe theory (see Chapter 1), thus allowing a test of the molecular field approximation. In the Lebwohl-Lasher model ε_{ij} is a constant controlling the interaction strength, and equals ε for nearest neighbour interactions but zero otherwise, thus reducing the amount of computation required. Later work on this model has investigated the effect of N (the number of particles) on the various transition properties (Jansen et al, 1977) and various modifications to the model have also been studied, for example, the effect of different pair potentials. In particular, potentials representative of dispersion forces and therefore dependent on the orientation of the intermolecular vector, and those present between biaxial particles. (Luckhurst and Romano, 1980; Humph-ries et al, 1981). Other work in this area can be summed in a few references : Vieillard-Baron (1974), Meirovitch (1977), Miller (1979), Zannoni (1979), Luckhurst et al (1981,1982), Luckhurst and Simpson (1982a, 1983), Tsylalo and Bagmet (1976, 1978), Zannoni and Guerra (1981), Bagmet (1982), the later three being molecular dynamics simulations.

The work in Chapters 3 to 6 of this thesis is based on the Lebwohl-Lasher model with the approximations that the molecules are cylindrically symmetric and that they are fixed at the lattice points of some predefined lattice (either simple cubic or face centred cubic - see Appendix 4).

As mentioned earlier, this later approximation removes the translational degrees of freedom without affecting the orientational properties significantly, whilst the first allows a great deal of simplification to made in the approximation for the pair potential, and as we have seen in Chapter 1 means that the averages of the even valued Legendre polynomials alone are sufficient to fully describe the long range orientational order present.

One of the most important steps in the Monte Carlo process is the generation of a new configuration in the chain of events. This new configuration must initially be chosen such that it occurs with equal probability throughout all phase space. Firstly a particle is selected either at random or taken sequentially and given a random displacement. For cylind-rically symmetric molecules this can be achieved in two ways: To define the orientation of a cylind-rically symmetric particle, two variables are required, the azimuthal angle, α, and the polar angle, β. However, it is more convenient to store $\cos\beta$ since a new configuration with the required probability density can now easily be generated using:-

$$\alpha_{new} = \alpha_{old} + \Delta\xi \qquad 2.10$$

and

$$(\cos\beta)_{new} = \lambda \qquad 2.11$$

Here ξ and λ are random numbers (See Appendix 3) uniformly distributed in the range +1 to -1 and Δ is the maximum displacement providing control of the acceptance-rejection ratio.

A variation to this method is to increment $\cos\beta$ in a similar way to α, with appropriate action being taken to ensure it does not exceed its permitted bounds of +1 and -1. This technique is discussed in further detail in Chapter 5.

An alternative method was originally proposed by Barker and Watts (1969) in their simulation of water. It involves selecting a molecule, again either taken sequentially or at random, and rotating it by a controlled random amount about a laboratory axis selected at random. In this case it is more convenient to represent the molecules by unit vectors, so the orientation of the i^{th} molecule can be represented by:-

$$\underline{l}^i = (n_x, n_y, n_z) \qquad 2.12$$

where
$$n_x = \cos\alpha\sin\beta \qquad 2.13$$
$$n_y = \sin\alpha\sin\beta \qquad 2.14$$
$$n_z = \cos\beta \qquad 2.15$$

A new configuration is then generated using the following relationships:-

$$(n_x)_{new} = (n_x)_{old} \qquad 2.16$$
$$(n_y)_{new} = \cos\theta(n_y)_{old} + \sin\theta(n_z)_{old} \qquad 2.17$$
$$(n_z)_{new} = \cos\theta(n_z)_{old} - \sin\theta(n_y)_{old} \qquad 2.18$$

Where the equations correspond to a rotation of θ about the laboratory x axis. Equations of a similar form occur for rotations selected about the y and z axes. The rotation angle, θ is generated using:-

$$\theta = \Delta\xi \qquad 2.19$$

Where again Δ is the maximum displacement, chosen to achieve an optimum acceptance-rejection ratio and ξ is a random number generated in the range +1 to -1. Clearly this method invokes a slight computational overhead, since extra multiplications are involved, however as we shall see in Chapter 5 it does have certain advantages.

One of the most useful properties available from

simulations of anisotropic systems are the orientational order parameters. For uniaxial systems these are just the averages of the even ranked Legendre polynomials (see Appendix 7), and furthermore are normally measured in real experiments. In computer simulations these can be calculated directly provided the director orientation is known. Indeed in certain cases, as we shall see later in this thesis, the director can be pinned either by some external force, by using a suitable pair potential or by using a large enough system, thus allowing the direct calculation of $\bar{P}_2$, $\bar{P}_4$ etc. Given that the order parameter of the j^{th} configuration is $\bar{P}_L^{(j)}$, the average order parameter over M configurations is simply:-

$$\bar{P}_L = \frac{1}{M} \sum_{j=1}^{M} \bar{P}_L^{(j)} \qquad 2.20$$

However, in the situation where the director does fluctuate, complications arise and only $\bar{P}_2$ can be calculated with relative ease. Now the director orientation is unknown and will in general vary from configuration to configuration. Working in a cartesian coordinate system, a tensor can be defined (Buckingham, 1967 ; de Gennes, 1969; Vieillard-Baron, 1974) known as 'the Q-tensor' as:-

$$Q_{ab} = \frac{1}{N} \sum_{i=1}^{N} (3\overline{l_a^i l_b^i} - \delta_{ab})/2 \qquad 2.21$$

where a and b denote the x, y and z laboratory axes, N is the number of particles in the system, and δ_{ab} is the kronecker delta which is zero unless a and b are equal, when it equals one. Thus the Q-tensor of a particular configuration is:-

$$Q = \frac{3}{2N} \sum_{i=1}^{N} \begin{bmatrix} \sin^2\beta\cos^2\alpha - \frac{1}{3} & \sin^2\beta\cos\alpha\sin\alpha & \sin\beta\cos\beta\cos\alpha \\ \sin^2\beta\cos\alpha\sin\alpha & \sin^2\beta\sin^2\alpha - \frac{1}{3} & \sin\beta\cos\beta\sin\beta \\ \sin\beta\cos\beta\cos\alpha & \sin\beta\cos\beta\sin\alpha & \cos^2\beta - \frac{1}{3} \end{bmatrix} \qquad 2.22$$

In the special case that the director axis is parallel with a laboratory axis, the off diagonal elements vanish. However, generally this will not be the case, although it can be achieved by diagonalising the matrix, which for a real, symmetric matrix of this order is relatively simple. This process corresponds to rotating the laboratory frame of reference to coincide with the director frame. With this definition of Q, the largest resulting eigenvalue is simply the second rank order parameter of the j^{th} configuration, $\bar{P}_2^{(j)}$ and its corresponding eigenvector is the orientation of the director in the laboratory frame of reference. The other two eigenvalues provide a check for the uniaxiality of the system, as in this case they should both equal - 1/2 the value of $\bar{P}_2$. In principle the Q-tensor should be set up and diagonalised for each new configuration generated. However, this is rather wasteful of computer time as the director will not change orientation significantly from one configuration to the next, and so two strategies can be adopted. Firstly the Q-tensor can be set up at longer intervals, now after a number of configurations, a reasonable number being after each cycle, where a cycle is defined as being N attempted moves in the Monte Carlo chain. The tensor is then diagonalised and the overall average order parameter is just the average of the order parameters evaluated at the end of each cycle. A second, alternative method is to average the Q-tensor over a number of configurations during which time the director is assumed not fluctuate. This later technique, although giving statistically better results has to be used with caution, as even a slight director fluctuation during the averaging process will give a misleading small order parameter. The final order parameter is then the average of the order parameters obtained from the averaged Q-tensor. Throughout parts of this thesis both techniques are used, and in most

cases give identical results (see Chapter 4).

In principle higher ranked order parameters can be evaluated using a similar process and tensors of higher order. However, the diagonalisation of these large tensors is computationally expensive, and higher ranked order parameters are easily calculated by other methods. One obvious method is after diagonalisation of the Q-tensor to transform all the the orientations of the molecules to the director frame, however, for large systems this becomes time consuming. An easier route is via the pair distribution functions.

As we saw in Chapter 1, the pair distribution function is perhaps the most important orientational property available, being defined as:-

$$G_L(r_{12}) = \overline{P_L(\cos\beta_{12})r_{12}} \qquad 2.23$$

since they provide a route not only to the short range order parameters σ_L, but in their long range limit, they tend to the square of the corresponding long range order parameter. For example:-

$$\lim_{r_{12}\to\infty} G_4(r_{12}) = \bar{P}_4^2 \qquad 2.24$$

The short range order parameter, σ_2 allows an alternative means of the calculation of the internal energy for the Lebwold-Lasher model (Zannoni, 1979) since:-

$$\bar{U}/\epsilon = -\frac{z}{2}\sigma_2 \qquad 2.25$$

where z is the lattice coordination number. Furthermore, the pair correlation functions provide a direct test of the molecular field approximation as will be discussed in detail in Chapter 3.

On a lattice the calculation of $G_L(r)$ is relatively

simple, since all the intermolecular separations are known. Therefore in order to calculate a particular pair correlation function, the cosines of angles between all pairs of molecules only have to evaluated, normally at the end of each cycle. In doing so however, only pairs of molecules with intermolecular separations less than half the cell dimension must be considered, as periodic boundary conditions will cause correlations to be counted twice at distances greater than this cut off. The extrapolation to long range must therefore be taken with caution, since only correlations up to the cut off are calculated. However, throughout this thesis it will be seen that the limiting value is reached long before the cut off, thus permitting the valid calculation of long range parameters from the long range limits.

In computer simulations the estimation of errors is of extreme importance. Clearly, properties can be recalculated at each new configuration generated by the Monte-Carlo chain thus providing very accurate averages. However, in general, the individual values forming the averages will be correlated with each other, thus any attempt to estimate the standard deviation will prove inaccurate. To overcome this problem, the simulations are normally broken up into steps (sometimes called 'macrosteps') over which time averages are calculated. The total average of the property is then the average of all the steps, and now assuming the sub averages to be uncorrelated, standard deviations can be evaluated. The length of each step determines whether they are uncorrelated or not. Clearly they should be as long as possible, yet throughout the entire simulation there should be sufficient to provide a reasonable estimate of the standard deviation. Generally, the number calculated represents a compromise between these two factors. Throughout this work, the averages presented (when they given error estimates) represent a break down of the total run into anything between 20 and 100 subaverages, each of anything up to 500 cycles.

Chapter 3

The Lebwohl-Lasher model and the molecular field approximation

3.1 Introduction

One of the earliest and most significant simulations of anisotropic systems was that performed by Lebwohl and Lasher (1972). This important set of calculations involved the isolation of a first order transition between an orientationally ordered and disordered phase, as observed in the nematic-isotropic phase transition, using a relatively simple model. The model consisted of cylindrically symmetric particles, representing molecules restricted to the sites of a simple cubic lattice and interacting via the simple anisotropic potential:-

$$U_{ij} = - \epsilon_{ij} P_2(\cos\beta_{ij}). \qquad 3.1$$

Here ϵ_{ij} is a positive constant which equals ϵ if molecules i and j are nearest neighbours but is zero otherwise, and β_{ij} is the angle between the symmetry axes of molecules i and j. The transition was later studied in slightly more detail by Jansen, Vertogen and Ypma (1977) and Zannoni (1979) again by the Monte-Carlo technique (see Chapter 2) and also by the method of molecular dynamics (Zannoni and Guerra, 1981). However, all of these simulations were restrictive, either by using a relatively small number of molecules (eg 10^3) which has tended to show continuous properties throughout the transition, or by studying a range of temperatures very uncharacteristic of nematogens. For example, Zannoni (1979) studied the model using 10^3 particles at temperatures as low as $T/T_{NI} = 0.46$. Therefore one of the aims of this Chapter is to investigate the nematic-isotropic phase transition in the temperature region, close to the transition, characteristic of real

nematogens, i.e. from $T/T_{NI} = 0.9$ to $T/T_{NI} = 1.1$ and to study a larger system of 20^3 particles with the aim of improving the sharpness of the transition.

The Lebwohl-Lasher model has also been studied for a system of 50^3 particles using the stochastic models technique (Meirovitch, 1977), a method of unproven reliability, at least in the simulation of anisotropic systems. A comparison of this model with other work will be made later.

In addition, a detailed knowledge of the temperature dependence of the second rank order parameter and other properties in the Lebwohl-Lasher model close to the nematic-isotropic phase transition provides a comprehensive test of analytic theories.

One of the most successful analytic theories describing the properties of the nematic-isotropic phase transition was proposed by Maier and Saupe (1958, 1959, 1960), the details of which are discussed in Chapter 1. The major approximations used in this theory are the molecular field approximation which is employed to simplify greatly the orientational distribution function, and the description of the anisotropic pair potential, which for true nematogens would be extremely complex. The latter approximation invalidates any unambiguous comparison with real experimental data, so to test the approximations in the theory we have to resort to computer simulation studies. The Lebwohl-Lasher model has the immediate advantage in that the simple potential used (equation 3.1) is consistent with that employed in the Maier-Saupe theory, although it has been shown that other pair potentials, for example a pair potential which depends on the orientation of the intermolecular vector, also yields the same single particle pseudo potential as that used in the Maier-Saupe theory. (Humphries et al., 1981). Indeed, it is for this type of potential that Maier and Saupe based their original derivation.

There are however, two important features of the Lebwohl-Lasher model that have not been studied to test the validity of the molecular field approximation, that of lattice coordination number, and the effect of increasing the range of the interaction potential, each of which is very important in their own right, since in the limit that all particles interact equally with all others the molecular field approximation becomes exact. The second aim therefore of this Chapter is to investigate the effect of increasing the lattice coordination number, the effect of increasing the range of the pair potential and finally to combine these two features and compare all the results for these systems with the predictions of the Maier-Saupe theory.

3.2 The models

The four models, labelled I to IV, used in the simulations are now described in detail.

Model I

This model is exactly identical to the Lebwohl-Lasher model but using a larger system of 20^3 particles on the sites of a simple cubic lattice and interacting via the nearest neighbour pair potential defined in equation 3.1.

Model II

This differs from Model I in that the particles now lie at the sites of a face centred cubic lattice (see Appendix 4), thus doubling the coordination number, z, from 6 to 12.

Model III

This model investigates the second effect, that of increasing the range of the potential. The coordination number in the first shell was kept at 6 (i.e. a simple cubic lattice), but each molecular interaction extended

to the next two shells of molecules. Thus there were 6 pair interactions arising from shell 1, 12 from shell 2 and 8 from shell 3. (See Appendix 4). As with anisotropic dispersion forces, it is assumed that the strength of interaction diminishes as r_{ij}^{-6}, the anisotropic pair potential is then:-

$$U_{ij} = - \epsilon(r_{ij}^{*})^{-6} P_2(\cos\beta_{ij}) \qquad 3.2$$

where r_{ij}^{*} is the scaled separation, r_{ij}/a, where a is the nearest neighbour separation.

Model IV

Model IV combines the two important features of Models II and III. The particles are confined to the sites of a face centred cubic lattice and the range of the potential extended to the next 12 interaction shells (see Appendix 4). This corresponds to all pair interactions at separations less than half the cell edge length. The anisotropic potential used was as defined in equation 3.2 although in this case, the nearest neighbour separation, a, is actually the lattice spacing divided by $2^{1/2}$.

The outline of the remainder of this Chapter is as follows. In the next section explicit computational details are given for all four models followed by section 3.4 which discusses the results. Next the results from Model 1 are compared with other simulations using the Lebwohl-Lasher model (section 3.5) and the results of all four models are used to test the predictions of the Maier-Saupe theory in section 3.6. Section 3.7 compares the results with a theory based on a two site cluster expansion and in 3.8 the results from Model 1 are compared tentatively with experimental results. Finally in section 3.9 an important feature observed in Model I is discussed, that of director pinning.

3.3 Computational details

For each of the four models the Monte-Carlo method proposed by Metropolis *et al.* (1953) was used (see Chapter 2). Model I consisted of a system of 20^3 particles although for Models II, III and IV, fewer were employed because of restricted computational resources. For Models II and IV involving face centred cubic lattices, 864 ($=4\times6^3$) and 500 ($=4\times5^3$) particles respectively were used and for the simple cubic lattice in Model III, the system consisted of 10^3 particles.

The orientations of particles in Models I, II and III were stored using the azimuthal angle, α, and the polar angle β, via $\cos\beta$. A new configuration was created by generating a random number uniformly in the range of 0 to +1 for Model I and -1 to +1 for Model II and III, and identifying this with $\cos\beta$, thus:-

$$(\cos\beta)_{new} = \xi \qquad 3.3$$

and for the azimuthal angle:-

$$\alpha_{new} = \alpha_{old} + \Delta\xi. \qquad 3.4$$

Here ξ is a random number generated in the range 0 to +1 and Δ is the allowed maximum displacement. In general $\cos\beta$ should always be chosen in the full range of -1 to +1, but in this case, the potential is independent of the sign of $\cos\beta$ and so in this instance is unimportant. In Model I, it was observed that the acceptance-rejection ratio was almost totally insensitive to the magnitude of Δ, because of the effect of pinning of the director (see section 3.9 and Chapter 5). However, within the temperature range studied, the ratio was still acceptable, varying from about 0.5 at $T^*=1.0$ to approximately 2.3 at $T^*=1.3$. (Here T^* is the reduced temperature defined as:-

$$T^* = kT/\epsilon \qquad 3.5$$

where k is the Boltzmann constant, and ϵ the strength parameter used in equation 3.1). In Model IV the molecular orientations were stored as unit vectors whose components in the laboratory frame were changed using the method outlined by Barker and Watts (1969) (see Chapter 2).

The initial configuration in the simulation with Model I was created by selecting the azimuthal angle, β, randomly in the range 0 to 2π, and the polar angle, β, in the range 0 to $\pi/2$. As a consequence this gives a partially ordered system with $\bar{P}_2$ approximately 0.25 and the director parallel with the laboratory z axis. The model was studied over a total of 14 temperatures ranging from T^*=1.000 to T^*=1.282. For the first temperature, at T^*=1.000, equilibration and production stages of 12 and 8 million moves respectively were performed, with subsequent calculations at higher temperatures using the final configuration of the preceeding lower temperature simulation as a starting point. For these calculations typical equilibration and production stages of 5 and 10 million moves respectively were used.

For models II, III and IV, the starting configuration was taken to be a perfectly ordered system with the molecular axes parallel with the laboratory z direction with calculations at higher temperatures started from the last configuration of the production run at the proceeding temperature. The equilibration and production runs for Model II were typically 3 and 6 million configurations respectively, although slightly less for Models III and IV, with between 1 and 2 million moves for equilibration and about 3 million for production in Model III and about 1 million for production in Model IV.

For all models the average potential energy per particle, U^* (= $\bar{U}/N\epsilon$) was evaluated as a function of the

reduced temperature taking into account all the interactions as described in the model definitions in section 3.2. The heat capacity at constant volume with respect to T^* was also calculated, by numerical differentiation of the temperature dependence of $\bar{U}^*$, since

$$C_v^* = (\partial \bar{U}^*/\partial T^*)_v \qquad 3.6$$

Furthermore, C_v^* was also calculated from the fluctuations in the internal energy for Model IV,:-

$$C_v^* = (\overline{U^{*2}} - \bar{U}^{*2})/T^{*2} \qquad 3.7$$

Since in Model I, it was observed that the director orientation remained fixed parallel to the laboratory z axis throughout the duration of the simulation, the second rank orientational order parameter, $\bar{P}_2^j$ of the j^{th} configuration was calculated directly as:-

$$\bar{P}_2^j = \frac{1}{N} \sum_{i=1}^{N} 3/2 \cos^2\beta_i - 1/2 \qquad 3.8$$

Here β_i is the angle describing the orienatation of the i^{th} molecule in the laboratory frame. In practice $\bar{P}_2^j$ was evaluated at the end of each cycle and then averaged over M cycles to give $\bar{P}_2$, i.e.

$$\bar{P}_2 = \frac{1}{M} \sum_{i=1}^{M} \bar{P}_2^j \qquad 3.9$$

However for Models II to IV, the director orientation was observed to fluctuate, and so a different procedure had to be adopted. The Q-tensor was set up and diagonalised at the end of each cycle, and the largest eigenvalue, $\bar{P}_2$ averaged over all cycles, where the tensor is defined as:-

$$Q_{ab} = (\overline{3l_a l_b} - \delta_{ab})/2 \qquad 3.10$$

In Model IV, the pair correlation functions $G_2(r_{ij}^*)$ and $G_4(r_{ij}^*)$ were also calculated, although not at every temperature, over stages during the production runs. They were evaluated again at the end of each cycle and averaged over a total of 500 cycles, $\bar{P}_2$ was also calculated at the same stage to enable a more meaningful comparison with molecular field theory.

The errors in the quantities $\bar{P}_2$, $\bar{U}^*$ and C_V^* (for Model IV) were estimated by dividing the production stage into typically 10 macrosteps from which the total average and standard deviations were calculated.

3.4 Results

The results for the internal energy, $\bar{U}^*$, heat capacity at constant volume, C_V^* and the second rank order parameter, $\bar{P}_2$ are shown as functions of the reduced temperature, T^* in Figures 3.1, 3.2 and 3.3 respectively for all four models, as the solid squares.

The internal energy, in Figure 3.1, is essentially a continuous function of temperature suggesting that either the entropy of transition is small, or more probably, especially for Models II, III, IV finite size effects are occuring which tend to smooth out the transition. However, before the entropy change can be measured, the exact location of the transition temperatures must be determined. This is readily obtained from the heat capacity in Figure 3.2 where in all cases a divergence in C_V^* is observed. This can be associated with a transition from an orientationly ordered phase to one of disorder (see Figure 3.3), i.e. the nematic-isotropic phase transition. The exact location of the transition can be regarded as being midway between temperature on either side of the divergence. This gives transition temperatures, T_{NI}^* as listed in Table 3.1 for the four models. The assignment of the order of the transitions is not easy to evaluate, since the plots of the heat capacity are all consistent with first or higher order

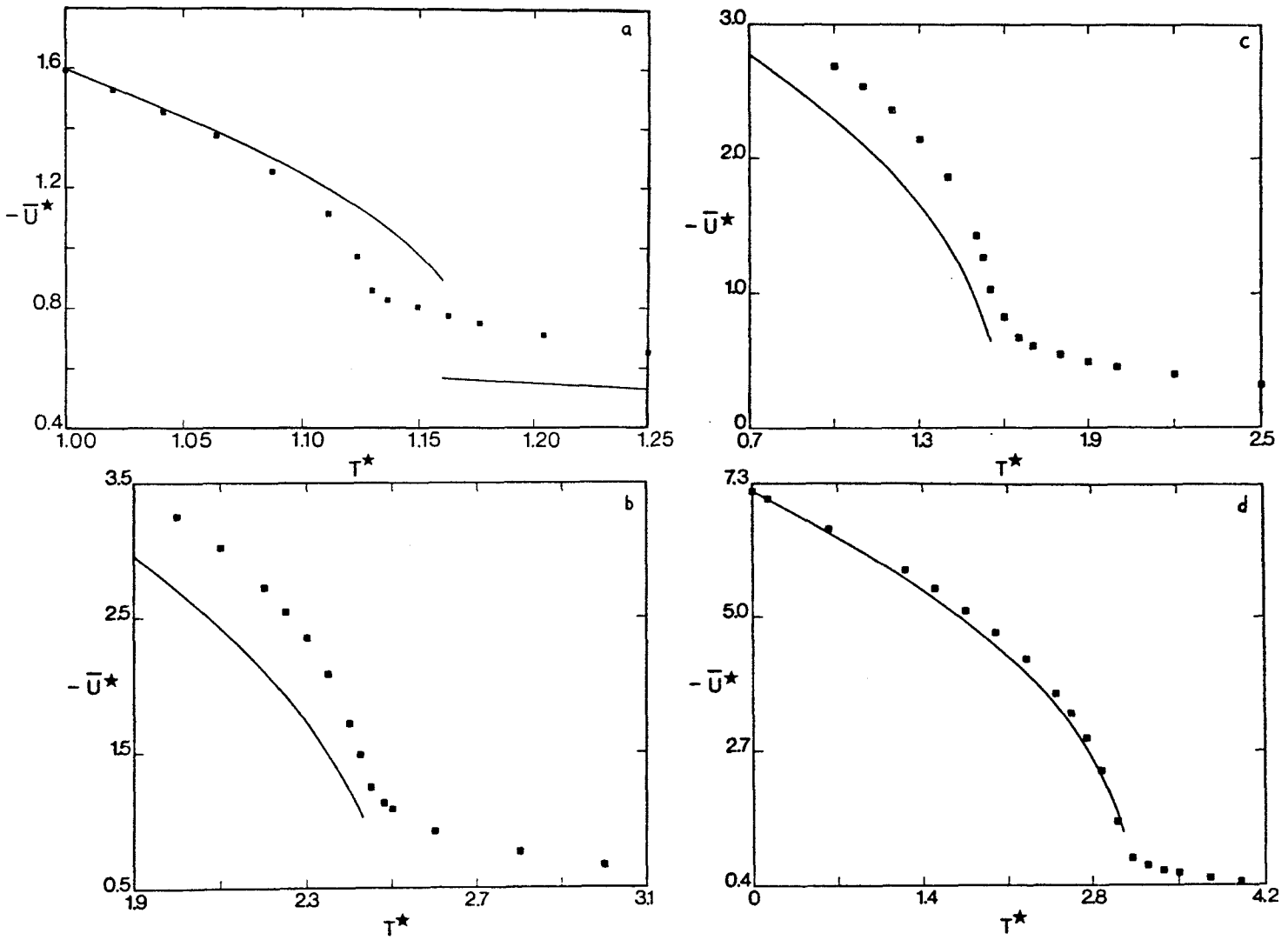

Fig 3.1 The scaled temperature dependence of the internal energy per particle for models I (a), II (b), III (c) and IV (d). The solid curves in b), c) and d) are the predictions of the Maier-Saupe theory scaled to the same transition temperatures, while in a) the solid curve is the prediction of the two site cluster expansion.

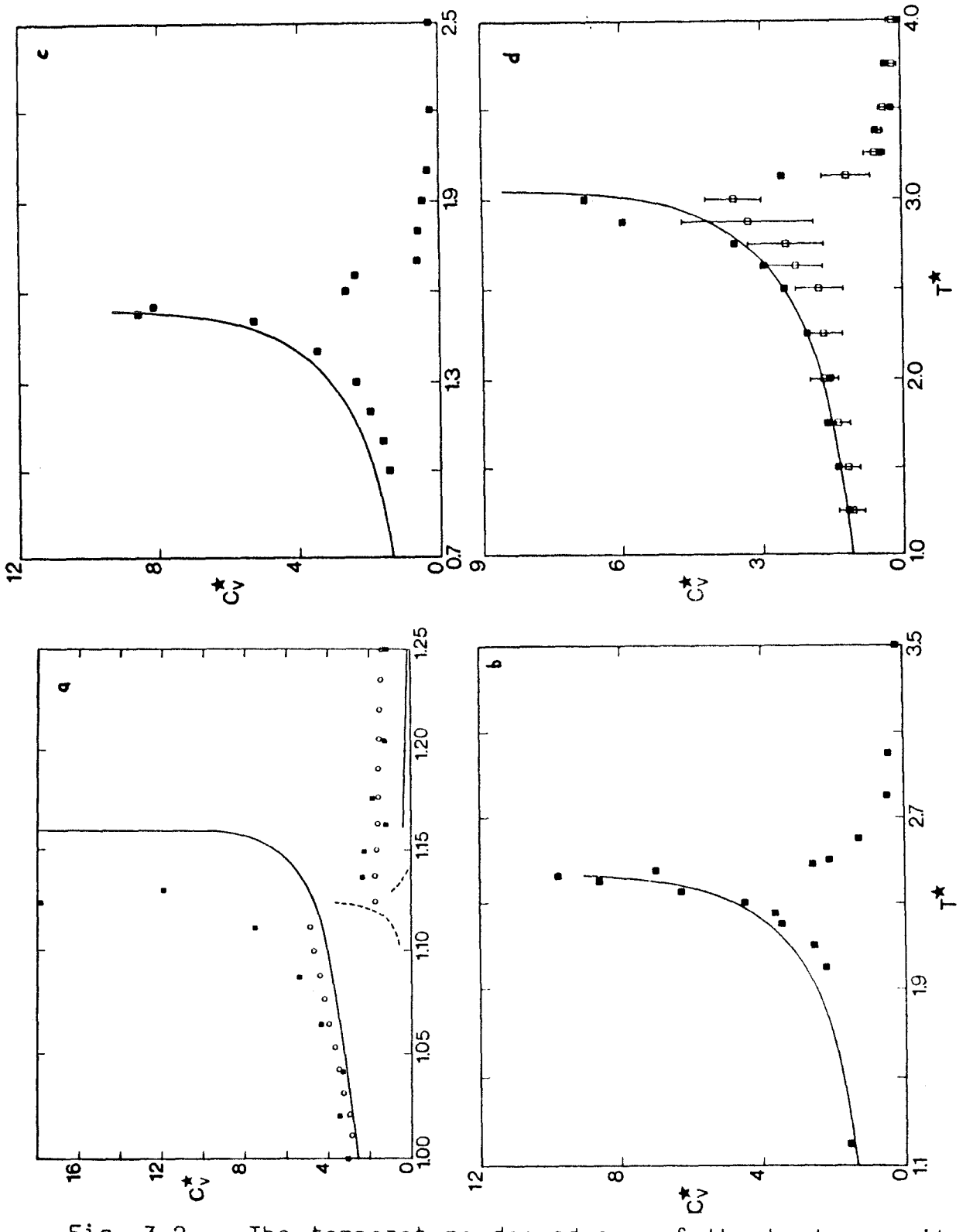

Fig 3.2 The temperature dependence of the heat capacity at constant volume per particle for Models I, II, III and IV. (Diagrams a, b, c and d respectively). The solid squares are results obtained from the gradient of the internal energy while the open squares are results derived from energy fluctuations (d). The molecular field theory predictions are shown by the solid curves scaled to the same transition temperatures in plots b), c) and d), while in a) the solid curve is the prediction of the two site cluster expansion. In a) the dashed curve is C_V measured for PAA and the open circles are results obtained by Jansen et al (1977).

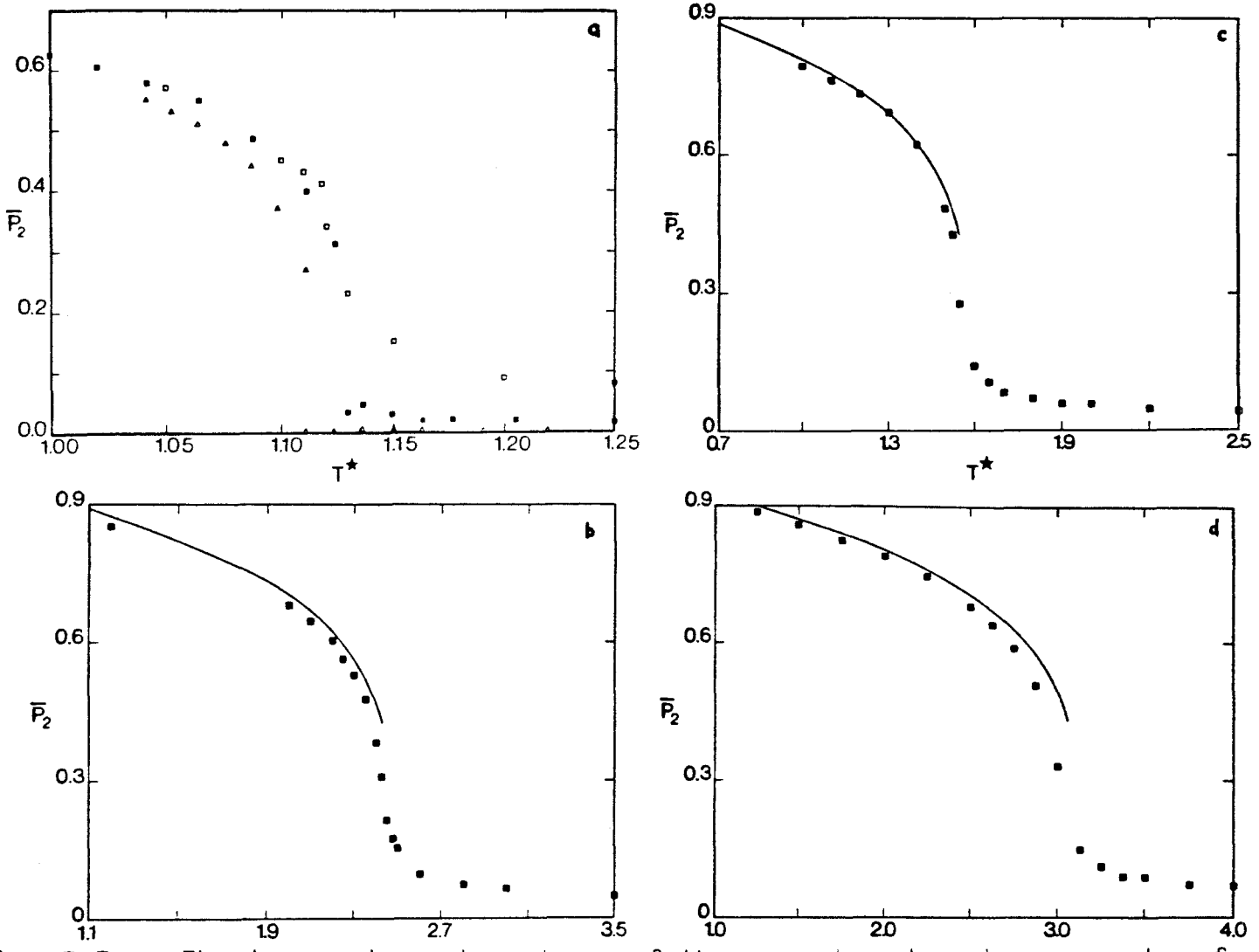

Fig 3.3 The temperature dependence of the second rank order parameter for Models I to IV (a to d respectively). The solid curves in b), c) and d) are the molecular field predictions scaled to the same transition temperatures. The open squares in a) are results obtained by Zannoni (1979) and the open triangles are data calculated by Meirovitch (1977).

transitions. However, extrapolation of $\bar{U}^*$ at T_{NI}^* from both the nematic and isotropic phases indicates a small but nonetheless non-zero change in $\bar{U}^*$, suggesting the occurance of first order phase transitions. From this finite change in $\bar{U}^*$ at the transition, the entropy of transition $\Delta S/R$ can be calculated and is also listed in Table 3.1 for all four Models. The relatively large errors in $\Delta S/R$ arise from the difficult extrapolation of the internal energy from the ordered and disordered phases and indeed could be larger, since the uncertainties in the transition temperatures have not been taken into account. In Model IV the heat capacity was also calculated from the fluctuations in the internal energy, as defined by equation 3.7, and these results are shown as the open squares on the fourth diagram in Figure 3.2. To within experimental error, both sets of results agree and diverge at the same transition temperature. This observation is comforting since it does provide a check to the two methods of calculation of C_V^* although C_v^* calculated by spline fitting the internal energy is probably more reliable than that evaluated from the energy fluctuations, since the latter method requires efficient sampling of states of both high and low energy.

The order parameter, $\bar{P}_2$ plotted in Figure 3.3 as a function of T^* is again essentially continuous throughout the temperature ranges studied, although it changes most rapidly in the temperature region where the heat capacity diverges. However, in the isotropic phase it does not equal zero especially in Models II, III and IV, presumably because of the relatively small numbers of particles employed. A knowledge of T_{NI}^* allows $\bar{P}_2$ to be found at the transition by a careful extrapolation and again is listed in Table 3.1.

Finally, we look briefly at the orientational correlation functions, $G_2(r_{ij}^*)$ and $G_4(r_{ij}^*)$ plotted in Figure 3.4 for Model IV. The relevance of the form of the plots will be discussed in more detail later when a comparison with molecular field theory will be made.

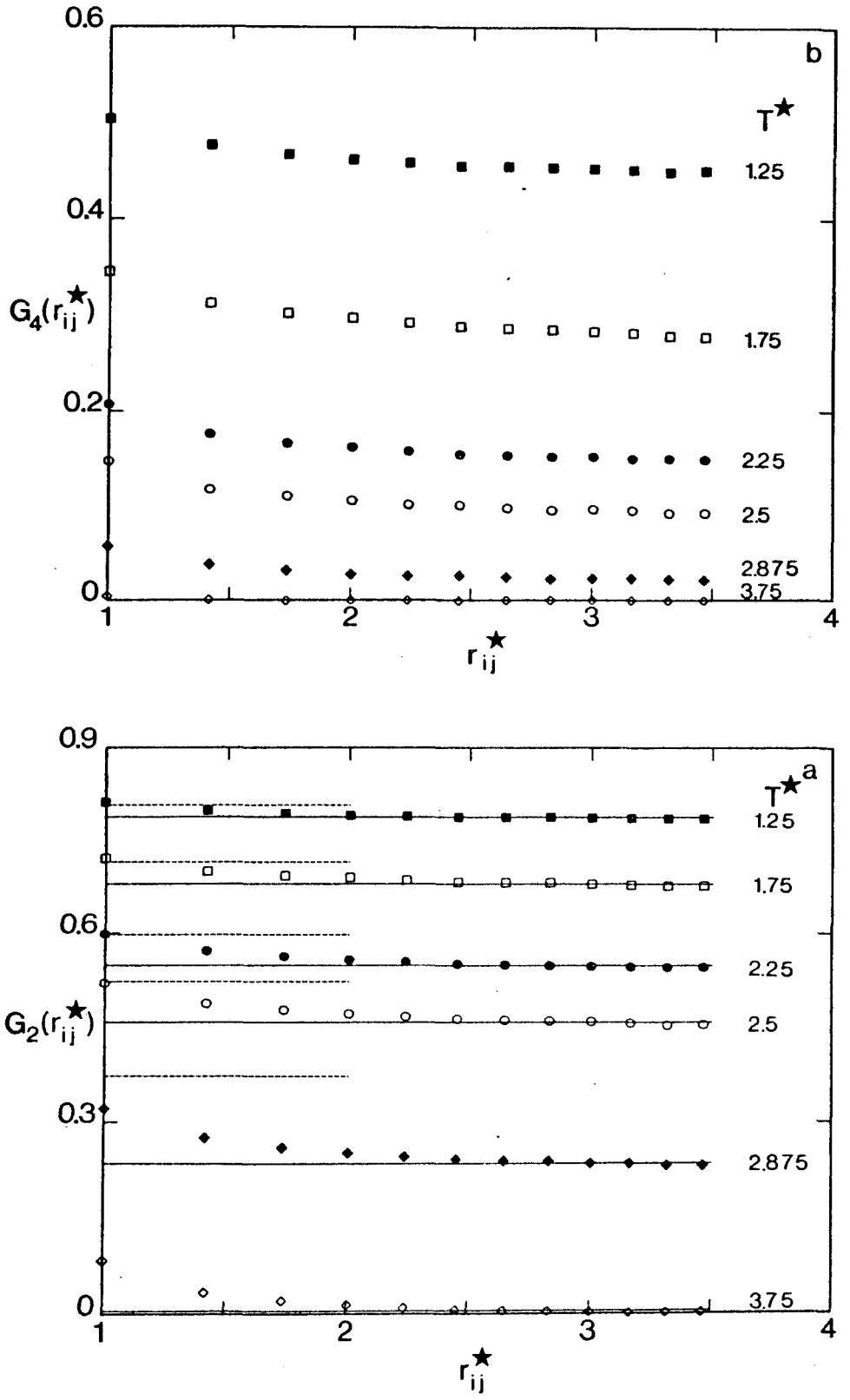

Fig 3.4 The distance dependence of the second (a) and fourth rank (b) orientation pair correlation functions calculated in Model IV. The solid lines in a) are the large separation limits while the Maier-Saupe predictions at the same reduced temperature are given by the dashed lines.

However, the consistency of $G_2(r_{ij}^*)$ with the internal energy can be demonstrated at this stage since (Zannoni, 1979):-

$$\bar{U} = -1/2 \sum_n z_n (r_n^*)^{-6} G_2(r_n^*), \qquad 3.11$$

where z_n is the number of molecules in the n^{th} coordination shell (see Appendix 4) at a scaled distance of r_n^* from a central particle. The values of $\bar{U}^*$ evaluated from the observed $G_2(r)$ with the summation truncated at the same point as the pair potential in the simulation are compared with $\bar{U}^*$ calculated directly during the simulation in Table 3.2, and there is excellent agreement. A further check on the calculation of $G_2(r_{ij}^*)$ and $G_4(r_{ij}^*)$ can be made by comparing the long range limiting values with the corresponding ranked order parameter, since in the limit of large separations the orientational correlations between molecules are lost and $G_L(r)$ tends to $\bar{P}_L^2$. Thus the limit of $G_2(r_{ij}^*)$ can be checked against $\bar{P}_2$ evaluated during the simulation, in particular against $\bar{P}_2$ calculated over the same 500 cycles in the production run. This value of $\bar{P}_2^2$ is plotted as the solid line in Figure 3.4a and indeed does show excellent agreement with the long range limiting values of $G_2(r_{ij}^*)$. Therefore we can expect to be able to adopt this method to calculate $\bar{P}_4$ from $G_4(r_{ij}^*)$, the values of which are listed in Table 3.2.

3.5 Comparison with other simulations

The comparison of the results is only made with Model I, since virtually all similar work has employed this model. Firstly the comparison of the transitional properties of T_{NI}^*, $\bar{P}_2^{NI}$ and $\Delta S/R$. These are given in Table 3.1 where it can be seen that the transition for Model I of $T_{NI}^* = 1.127 \pm 0.003$ is comparible with that of 1.124 ± 0.006 found by Lebwohl and Lasher (1972, 1973) although greater than $T_{NI}^* = 1.119 \pm 0.001$ obtained by Jansen, Vertogen and Ypma (1977)

and T^*_{NI} = 1.111±0.004 found by Meirovitch (1977). The reason for this discrepency is not clear, although in the latter case it could stem from the use of the stochastic models technique of simulation. However, for the order parameter at the transition the agreement is reversed with poor accordance between the results of Lebwohl and Lasher and the results of Model I. To within the experimental error, the values of $\Delta S/R$ agree, all being very small.

The temperature dependence of the heat capcity observed by Jansen et al. is shown in Figure 3.2 as the open circles and clearly their results show a small discontinuity at the transition typical of a second order transition rather than a divergence as shown by the solid squares. The difference is again unaccountable, especially in view of the apparent consistency with the methods of calculation of C_v^* both by numerical differentiation and from the fluctuations, observed in Model IV.

Finally the comparison with $\bar{P}_2$ is made. Unfortunately the temperature dependence of $\bar{P}_2$ is not accurately available from the work by Lebwohl and Lasher although it is known from the work of Zannoni (1979) for a system of 10^3 particles. These results, together with the findings by Meirovitch are shown in Figure 3.3a as the open squares and open triangles respectively. In the nematic phase very good agreement with the results obtained by Zannoni is observed although in the isotropic phase better agreement is found with the results of Meirovitch. This difference can be attributed to the relatively small system studied by Zannoni of 10^3 particles compared with 20^3 used in Model I. Furthermore, the discrepency with Meirovitch's results in the nematic phase can be accounted for by the difference in the observed transition temperature, since if the temperatures were reduced to give the same transition, then virtually perfect agreement would be obtained.

3.6 Comparison with molecular field theory

One of the most successful theories describing the orientational properties of nematogens was developed by Maier and Saupe (1958, 1959, 1960). The anisotropic pair potential used in their theory is consistent with those used in this Chapter, thus allowing various elements of the theory to be tested by computer simulation, in particular the molecular field or single site cluster approximation. The predictions of this theory have been discussed in relative detail in Chapter 1, although the transitional properties are given again in Table 3.1. To compare the theory with Models I to IV, the interaction strength parameter $\bar{u}_2$ in the pseudo potential must be modified slightly to account for the variations in the range and number of interactions used in the simulation. Thus, as we have seen in Chapter 1, the pseudo-potential in the Maier-Saupe theory can be written as:-

$$U(\beta) = - \bar{u}_2 \bar{P}_2 P_2(\cos\beta), \qquad 3.12$$

where β is the angle between the molecular symmetry axis and the director. The molecular field strength parameter, $\bar{u}_2$ is defined by:-

$$\bar{u}_2 = \rho \int_0^\infty u_2(r_{ij}) g(r_{ij}) 4\pi r_{ij}^2 dr_{ij}. \qquad 3.13$$

Here ρ is the number density, $g(r_{ij})$ is the radial distribution function and $u_2(r_{ij})$ gives the distance dependence of the anisotropic pair potential. For a lattice system, this equation reduces to:-

$$\bar{u}_2 = \varepsilon \sum_n z_n (r_n^*)^{-6} \qquad 3.14$$

So for the models used in this Chapter $\bar{u}_2^*$ is 6, 12, 7.796 and 14.31 for Models I, II, III and IV respectively, where

$\bar{u}^*_2$ is $\bar{u}_2/\epsilon$. This results in predicted transition temperatures of $T^*=1.321$, $T^*=2.642$, $T^*=1.717$ and $T^*=3.151$ for Models I, II, III and IV thus overestimations of 17%, 5%, 10% and 3% occur. This means that theory progressively improves when either the number of interactions or the potential range increases, and combining both effects gives almost perfect agreement as seen for Model IV. This is in complete accord with our expectations, since in the limit that the range of the potential and the coordination number become infinite the molecular field approximation becomes exact. This trend towards the theoretical predictions of the transition temperature for a particular model can be seen in the ratio $T^*_{NI}/\bar{u}^*_2$, which for Models I, II, III and IV is 0.1878 ± 0.0005, 0.203 ± 0.003, 0.198 ± 0.003, 0.214 ± 0.003 and for molecular field theory is predicted to be 0.2202. Thus an almost linear improvement in $T^*_{NI}/\bar{u}_2$ with $\bar{u}^*_2$ is observed, these figures are also listed in Table 3.1.

Although a gradual improvement in the predictions of the transition temperature is observed on increasing the potential range and coordination, the value of the second rank order parameter at the transition and the entropy of transition are virtually constant for all four Models (see Table 3.1). Clearly the molecular field approximation grossly overestimates the entropy by almost an order of magnitude, and although the errors in the simulated values of $\Delta S/R$ are relatively large, they cannot absorb the theoretical overestimation. For all four models the order parameter at the transition is less than the predicted value of $\bar{P}_2=0.417$. Surprisingly worse agreement with the molecular field value is seen in Model IV, although this is probably related to the relatively small system size of only 500 particles used in this case.

It would appear therefore that the Maier-Saupe predictions of the nematic-isotropic transition temperature improve with both increased coordination number and potential range although the improvement in the predictions

of both $\bar{P}_2^{NI}$ and $\Delta S/R$ is poor. To understand why these properties are poorly estimated by theory we must turn our attention to the angular correlation functions.

The molecular field approximation predicts the angular pair correlation functions to be independent of separation and equal to the order parameters of corresponding rank squared. The results observed for Model IV for $G_2(r^*_{ij})$ (c.f. figure 3.4) do indeed show that these two predictions are true, but only for separations greater than scaled distances of about $r^*_{ij}=3$. For shorter separations the angular correlations increase with decreasing r^*_{ij}. Thus $\bar{P}_2$ taken from the simulation as shown by the solid lines in Figure 3.4 does coincide with the limiting values as we have already discussed. We know that the Maier-Saupe theory overestimates $\bar{P}_2$ both at the transition temperature and at lower reduced temperatures, thus it must also overpredict $G_2(r^*_{ij})$, this is shown by the dashed lines in Figure 3.4a which are calculated at the same reduced temperature. Indeed much better agreement between the theory and the simulation is found at short separations, especially at low temperatures where the values of $G_2(1)$ and the theoretical value agree almost exactly. This is caused by a fortuitious cancellation of errors, that of the molecular field theory underestimating the short range correlations, being compensated for by the overestimation of the long range order parameter. This cancellation of error, has some important consequences, as we shall see later when we compare the predictions of the internal energy with the simulation. Furthermore, in the isotropic phase, molecular field theory says that all short range correlations should vanish, which as we can see for the plot of $T^*=3.75$ in Figure 3.4a is untrue. Thus, the failure of the theory to predict the short range order present in the isotropic phase means that the entropy of transition will be overestimated, which is indeed the case.

The second rank angular pair correlations have also been evaluated by Zannoni (1979) for a system of 10^3 particles on a cubic lattice. In this case a much greater difference between the long and short range correlations was observed. To quantify this difference we define a excess second rank correlation:-

$$\Delta\sigma_2 = \sigma_2 - \bar{P}_2^2 \qquad 3.15$$

where σ_2 is the short range angular correlation $G_2(1)$, or the short range order parameter, and P_2 is that calculated from the square of the limiting value. In the molecular field limit $\Delta\sigma_2$ will equal zero since here, correlations are independent of separation. Figure 3.5 shows how $\Delta\sigma_2$ varies with the reduced temperature for Model IV as indicated by the solid squares, and for the system studied by Zannoni (solid diamonds). It is also possible to calculate $\Delta\sigma_2$ for Models I and II, since in these systems only nearest neighbour interactions are involved and therefore the short range order parameter is proportional to the internal energy, since:-

$$U^* = -z\sigma_2/2, \qquad 3.16$$

where z is the coordination number. The results for Models I and II are shown as the open squares and open circles respectively on Figure 3.5. Clearly the excess correlations are largest at the transition in both isotropic and nematic phases and decrease rapidly on going away from the transition. For Model I, $\Delta\sigma_2$ is discontinuous at the transition, although essentially continuous for the system of 10^3 particles and Models II and IV. Also the excess correlations are greatest for Model I and decrease with systems of increasing interactions and therefore approach the molecular field limit of zero for all temperatures.

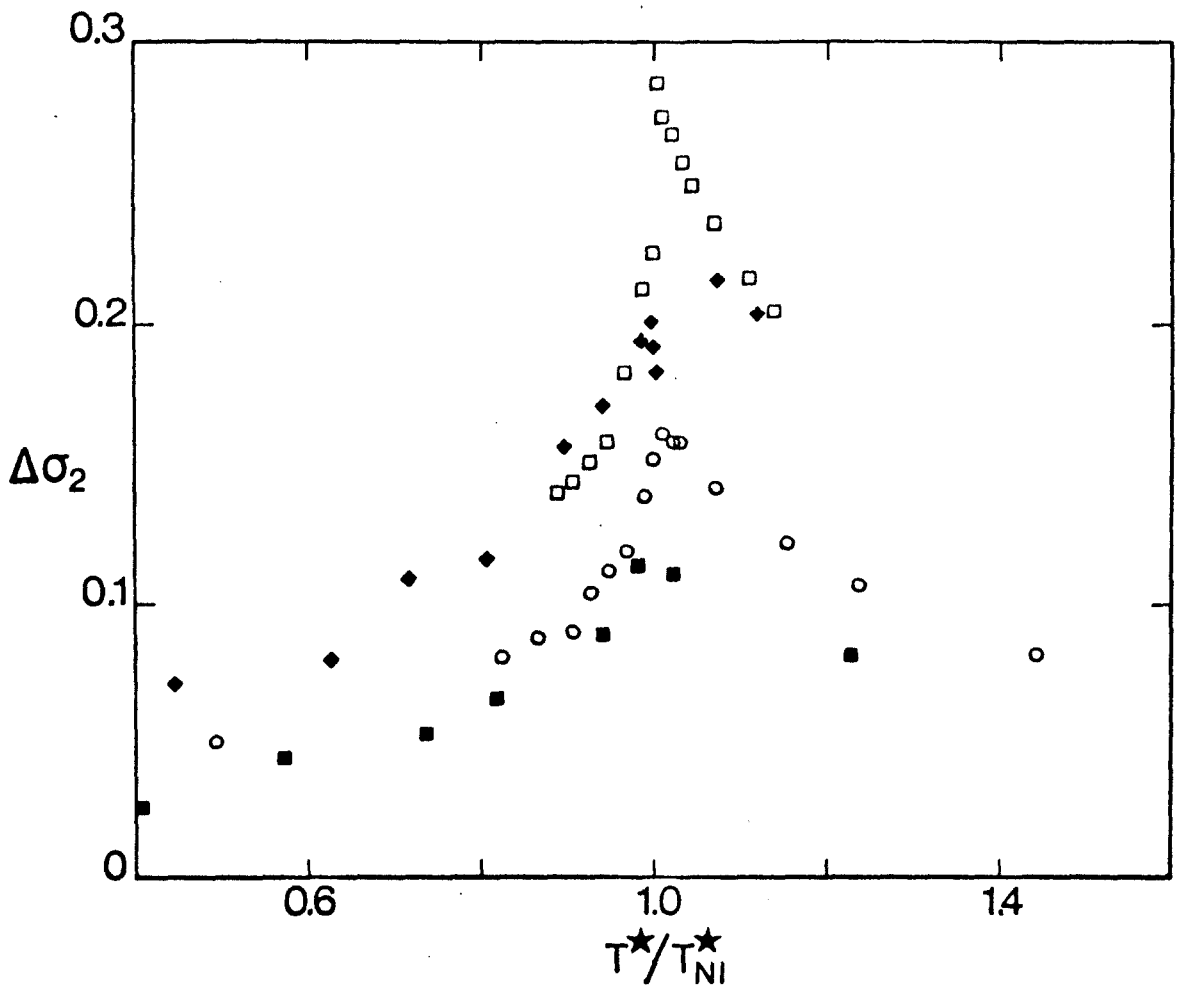

Fig 3.5 The variation of the excess second rank pair correlation function with temperature for Model I (the open squares), Model II (the open circles) and Model IV (solid squares). The results obtained by Zannoni (1979) are given by the solid diamonds.

Finally we compare the theory's predictions of the temperature dependence of the internal energy, heat capacity and second rank order parameter as shown by the solid curves in Figures 3.1, 3.2 and 3.3. (The curves on the diagram representing Model I correspond to predictions of the 2-site cluster approximation, and will be discussed in the next section). To enable a meaningful comparison, $\bar{U}_2$ has been modified such that in all cases the predictions of the molecular field theory transition temperature equals the simulated transition temperature. More will be said of this scaling later. This compensates therefore, for the overestimation of the transition temperature by the theory. Firstly comparing the internal energy in Figure 3.1. The best agreement is observed with Model IV, a direct consequence of the fortuitious cancellation of errors discussed earlier, i.e. that of an underestimation of the short range correlations and an overestimation of the long range order. However, the agreement is not as impressive for Models II and III, where the internal energy by the Maier-Saupe theory is lower than that found in the simulation. Turning to the heat capacity in Figure 3.2 indicates good agreement for Models II, III and IV in the nematic phase, although in the isotropic phase it fails completely where the short range order and its temperature dependence is much larger than the theoretical value of zero. Finally we look at the dependence of the long range order parameters with temperature, firstly with $\bar{P}_2$ as plotted in Figure 3.3. In all three Models (II, III and IV) the theoretical agreement with $\bar{P}_2$ in the nematic phase is very good now that the overestimation of T^*_{NI} has been accounted for. However, the observed values in the isotropic phase are greater than the zero predictions of theory, although this difference can be attributed to the finite sizes of the systems used. The fourth rank long range order parameter can also be calculated from theory (see Chapter 1) and therefore can be compared with $\bar{P}_4$ obtained from the

limiting values of $G_4(r_{ij}^*)$. According to the Maier-Saupe theory, the angular dependence of the pseudo potential is contained in just $P_2(\cos\beta)$. This can therefore be tested since two order parameters are known, for example, given a value of $\bar{P}_2$, the coefficient of $P_2(\cos\beta)$ can be evaluated in the pseudo-potential and then used to calculate $\bar{P}_4$. This comparison is shown in Table 3.2 where the predicted values of $\bar{P}_4$ are in excellent accord with the values obtained from the simulation, thus indicating that the angular dependence of the potential of mean torque or pseudo potential is indeed given correctly by the Maier-Saupe theory.

To complete the comparison with the molecular field theory we shall now return to Model I, which was studied over a temperature range much closer to the transition. Thus, in Figure 3.6 is plotted the variation of $\bar{P}_2$ in the nematic phase with the reduced temperature, T^*/T^*_{NI}. The solid curve represents the Maier-Saupe prediction scaled to the same transition temperature, and over this much reduced temperature range, the agreement is not as good as we have seen previously in the comparison with Models II, III and IV. Here $\bar{P}_2$ is constantly overestimated especially as the transition is approached. The source of this discrepency has already been discussed, i.e. the theory's overestimation of long range correlations. However, another source of error can now be investigated, that concerning the singlet orientational distribution function. In the Maier-Saupe theory this is given by:-

$$f(\beta) = \exp(aP_2(\cos\beta))/\int d\beta \sin\beta \exp(aP_2(\cos\beta)) \qquad 3.17$$

where a is the coefficient of mean torque, which for Model I is:-

$$a = 6\,\bar{P}_2/T^*. \qquad 3.18$$

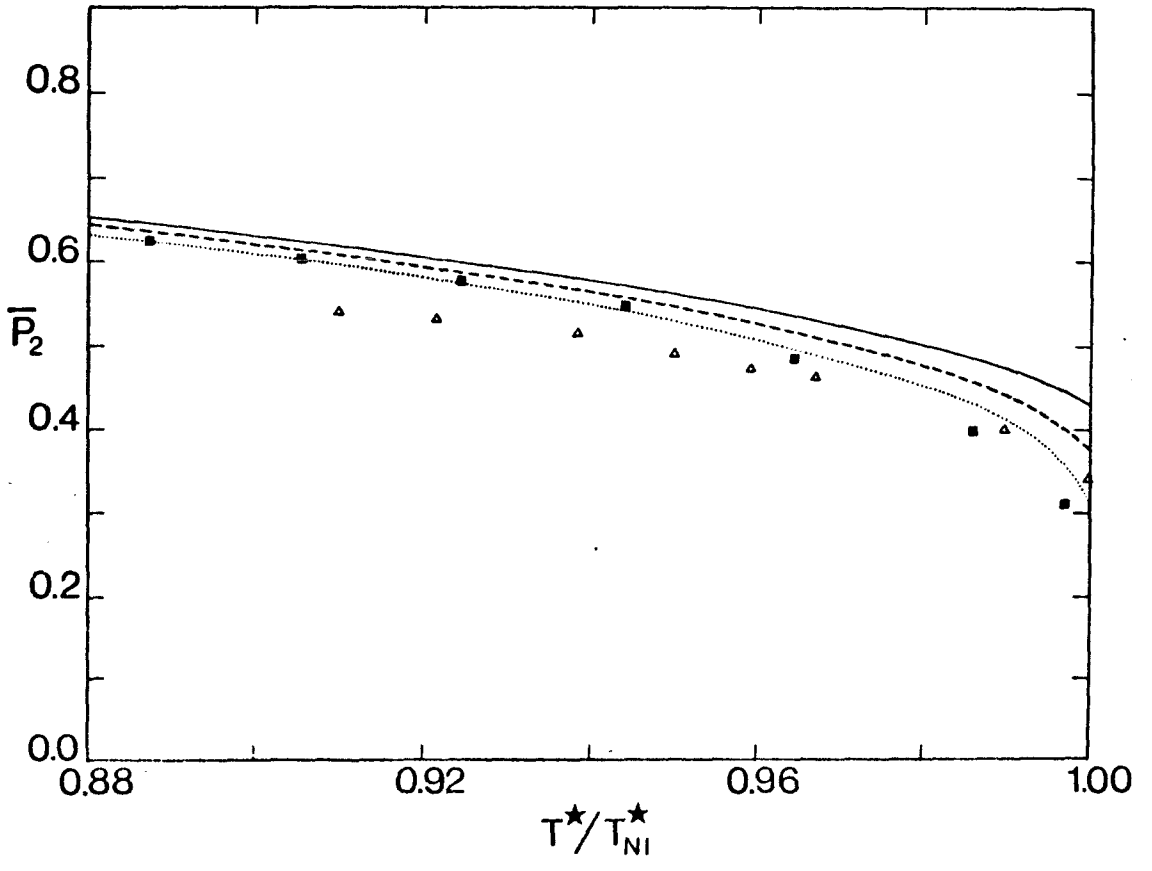

Fig 3.6 The temperature dependence of second rank order parameter for Model I (solid squares) in the nematic phase. The experimental results for PAA obtained at constant volume are given by the open triangles. The dependence predicted by the Maier-Saupe theory is given as the solid curve, by the two side cluster expansion as the dashed curve and by the Maier-Saupe theory after admitting the free energy to be in error by the dotted curve.

The orientational form of $f(\beta)$ calculated by both Monte-Carlo (see Chapter 5) and molecular dynamics (Zannoni and Guerra, 1981) methods has been shown to be of an identical form to that given by this equation, thus we can proceed to check the linear dependence of a on $\bar{P}_2$. Therefore, knowing $\bar{P}_2$ calculated from the simulation allows us to use this to find the theoretical value of a, and hence the ratio $T^*/\bar{P}_2$, which according to theory will be constant. Table 3.3 gives $aT^*/\bar{P}_2$ at the different temperatures studied and indeed to within experimental error it is constant. Therefore the linear dependence of a on $\bar{P}_2$ provides no justification for the employment of quadratic as well as linear terms in $\bar{P}_2$ as was suggested by Horn and Faber (1979), and Kvenzel and Katriel (1982). However, the constant value of $aT^*/\bar{P}_2$ of 5.05 ± 0.02 is not in accord with the Maier-Saupe value of 6, being just the coordination number. Strictly speaking this difference should be associated with the product, $z\varepsilon$, but since ε is used to scale the temperature we shall assume the error to be entirely in z an refer to it as an effective coordination number. Therefore this effective coordination can be used to rescale the theoretically predicted transition temperature since:-

$$T^*_{NI} = 0.2203z \qquad 3.19$$

to give a value of $T^*=1.113$, a value much closer to the simulated value of $T^*=1.127$.

Although using the effective coordination forces agreement to the nematic-isotropic transition temperature, it does nothing to the value of the order parameter at the transition. To obtain better agreement, we would have to admit that the Maier-Saupe free energy from which the location of the transition is evaluated is incorrect. To test this we shall regard the numerical factor in the above equation to be in error, thus treating T^*_{NI}/z as an

adjustable parameter. However there is an upper limit of $T^*_{NI}/z=0.2228$, above which an ordered phase ceases to exist, at which point $\bar{P}_2$ is equal to 0.324. Therefore we will not be fit our results exactly since we have found that $\bar{P}_2^{NI}=0.27$. However, we can still attempt to make a comparison as shown by the dotted line in Figure 3.6, where the maximum value of $T^*_{NI}/z=0.2228$ has been used. The agreement is now very good, especially at low temperatures, although at the transition there is still a slight deviation from the simulated values.

To summarise this comparison with the molecular field theory, we have seen that on increasing the coordination number and the range of the interaction potential the molecular field limit is approached, as we would expect. In addition the theory underestimates the short range angular correlations, which combined with the overestimation of the long range correlations gives fortuitious agreement with the internal energy. Secondly the overestimation of the nematic-isotropic transition temperature can be expressed in terms of an effective coordination number since it is observed that the coefficient a $(=z\bar{P}_2/T^*)$ is directly proportional to $\bar{P}_2$, thus confirming part of the form of the singlet distribution function, and finally we have seen that part of the error in the order parameter at the transition can be accounted for by assuming the Maier-Saupe free energy to be in error.

3.7 Comparison with cluster expansion theory

In Chapter 1 a description of the two site cluster expansion theory was given. Here we shall briefly outline the theory's predictions and make comparisons with both molecular field theory and the simulations. Firstly looking at the transitional properties given in Table 3.1. These have been calculated by Sheng and Wojtowicz (1976) for various coordination numbers, and although they did not evaluate the properties of a 12 coordinate system, values

have been obtained by extrapolation and are presented here. Thus on going from z=6 to z=12, $\bar{P}_2^{NI}$ and $T_{NI}/\bar{u}_2$ both increase by about 7% towards the molecular field limit corresponding to infinite coordination. This is in accord with our simulated values, although this theory still greatly overestimates the entropy of transition but not to the same extent as the molecular field theory.

Finally, predictions of the two site cluster expansion can be compared with the temperature dependence of the simulated values of $\bar{U}^*$, C_v^* and $\bar{P}_2$. This dependence is shown by the solid curves in the plots for Model I in Figure 3.1 and 3.2 for $\bar{U}^*$ and C_v^* respectively, and clearly improves greatly on the molecular field predictions in the isotropic phase by permitting a certain degree of short range order. Indeed, if allowance for the overestimation of the transition temperature is made, then excellent agreement would be observed also in the nematic phase. The two site cluster prediction of the temperature dependence of $\bar{P}_2$ is shown in Figure 3.6 by the dashed curve scaled to the same reduced transition temperature and actually falls midway between the molecular field prediction and the dependence when allowance for the error in the free energy is made.

3.8 Comparison with real nematics

Since the Lebwohl-Lasher model does not correspond to any real molecular system, since no nematic has perfect long range spatial order, any comparison with real systems must be made with caution. Furthermore, no real nematic molecule is cylindrically symmetric and it is improbably that its anisotropic pair potential can be written as the simple form given by Equation 3.1. However, computer simulations of spatially disordered systems have failed to discern a dramatic difference with orientational properties calculated in lattice models (Luckhurst and Romano, 1980). It has also been suggested that nematogens can be regarded as being formed of systems of groups of molecules, each group being

approximately cylind-rically symmetric, therefore justifying the use of such a simple potential (Luckhurst and Zannoni, 1977). Therefore, with these factors in mind we shall attempt to compare the simulated properties of Model I with those of a real nematogen, in this case with 4, 4-dimethoxyazoxybenzene (PAA). This molecule is relatively rigid and furthermore has been very comprehensively studied at various temperatures and pressures, thus providing us with data at constant volumne (McColl and Shih, 1972).

The experimental observations for $\bar{P}_2$ as a function of the reduced temperature, T/T_{NI} are shown as the open triangles in Figure 3.6 and reasonable agreement with simulation is observed at the transition, although it becomes progressively worse with decreasing temperature.

Secondly, the heat capacity at constant pressure has been measured as a function of temperature (Chandrasekhar et al, 1970), from which C_v can be calculated, since:-

$$C_v = C_p + \alpha^2 TV/k_T \qquad 3.20$$

Here k_T is the isothermal compressibility and α is the cubic expansitivity which are both known for PAA. However, C_p measured experimentally contains a relatively large scalar contribution which has to be removed before a comparison with the simulated results containing only anisotropic contributions can be made. The removed contribution was taken to be an amount derived from the extrapolation of C_p in the isotropic phase back to the nematic thus, leaving just the anisotropic contribution to C_p. C_v calculated using this technique and equation 3.20 is shown in Figure 3.1 for Model I as the dashed curve as a function of temperature. The agreement is very poor, with the divergence being much less than that observed in the simulation. It could however, be improved slightly if a smaller scalar contribution was removed, although the overall improvement would be insignificant. The total failure of this data is surprising

since Sheng and Wojtowicz claim good agreement for C_v with their two site cluster theory, although their results suggest that they have compared C_p and not C_v with their constant volume theory.

Finally, the entropy of transition can be compared since there have been numerous experiments to measure the enthalpy change at the nematic-isotropic transition for PAA, (Martire, 1979) an average value for $\Delta S_p/R$ being 0.19 ± 0.01. To convert this to a value at constant volume we use:-

$$\Delta S_v = \Delta S_p - \alpha\Delta V/k_T \qquad 3.21$$

For PAA the requisite values of α and k_T are $12\pm2\times10^{-4}$ K^{-1} (Chandrasekhar et al, 1970) and $75\pm5\times10^{-11}$ m^2N^{-1} (Chandrasekher and Madhusudana, 1971) respectively, and the change in molar volume at the transition is $0.81\pm0.08\times10^{-6}m^3$ mol^{-1} (Martire, 1979). This gives $\Delta S_v/R = 0.05\pm0.03$, which is essentially identical to the simulated value of 0.06 ± 0.01.

3.9 Director Pinning

Throughout the entire simulation for Model I consisting of 20^3 particles, it was observed that the director remained exactly fixed along the direction in which it was initially defined that is, along the laboratory z axis. Each simulation at a new temperature used the configuration from the preceeding lower temperature simulation as a starting point, thus in all, the director remained fixed for a total of about 14×10^3 cycles, since each run in the nematic phase consisted of approximately 2×10^3 cycles.

The reason for this pinning is not obvious, at first it was thought that it could be due to the way in which new configurations were generated, since $\cos\beta$ was generated in the restricted range of 0 to +1, thus removing the full rotational symmetry. However, a subsequent simulation on a system of 10^3 molecules at $T^*=1.0$ proved this not to be the

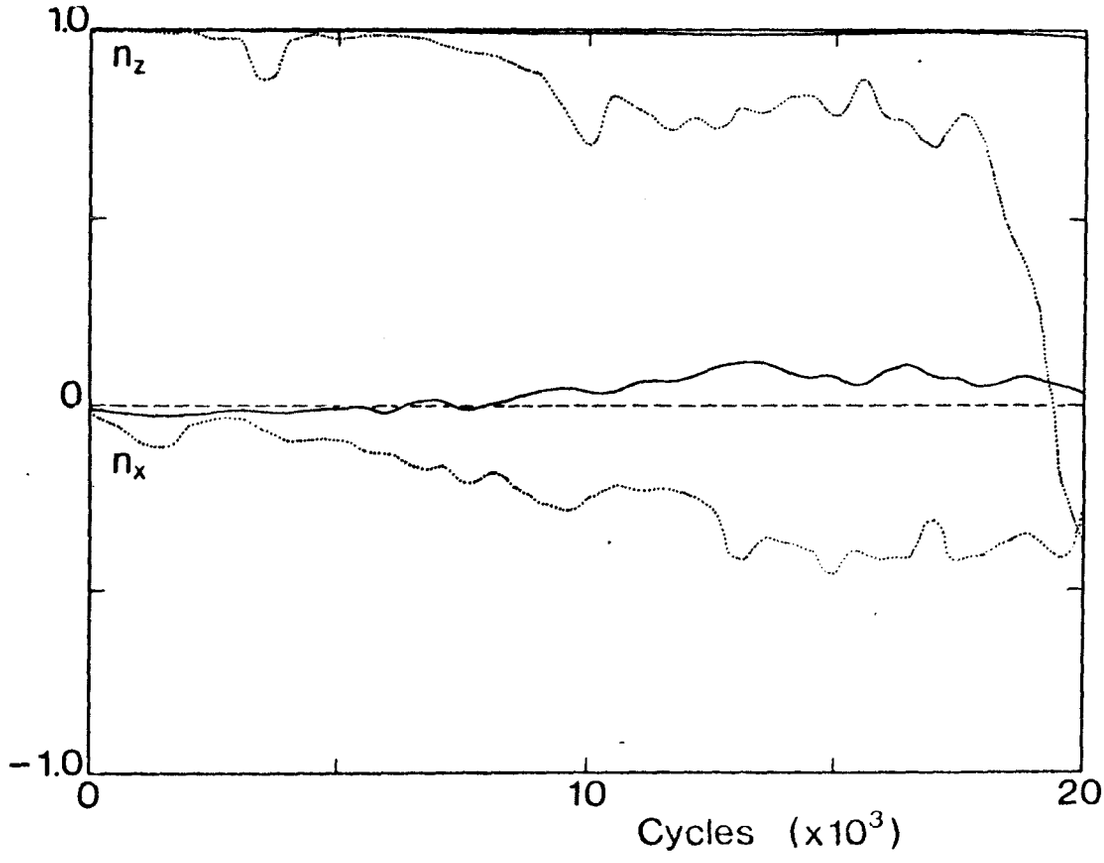

Fig 3.7 The direction cosines n_z and n_x of the director in the laboratory frame as a function of the number of cycles in Model I at $T^* = 1.000$, for 8000 particles (solid curves) and 1000 particles (dotted curves).

case. In this calculation, the Q-tensor was evaluated and diagonalised at the end of each cycle, from which the director orientation was found. The direction cosines made by the director with the x and z laboratory axes for this system are plotted in Figure 3.7 as the dotted curves as a function of cycle number and clearly shows the director reorientating considerably over this run of 20×10^3 cycles. A similar calculation with 20^3 particles shows the director remaining pinned very accurately over this length of run as shown by the solid curve in Figure 3.7, thus proving it is not the method of generating $\cos\beta$ that is responsible for the director pinning. Instead, the reluctance for the director to reorientate must be due to the fact that this system is much larger, a conclusion which is very reasonable, since if one considers that in order for the director to reorientate over a given period, the majority of molecules must reorientate in that direction, an event which becomes more and more statistically improbable with increasing numbers of particles.

This therefore provides an easy method of performing simulations in which it is important that the director remains fixed during the course of a calculation. As we shall see later in this thesis, this can also be achieved in other ways, either by a judicious choice of pair potential (see Chapter 4) or by subjecting the nematic to external forces (Chapters 5 and 6), therefore allowing the relative ease of calculation of various important functions and properties.

Chapter 4

The Effect of dipolar interactions

4.1 Introduction

The nature of liquid crystalline molecules is such that severe approximations have to be used in simulating their physical properties. The first simulations of these anisotropic systems employed a pair potential of a simple P_2 interaction (Lebwohl and Lasher, 1972, 1973;Lasher, 1972 a,b; Jansen et al., 1977) between neighbouring molecules, thus assuming the molecules to be rigid and cylindrically symmetric. Later modifications to the pair potentials have included the assumption that the molecules are symmetric tops (Zannoni and Guerra, 1981) biaxial (Luckhurst and Romano, 1980) and to extend the simple P_2 potential to be representative of the anisotropic dispersion forces potential (Humphries et al., 1981). However, one feature of real liquid crystal molecules is that they often possess dipole moments. The object of this chapter therefore, is to investigate the effect of dipolar forces on the orientational properties of a system which has been previously well studied. In this case, the system with particles interacting via the full dispersion forces potential (Humphries et al, 1981).

The outline of the chapter is as follows: in the next section the exact nature of the pair potential will be discussed, together with appoximations made, computational difficulties and problems initially encountered. The following two sections describe the computational details and results. Finally, these results are compared with those obtained from similar systems but by different techniques, for example with molecular field and other higher order analytic methods.

4.2 The pair potential

As we have seen in Chapter 1, the dipolar potential between two similar linear molecules can be written as (Hansen and McDonald, 1976):-

$$U_{12}(dip) = \frac{\mu^2}{4\pi\varepsilon_o r^3} (\underline{z}_1 \cdot \underline{z}_2) - 3(\underline{z}_1 \cdot \underline{R})(\underline{z}_2 \cdot \underline{R})) \quad 4.1$$

where $\underline{z}_1$ and $\underline{z}_2$ are unit vectors describing the orientations of the dipole moments, μ, parallel with the molecular symmetry axes separated by a distance r and ε_o is the permittivity of free space. The form of this potential is more easy to visualise and more recognisable in terms of spherical polar coordinates in a molecular axis system (Hirschfelder *et al.* 1964):-

$$U_{12}(dip) = \frac{-\mu^2}{4\pi\varepsilon_o r^3} (2\cos\theta_1\cos\theta_2 - \sin\theta_1\sin\theta_2\cos\phi) \quad 4.2$$

Here θ_1, θ_2 define the orientations of dipoles 1 and 2 in the molecular frame with respect to the intermolecular vector and ϕ is as defined in Figure 4.1. Computationally the vector notation is more attractive since fewer time consuming trigonometric function evaluations are required.

The nature of the dipolar interactions are such, that even at large r, the potential still has a significant effect on the total potential energy, therefore long range interactions have to be included. This leads to various computation problems. One obvious method of calculation would be to simply sum over all pairs of molecules in the system, imposing a spherical cut-off when some convergence criteria is satisfied. However, the cut-off would have to be very large resulting in a prohibitive number of interactions being calculated. A much more rapidly convergent method, and

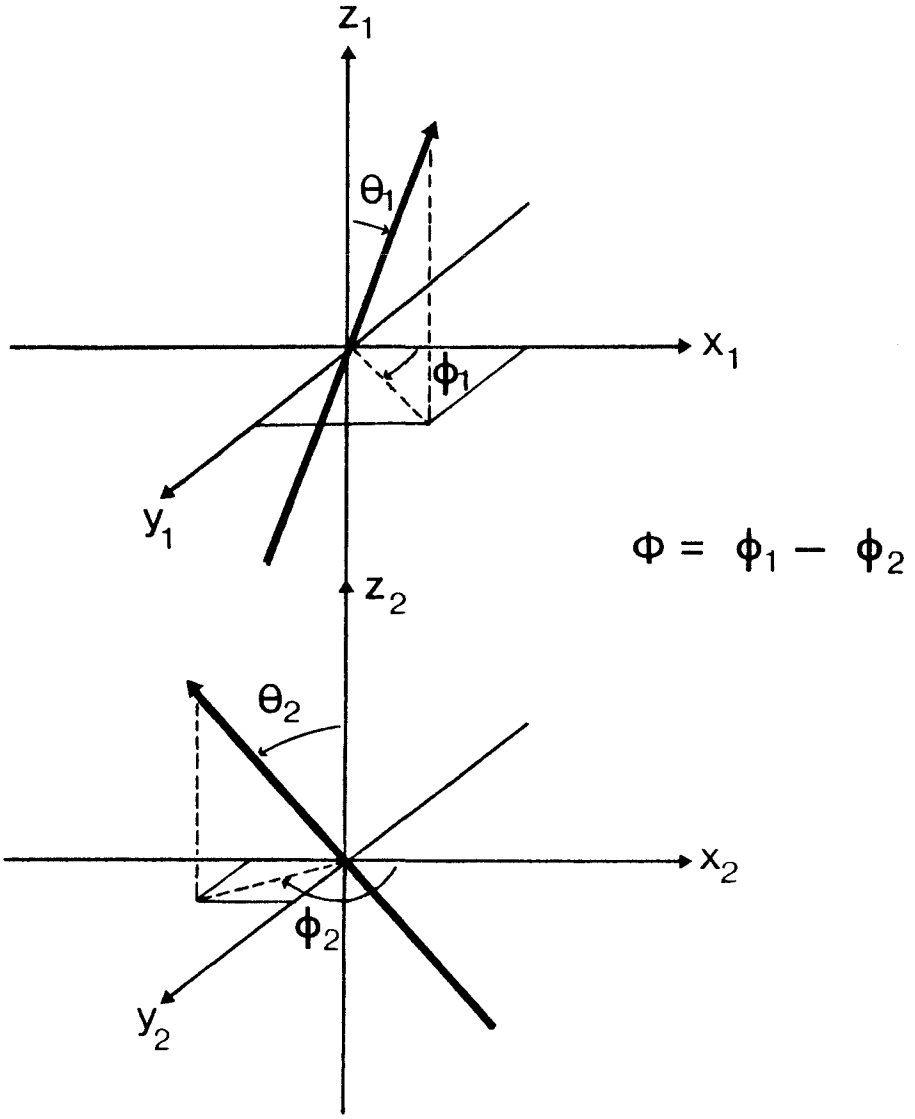

Fig 4.1 Definition of the angular variables, θ_1, θ_2 and $\emptyset$ in Equation 4.2 for two linear molecules.

indeed what was used in this simulation, is an extension of the method originally proposed by Ewald (1921) for electrically neutral systems. He encountered similar problems calculating Madelung constants in ionic crystals where regular arrays of long range interacting point charges exist. Later the method was adapted by Kornfeld (1924) to include lattices of dipoles and quadrupoles. Simply, it involves converting what would be a slowly convergent series in real space to a more complicated but rapidly convergent summation in real and reciprocal space. Thus starting with the expression given by Ewald, we shall express it in a form suitable for the computer simulation of dipoles on a lattice.

The potential at $\underline{r}$ due to N-point charges on an infinite repeating regular cubic lattice of side L is given by the Ewald expression as (Adams and McDonald, 1976):-

$$V_q(r) = \sum_{n\neq 0} \sum_{j} q_j A(n;\eta)\exp(-2\pi i \underline{n}.\underline{R}_j/L) + \sum_{j} q_j \operatorname{erfc}(\eta R_j)/R_j \qquad 4.3$$

where $\underline{n}$ is a reciprocal lattice vector of a cubic array of particles, η is some adjustable parameter having dimensions L^{-1}, carefully chosen for optimum convergence. $\underline{R}_j$ is the vector between the j^{th} point charge and the charge at $\underline{r}$, thus:-

$$\underline{R}_j = \underline{r}_j - \underline{r} \qquad 4.4$$

and $A(n;\eta)$ is defined by

$$A(n;\eta) = \frac{1}{\pi L n^2} \exp\,(-\pi n/\eta L)^2 \qquad 4.5$$

The final term is the complementary error function,

related to the error function, erf, by

$$\text{erfc}(z) = 1 - \text{erf}(z)$$

$$= 1 - \frac{2}{\pi^{\frac{1}{2}}} \int_0^z e^{-t^2} dt \qquad 4.6$$

The potential due to a single charge is q_j/R and for a single dipole is $-\mu_j . \nabla .(1/\underline{R}_j)$. So we can obtain an expression for an infinite lattice of regular repeating dipoles by replacing q_j by $-\mu_j$ and differentiating. To differentiate the error function, we make use of the relationship (Abramowitz and Stegun, 1965):-

$$\frac{\partial}{\partial z} \text{erfc}(z) = - \frac{2}{\pi^{\frac{1}{2}}} e^{-z^2} \qquad 4.7$$

So now:-

$$V_\mu(r) = \frac{2\pi i}{L} \sum_{n \neq o} \sum_j (\mu_j . \underline{n}) A(n;\eta) \exp(-2\pi i \underline{n} . \underline{R}_j / L)$$

$$+ \sum_J (\mu_j . \underline{R}_j) \frac{1}{R_J^3} \left[\text{erfc}(\eta \underline{R}_j) + \frac{2\eta}{\pi^{\frac{1}{2}}} \frac{1}{R_j^2} \exp(-\eta^2 R_j^2) \right] \qquad 4.8$$

The total interaction energy of a dipole placed at $\underline{r}$ is thus:-

$$U(r) = \mu \nabla . V_\mu(\underline{r}) \qquad 4.9$$

So differentiation again yields:-

$$U(r) = \frac{4\pi^2}{L^2} \sum_{n \neq o} \sum_J (\underline{\mu}_j . \underline{n}) (\underline{\mu} . \underline{n}) A(n;\eta) \exp(-2\pi i \underline{n} \underline{R}_j / L)$$

$$+ \sum_J (\mu_j\mu) B(R_j) - \sum_J (\mu.\underline{R}_j)(\mu_j.\underline{R}_j)C(R_j) \qquad 4.10$$

where

$$B(r) = \text{erfc}(\eta r)(\eta r)/r^3 + \frac{2\eta}{\pi^{\frac{1}{2}}}.\exp(-\eta^2 r^2)/r^2 \qquad 4.11$$

and

$$C(r) = 3\text{erfc}(\eta r)/r^5 + (2\eta/\pi^{\frac{1}{2}})(2\eta^2+3/r^2)\exp(-\eta^2 r^2)/r \qquad 4.12$$

Equation 4.10 is the general expression for the interaction energy of a single dipole inserted in the lattice. In our case the test molecule is itself part of the repeating lattice. If a dipole, $\underline{\mu}$ is placed at $\underline{r}$ and the reference dipole, $\underline{\mu}_i$ at $\underline{r}_i$, then their energy of interaction, if they are both parallel is:-

$$(\underline{\mu}.\underline{\mu} - 3(\mu.\underline{R})^2/R_i^2)R_i^3 \qquad 4.13$$

which must equal zero, even when $\underline{r} \to \underline{r}_i$. However C(r) and B(r) both tend to infinity as $\underline{r} \to \underline{r}_i$. To avoid this difficulty we can remove the term for i=j in equation 4.10. thus:-

$$U(r) = \frac{4\pi^2}{L^2} \sum_{n\neq o} \sum_j (\underline{\mu}_i.\underline{n})(\underline{\mu}_j.\underline{n})A(n;\mu)\exp(-2\pi i\underline{n}.\underline{r}_{ij}/L)$$

$$+ \sum_{j(\neq i)} (\underline{\mu}_i.\underline{\mu}_j)B(r_{ij}) - \sum_{j(\neq i)} (\underline{\mu}_i.\underline{r}_{ij})(\underline{\mu}_j.\underline{r}_{ij})C(r_{ij})$$

$$+ \lim_{r\to 0} \left[(\underline{\mu}_i\underline{\mu}_i)B(r_i) - (\mu_i R_i)(\mu_i R_i)C(r_i)\right] \qquad 4.14$$

So if we take this limit along the path defined by

$$\underline{\mu}.\underline{\mu} = 3(\underline{\mu}.\underline{R}_i)^2/R_i^2 \qquad 4.15$$

The final limiting term in equation 4.14 becomes

$$\lim_{r\to 0} (\underline{\mu}_i\underline{\mu}_i)B(r_i) - \frac{1}{3}(\underline{\mu}_i\underline{\mu}_i)R_i^2C(r_i)$$

$$= \frac{-4\eta^3\mu^2}{3\sqrt{\pi}} \qquad 4.16$$

Summing over all i molecules and dividing by N to obtain the total lattice energy per dipole gives:-

$$\frac{U}{N}dip = \frac{4\pi^2}{NL^2} \sum_{n\neq o} \sum_{i} \sum_{j} (\underline{\mu}_j.\underline{n})(\underline{\mu}_i.\underline{n})A(n;\eta)\exp(-2\pi i\underline{n}.\underline{r}_{ij}/L)$$

$$+ \frac{1}{N} \sum_{i} \sum_{j<} (\underline{\mu}_i\underline{\mu}_j)B(r_{ij}) - (\underline{\mu}_i\underline{r}_{ij})(\underline{\mu}_j.\underline{r}_{ij})C(r_{ij})$$

$$- 2\eta^3\mu^2/3\sqrt{\pi} \qquad 4.17$$

This expression can be more conveniently expressed using standard trigonometric relationships and employing the fact that the summation over i and j in the first term reduces to a single summation squared over one of the subscripts, we finally obtain:-

$$U_{dip} = \frac{2\pi}{NL^2} \sum_{n\neq o} A(n;\eta) \left[\left(\sum_{j} (\underline{\mu}_j.\underline{n})\cos(2\pi\underline{n}.\underline{r}_{ij}/L)^2 \right) \right.$$

$$\left. + \left(\sum_{j} (\mu_j.\underline{n})\sin(2\pi\underline{n}.\underline{r}_{ij}/L)^2 \right) \right]$$

$$+ \frac{1}{N} \sum_{j>i} (\underline{\mu}_i \cdot \underline{\mu}_j) B(r_{ij}) - (\underline{\mu}_i \cdot \underline{r}_{ij})(\underline{\mu}_j \cdot \underline{r}_{ij}) C(r_j)$$

$$- 2\eta^3 \mu^2 / 3\pi \qquad 4.18$$

In the calculations the summations must be truncated. The first by summing over a finite number of vectors only, and the second double summation only summed for $r_{ij} < L$. For a given number of vectors the parameter η was adjusted using the following trial and error procedure to reduce the error in the total dipolar potential energy. A very large lattice was set up and the dipolar potential energy was calculated by simply summing up all pair dipolar interactions for an antiferroelectric system (see Figure 4.5) and comparing it with that obtained using the above equation for the similar configuration. The results for the Ewald summution on an 8x8x8 cubic lattice and those from direct summations for η = 4.0 and 5.0 on 20x20x20 and 30x30x30 cubic lattices with a reduced dipole moment of 1.0 in all cases yielded a result of:-

$$U_{dip}/N = -4.17824 \ \gamma^2 \varepsilon \qquad 4.19$$

Where $\gamma^2 \varepsilon$ are scaling units which will be discussed later.

We now turn to the dispersion part of the potential. As we have seen in Chapter 1, if assuming cylind-rically symmetric molecules, the anisotropic dispersion pair potential can be written as (Kohin, 1960):-

$$U_{12} = \frac{\gamma^2\varepsilon}{r_{12}^6}\left[1 - \frac{3}{2}(\underline{z}_1\cdot\underline{r}_{12})^2 - \frac{3}{2}(\underline{z}_2\cdot\underline{r}_{12})^2\right]$$

$$+ \frac{3}{2}\frac{\gamma^2\varepsilon}{r_{12}^6}\left[(\underline{z}_1\cdot\underline{r}_{12})^2 + (\underline{z}_2\cdot\underline{r}_{12})^2 - 9(\underline{z}_1\cdot\underline{r}_{12})^2(\underline{z}_2\cdot\underline{r}_{12})^2\right.$$

$$\left. + 6(\underline{z}_1\cdot\underline{r}_2)(\underline{z}_2\cdot\underline{r}_{12})(\underline{z}_1\cdot\underline{z}_2) - (\underline{z}_1\cdot\underline{z}_2)^2\right] \quad 4.20$$

Where r_{12} is the separation of molecules 1 and 2, $\underline{z}_1$, $\underline{z}_2$, and $\underline{r}_{12}$ are unit vectors describing the orientation of molecules 1 and 2 and the intermolecular separation respectively. γ is the relative anisotropy in the polarisability

$$\gamma = \left[(\alpha_{||} - \alpha_{\perp})/(\alpha_{||}+2\alpha_{\perp})\right] \quad 4.21$$

and ε is the scalar component of the dispersion interaction, which together with γ^2 will be used to scale the potential with temperature and the dipolar interaction. Thus we shall define a reduced temperature, T^* as:-

$$T^* = \frac{kT}{\gamma^2\varepsilon} \quad 4.22$$

In general the temperature could have been scaled with $\gamma\varepsilon$, but molecular field theory suggests $\gamma^2\varepsilon$ to be a more suitable factor (Humphries *et al,* 1981) . In order to make a meaningful comparision with previous work, we shall set $\gamma^2\varepsilon = 0.8$ (Humphries *et al,* 1981).

As mentioned earlier, the dipolar pair potential was also scaled with $\gamma^2\varepsilon$, thus defining a dimensionless reduced squared dipole moment, M^2 as:-

$$M^2 = \frac{\mu^2}{4\pi\varepsilon_0 a^3 \gamma^2 \varepsilon} \qquad 4.23$$

Here a is the nearest neighbour intermolecular separation. Assuming, that for a pure dispersion potential only, $kT/\gamma^2\varepsilon$ = 2.22 (Humphries et al, 1981), and for a typical molecule, μ~4.8 Debyes (See for example Dunmur and Miller, 1980), T_{NI} = 400K, a = 10Å, we get a value of M^2 = 1.0. This therefore gives a total pair potential of

$$U^* = \frac{U_{12}}{\gamma^2\varepsilon} = \left(\frac{a}{r}\right)^6 \phi' + M^2\left(\frac{a}{r}\right)^3 \phi'' \qquad 4.24$$

Where ϕ' and ϕ'' are the anisotropic angular parts of the dispersion and dipolar pair potentials respectively, as defined earlier.

At this point we shall examine the form of the two potentials. Firstly, the dipolar interaction given by equation 4.2. In Figure 4.2 the dipolar potential energy surface together with a contour plot of the same surface is plotted. The x and y coordinates correspond to θ_1 and θ_2 respectively, the angles each molecule make with the intermolecular vector. ϕ is constant at 0° (see figure 4.1). Minima of $-2\mu^2$ are observed when the molecules are parallel to each other and to the intermolecular vector (at the four corners of the surface and the centre (ie θ_1 = 0°, θ_2 = 0°, θ_1 = 360° etc, and θ_1 = 180°, θ_2 =180°)). When the molecules are antiparallel to each other and perpendicular to the intermolecular vector the minima are $-\mu^2$ and actually occur as saddle points on the surface.

The surface obtained for the dispersion potential is plotted in Figure 4.3. Here again the surface represents molecules in the same plane (ie with $\phi_1 - \phi_2 = 0$). The minima are again with the molecules parallel to each other and to the intermolecular vector and as before, the minimum

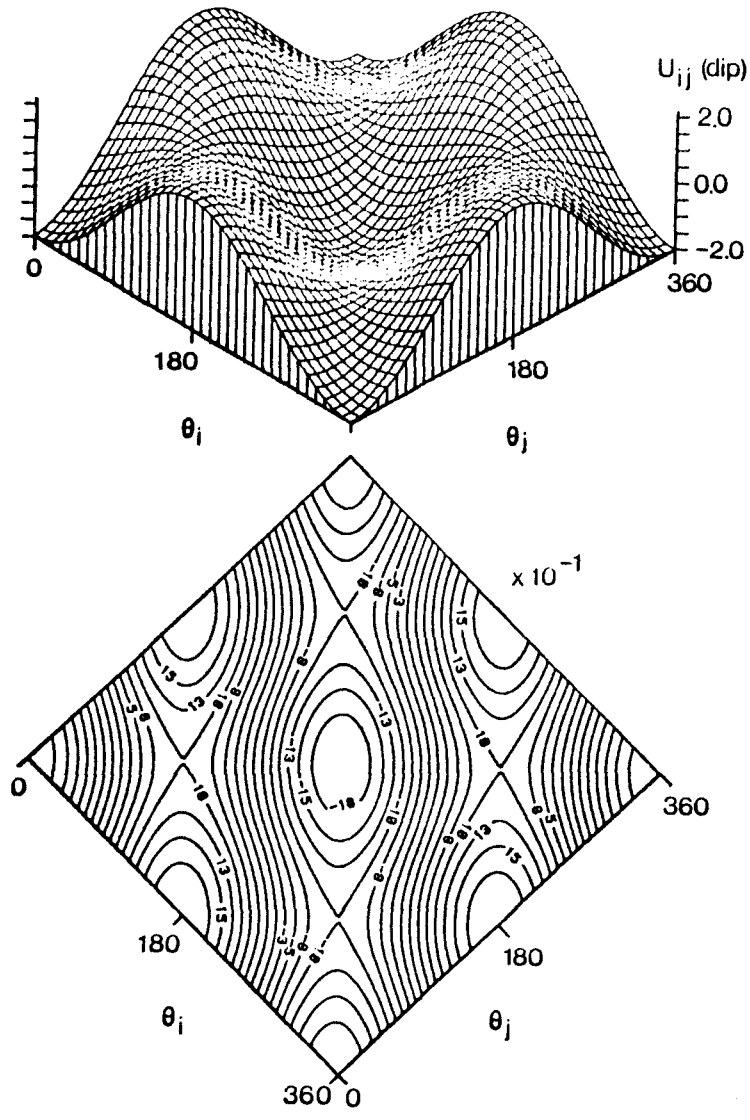

Fig 4.2 Dipolar potential energy surface as a function of θ_i and θ_j for two linear molecules, as defined by Equation 4.2. The angle ϕ equals 0^0. The lower diagram is a contour plot of the surface.

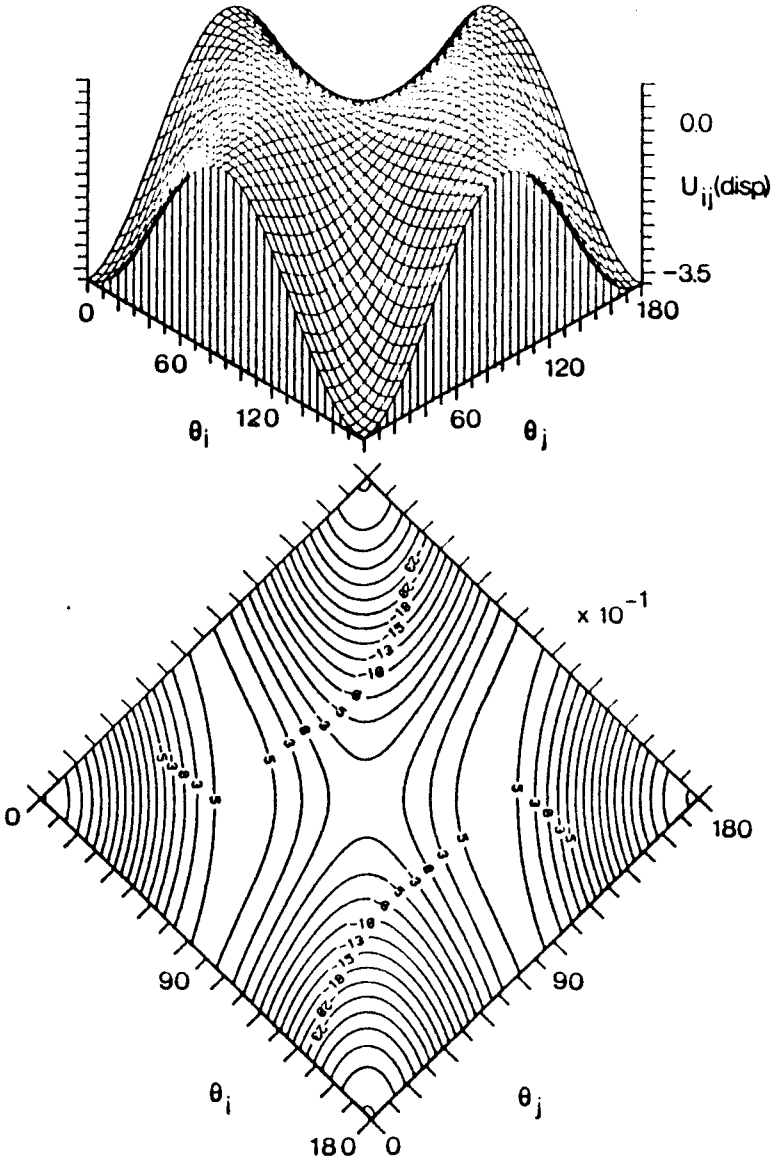

Fig 4.3 Dispersion potential energy surface as a function of θ_i and θ_j for two linear molecules. The angle ϕ equals 0^0. The lower diagram is a contour plot of the surface.

representing the configuration with parallel molecules perpendicular to the intermolecular vector is at a saddle point on the surface.

Initially the simulation was run with a full range dispersion potential and zero dipolar interaction. However, the nature of the potential was such, that with the inclusion of the interactions from the second and subsequent shells of molecules, a configuration with a potential energy lower than the ordered antiferroelectric state was observed at very low temperatures. This staggered configuration is shown in Figure 4.4, where the molecules tend to lie along the (1,1,1) (1,1,-1),(1,-1,1) etc. lattice vectors. This system is spherically symmetric and has an order parameter of zero, and is therefore totally unsuitable for the simulation of nematics. The dispersion interaction was therefore truncated to include nearest neighbour interactions only while retaining a full range dipolar interaction. This has a totally ordered ground state configuration and is antiferroelectric as shown in Figure 4.5, where the dots at the end of each line represent a pole of the dipole moment.

4.3 Computational Details

The study was performed using the standard Monte-Carlo technique developed for the simulation of simple liquids (Metropolis *et al,* 1953). The centres of mass of the molecules were restricted to lie on the lattice points of an 8x8x8 simple cubic lattice (N=512), with usual cubic periodic boundary conditions, as defined in Chapter 2. Ideally we would have liked to study a 10x10x10 system, in order to make a more meaningful comparison with previous work (Humphries *et al,* 1981). Unfortunately, the lack of computational resources prevented this.

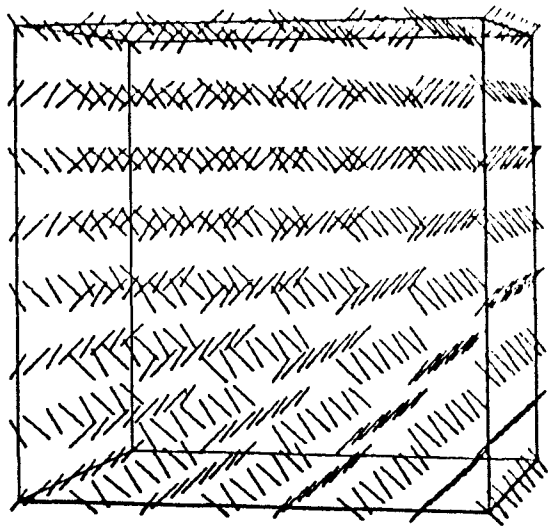

Fig 4.4 The 'staggered' low temperature configuration observed in the case of a full ranged dispersion potential only.

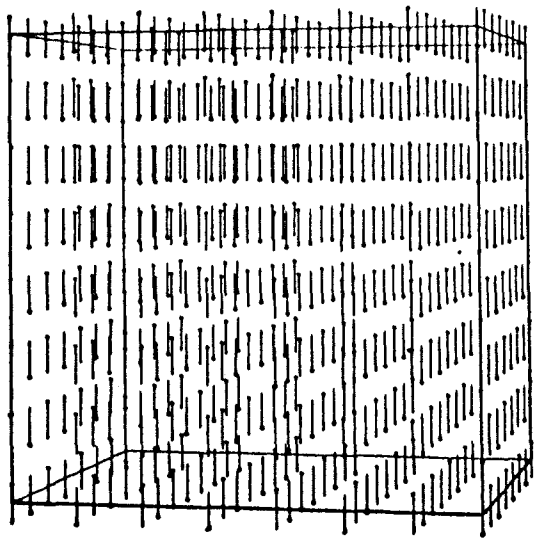

Fig 4.5 The ground state antiferroelectric configuration for the molecules interacting via a full ranged dipolar, nearest neighbour dispersion potential.

The molecules interacted via the nearest neighbour dispersion potential (Equation 4.20) and the full ranged dipole-dipole interaction, calculated using the Ewald sum mation (Equation 4.18), with a spherical cut-off at half the box length for the real space term and the summation over the reciprocal space term (the first term) performed over 297 lattice vectors (ie up to a maximum distance of 5a). η was chosen to be 4.0. The orientations of molecules were stored in unit vector notation (ie as direction cosines) with the laboratory z axis parallel with one of the nearest neighbour intermolecular vectors. To generate a new configuration in the Monte-Carlo chain, molecules were sampled sequentially, and re-orientated using the method developed by Barker and Watts (1969). The acceptance-rejection ratio was controlled to be approximately one by adjusting the permitted maximum rotation.

The simulations consisted of two stages, an equilibration stage, where the averages calculated in the program were monitored but discarded and a longer production phase where various thermodynamic and orientational properties were calculated.

The first run was at a reduced temperature of $T^* = 2.5$ where the starting configuration was chosen to an all aligned, antiferroelectric state with the molecular axes parallel with the laboratory z-axis. This configuration is depicted in Figure 4.5. An antiferroelectric state was chosen to speed up the convergence of the orientations of the dipoles. If for example a ferroelectric state was chosen then at low temperatures, where, to achieve good acceptance rejection ratios small maximum displacements are required, it would be very unlikely and probably impossible for a dipole to completely rotate through an angle close to 180^0. Thus a more stable antiferroelectric state would never actually be reached. The starting configuration at a new temperature was chosen to be one from either a run in the

ordered phase, or in the case of high temperature isotropic calculations from either the nematic or the isotropic phase. In either case, the starting configuration for a nematic phase calculation was never chosen to be isotropic. This is due entirely to the nature of the potential, since the dispersion part has three degenerate ground states, each with the molecular symmetry axes parallel with the three crystal axes. Furthermore each of these degeneracies has a double degeneracy from the dipolar contribution, since antiferroelectric states can be formed with dipoles pointing in two directions. This means our system has six degenerate ground states. If therefore an isotropic state was cooled to the nematic phase, invariably within the sample, domains of local order would form. From statistical arguments there would be an equal probability for any of the six degenerate states forming into a domain. This multi-domain structure would take a very long time to equilibrate fully to a monodomain system which is required to calculate bulk properites. This effect has been discussed for p-fold degenerate systems in d-dimensional space where it is suggested that the domain sizes would equilibrate as a power function of time, therefore a monodomain system would never occur (Safran, 1981). A typical configuration showing a monodomain sample is shown in Figure 4.6 taken at a reduced temperature of $T^* = 2.5$. Again the dots at the ends of each molecule represent one end of the dipole moment.

During the production stage the average dispersion ($\bar{U}^*_{disp}$) and dipolar ($\bar{U}^*_{dip}$) contributions to the total average internal energy ($\bar{U}^*_{tot}$) were calculated, from which the heat capacity at constant volume was evaluated using

$$C_v^* = (\overline{U^{*2}_{tot}} - \overline{U^*_{tot}}^2)/T^{*2} \qquad 4.25$$

The orientational second rank order parameter, defined as the average of the second Legendre polynomial was also

calculated as:-

$$\bar{P}_2 = \frac{3}{2}\overline{\cos^2\beta} - \frac{1}{2} \qquad 4.26$$

where the bar indicates an ensemble average, and β is the angle between the molecular symmetry axis and the director axis for the orientationally ordered phase. In this instance it was calculated by evaluating the Q-tensor.

$$Q_{ab} = (3\,\overline{z_a z_b} - \delta_{ab})/2 \qquad 4.27$$

Here a and b denote laboratory axes, z_a and z_b the direction cosines and δ_{ab} the Kroneker delta. Averages of the Q-tensor were taken over a number of cycles (defined as 1 macrostep) during which time the director does not move. Each macrostep was actually 50 cycles after which time the Q-tensor was diagonalised and the largest eigenvalue identified with the order parameter, $\bar{P}_2$, defined above in equation 4.26 (Buckingham 1967). Each typical production stage consisted of 50 macro-steps, although 125 were used close to the transition because of large fluctuations in the internal energy and order parameter in this region. Explicit details of starting configurations, lengths of equilibration and production runs are given in Table 4.1. Futhermore during some of the production stages (see Table 4.1), the orientations of all the molecules at the end of each cycle were written onto magnetic tape for the following further analysis.

Since, as we shall show, the director is pinned along some arbitrary laboratory axis, (in our case the z-axis), the singlet distribution function can be readily calculated; this is defined as the probability of finding a molecule within a volume element between $\cos\beta$ and $\cos\beta+d\cos\beta$ where β is the angle the particle makes with the director. This was calculated by dividing the $\cos\beta$ space (to give equal volume

elements) into 100 equal divisions and incrementing a counter array (of 100 buckets) for the orientations of all molecules for all cycles.

Various pair correlation functions were also calculated. In particular:-

$$G_1(r_{ij}) = < P_1(\cos\theta)>_{r_{ij}} \qquad 4.28$$

$$G_2(r_{ij}) = < P_2(\cos\theta)>_{r_{ij}} \qquad 4.29$$

$$G_4(r_{ij}) = < P_4(\cos\theta)>_{r_{ij}} \qquad 4.30$$

Here P_1, P_2 and P_4 are Legendre polynomials and θ is the angle between molecules at a distance r_{ij}. Computationally these were calculated by firstly labelling the x, y, z coordinates of all the molecules with integer labels. The square of the distance between particles i and j is:-

$$r_{ij}^2 = (x_i - x_j)^2 + (y_i - y_j)^2 + (z_i - z_j)^2 \qquad 4.31$$

Taking into account the periodicity of the system using the minimum image convention, r_{ij}^2 was used as an array pointer, to store the necessary values of $\cos\theta$, $\cos^2\theta$ and $\cos^4\theta$. The correlation between molecules at distances greater than half the sample size were not counted.

A subset of pair correlation functions were also calculated. We will show that the director is pinned along the z-axis, thus pair correlations for pairs of molecules parallel and perpendicular to the director were evaluated, defined by:-

$$G_L^{\parallel,\perp}(r_{ij}) = < P_2(\cos\theta) >^{\parallel,\perp}_{r_{ij}} \qquad 4.32$$

Where L = 1,2 and 4. These were calculated in exactly the same way as for the total pair correlation functions, except that molecules with intermolecular vectors parallel and

perpendicular to the director were considered.

As a check to the pinning of the director along the laboratory z-axis, various order parameters were calculated directly with respect to this axis, defined by:-

$$\bar{P}_1 = \langle \cos \beta \rangle \qquad 4.33$$

$$\bar{P}_2 = \frac{3}{2} \langle \cos^2\beta \rangle - \frac{1}{2} \qquad 4.34$$

$$\bar{P}_4 = \frac{35}{8}\langle \cos^4\beta \rangle - \frac{15}{4}\langle \cos^2\beta \rangle + \frac{3}{8} \qquad 4.35$$

Here β is the angle between the dipolar axis and the laboratory z-axis. The second rank order parameter was then compared with that evaluated by setting up and diagonalising the Q-tensor (Equation 4.27) at the end of each cycle, and with that calculated by averaging the Q-tensor over the previously defined macrosteps.

4.4 Discussion of Results

Thermodynamic Properties

The thermodynamic properties obtainable directly from the simulation were the internal energies, $\bar{U}^*_{disp}$, $\bar{U}^*_{dip}$ and $\bar{U}^*_{tot}$ and the heat capacity at constant volume calculated from the energy fluctuations by equation 4.25. Figure 4.7 shows these internal energies plotted as a function of the reduced temperature T^*, the actual values are listed in Table 4.2 with their associated error. The behaviour of $\bar{U}^*_{tot}$ clearly indicates a phase transition occuring in the region of $T^*=2.7$ to $T^*=2.8$. The transition between an ordered and disordered phase is also emphasized in the plot of the dispersion contribution to the internal energy U^*_{disp}, although very much less so by the dipolar energy, which is essentially a continuous function of temperature. The exact location of the transition is most accurately determined from the divergence of the heat

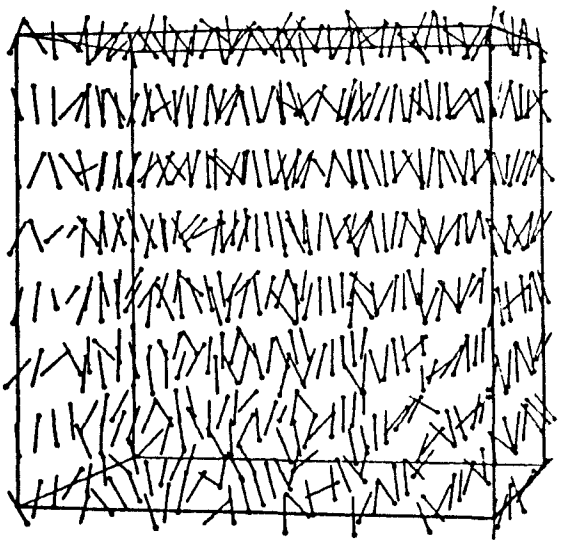

Fig 4.6 A typical configuration taken at the end of the production stage at T* = 2.5

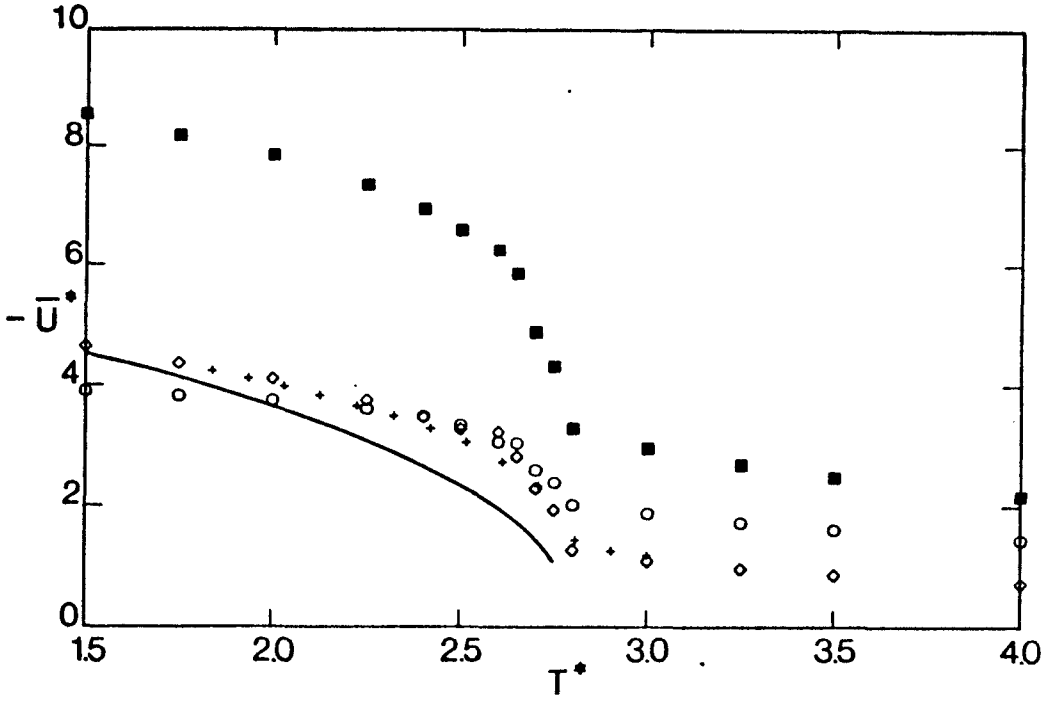

Fig 4.7 The reduced temperature dependence of the total internal energy (■) and the contribution from the dispersion (◇) and dipolar (O) terms. The crosses are the unscaled values quoted by Humphries et al (1981) and the curve is the Maier-Saupe prediction based on a pseudo potential derived from dispersion forces.

capacity. In this simulation it was calculated both from energy fluctuations and by fitting the internal energy, U^*_{tot} versus T^* with a cubic spline interpolation procedure (CERN routine E209) and obtaining the first derivative numerically since:-

$$C_v^* = \left(\frac{\partial \bar{U}^*}{\partial T^*}\right)_v \qquad 4.36$$

The results given by both methods are plotted in Figure 4.8 with the fluctuation and spline results given by the open circles and solid squares respectively. The results are also tabulated in Table 4.2. As we would expect the values obtained from the energy fluctuations are not in exact agreement with those evaluated from the spline interpolating routine. This is due largely to the fact that in calculating the derivative at a particular point the spline fitting routine uses data points before and after that point, and in doing so calculates a more accurate value, whereas, the value from the fluctuations relies on sampling configurations of both high and low energy states from the Boltzmann distribution, which would only be achieved after prohibitively long production runs. However, both sets of results do indeed show a divergence at the transition. This can be accurately located at $T^* = 2.75 \pm 0.03$. From the divergence of the heat capacity the transition can be predicted to be of first, or weakly first order.

Since we know the exact location of the transition we can now turn back to the plot of the internal energy and attempt to evaluate the entropy of transition. The determination of this quantity requires very careful extrapolation of the internal energy especially in the nematic phase. However, if in this phase, we ignore the points close to the transition where the internal energy changes most rapidly a reasonable estimate can be made. The

resulting value for $\Delta S/Nk$ which is independent of any scaling factors in the temperature or internal energy is 0.70 ± 0.10, (where the error stems entirely from the uncertainty in measuring the change in the internal energy, not from the uncertainty in the transition temperature). This value is larger than that obtained in the simulation using the nearest neighbour dispersion potential of $\Delta S/Nk = 0.29 \pm 0.01$ (Humphries *et al*, 1981) and very much higher than that evaluated from simulations using the simple P_2 potential (Luckhurst and Simpson, 1982).

For the sake of completeness the nearest neighbour dispersion potential results for the internal energy scaled to the same transition temperature are plotted on Figure 4.7 as the crosses and are virtually superimposable. Thus the difference in entropy at the transition stems from the inclusion of our dipolar interactions.

Analytic theories, for example Maier-Saupe molecular field theory predicts a value for the entropy of transition of $\Delta S/Nk = 0.417$. This value will be compared and discussed further later.

Orientational Properties

The only orientational property calculated directly in the simulation was the second rank order parameter $\bar{P}_2$, which was evaluated from the Q-tensor averaged over macrosteps of 50 cycles. Its temperature dependence is shown in Figure 4.9 as the solid squares, and clearly reinforces our previous observation of a transition at $T^* = 2.75$. The order parameter through the transition is essentially continuous, and has a non-zero value in the isotropic phase. This continuity and low order in the isotropic phase stems from the relatively small size of the system. The order parameter at the transition is 0.36 ± 0.15, where again the uncertainty arises from the error in the order parameter only. The relatively large error at the transition can be attributed to the system existing in two

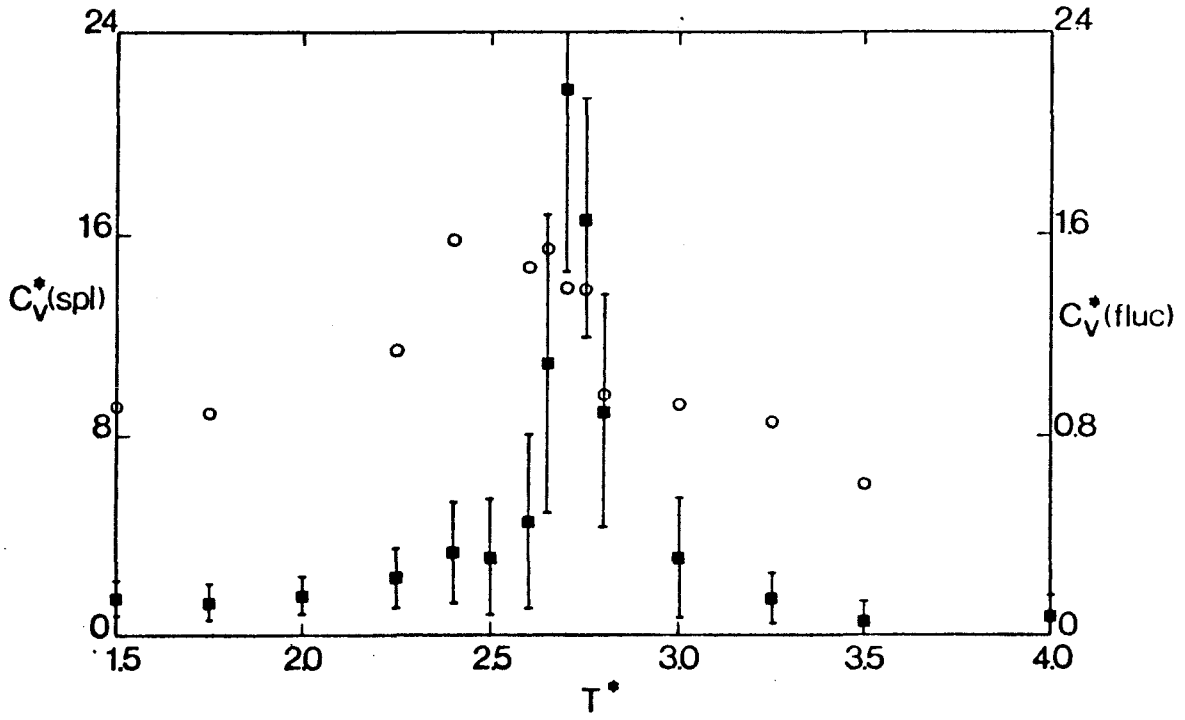

Fig 4.8 The reduced temperature dependence of the heat capacity, calculated from the energy fluctuations (O) and numerical differentiation of the internal energy (■).

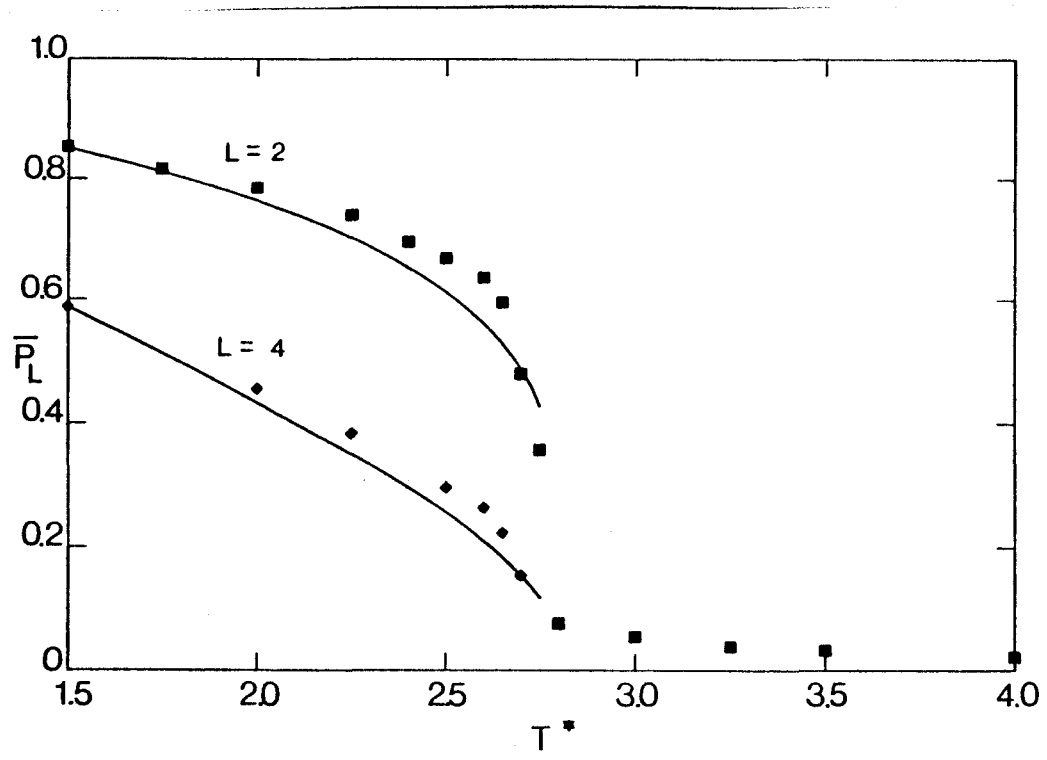

Fig 4.9 The reduced temperature dependence of the second and fourth rank order parameters. The curves are the Maier-Saupe predictions.

states for the duration of the production run, i.e. in states with order of approximately $\bar{P}_2 = 0.15$ and $\bar{P}_2 = 0.45$, as can be seen in the histogram plotted in Figure 4.10 where the frequency of $\bar{P}_2$ calculated over each macrostep is plotted. The distribution is essentially bi-model and similar to that observed by Jansen et al (1977). The order parameter evaluated during macrosteps was calculated assuming the director did not fluctuate within each macrostep. Indeed, analysis of the data stored on magnetic tape does show this to be true. Furthermore, the director is accurately pinned along the z-laboratory axis for the duration of the entire simulation in the nematic phase. This can be seen from the virtually indentical values of $\bar{P}_2$ calculated from the evaluation of the Q-tensor at the end of each cycle, and from $\bar{P}_2$ calculated with respect to the z-axis directly using equation 4.34. These are listed in Table 4.3. The greatest deviations occur close to the transition temperature, although within experimental error they are equal. If director fluctuations about the z-axis occur, it would be expected that the average order parameter calculated with respect to the z-axis would be less than that calculated by averaging the Q-tensor over macrosteps, which would be less than the average value calculated from the Q-tensor at each cycle. Unfortunately, close to the transition where this trend should be more evident, it was not possible to write the entire production history onto magnetic tape (see Table 4.1), so two of the three averages are over different stages in the production phase. However, at $T^* = 2.7$ $\bar{P}_2$ calculated directly with respect to the z-axis is very slightly less than that evaluated from the un-averaged Q-tensor. In the isotropic phase the order parameter calculated with respect to the laboratory z-axis has no physical significance since a preferred director axis no longer exists.

Since the director is pinned accurately along the z laboratory axis the calculation of the fourth rank order

parameter, $\bar{P}_4$ defined by equation 4.35 becomes valid. The results for P_4 are plotted on figure 4.9 and listed in Table 4.4 and again reinforce the observation of a transition from an orientationally ordered to disordered phase.

The first rank order parameter, P_1, was also calculated from the data stored on magnetic tape using equation 4.33, the values of which are listed in Table 4.4. Within experimental error, all the values are equal to zero, indicating the orientations of the dipoles are totally random. This is exactly what we would hope for, since in real dipolar nematics, the systems as a bulk have no net polarity.

We now turn to the results calculated for the singlet orientational distribution functions. Figures 4.11 to 4.17 show these functions as crosses for temperatures in the nematic phase, normalised such that the area under each graph is unity. Experimentally it has been shown that the form of the distribution function is in accord with the Maier-Saupe prediction, so it can be written as:-

$$f(b) = a \exp (b P_2(\cos\beta)) \qquad 4.37$$

where a is related to the orientational partition function, and according to this theory, b is proportional to $\bar{P}_2$. As a test of the Maier-Saupe prediction for the singlet distribution function, the experimental data was fitted to Equation 4.37 using a non-linear optimisation procedure (CERN library routine D506-MINUIT5). The optimum values for a and b are given in Table 4.5. The solid curves on Figures 4.11 to 4.17 are the best fits to the simulated data. In each case an excellent fit is obtained indicating the success of the Maier Saupe theory in predicting the form of the singlet distribution function. This agreement is in contrast with that found for molecules interacting via a simple P_2 potential (Luckhurst *et al.* 1981) where fourth rank terms had to be included in equation 4.37 to fit the singlet distribution function. We know from the theory that

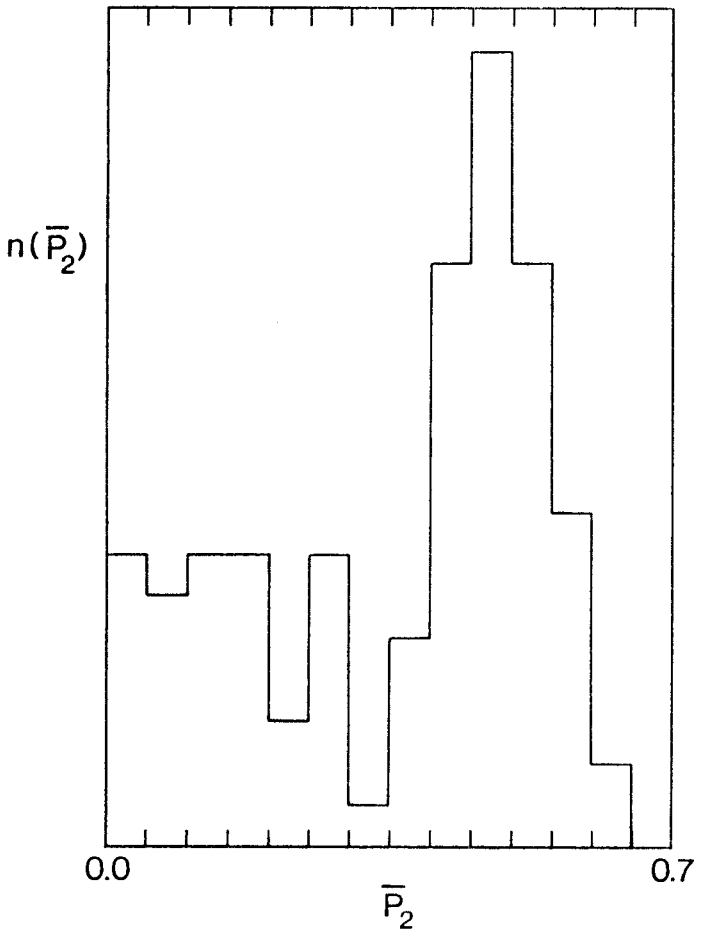

Fig 4.10 A histogram showing the order parameter frequency over 100 macrosteps at the transition temperature of T* = 2.75.

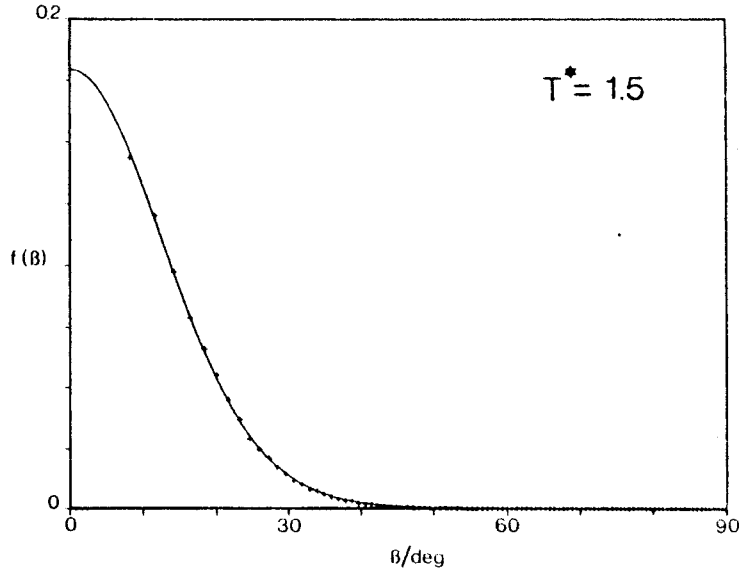

Fig 4.11 The singlet orientational distribution functions calculated during the simulation (+) at the reduced temperature indicated. The curve is the best fit to the equation:- $f(\beta) = a\exp(b\ P_2(\cos\beta))$.

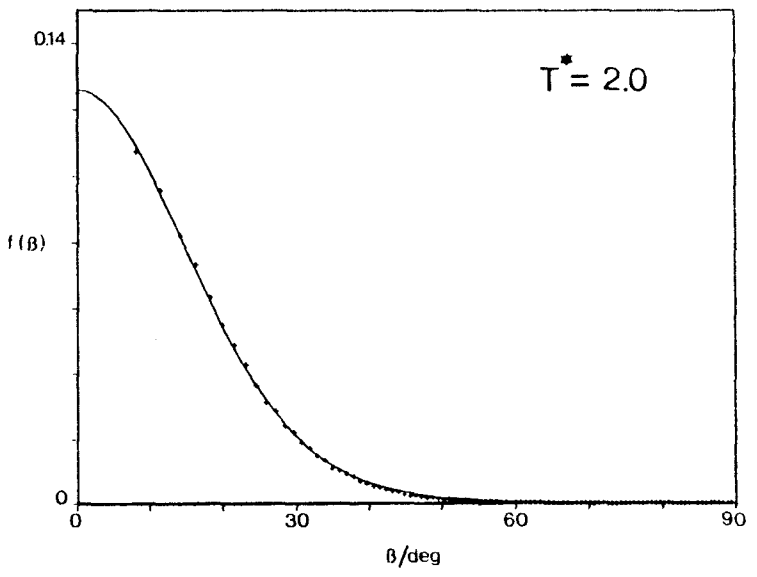

Fig 4.12

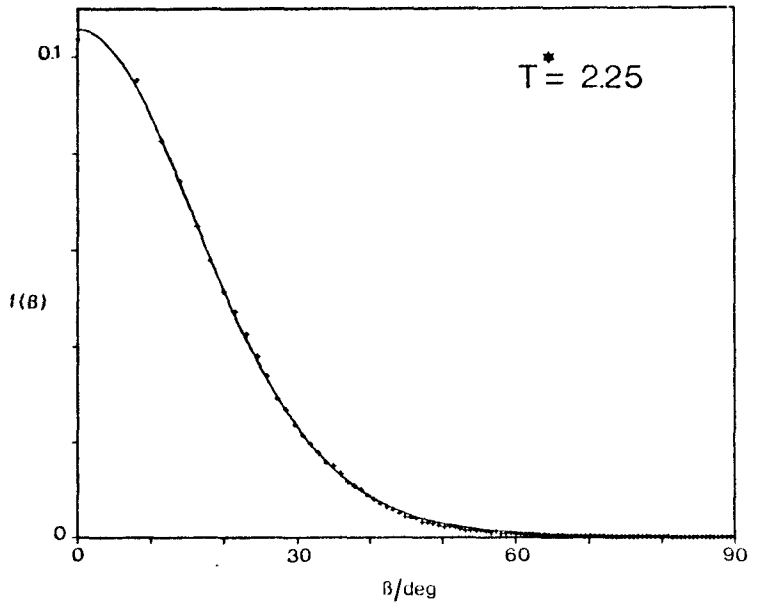

Fig 4.13

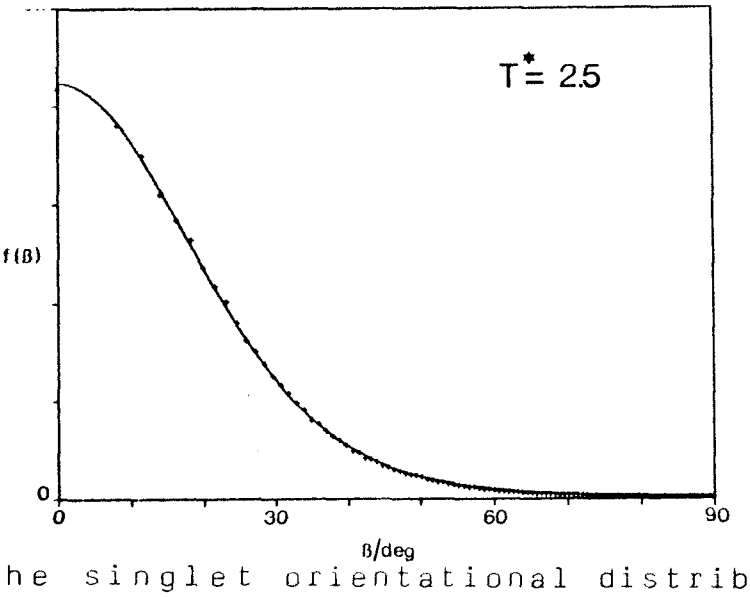

Fig 4.14 The singlet orientational distribution functions calculated during the simulations (+) at the reduced temperatures indicated. The curves are the best fits to the equation:- $f(\beta) = a\exp(b\ P_2(\cos\beta))$.

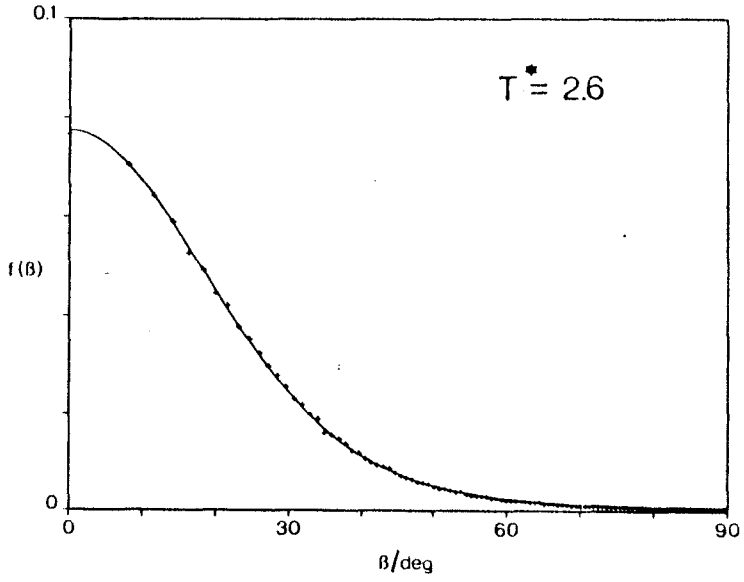

Fig 4.15

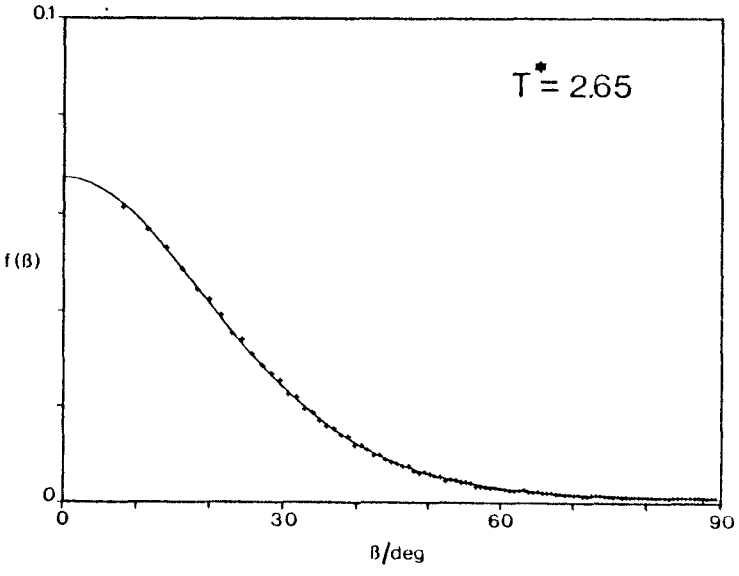

Fig 4.16

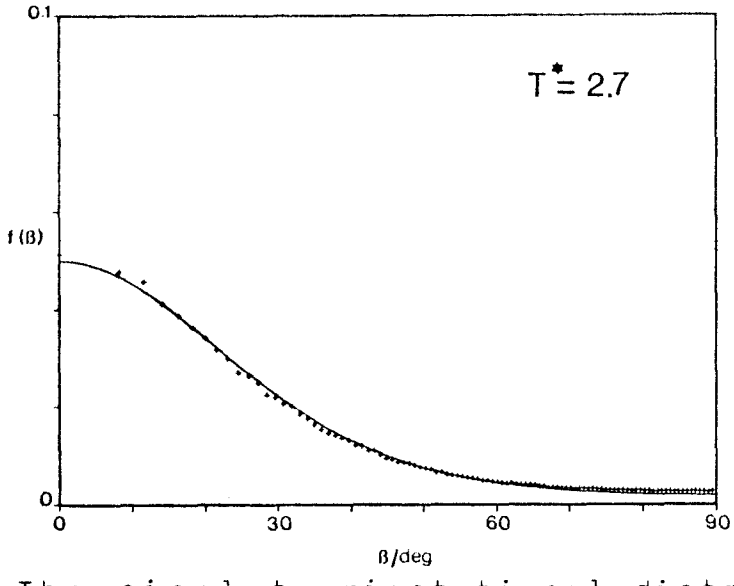

Fig 4.17 The singlet orientational distribution functions calculated during the simulations (+) at the reduced temperatures indicated. The curves are the best fits to the equation:- $f(\beta) = a\exp(b\ P_2(\cos\beta))$.

the coefficient b is predicted to be linearly proportional to the order parameter, $\bar{P}_2$ and inversely proportional to temperature, T^*, so:-

$$b = \frac{m \bar{P}_2}{T^{*2}} \qquad 4.38$$

Here m is a constant related to the strength of the potential of mean torque, or in this case equal to $z\gamma^2\varepsilon$, where z is the coordination number, 6 (Humphries et al 1981) Figure 4.18 shows a plot of b versus $\bar{P}_2/T^*$, with $\bar{P}_2/T^*$, with $\bar{P}_2$ and T^* taken from the Q-tensor diagonalised at the end of each cycle. The points form a very good straight line, again reinforcing the success of the Maier-Saupe form of the singlet distribution function. Linear least squares analysis of the data points gives a slope of 12.08 ± 0.12 and an intercept of 0.09 ± 0.04, with the inclusion of a point at the origin corresponding to the isotropic phase. The value of the slope will be discussed further in the final section.

We can now turn our attention to the pair correlation function of rank 1, 2 and 4 defined by equations 4.28, 4.29 and 4.30 the results of which are plotted in Figures 4.19, 4.20 and 4.21 and listed in Tables 4.6, 4.7 and 4.8 respectively. The first rank correlation function has been normalised by dividing the correlations by these for the ground state, antiferroelectric configuration. This is because, for $G_1(r)$ for a completely ordered antiferroelectric system, two types of correlations occur depending on the coordination shell. One in which 2n dipoles are parallel, and 4n antiparallel, giving an average pair correlation of -1/3, and the other in which all dipoles are parallel resulting in an average correlation of 1. Thus normalisation gives the same correlations for all coordination shells. At first sight the correlations appear to tend to positive limiting values, which is unexpected, since their long range limits should simply be the square

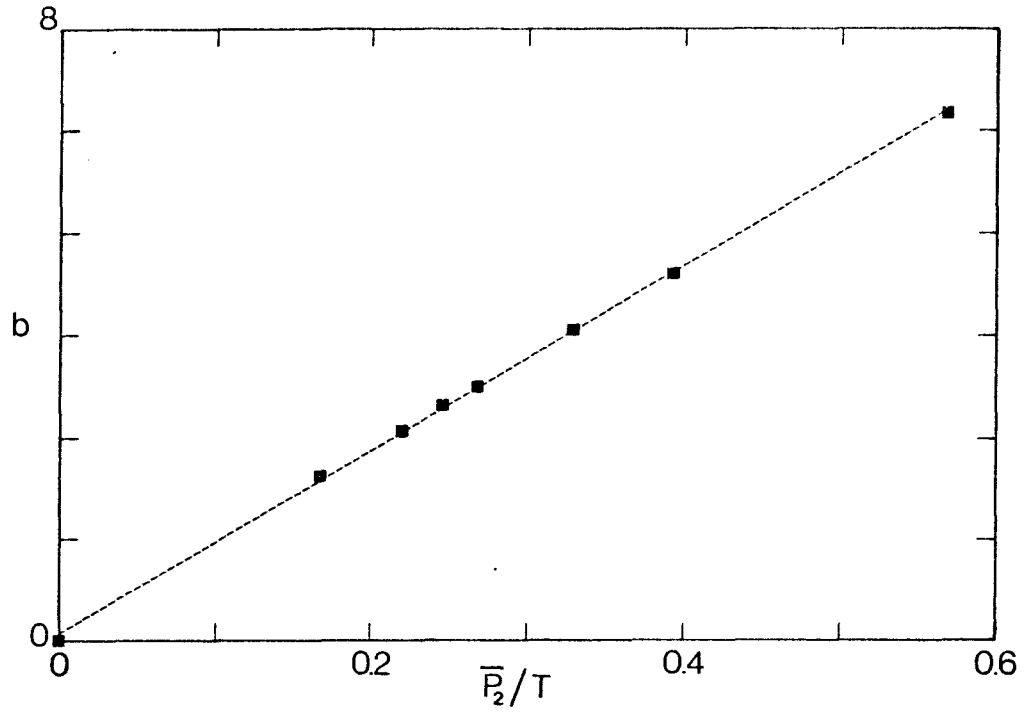

Fig 4.18 The dependence of the coefficient b versus the quantity $\bar{P}_2/T^*$. A linear least squares analysis gives the slope equal to 12.08±0.012 with an intercept of 0.09±0.04.

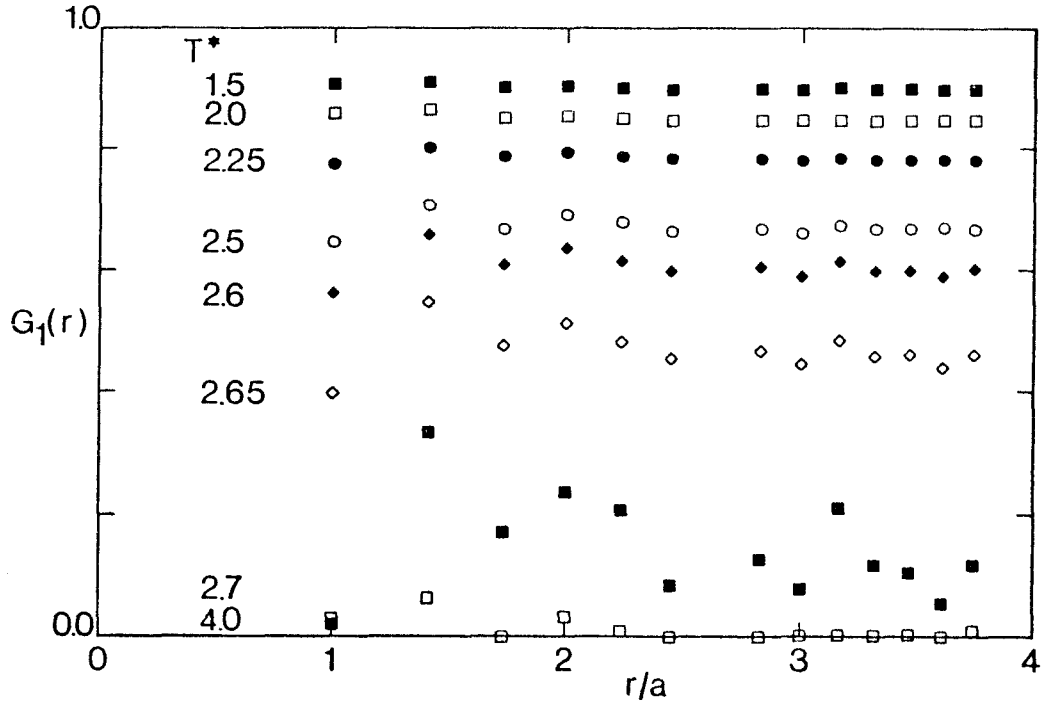

Fig 4.19 The total normalised first rank pair correlation function, $G_1(r)$ as a function of the intermolecular separation, r/a, where a is the nearest neighbour separation.

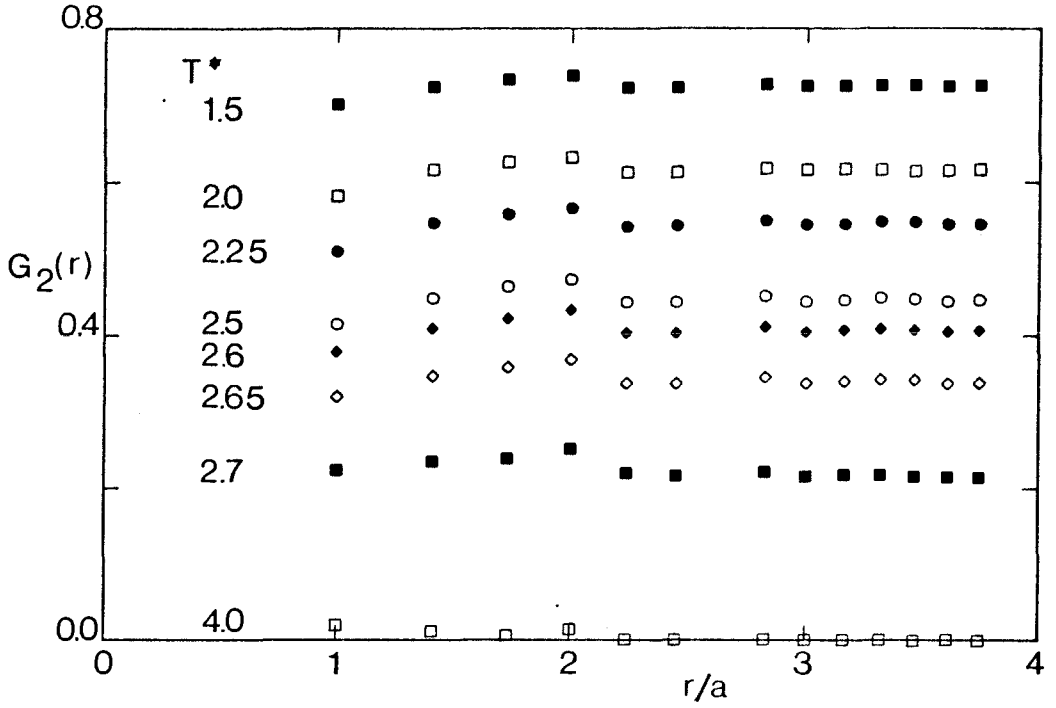

Fig 4.20 The total second rank pair correlation function, $G_2(r)$ as a function of the intermolecular separation, r/a, where a is the nearest neighbour separation.

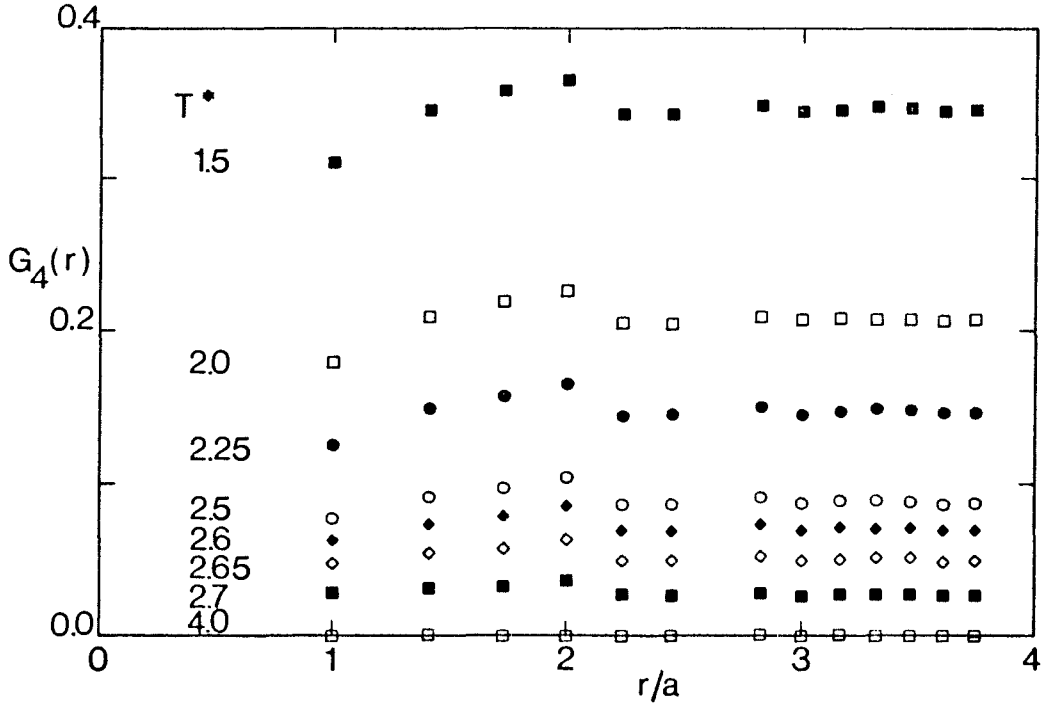

Fig 4.21 The total fourth rank pair correlation function, $G_4(r)$ as a function of the intermolecular separation, r/a, where a is the nearest neighbour separation.

root of $\bar{P}_1$ which we know is zero. However, close observation near the transition (eg at $T^* = 2.7$) does show a slight tendency for the correlations to vanish. The reason for the non-convergance of the dipolar correlations at lower temperatures is not immediately clear, although one explaination is related to the relatively small size of the system in comparison with the long range nature of the dipolar potential. Thus for our system with infinite repeating images of itself there will always be a periodic long range correlation present with a periodicity equal to the cell dimension. Furthermore, the dispersion forces contribution to the potential is mainly responsible for the tendency to align molecules parallel with each other, regardless of the orientation of the dipole. All the dipolar term has to do therefore, is to remove the degeneracy of orientation, with the dipole up or down to give an antiferroelectric state. Thus for increasing temperature, the second rank correlations will decrease because of the decrease in long range order, thus decreasing the first rank angular correlations while the antiferroelectricity in the system remains. So although, overall, the order in the system is decreasing for increases in temperature, the dipolar antiferroelectric correlations remain.

The second and fourth rank order parameter, $\bar{P}_2$ and $\bar{P}_4$ can be calculated from the square of the long range limiting values of $G_2(r)$ and $G_4(r)$ plotted in Figures 4.20 and 4.21. These are also given in Table 4.3 and Table 4.4 and show excellent agreement with values obtained using direct calculation. One interesting feature of the plots is the increased correlations present at r=2a where a is the nearest neighbour separation, being especially obvious for the fourth rank correlation function. Furthermore, the short range correlation at r=a is less than the value at r=2a and even less than the long range limit. This feature is of particular interest in the comparison with the predictions of the Maier-Saupe theory and will be discussed in the next

section.

The results for the six pair correlations functions, $G_1^{||,\perp}(r_{ij})$, $G_2^{||,\perp}(r_{ij})$ and $G_4^{||,\perp}(r_{ij})$ are plotted in Figures 4.22 and 4.23 and 4.24 and listed in Table 4.6, 4.7 and 4.8. The solid and open symbols represent pair correlations parallel and perpendicular to the director axis respectively. In the second and fourth rank cases, both sets of correlations are virtually identical, with the exception of the nearest neighbour contributions, which for all temperatures are smaller for correlations perpendicular rather than parallel to the director axis. Also, as we saw earlier, the correlations are a maximum at r=2a.

The first rank functions clearly indicate how the dipoles within the system are correlated. The molecules parallel to the director exhibit positive correlations for all values of r, thus confirming the molecular tendency to align head to tail, while molecules perpendicular to the director show both positive and negative correlations with nearest and next nearest neighbours antiparallel. However, in the third shell, at r=2a, all the dipoles are parallel, again a result consistant with the antiferroelectric nature of our system.

We now turn to the observation of increased orientational correlations at r=2a and a reduction for nearest neighbours correlations at r=a. Looking at the plots of $G_2^{||,\perp}(r)$ and $G_4^{||,\perp}(r)$ in Figures 4.24 and 4.25, the short ranged nearest neighbour parallel correlations are always less than the perpendicular values, indicating that molecules with intermolecular vectors perpendicular to the director tend to be more correlated than pairs of molecules with intermolecular vectors parallel to the director. Pair potential arguments would suggest the reverse of this is to be expected, since both the nearest neighbour dispersion and the dipolar terms in the pair potential favour nearest neighbour molecules parallel to each other and to the intermolecular vector, rather than parallel molecules

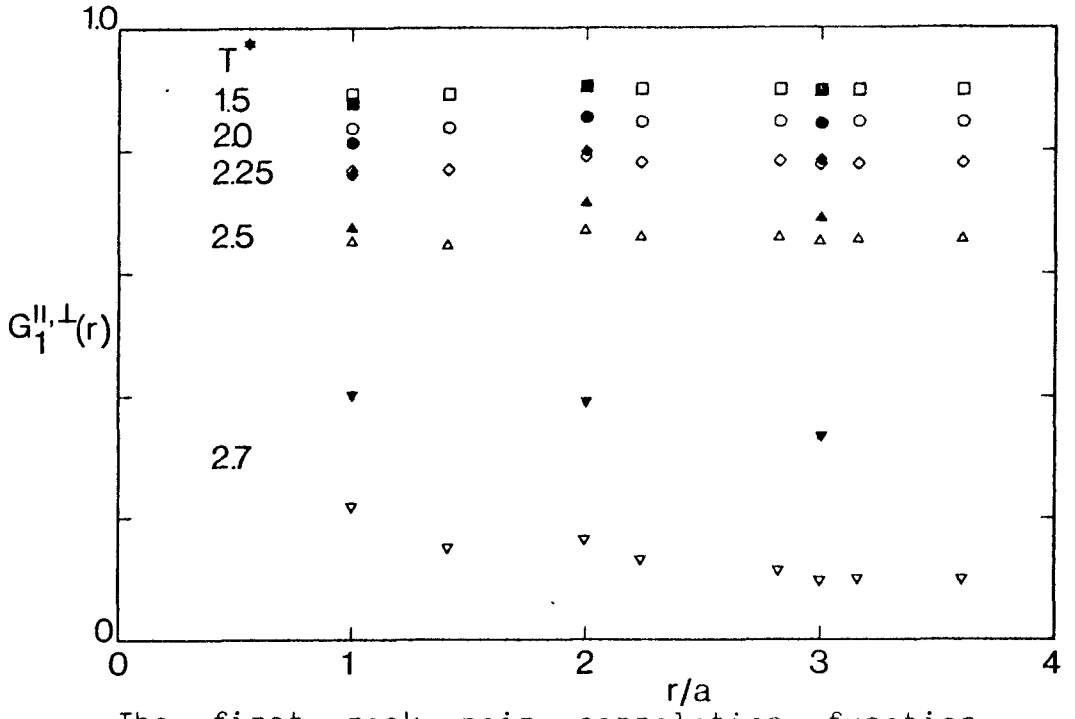

Fig 4.22 The first rank pair correlation function, calculated using pairs of molecules parallel ($G_2^{\parallel}(r)$, the open symbols) and perpendicular ($G_2^{\perp}(r)$, the solid symbols) to the director.

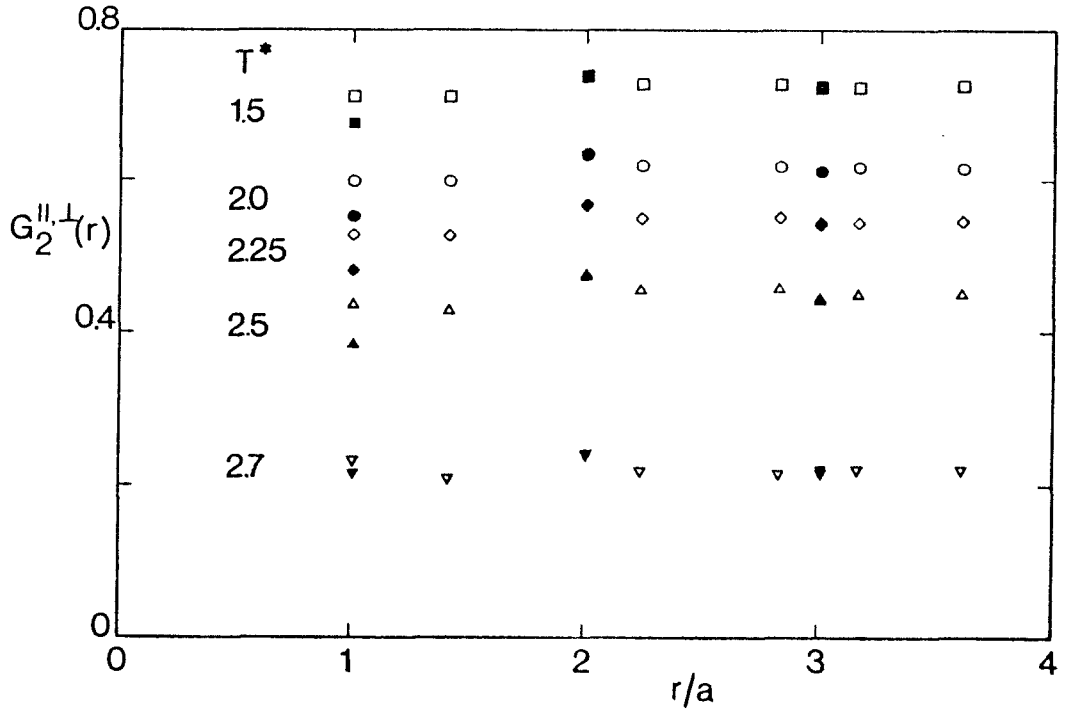

Fig 4.23 The second rank pair correlation function, calculated using pairs of molecules parallel ($G_2^{\parallel}(r)$, the open symbols) and perpendicular ($G_2^{\perp}(r)$, the solid symbols) to the director.

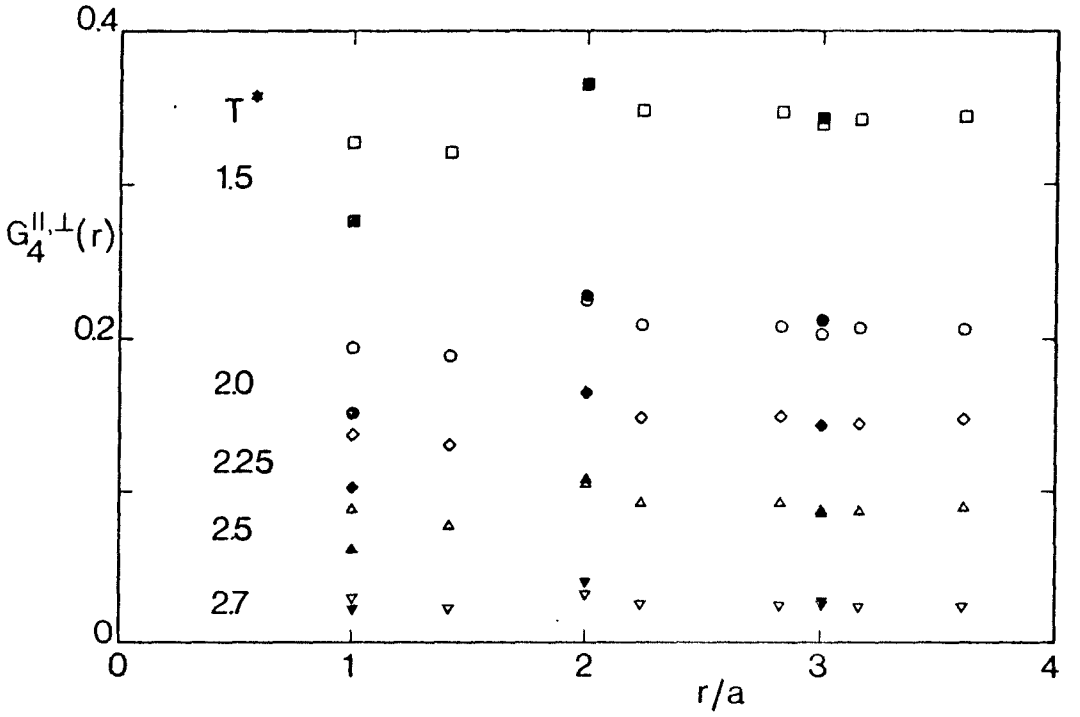

Fig 4.24 The fourth rank pair correlation function, calculated using pairs of molecules parallel ($G_2^{\parallel}(r)$, the open symbols) and perpendicular ($G_2^{\perp}(r)$, the solid symbols) to the director.

perpendicular to the intermolecular vector. This would therefore reverse the order of the short range parallel and perpendicular correlations.

However, the effect of additional correlations of r=2a at the expense of a reduction in nearest neighbour correlations has also been observed in the simulation of particles on a cubic lattice interacting via dipolar forces only (Romano, 1982), and it has recently been suggested that for such a system, a ground state exists in which the potential energy is exactly the same as that in the totally ordered antiferroelectric state, although the order parameter is less than one. (Adams, 1982). Thus it is almost certainly the presence of the full ranged dipolar forces that give this unexpected behaviour in the pair correlation functions. The dominating contribution to the dipolar potential comes from nearest neighbour interactions which favour parallel or antiparallel orientations depending on whether they are parallel or perpendicular to the intermolecular vector. However, a considerable interaction also arises from the twelve molecules in the second coordination shell at r= $\sqrt{2}$a, and from the eight molecules in the third shell at r= $\sqrt{3}$a. The twelve molecules in the second shell consists of four with intermolecular vectors perpendicular to the director axis, while the other eight molecules (assuming them all parallel) make an angle of 45^0 with the intermolecular vector. A similar situation is observed in the third shell where all eight molecular dipoles make an angle of 55^0 or 35^0 with the intermolecular vector. Turning back to the dipolar interaction equation (Equation 4.2) the most stable state with the molecules parallel occurs when the dipoles are parallel to each other and to the intermolecular vector, or antiparallel when perpendicular to the intermolecular vector. However, assuming a reference dipole parallel with the laboratory z-axis, then for an intermolecular vector of 45^0, 55^0 or 35^0 the most stable configuration for the second molecule is at

360^0- 45^0, 55^0 or 35^0 to the intermolecular vector. Indeed, this is a general result for pairs of dipoles in the same plane. Thus for a dipole making an angle Ø with some arbitrary intermolecular vector, the most stable orientation of the second dipole is at 360^0-Ø to the intermolecular vector. So considering a system with the director pinned along the z-axis say, by dominant nearest neighbour dispersion forces, then dipolar forces will assist the stability of pairs of molecules that are parallel or antiparallel and parallel or perpendicular to the director. However, pairs of molecules whose intermolecular vector is not parallel or perpendicular to the director will tend to rotate with respect to it, thus destabilising the whole system slightly. Which will reduce correlations in the second and third coordination shells. This is indeed the case as when $G_2(r)$ and $G_4(r)$ are calculated for the Lebwohl-Lasher (1972) model short range correlations are seen to be much larger than their long range limiting values. (Zannoni, 1979) Therefore, it is the inclusion of long range dipolar forces that tend to reduce correlations up to a seperation of about r=2a. Based on these arguments alone however, nearest neighbour correlations should not be reduced, because here the intermolecular vectors are parallel or perpendicular to the director axis. Thus, the destabilisation between a reference molecule and one in its second shell must also destabilise nearest neighbours via indirect correlations. The same situation arises at r=2a, but as the molecules are more distant from the reference molecule, the net destabilisation is less, therefore the correlations appear greater. Thus a maximum is observed in the pair correlations at r=2a, while shorter ranged correlations are reduced. Furthermore as was previously mentioned in section 4.2, the minimum for antiparallel dipoles, perpendicular to the intermolecular vector, is actually a saddle point. Thus it is energetically more favourable for nearest neighbouring molecules with this

configuration to try and rotate to a configuration of lower potential energy, so again reducing short range correlations. This situation can be reasonably seen in Figure 4.2.

4.5 Comparison of results with theory and other work

In the previous Chapter, we saw how the Maier-Saupe theory fails to predict various properties at the nematic-isotropic transition when compared with those obtained from simulations with particles interacting via a $U_{ij}=-\varepsilon P_2(\cos\theta_{ij})$ type potential. In particular for a six coordinate system, the transition temperature is overestimated by 17%, the order parameter at the transition by 46% and the entropy of transition by over 500%. These failures can partially be attributed to the assumptions in the theory that both long and short range correlations are equal, which the plot of $G_2(r)$ in Chapter 3, has clearly shown to be false. We know that in Maier-Saupe theory the internal energy is related to the short range order parameter σ_2 by:-

$$\bar{U}^* = -\frac{z\sigma_2^2}{2} \qquad 4.39$$

where z is the coordination number. However, it was observed that $\bar{U}^*$ was in relatively good agreement with simulation, although probably due only to the cancellation of errors caused by the overestimation of the temperature and entropy of transition. The long range order parameter at the transition is therefore poor due to the short range order failure. Furthermore, Maier Saupe theory predicts the singlet orientational distributions to depend on second rank terms only, but as we shall see in the next chapter where the singlet distribution is calculated for particles interacting via a second rank potential, fourth rank terms have to be included to fit the exact functional form of the

singlet distribution function.

At this point it is worthwhile comparing the results with those obtained from previous work. The only similar simulation (Humphries et al, 1981) was for molecules interacting via a nearest neighbour dispersion potential only. Here the nematic-isotropic phase transition was reported to be equal to $T^*_{NI} = 2.22$, thus the dipole interaction has shifted the transition by 21%. As we have already seen, the results for the internal energy for this dispersion simulation scaled to the same transition temperature are plotted in figure 4.7 as the crosses and show excellent agreement with the dispersion energy contributions obtained in this simulation.

The predicted molecular field transition temperature occurs at $T^*=2.642$ (Humphries et al, 1981), thus, without any dipolar terms in the potential the transition is overestimated by 18%. However, with these interactions we have seen that the transition is shifted to $T^*=2.75$, now an overestimation of only 4%. This remarkable good agreement can be explained as follows. The transition temperature in the molecular field theory is obtained using the relationship for the change in free energy, ΔA, between the stable and isotropic phases. ie

$$\Delta A = \Delta U - T\Delta S \qquad 4.40$$

where ΔU is the change in internal energy, and ΔS the change in entropy at the transition. We know from equation 4.39 that the short range order parameter is related to the internal energy. Molecular field theory predicts that pair correlations are independent of separation, thus $G_2(r)$ is the same for all r. Hence, the short range order parameter is just the square of the long range order parameter (Zannoni, 1979). As we have seen in the previous section, the effect of dipolar interactions is to reduce short range correlations, and indeed, this simulation does show that the

second (and fourth) rank correlations are virtually independent of separation. As we have seen in Chapter 3, in the simple Lebwohl-Lasher model, short range correlations are evaluated to be greater than long range correlations, thus the transition temperature in the molecular field theory is overestimated as it takes no account of these excess short range correlations. Therefore in a simulation in which correlations are in accord with those predicted by theory, we would expect much better agreement with the transition temperature. Furthermore, the transition temperature depends on the entropy (see equation 4.40). However, the entropy is related to the n-body distribution function (Luckhurst, 1979) which, in the molecular field limit is a function of the singlet orientational distribution function. We have seen that the singlet distribution functions fit very accurately the Maier-Saupe functional form, thus the entropy at the transition will be in much better agreement. With good agreement for the two terms in equation 4.40 we would expect reasonable agreement with the transition temperature, which is indeed the case.

The Maier-Saupe predic-tions of $\bar{P}_2$ and $\bar{P}_4$ are shown on figure 4.9 as the solid curves and also show excellent agreement with the simulated values. Table 4.4 lists the simulated values of $\bar{P}_4$ together with the theoretical prediction calculated using a value of ε in the theory scaled such that the second rank order parameters are indentical. Within experimental error, the fourth rank order parameter obtained in this way is equal to that calculated in the simulation, thus indicating the success of the Maier-Saupe theory in predicting the ratio of $\bar{P}_2$ to $\bar{P}_4$.

However, the above arguments assume that the dipolar terms in the pair potential in the simulations have no direct effect on the internal energy and entropy in equations 4.40. In otherwords, the dipolar terms simply reduce short range correlations. Therefore, taking no account of the dipolar contribution to the internal energy

and comparing only the dispersion energy we see that Maier-Saupe theory predicts reasonably well the dispersion energy at the transition as shown by the solid curve in Figure 4.23. In addition, the entropy of transition calculated from the change in the dispersion contribution to the total energy only is $\Delta S/Nk=0.45\pm0.05$ which again is in excellent accord with the molecular field prediction of $\Delta S/Nk=0.417$.

We now return to the comparison of the singlet orientational distribution functions with molecular field theory. Figure 4.18 shows the linear dependence of the coefficient b versus $\bar{P}_2/T^*$, the slope of which is 12.08 ± 0.12 and has an intercept of 0.09 ± 0.04. The Maier-Saupe prediction is 12, being the product of the coordination number and a factor of 2, arising because of the pseudo potential derived for anisotropic dispersion forces. (Humphries et al, 1981). Therefore again the dipolar term in the pair potential has fortuitiously given very good agreement with molecular field prediction.

We can now make a brief comparison with other theories proposed to attempt to explain the effect of dipolar interactions on nematic order. The earliest work, although not designed specifically for the explaination of nematic order was developed by Krieger and James (1954). This work contains all the important elements of the Maier-Saupe theory, together with the effect of P_1 interactions. They assume an interaction potential of the form:-

$$U(\beta_{ij}) = AP_1(\cos\beta_{ij}) + BP_2(\cos\beta_{ij}) \qquad 4.41$$

for various ratios of the coefficients A and B. Obviously for A=0 the Maier-Saupe form is reached. Although this pseudo-potential is not strictly representative of a true dipolar interaction, since the P_1 interaction, like the P_2 term is totally independent of the orientation of the intermolecular vector, it does indicate that for certain

ratios of A/B various transitional effects do occur. For example for small values of A, at temperatures below the nematic-isotropic phase transition, a second order transition occurs in which the dipoles in the system become disordered. For larger values of A, however, this second order transition collapses and now the temperature of the nematic-isotropic transition increases and approaches infinity as A tends to infinity. This is obviously the region in which this simulation was carried out, and is clearly in accord with our observations of the increase in transition temperature with the inclusion of dipolar interactions. However, because of the extreme simplicity of this theoretical model it is not very informative to make a more quantitative comparison. This theoretical work also includes a refinement, in that Chang's constant coupling method (Chang, 1937) is applied, ie the effect of an infinite field of molecules on the orientations of two molecules rather than one, as in the simple molecular field treatment. The predictions however are still in agreement with a shift in the transition temperature. This later treatment has also, been applied (Madusudana and Chandrasekhar, 1975) to the relatively successful prediction of the temperature dependence of dielectric constants. To date, however, a more realistic analytic theory describing the effects of true dipolar interactions has yet to be developed.

Finally in this chapter we make a tentative prediction of values for the kirkwood correlation factor, g_1, for our system, and in particular $g_{||}$ and $g_{\perp}$. This can be defined as (Kirkwood, 1939; Ben-Reuven and Gershon, 1969):-

$$g_1 = 1 + \int_c^{\infty} G_1(r_{ij}) dr_{ij} \qquad 4.42$$

Earlier we have seen how the convergence to zero of the first rank pair correlation was hampered by the long range antiferroelectricity in our system caused by the regular

repeating periodicity of the boundary conditions. Therefore the integral in the above equation, at least for our system, will never converge, thus making it impossible to estimate g_1. However, we can make guesses at the values of $g_{||}$ and $g_{\perp}$ from the correlation functions $G_1^{||}(r)$ and $G_1^{\perp}(r)$ respectively. The unnormalised plot in figure 4.22 shows that perpendicular to the director the molecules tend to align antiparallel, thus, the integral in equation 4.42 will vanish, giving an average $g_{\perp}$ correlation of about 1, whilst molecules parallel to the director are all parallel, giving in our case $g_{||}$ less than or equal to 8. For larger systems this value will very slowly converge to some very large value.

Finally, a few concluding remarks related to the inclusion of dipolar interactions into the total pair potential. We have seen that with dipolar interactions present all the essential properties previously simulated in anisotropic systems remain. Furthermore, we have seen that they tend to destabilise short range interactions giving, fortuitiously maybe, excellent agreement with the predictions of Maier-Saupe theory. Therefore this simulation has allowed us to understand more fully the effect of various assumptions made in such a simple theory, and hopefully this understanding can be applied to future theories.

Chapter 5

The Effect of External fields

5.1 Introduction

As we have seen in Chapter 3 the calculation of important distribution functions in computer simulations of nematic liquid crystals can be difficult because of fluctuations in the orientation of the director. In a real nematic, in the absence of any external force the director orientation appears isotropically distributed, so experiments are usually conducted in the presence of external fields, where a combination of two effects occur. In magnetic fields greater than about 0.1T the director becomes aligned, either parallel or perpendicular to the field. At this stage the director still fluctuates, although on average it is fixed. However, on increasing the field the director fluctuations eventually become quenched and finally at fields much higher than present technology will permit, the molecular fluctuations are predicted to become quenched. The quenching of the director modes has been observed experimentally by Poggi and Filippini (1977) in 7CB (Malraison et al 1980). They used magnetic fields up to 120KOe and observed that the optical birefringence (which is approximately proportional to the order parameter) increased linearly with the field. Indeed, this increase in order as a result of the quenching of the director fluctuations has been predicted theoretically by de Gennes (1974). More recent work by Keyes and Shane (1979) has lead to the belief that at very large fields a critical point would occur, since they observed that the latent heat of the nematic-isotropic phase transition reduces with increasing field. However work by Rosenblatt (1982) on 8CB in fields up to 187KOe suggests that the critical point is not as close as it was originally believed.

Molecular field theory, for example (Wojtowicz and Sheng, 1974) predicts that on increasing the external field in a nematic system, the latent heat of transition should indeed decrease until a critical point is reached when the nematic and 'isotropic' phases become identical. This point, however will be discussed in detail later in this chapter. To date only one simulation has been reported for an anisotropic system in an external field (Vieillard-Baron, 1974), although in this case the field was excessively large resulting in the director pinning at the expense of an almost total quenching of the molecular fluctuations.

The objectives of this chapter are therefore as follows: to investigate the magnitude of the external field required to quench the director fluctuations, without, hopefully, affecting the molecular modes and to look at the behaviour of the system in a large magnetic field. The first point would therefore allow the calculation of various distribution functions, for example, the singlet orientational distribution function and in addition, the pinning of the director would in principle provide a route to the calculation of the Frank elastic constants, either directly using a Freedericksz transition technqiue (Freedericksz and Tsvetkov, 1933) or indirectly from the singlet distribution function and direct correlation functions (Poniewierski and Stecki, 1979).

5.2 The Model

As in Chapter 3, the relatively sucessful Lebwohl-Lasher (1972) has been used with the system subject to an external field. The molecules, therefore, are taken to be cylindrically symmetric with their centres located on the sites of a simple cubic lattice and interacting via the pair potential:-

$$U_{ij} = \epsilon_{ij} P_2(\cos\beta_{ij}) \qquad 5.1$$

where $P_2(\cos\beta_{ij})$ is the second Legendre polynomial, β_{ij} is the angle between the symmetry axes of molecules i and j, and ε_{ij} is the positive constant, ε, if molecules i and j are nearest neighbours, but is zero otherwise. In order to incorporate a magnetic like external field a term is added to the pair potential such that each molecule experiences a second rank interaction of the form:-

$$U_i^{field}/\varepsilon = -\chi P_2(\cos\beta_i') \qquad 5.2$$

where β_i' is the angle between the symmetry axis of the i^{th} molecule and the direction of the applied field. χ is a constant governing the strength of the external field, which for a magnetic field will be a function of the flux density, B, and dependent on the anisotropy of the diamagnetic susceptibility $\Delta\chi$. In these calculations we take χ to be positive so that the molecules will tend to lie parallel with the field. The total potential energy of a system of N molecules is:-

$$U_{tot}/\varepsilon = -\frac{1}{2}\sum_i^N \sum_j^N P_2(\cos\beta_{ij}) - \sum_i^N P_2(\cos\beta_i') \qquad 5.3$$

where the factor of 1/2 arises because all i and j interactions are counted twice in the double summation. We can also define the average internal energy per particle $\bar{U}^*$ as:-

$$\bar{U}^* = \bar{U}/N\varepsilon \qquad 5.4$$

Throughout the simulations a reduced temperature is used, defined as:-

$$T^* = kT/\varepsilon \qquad 5.5$$

In order to investigate the pinning of the director by the external field two methods can be adopted. The Q-tensor could either be averaged over the entire production stage, from which the average director could be extracted from the eigenvectors, or two order parameters could be calculated, one with respect to the field defined as:-

$$\bar{P}_2^{field} = \overline{P_2(\cos\beta_i')} \qquad 5.6$$

where β_i' is as defined previously and the other order parameter with respect to the director.

In this simulation the second method was used, since averaging the Q-tensor over the entire production run presents some computational problems. The order parameter with respect to the director axis was calculated by setting up the Q-tensor (Buckingham, 1967) at the end of each cycle (1 cycle = N attempted moves), where:-

$$Q_{ab} = \frac{1}{N}\sum_{i=1}^{N} \overline{(3l_a^{(i)}l_b^{(i)} - \delta_{ab})/2} \qquad 5.7$$

and a and b denote the laboratory x,y and z axes. $l^{(i)}$ are the direction cosines describing the orientation of the i^{th} molecule with that laboratory axis. The largest eigenvalue of the diagonalised tensor, the order parameter, defined as:-

$$\bar{P}_2 = \overline{P_2(\cos\beta_i)} \qquad 5.8$$

was averaged at the end of each cycle over all cylces during the production stage of the simulation. Here β_i is the angle

between the i^{th} molecule and the director axis. Clearly for a system in which the external pinning field is zero, there will be no prefered director orientation, thus $\bar{P}_2$ (field) will be zero if sufficient configurations are generated, and conversely in a system in which the director is totally pinned both order parameters will be identical.

5.3 Computational details

Using the Lebwohl-Lasher model described earlier three different systems were studied.

System A

Here the properties of 1000 particles were evaluated as a function of the applied external field at an angle of 10^0 to the laboratory z-axis and with an azimuthal angle of 0^0. The temperature was kept constant at $T^* = 1.0$.

System B

This was identical with system A except that in order to achieve a smaller perturbation to the order with the pinning of the director, a larger system of 8000 particles was studied. The field was applied along the laboratory x-axis.

System C

In this case, the properties of 1000 molecules were investigated as a function of the reduced temperature T^*, but with the external field constant at a value of $X = 0.2$ parallel to the laboratory z-axis.

For systems A and C, the angular variables were stored as $\cos\theta$ and ϕ, where θ and ϕ are the spherical polar angles defining the orientations of the molecular symmetry axes in the laboratory frame. A new configuration

was generated initially in the following way. The new value of cosθ was chosen from a distribution of random numbers in the range of +1 to -1, while the azimuthal angle Ø was incremented according to:-

$$\emptyset_{new} = \emptyset_{old} + \Delta\xi \qquad 5.9$$

where again ξ is a random number uniformly distributed in the range of +1 to -1 and Δ is the maximum permitted displacement. However for these two systems (A and C), in which the external field is at 10^0 and parallel with the z-axis, it was found impossible to achieve a good acceptance-rejection ratio. This failure stems from the alignment of the director close to the z-axis, since the energy of such a large system is almost totally independent of the azimuthal angle of the molecules, the angle which we use to control the acceptance-rejection ratio. This difficulty was overcome by incrementing cosθ in a similar way to Ø, but ensuring that its value was maintained within the permitted limits of +1 and -1, such that if it exceeded +1 by an amount λ then a value of -1+λ was taken, and less than -1 a value of 1-λ was used. This can be expressed mathematically as:-

$$\cos\theta_{new} = \cos\theta_{old} + \Delta_\theta\xi \qquad 5.10$$

where Δθ is the maximum allowed displacement for cosθ. If $\cos\theta_{new}$ was greater than +1 or less than -1, the following action was taken.

$$\cos\theta_{new} = \cos\theta_{new} - 2\,\mathrm{sgn}(\cos\theta_{new}) \qquad 5.11$$

where sgn ( ) is a function returning the value of +1 and

-1 if $\cos\theta_{new}$ is positive or negative respectively. An alternate solution would have been to apply a field at a much larger angle to the z-axis. Indeed, this was the case in System B where the field was applied parallel with the x-axis, although in this simulation the molecular orientations were stored as their respective direction cosines. Thus new orientations were generated using the algorithm of Barker and Watts (1969), in which a laboratory axis is selected at random, and a random rotation of a controlled maximum amount performed about this axis. (see Chapter 2)

In all three systems the starting configuration was taken to be a completely ordered state with the particles parallel with the laboratory z-axis. In systems A and B the first simulations were with an external field strength of X=0.1 with T^*=1.0. In both cases the first run consisted of an initial equilibration stage of approximately 10 million configurations, during which time the eigenvectors from the Q-tensor did indeed show that the director had reorientated parallel with the external field, and a production run of 10 and 48 million configurations for systems A and B respectively. Subsequent runs at new field strengths were generally started from the configuration taken at the end of the production stage from the simulation with the closest value of X, with equilibration stages of typically 2 and 16 million configurations, and production stages of 10 and 48 million configurations respectively for systems A and B. In addition, for system B, some of the runs at lower external field strengths were started from totally random states to ensure that the director pinning was caused by the field and not as a consequence of the size of the system causing the director to remain fixed. For system C, the first run was at T^*=1.0 with typical equilibration and production stages of 2 and 8 million moves respectively. The starting configuration for additional higher temperatures was taken as the final production stage configuration at the closest, lowest temperature.

Furthermore, in systems A and B, a run was performed in which the singlet distribution function was calculated. This as achieved by dividing the range for $|\cos\beta'_1|$ into 100 equal intervals. At the end of each cycle, the number of particles with orientations within these intervals was evaluated and averaged over 1000 cycles for both systems. For model A the singlet distribution function was calculated at a reduced temperature of $T^*=1.1146$ ($T^*/T^*_{NI} = 0.997$, where $kT_{NI}/\varepsilon = 1.118$ (Zannoni, 1979) and the director pinned in an external field of $X=0.1$. This temperature corresponds to a reduced temperature similar to that used in the x-ray scattering determinations of $f(\beta)$ for 4-4'-di-n-octyl-oxyazoxybenzene (Leadbetter and Norris, 1979). In system B however, a temperature of $T^*=1.0$ and an external field of $\chi=0.05$ was used.

5.4 Discussion of Results

For systems A and B, the observed dependence of the two order parameters are plotted in Figures 5.1 and 5.2, with the solid and open squares representing $\bar{P}_2^{field}$ and $\bar{P}_2$ respectively. (Both sets of results are also listed in Tables 5.1 and 5.2). The internal energy, U^* is plotted in Figures 5.3 and 5.4 respectively for the two systems. In Figure 5.1 for system A which contains 1000 particles, it can be seen that the director is not pinned until $X \sim 0.2$, with the order parameters equal to about 0.69 in contrast with the zero field value of about 0.63. Hence the director becomes pinned, although at the expense of a 7% increase in the orientational order parameter $\bar{P}_2$. However for system B, where the two order parameters are plotted in Figure 5.2 as a function of X, a much lower external field is required to pin the director, with $\chi=0.01$ and a perturbation to the order parameter from 0.61 at zero field to that of 0.62 at $X=0.01$, an increase of only 2%. This result is in accord with our expectations in that as the number of particles in the system increases, the pinning field will decrease by a

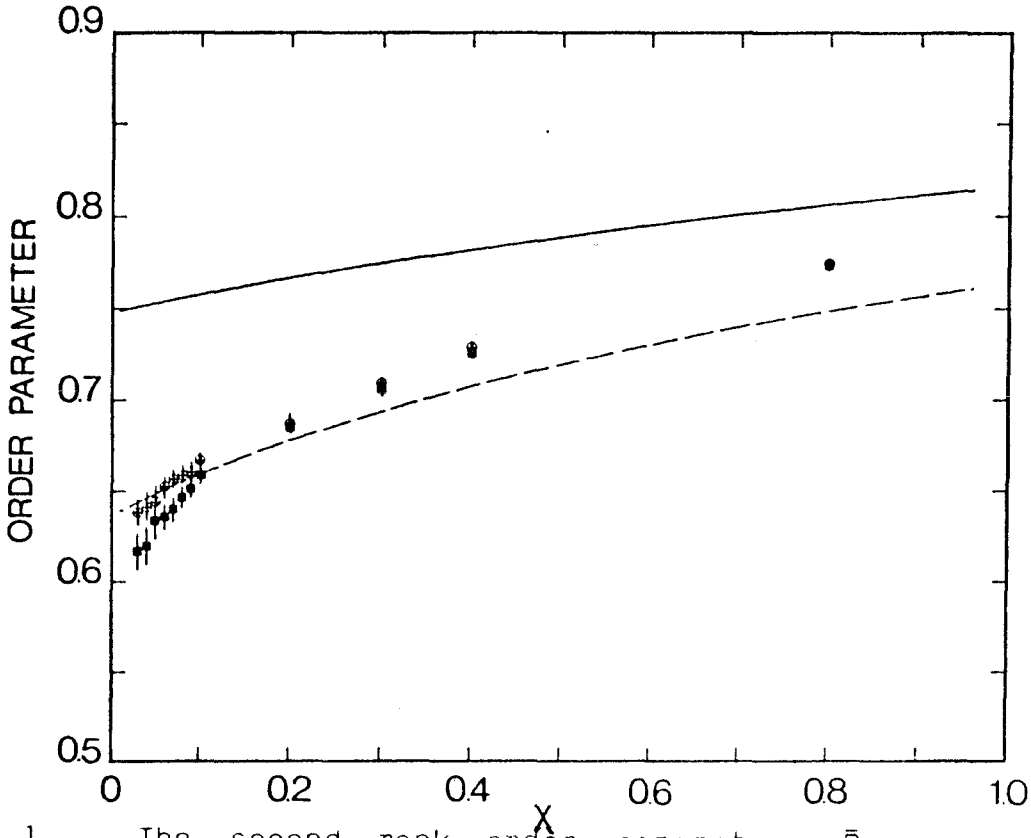

Fig 5.1 The second rank order parameter, $\bar{P}_2$, as a function of the external field, χ^*, for system A at a reduced temperature of $T^* = 1.0$. The open and solid symbols are $\bar{P}_2$ calculated with respect to the director and field respectively. The solid and dashed curves are the Maier-Saupe predictions calculated at the same reduced temperature and scaled to the same zero field transition temperature respectively.

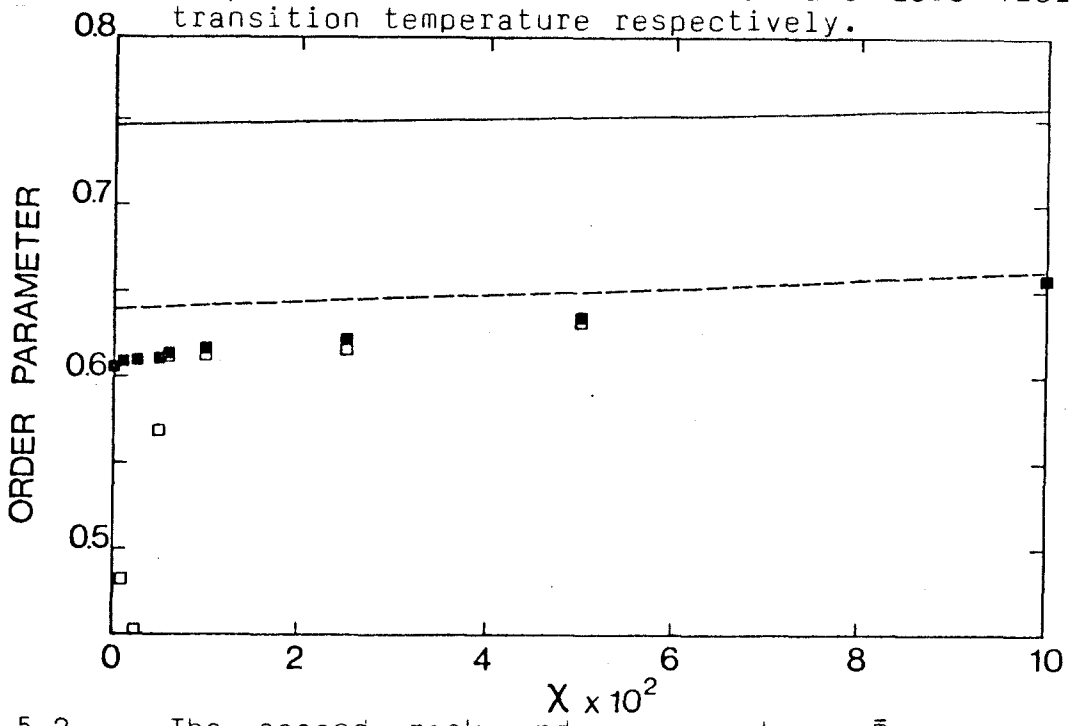

Fig 5.2 The second rank order parameter, $\bar{P}_2$, as a function of the external field, χ^*, for system B at a reduced temperature of $T^* = 1.0$. The open and solid symbols are $\bar{P}_2$ calculated with respect to the director and field respectively. The solid and dashed curves are the Maier-Saupe predictions calculated at the same reduced temperature and scaled to the same zero field transition temperature respectively.

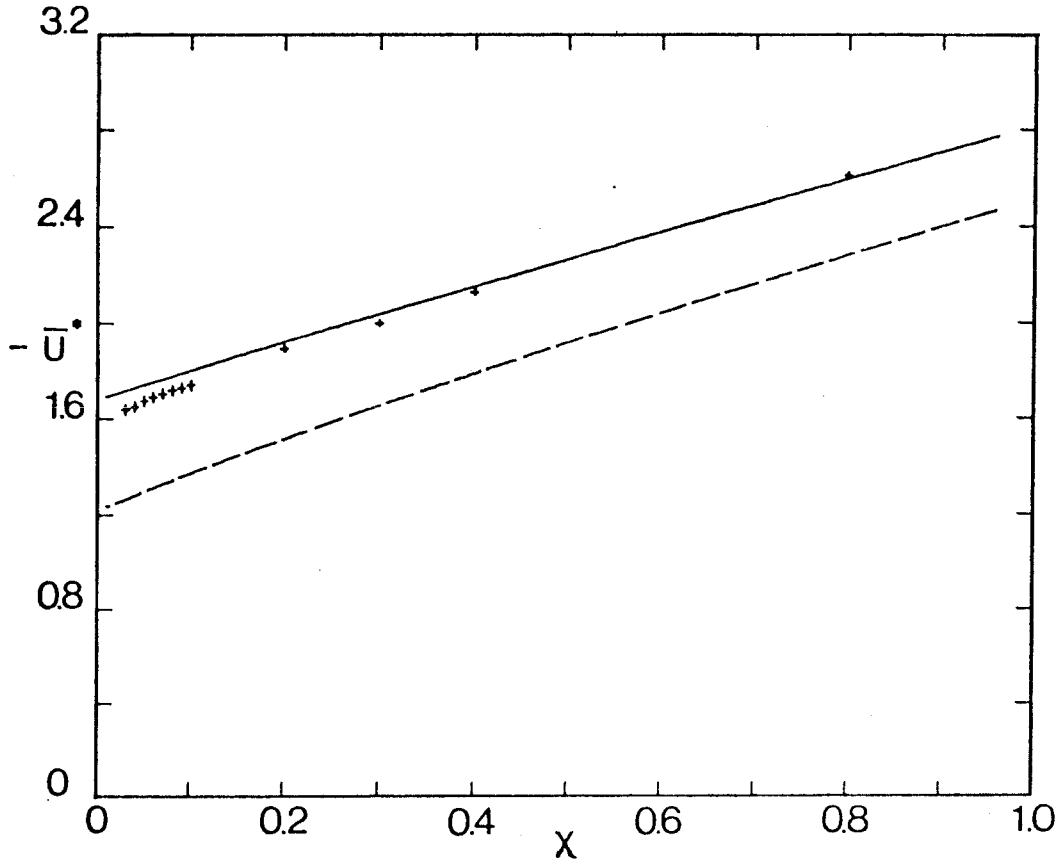

Fig 5.3 The scaled internal energy, $\bar{U}^*$ for system A as a function of the external field, χ, at a reduced temperature, T^* of 1.0. The solid and dashed curves are the Maier-Saupe predictions calculated at the same reduced temperature and scaled to the same zero field transition temperature.

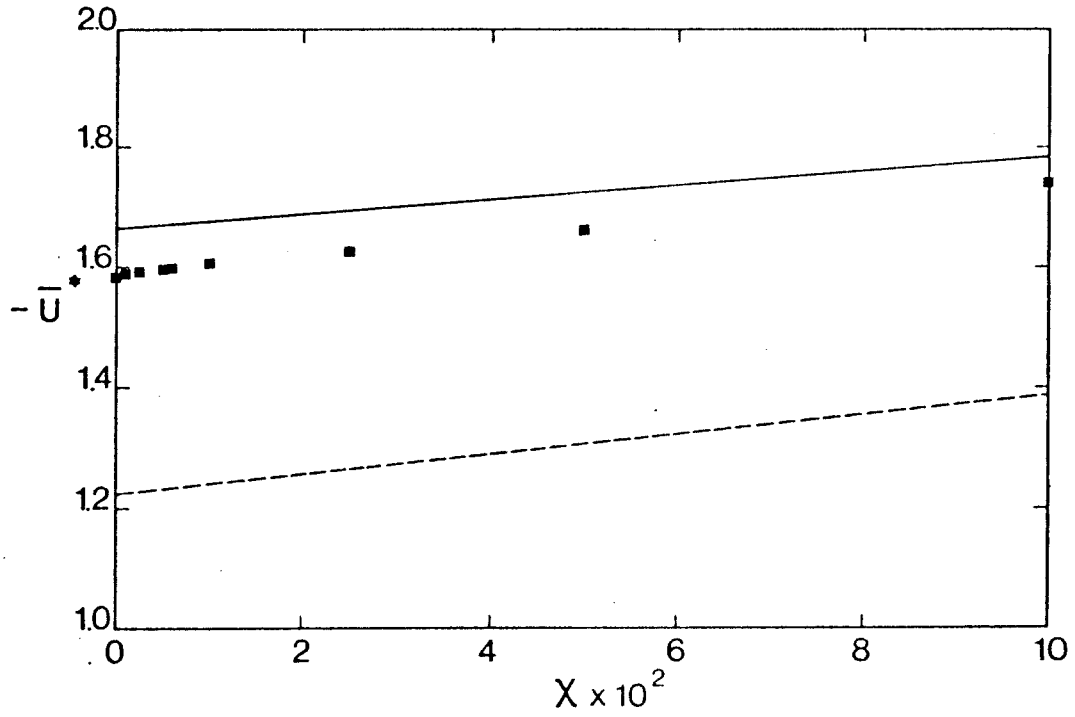

Fig 5.4 The scaled internal energy, $\bar{U}^*$ for system B as a function of the external field, χ, at a reduced temperature, T^* of 1.0. The solid and dashed curves are the Maier-Saupe predictions calculated at the same reduced temperature and scaled to the same zero transition temperature.

proportional amount, since the pinning force arises directly from the field interactions which are dependent on the number of particles in the system. Furthermore, as the size of the system increases we would expect the perturbation to the order parameter to be less at the point at which the director becomes pinned. Experimentally this effect has been observed, where, for fields of up to 187kOe in 8CB (Rosenblatt, 1982) the order parameter does increase slightly although as a consequence of the quenching of director and not in our case as a result of moleculer fluctuations.

In these simulations, if we assume the anisotropy in the diamagnetic susceptibility to be 1.25×10^{-7} erg G^{-2} cm^{-3} (Stinson and Lister, 1970) and $kT/\epsilon = 1.32116$ for the molecular field transition temperature, then a simulation field of $X=0.1$ actually corresponds to a real magnetic field of about 100 Megaoersted, thus the fields in these simulations actually correspond to very high unrealistic values. (Wojtowicz and Sheng, 1974).

The results for the singlet distribution functions calculated for systems A and B are shown in Figures 5.5 and 5.6 as the crosses. These agree qualitatively with the functions measured experimentally (Leadbetter and Norris, 1979) and a quantitative comparison will be made later.

Finally, we turn to the properties calculated for system C. Figure 5.7 shows the temperature dependence of the order parameter $\bar{P}_2$ as the solid squares at a constant field strength of $X=0.2$, and Figure 5.8 shows the total internal energy as a function of T^* as the solid squares. In addition these results are listed in Table 5.3. The open symbols marked on both plots indicate the results observed for the same system in the absence of an external field (Zannoni, 1979). Two features immediately obvious are that at a specific temperature the internal energy and order parameter are increased by about 15%, and the order parameter and internal energy are much more continuous

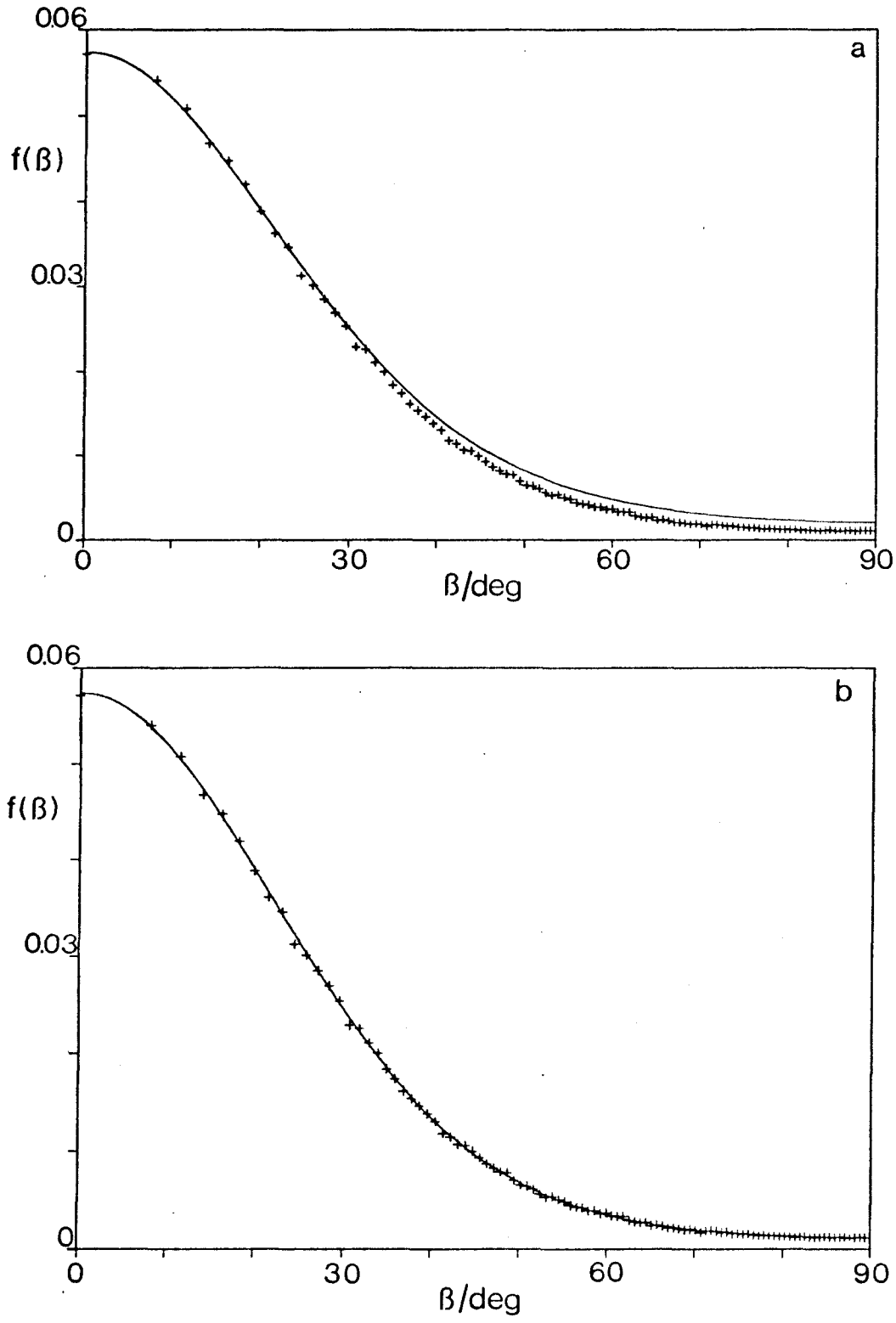

Fig 5.5 The singlet orientational distribution function calculated from system A with $T^* = 1.1146$ and $\chi=0.1$. The lines in 5.5a and 5.5b show the fits obtained using equations 5.25 and 5.27 respectively.

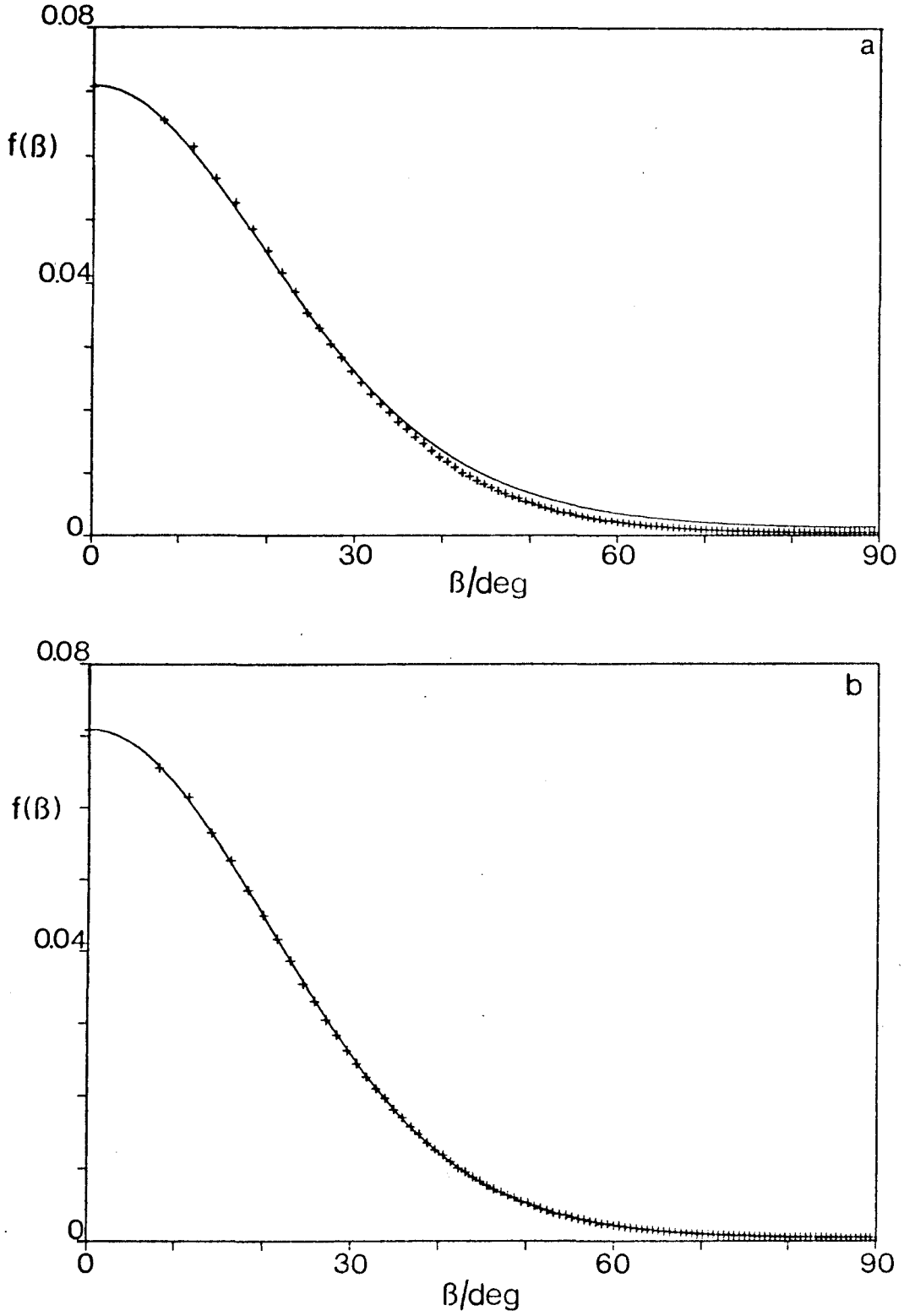

Fig 5.6 The singlet orientational distribution function calculated from system B with $T^* = 1.0$ and $\chi = 0.05$. The lines in 5.6a and 5.6b show the fits obtained using equations 5.25 and 5.27 respectively.

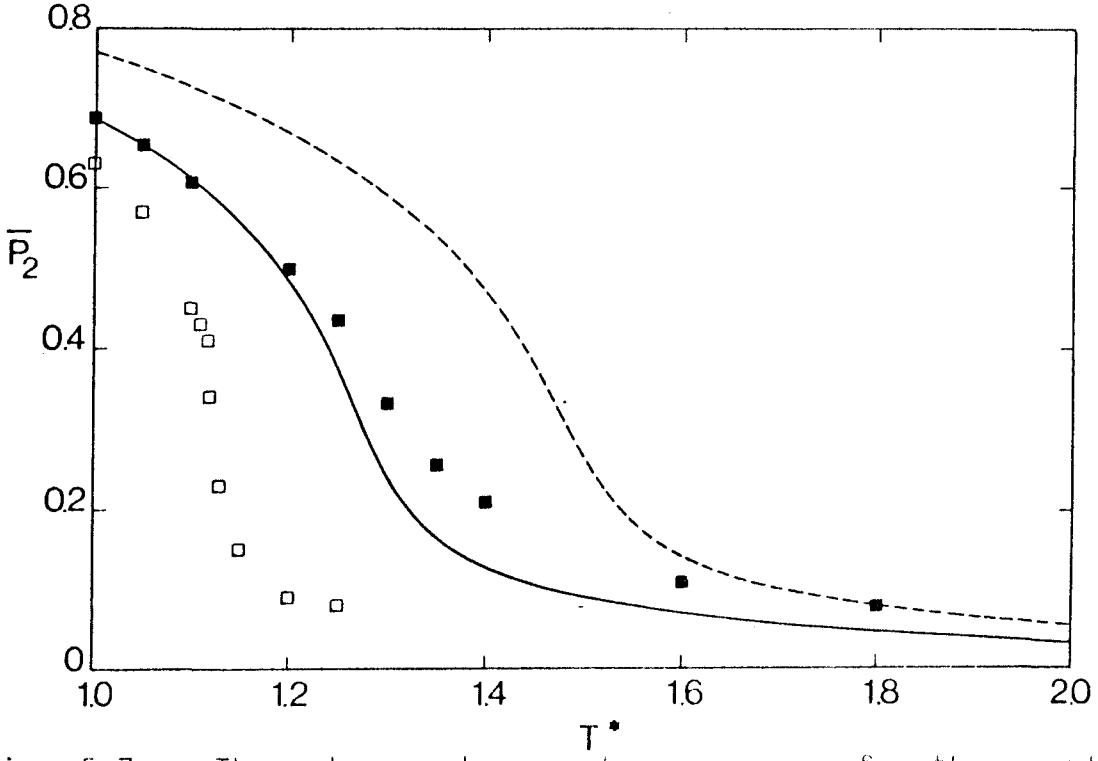

Fig 5.7 The temperature dependence of the order parameter calculated for system C, shown as the solid squares, at an external field of $\chi = 0.2$. The open squares are results obtained by Zannoni (1979) with $\chi = 0.0$. The dashed and solid curves are the Maier-Saupe predictions at the same reduced temperature and scaled to the same zero field transition temperature, respectively.

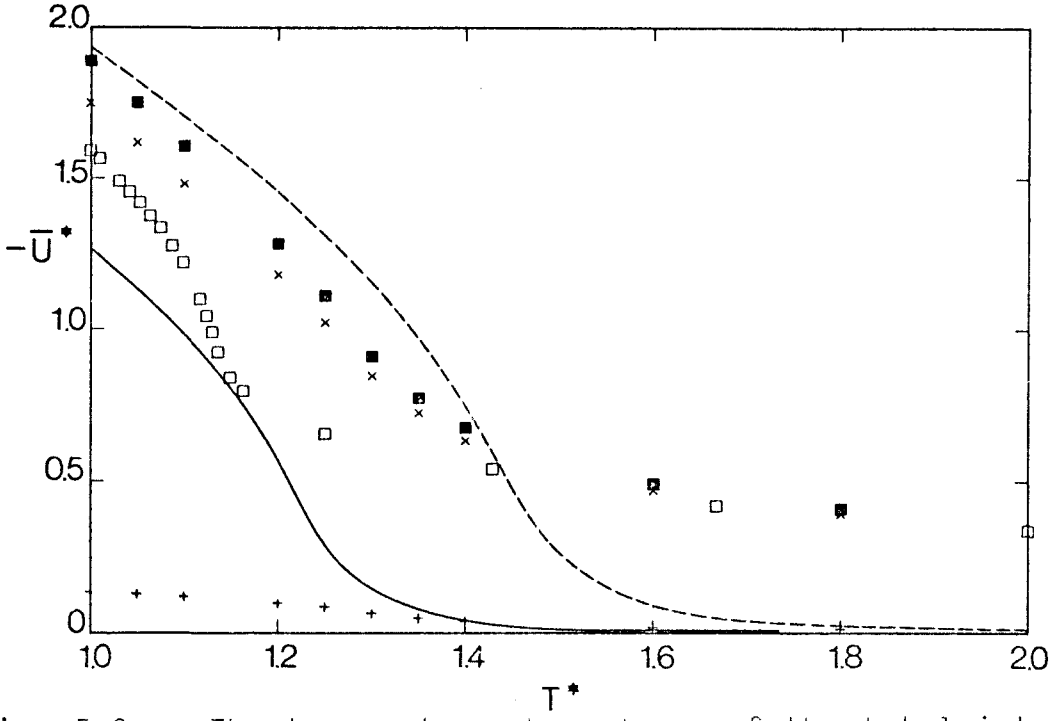

Fig 5.8 The temperature dependence of the total internal energy, calculated for system C, shown as the solid squares. The '×' and '+' represent the contributions to $\bar{U}^*$ arising from nearest neighbour and field interactions respectively, and the open squares are results obtained by Zannoni (1979) on a similar, system with $\chi = 0$. The dashed and solid curves are the Maier-Saupe predictions at the same reduced temperature and scaled to the same zero field transition temperature respectively.

through the transition as compared with the zero field simulation data.

At this point we can determine the heat capacity at constant volume using a numerical spline fitting procedure and obtaining the derivative of the internal energy with respect to temperature, since:-

$$C_v^* = (\partial \bar{U}^*/\partial T^*)_v \qquad 5.12$$

The solid squares on Figure 5.9 indicate C_v^* calculated in this manner, and show a maximum at $T^* = 1.30 \pm 0.05$. These values are also listed in Table 5.3. At the maximum value of C_v there is no divergence and this feature will also be discussed in the next section, where a comparison with molecular field theory will be made. The open squares correspond to C_v in the absence of an external field. (Humphries, 1982).

5.5 Comparison with Maier-Saupe molecular field theory

As we have seen in earlier chapters, the anisotropic single particle potential of mean torque, in the absence of any fields or higher rank terms is predicted to be:-

$$U(\beta) = -\epsilon z \bar{P}_2 P_2(\cos\beta) \qquad 5.13$$

However, in the presence of an external field of the form used in these simulations this becomes:-

$$U(\beta) = -\epsilon(z\bar{P}_2 + X)P_2(\cos\beta) \qquad 5.14$$

where z is the coordination number, which is 6 for a simple cubic lattice. The Maier-Saupe form of the singlet distribution function is therefore:-

$$f(\beta) = \exp(-U(\beta)/kT)$$

$$= \exp\left[\varepsilon/kT(z\bar{P}_2 + X)P_2(\cos\beta)\right]/Z \qquad 5.15$$

where, Z, the orientational partition function is:-

$$Z = \int_0^{\pi} \exp\ \varepsilon/kT(z\bar{P}_2 + X)P_2(\cos\beta)\ d\cos\beta \qquad 5.16$$

Hence the second rank order parameter in an external field is:-

$$\bar{P}_2 = Z^{-1}\int_0^{\pi} P_2(\cos\beta)\ \exp(\varepsilon/kT(z\bar{P}_2 + X)P_2(\cos\beta))d\cos\beta \qquad 5.17$$

and the internal energy per particle is:-

$$\bar{U}^* = -(z\bar{P}_2^2 + 2X\bar{P}_2)/2 \qquad 5.18$$

The predictions using this theory for the long range orientational order parameter as a function of external field at a reduced temperature of $kT/\varepsilon = 1.0$ is shown as the solid curves in Figures 5.1 and 5.2. As we have seen in Chapter 3, the molecular field theory overestimates the nematic-isotropic phase transition when compared directly with computer simulations, thus, at similar reduced temperatures the theoretically predicted order parameter is expected to be overestimated. This prediction is confirmed by the disagreement between the solid curves and data points in Figures 5.1 and 5.2. However, if the error arising from the transition temperature overestimation is removed, by scaling to the same zero field transition temperature reasonably good agreement is found, as indicated by the dashed lines in these two plots. In this case, the nematic

isotropic transition temperatures were taken to be $T^*_{NI} = 1.118$ and 1.125 for systems A and B respectively.

A similar comparison can be made for the internal energy with the aid of equations 5.17 and 5.18. The results of the theoretical predictions at the same reduced temperature are shown as the solid curves in Figures 5.3 and 5.4. Surprisingly at the same reduced temperatures of $T^* = 1.0$, much better agreement is obtained than when the temperature in the theory is scaled to the same zero field transition temperature, as shown by the dashed curve in Figures 5.3 and 5.4. This unusual reversal arises from the fact that for our model system the internal energy is related to the short range order parameter σ_2 and the long range order parameter by:-

$$\bar{U}^* = -(z\sigma_2 + 2X\bar{P}_2)/2 \qquad 5.19$$

where

$$\sigma_2 = \overline{P_2(\cos\beta_{ij})} \qquad 5.20$$

and i and j are nearest neighbours. We know from Chapter 3 that moleculer field theory underestimates σ_2 and overestimates the nematic-isotropic transition temperature and the order parameter at the transition. This results in a fortuitious cancellation of errors, since at the same reduced temperature the order parameter will be overestimated while the short range order parameter is underestimated, therefore giving good agreement in the simulated and predicted value of $\bar{U}^*$. Consequently, when we remove the overestimation in $\bar{P}_2$ by scaling to the same zero field transition temperature, the failure in the short ranged order parmeter becomes apparent by significantly underestimating the internal energy.

Before comparing system C with the molecular field

theory it is worth examining the theoretical predictions further. Figure 5.10 shows the temperature dependence of the order parameter $\bar{P}_2$, calculated using equation 5.17, at different external field strengths. At zero field, the curve describing $\bar{P}_2$ bends back on itself and as we have seen in Chapter 1 actually goes through a metastable state, while with large fields the curve is continuous and only approaches zero at infinite temperatures. Furthermore, at $X=0$ a solution exists at all temperatures with $\bar{P}_2=0$, although this solution vanishes in the presence of an external field. In order to locate and investigate the stability of the ordered phases, the Helmholtz free energy must be evaluated. We start with the entropy, S, which, according to molecular field theory is:-

$$S = -\frac{Nk}{Z}\langle \ln(f(\beta))\rangle \qquad 5.21$$

where, as before

$$f(\beta) = \exp(\varepsilon/kT(z\bar{P}_2 + X)P_2(\cos\beta))/Z \qquad 5.22$$

Hence

$$S = -Nk\frac{\varepsilon}{kT}(z\bar{P}_2 + X)\bar{P}_2 + Nk\ln Z \qquad 5.23$$

Thus

$$\frac{A}{NkT} = \frac{1}{2}z\frac{\varepsilon}{kT}\bar{P}_2 - \ln Z \qquad 5.24$$

which is identical to the expression for the free energy in the absence of an external field.

The difference in free energy, $\Delta A/NkT$, between the phase of order, and a phase of zero order is plotted in

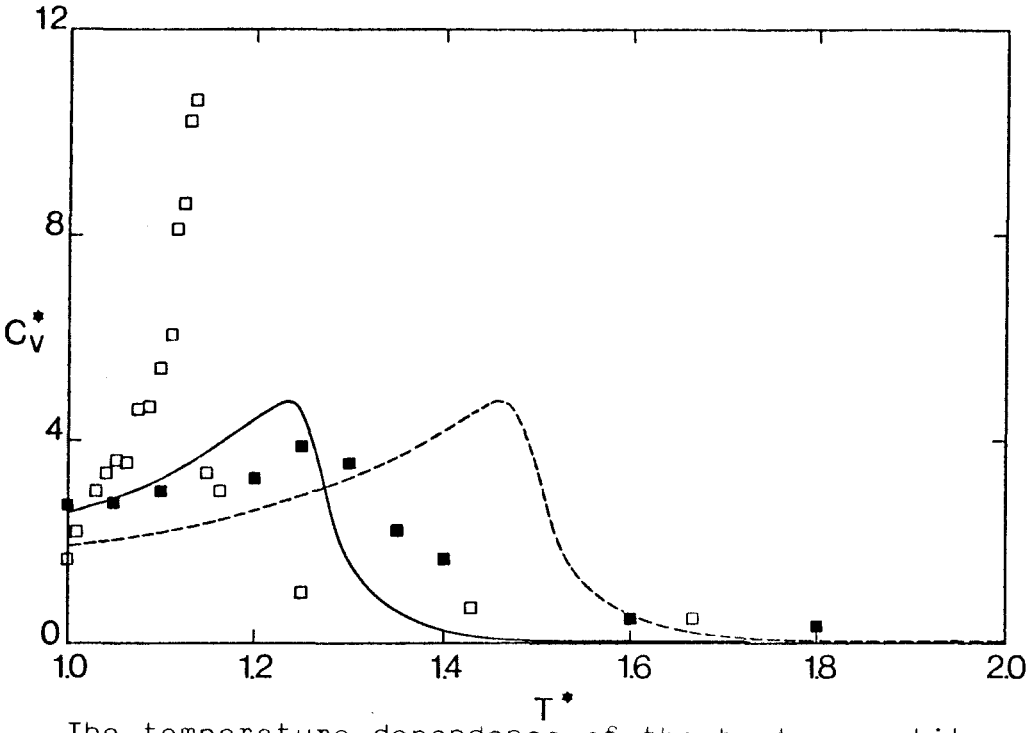

Fig 5.9 The temperature dependance of the heat capactity at constant volume for system C, shown as the solid squares. The open squares are results obtained in the absence of an external field (Humphries, 1982). The dashed and solid curves are the Maier-Saupe predictions calculated at the same reduced temperature, and scaled to the zero field transition temperature, respectively.

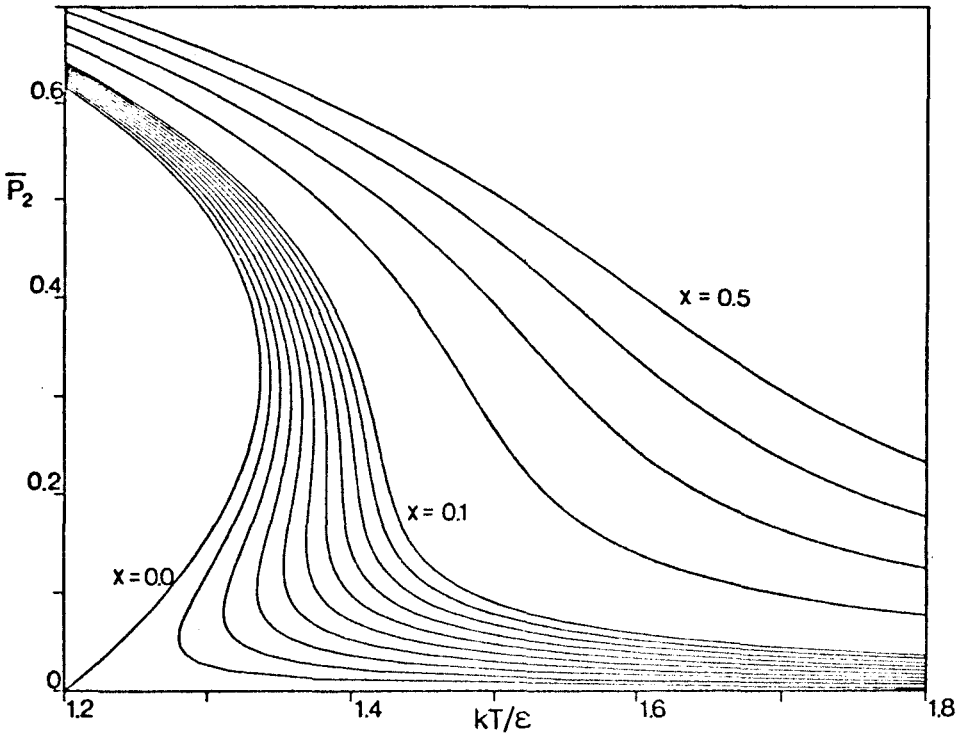

Fig 5.10 The orientational order parameter, $\bar{P}_2$ as a function for kT/ε for field strengths ranging from 0.0 to 0.5 as predicted by the modified Maier-Saupe theory via equation 5.17, with a coordination number of 6.

Figure 5.11 as a function of reduced temperature, kT/ε, for various external field strengths. As we have seen in Chapter 1 for the normal Maier-Saupe theory, the self consistancy relationship given by equation 5.17 for $\bar{P}_2$ has a solution of $\bar{P}_2 = 0$ for all temperatures provided $X=0$, and in the range of $kT/\varepsilon = 1.2$ to $kT/\varepsilon = 1.337$ a third non-negative solution of $\bar{P}_2$ exists. This can be seen in Figure 5.10 for the curve with $X=0$. To determine which of these ordered phases are stable we have to examine the free energy. Thus, looking at the free energy, starting at the extreme left hand side of the $X=0$ curve in Figure 5.11 the curve gradually increases to a maximum at $kT/\varepsilon=1.337$ and then suddenly drops back and remains positive until $kT/\varepsilon=1.32116$. This is the region in which a third non-negative lower solution of $\bar{P}_2$ exists, and because the free energy of this portion of the curve is the larger value of the two possible solutions it is actually metastable. The free energy then becomes negative and the stable nematic phase is reached. In addition, a solution in which $\Delta A/NkT=0$ exists corresponding to a stable isotropic phase at temperatures greater than $kT/\varepsilon=1.32116$. Thus a first order transition between an ordered and an isotropic phase occurs at $kT/\varepsilon=1.32116$.

When external fields of up to $X=0.063$ are applied a similar situation arises. Here, as with the zero field case, a first order transition occurs, although now from the nematic phase, to, a phase of lower order, a paranematic phase. In addition, a metastable state also exists as indicated by the 'loops' in the free energy. On increasing the field strength the change in the order parameter at the transition gradually decreases since the order in the paranematic phase increases and $\bar{P}_2$ in the nematic phase decreases. Thus the latent heat of transition decreases until at a value of $X=0.063$ a critical point occurs in which the transition no longer occurs as first order. Thus at this

critical point the transition becomes second order (Wojtowicz and Sheng, 1974) although for higher fields no transition occurs at all since both phases now become identical. This critical point can be more readily seen in Figure 5.12, where the first order phase transition temperature, between the nematic and paranematic (or isotropic at $X=0$) is plotted as a function of the applied external field. On the lower right hand side of the curve the stable nematic phase exists while on the other side the field induced paranematic phase is stable. Therefore at fields greater than $\chi = 0.063$, no transition occurs between these two phases.

Returning to the simulation of system C, it is clear that for a field of $X=0.2$ we are well beyond the critical point. On the basis of molecular field theory alone we would not expect a transition to occur. Indeed the plots of the order parameter and internal energy as a function of temperature in Figure 5.7 and 5.8 support this conclusion, since they are more continuous through the transition region than we would expect for similar sized systems interacting via a simple P_2 potential.

The dashed curve in Figure 5.7 shows the molecular field prediction and as expected overestimates the order parameter at the same scaled temperature. As before, to remove the failure of the overestimation of the transition temperature the solid curve shows the dependence of the order parameter with the temperature scaled such that the transition temperatures at zero field are identical. In the region of high order, very good agreement is now found, although in the high temperature region the molecular field prediction underestimates the order. This failure probably arises from the known failure of the simulation using the normal Lebwohl-Lasher model to obtain a zero order parameter

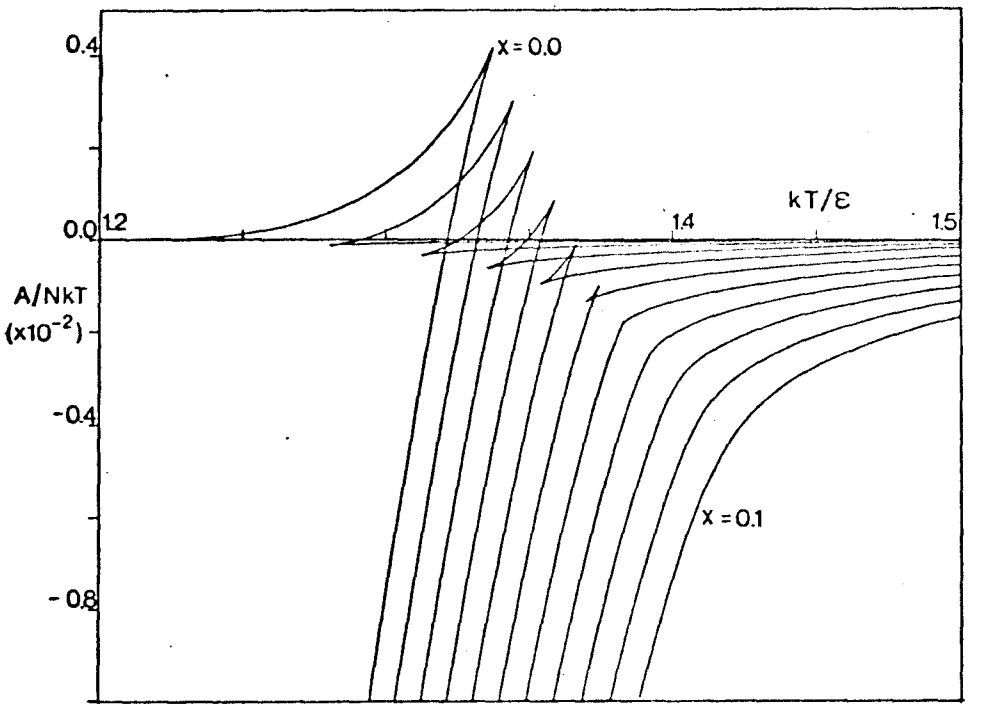

Fig 5.11 The Helmholtz free energy, A/NkT as a function of kT/ε for field strengths ranging from 0.0 to 0.1 as predicted by Maier-Saupe theory using equation 5.24 with a coordination number of 6.

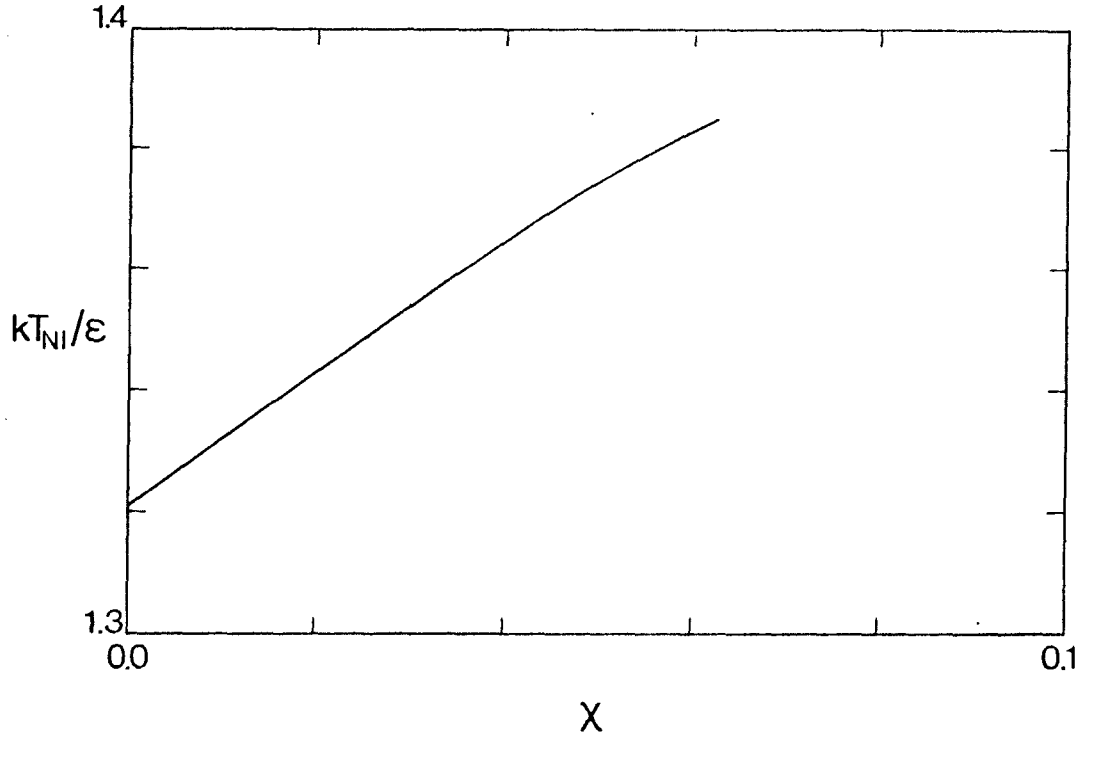

Fig 5.12 The transition temperature of the Maier-Saupe theory in an external field as a function of the external field for a coordination number of 6. Between fields of χ = 0 and χ = 0.063 a first order phase transition occurs, although this ceases to exist for higher field strengths.

in the isotropic phase due to finite size effects.

The internal energy calculated using equation 5.18 is compared with the simulated values in Figure 5.8. As before, the dashed curve represents the molecular field prediction evaluated at the same scaled temperature. In the low temperature region, of high order, the agreement is very good, again due to the fortunate cancellation of errors explained previously in the discussion of system A and B. However, the agreement with the theoretical values at high temperatures is very poor. This is a consequence of the theory predicting the short range order parameter, σ_2, to be zero in the isotropic phase in the zero field case, where in fact it is not. From equation 5.19, which is

$$\bar{U}^* = -(z\sigma_2 + 2X\bar{P}_2)/2 \qquad 5.19$$

the internal energy depends predominantly on the value of σ_2, since in this case X=0.2 and $\bar{P}_2$ is less than 1, while z=6. Using this equation the energy contributions from the short range order and the external field on the long range order have been evaluated and are plotted as the 'X' and '+' respectively on Figure 5.8. As expected the contribution from the external field is very small. An interesting observation is that in the high temperature region, where the short range order is poorly estimated, the long range order is reasonable well predicted by the theory so it is not surprising that the agreement between the field contribution (which depends on $\bar{P}_2$) is good in this temperature region.

In comparing the thermodynamic properties of the theory and simulation we now turn to the heat capacity calculated at constant volume. Figure 5.9 shows the Maier-Saupe prediction calculated using a finite difference procedure to evaluate $(\partial U/\partial T)_V$. The curve is continuous throughout the entire temperature range and is in accord with the

observation that at X=0.2 the system is above the critical point beyond which a transition occurs between a phase of high and lower order. Furthermore, the shape of the curve is almost identical to that calculated by spline fitting the internal energy from the simulation, given by the solid squares, thus confirming the non-existance of a transition in the simulation.

Finally, we turn out attention to the singlet distribution functions obtained from the simulations of A and B. These results are plotted as the crosses in Figures 5.5 and 5.6 for systems A and B respectively. In 4'4-di-n-octyloxyazoxybenzene, the form of the singlet orientational distribution function is found to be similar to that predicted by molecular field theory. (Leadbetter and Norris, 1979). Hence

$$f(\beta) = \exp(aP_2(\cos\beta))/Z \qquad 5.25$$

In order to fit the simulated singlet distribution function, several methods could be adopted, for example, taking logs of both sides would allow a linear least squares analysis. However, this method proved unsatisfactory as it resulted in a much better fit to the 'tail' of the distribution function, which has less physical importance. Alternatively a non linear least squares fit could have been used, although in this case, problems arose because the fitting procedure entered different minima on the error surface for the 1000 and 8000 particle systems, causing inconsistancies to arise in the direct comparison of the parameters a and Z. In addition, two points could have been extracted from the simulated function and used simultaneously in equation 5.25. This is the method which was finally adopted, and since the long tail is both statistically and relatively physically unimportant, the two points chosen were the first point at $\beta=0$, and the point at half height, i.e. the point at $f(\beta)$ =

$f(\beta)_{max}/2$. This method has the advantage of giving a consistent fit to both sets of simulated data. The fits obtained in this manner are plotted in Figures 5.5a) and 5.6a) as the solid curves for systems A and B respectively and are seen to be good, although not perfect. The values for a and Z for systems A and B are given in Table 5.4. The value of a=2.21 for system A agrees reasonably well with that obtained experimentally of a=2.0 at the same reduced temperature (Leadbetter and Norris, 1979). However, in view of the complexity of the pair potential for a real nematagen as compared with our idealised model system this comparison will not be taken further.

We can however, compare the results with the predictions obtained from the molecular field theory, since, in this case:-

$$a = \varepsilon/kT(z\bar{P}_2 + \chi) \qquad 5.26$$

Firstly for system A, if we set $kT/\varepsilon = 1.1146$ (as used in the simulation) the molecular field theory yields an order parameter, $\bar{P}_2$ of 0.698 at $X=0.1$, which gives a=3.87. Again, this overestimation of 55% is exactly what is expected since the theory overestimates the transition temperature, and hence at the same scaled temperature will over predict $\bar{P}_2$. A similar behaviour is seen in system B, where the simulated value of a is 2.69 whereas, molecular field theory gives it as 4.56 an overestimation of 52%. This overestimation can be in part accounted for by scaling the systems to the same transition temperature, in particular, the transition temperature at zero field. Thus for system A, the transition temperature in the zero field model occurs at $kT_{NI}/\varepsilon=1.118$ (Zannoni, 1979). Using the molecular field prediction of $kT_{NI}/\varepsilon = 1.32116$ allows us to scale with these temperatures giving a value of a=2.45, which differs from the simulated value by only 10%. However, doing the same scaling for the larger system B, using, the value of

$kT_{NI}/\varepsilon=1.127$ (see Chapter 3) for the simulated transition temperature, gives an unexpected proportionally higher value of a=3.41, a difference of 24%. The origin of the worse prediction for a in system B is not immediately obvious. One possible reason is as follows: without any scaling we would expect the coefficient, a, to be overestimated by molecular field theory, since at the same reduced temperature theory gives a higher value of $\bar{P}_2$ which is related directly to a (c.f. Equation 5.26). Furthermore, the order parameter at the theoretically predicted transition temperature is overestimated, and also at the two temperatures used in the simulation, in systems A and B, where molecular field theory predicts $\bar{P}_2$ to be 0.698 and 0.752, a difference of 30% and 19% respectively from the simulated values of $\bar{P}_2$ = 0.52 and 0.611. Thus when scaling to the same zero field transition temperatures two effects have to be considered. Although the error caused by the overestimation of the transition is removed, an error caused by the overestimation of the order parameter has to be appreciated. The values of $\bar{P}_2$ when scaled to the same transition temperature at zero field, however, are 0.524 and 0.656 for systems A and B respectively, so actually scaling to the same transition temperature, fortuitiously removes the error in the order parameter more in system A than in system B which is at a lower temperature. Hence the agreement simply by scaling to the same transition temperature is better in system A than in system B.

This effect can also be seen if a third comparison is made, this time by removing the error associated with $\bar{P}_2$. So comparing at the same $\bar{P}_2$ values gives the coefficient a in the theory as 2.45 and 3.05 respectively for systems A and B. In this case a similar proportioned overestimation of 10% and 12% respectively is observed for both systems.

The fact that good agreement cannot be made whatever scaling is performed to remove various sources of error, is probably as a consequence of the singlet orientational

distribution function not obeying the Maier-Saupe molecular field form exactly, which consists of second rank terms only. However, in general we may expand the potential of mean torque, $U(\beta)$ as the infinite series:-

$$U(\beta)/kT = \sum_{L(even)\neq 0} a_L P_L(\cos\beta) \qquad 5.27$$

If we truncate this series to include second and fourth rank terms only, an approximation which has been proved successful by Humphries et al (1972), then we are able to obtain perfect agreement for both singlet distribution functions as shown by the solid curves in Figures 5.5b) and 5.6b). The fits were obtained using a non linear least squares procedure. In this case the values of Z, a_2 and a_4 are 220±5, 2.70±0.06 and -0.16±0.02 for system A, and 205±50, 3.43±0.06 and -0.27±0.02 for system B respectively. For both situations, although the simulation consists of second rank interactions only, higher rank terms in the potential of mean torque have to be included in order to predict the exact form of the singlet distribution function. Furthermore, it has been shown that fourth rank terms are required to fully account for the temperature dependance of $\bar{P}_2$ measured experimentally, (Humphries et al, 1972) thus justifying the addition of fourth rank interactions in the pseudo potential of mean torque. However, this could be as a consequence of effects from the alkyl chain present in the molecules used for comparison, since in 4-4'dimethoxyazoxybenzene, the ratio of a_4/a_2 was -0.187, although for the diethyl analogue the best ratio was found to be +0.116.

Finally a few concluding remarks. In this Chapter we have seen that we are able to pin the director in our model liquid crystal and for the 20x20x20 particle system, the perturbation to the order parameter is minimal. This allows very easy calculation of the singlet orientational

distribution function and the director pinning will be exploited further in the next chapter. Furthermore, the properties of the system beyond the magnetic critical point have been investigated and they agree within our expectations of the predictions of the molecular field theory.

Chapter 6

Computer simulation studies of surface alignment in nematics and their elastic constants

6.1 Introduction

One of the most common methods used to measure the Frank (1958) elastic constants of a nematic liquid cystal is to observe the Freedericksz effect. This technique involves subjecting the nematic to two opposing torques (fields), one of which is inhomogeneous. Normally this is achieved by sandwiching the nematic between two glass plates, treated in such a way that the director aligns either parallel or perpendicular to the surfaces, and applying a magnetic or electric field orthogonal to the director axis. At low external fields no change is observed and the director remains pinned by the surfaces. However, at a critical field the director at the centre of the cell starts to realign and continues to do so here and throughout the rest of the nematic as the field is increased, this effect is shown in Figure 1.5. From a knowledge of the geometry of the surface pinning forces, the direction of the external field and the value of the critical field one of the three elastic constants can be calculated. Further information about one of the other two elastic constants can also be obtained from the way in which the director changes beyond the critical point with varying external field.

The aim of this chapter is therefore twofold: Firstly to simulate the effect of surface aligning forces on the director, order parameter and thermodynamic properties for a nematic and secondly to attempt to observe the Freedericksz transition and hence evaluate the elastic constants.

The model nematogen used for the Monte Carlo simulation is the relatively successful Lebwohl-Lasher (1972) model. This model has the advantage of being relatively simple

while retaining all the essential physics required to describe the major physical properties (with the exception of spatial disorder) of a nematic liquid crystal. Furthermore, it can be compared easily with the predictions of the Maier-Saupe molecular field theory. The model consists of cylind-rically symmetric molecules with their centres of mass restricted to lie on the sites of a simple cubic lattice. The molecules interact via the pair potential:-

$$U_{ij} = -\epsilon_{ij} P_2(\cos\beta_{ij}), \qquad 6.1$$

where β_{ij} is the angle between the symmetry axes of molecules i and j, $P_2(\cos\beta)$ is the second Legendre polynomial and ϵ_{ij} is a positive constant, ϵ, if molecules i and j are nearest neighbours, but is otherwise zero. In order to incorporate surface forces, the model was modified slightly. The system was divided up into layers defined to lie parallel to the x-y plane. Surfaces were introduced simply by removing the periodicity in the z direction, although retaining normal periodic boundary conditions in the remaining two dimensions. Surface pinning was achieved by fixing the molecules in the top and bottom layers in some predefined direction. In reality this situation can be envisaged in two ways, either as the surface molecules exerting an infinite field prooucing total order in the first layer of molecules or alternatively, the perfectly ordered layers can be regarded as being the surface which applied a weaker constraint to the system bulk.

In order to simulate the Freedericksz transition an external magnetic field interaction was applied identical to that used in the previous chapter, ie

$$U_i^{field}/\epsilon = -\chi P_2(\cos\beta'_i), \qquad 6.2$$

where χ is a positive constant controlling the field strength and β_i' is the angle between the molecular symmetry axis and the external field. Thus for molecules with a positive anisotropic diamagnetic susceptibility the molcular symmetry axis aligns parallel with the field.

6.2 Molecular field theory

One of the assumptions used in the derivation of the Maier-Saupe molecular field theory, is that the system has uniaxial symmetry about the defined z-axis. Clearly, the Freedericksz transition removes the uniaxial symmetry and as a consequence this theory cannot be used in this case. However, it can be employed to describe the effect of surface forces on a nematic where uniaxial symmetry does prevail. We begin with the generalised expression for the potential of mean torque (Humphries et al, 1972):-

$$U(\beta) = \sum_{L(\text{even})} u_L \bar{P}_L P_L(\cos\beta). \qquad 6.3$$

To reduce the infinite number of terms in this expression we shall restrict our attention to second rank interactions only and so u_2 can be replaced by $z\varepsilon$ where z is the lattice coordination number giving:-

$$U(\beta) = - z\varepsilon \bar{P}_2 P_2(\cos\beta) \qquad 6.4$$

In a uniaxial system, sandwiched between two plates, the order parameter will clearly vary throughout the cell (although the variation could be very small), will have a minimum value at the centre and will be symmetric about this point. Therefore, a molecule in the sample will experience a molecular field generated by molecules at the same vertical distance from the surface, and an inhomogeneous field created by a region of molecules of higher and lower order.

In making a comparison with our simple cubic lattice system, the coordination number z, will be 6. If we define the system to consist of layers, parallel to the surfaces, then a molecule will experience the field created by four molecules in the same layer with an order parameter $\bar{P}_2^i$, say, and one above and below with order parameters $\bar{P}_2^{i+1}$ and $\bar{P}_2^{i-1}$ respectively. Thus the potential of mean torque becomes:-

$$U(\beta) = -\epsilon(4\bar{P}_2^i + \bar{P}_2^{i+1} + \bar{P}_2^{i-1})P_2(\cos\beta), \quad 6.5$$

where β is the orientation of the molecule in the i^{th} layer. The singlet orientational distribution function is therefore:-

$$f(\beta) = \frac{1}{Z} \exp\left(-\frac{\epsilon}{kT}(4\bar{P}_2^i + \bar{P}_2^{i+1} + \bar{P}_2^{i-1})\, P_2(\cos\beta)\right) \quad 6.6$$

and the second rank order parameter is the i^{th} layer is:-

$$\bar{P}_2^i = \frac{1}{Z}\int_0^{\pi} d\sin\beta d\beta P_2(\cos\beta)\exp\left(-\frac{\epsilon}{kT}(4P_2^i + \bar{P}_2^{i+1} + \bar{P}_2^{i-1})P_2(\cos\beta)\right) \quad 6.7$$

The order parameter of the top and bottom layers will be 1.0 since these represent the surface-nematic interaction for our model system, so assuming the system to be symmetric about the centre, then for a system of N layers, the order parameter in the i^{th} layer, $\bar{P}_2^i$ will equal $\bar{P}_2^{N-i+1}$. Therefore for N layers we have a set of N/2 self consistant simul-taneous equations, ((N+1)/2 if N is odd) which can be solved either iteratively for $\bar{P}_2^i$ or by minimising the sum of the squares of residuals between the order parameter(s) on the left and right hand sides of equation 6.7.

The results for a 10 layer system (excluding the surfaces) are shown in Figure 6.1. For a system of 10 or less layers there exists only one possible solution for $\bar{P}_2^i$

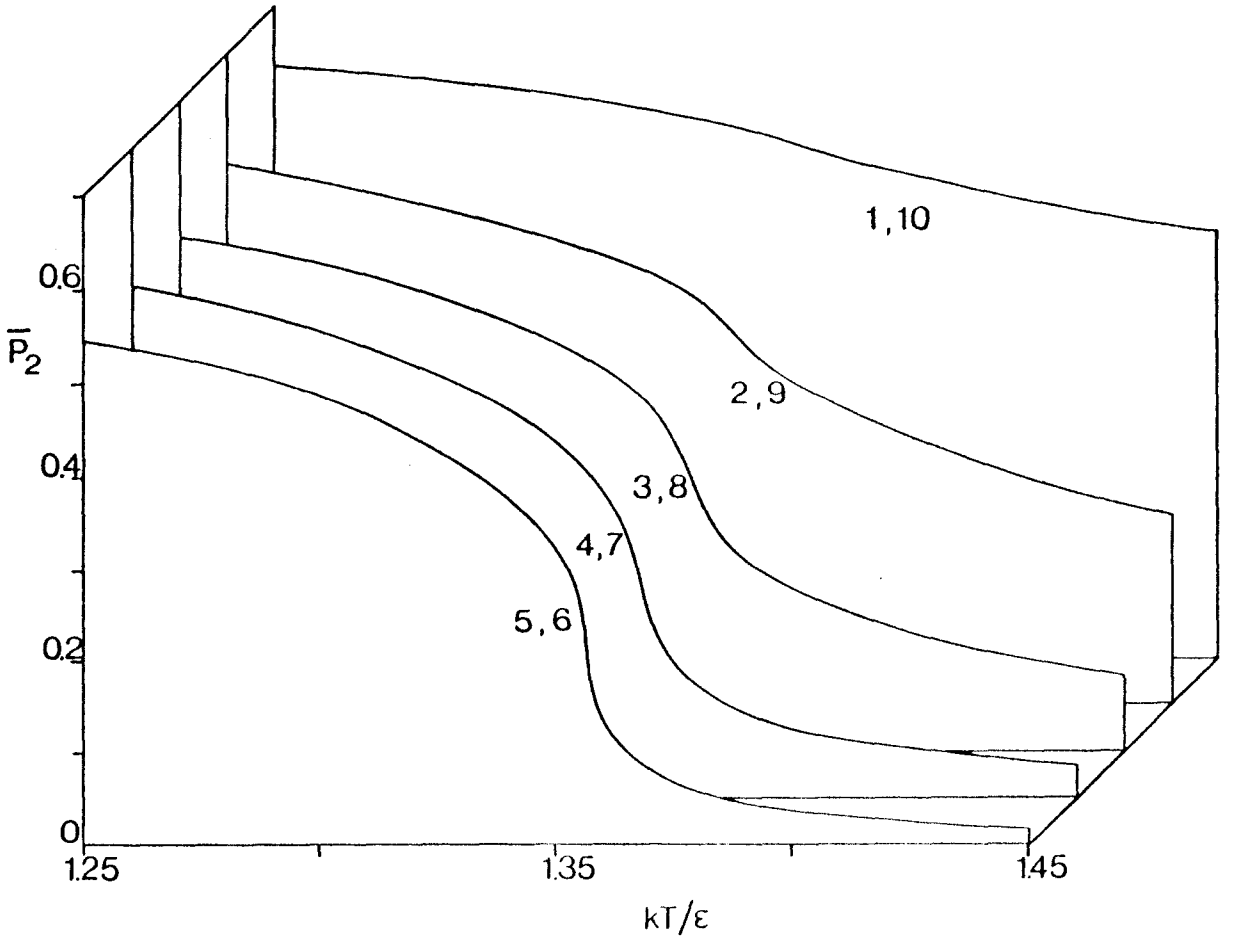

Fig 6.1 The molecular field predictions for the temperature dependence of the orientational order parameter, $\bar{P}_2$ calculated using equation 6.7 for a system of 10 layers. The coordination number, z, is 6.

at all temperatures. This is rather like the molecular field calculations in Chapter 5, where beyond the magnetic critical point a similar situation arose. Thus in this case we have a surface as opposed to a field induced critical point. The Helmholtz free energy is continuous over all temperatures indicating the non-existance of a transition between a phase of high orientational order and a para-nematic or isotropic phase. However, for systems of 11 layers or more, there are complications in the temperature range where the order parameter changes most rapidly. In this region the order parameter curve in the middle layer(s) actually bends back on itself, thus over a particular temperature range there exists three possible solutions for the order parameter. Since the order parameter in a given layer is a function of the order in neighbouring layers then it follows that three possible solutions will now exist in these neighbouring layers and subsequent layers back to the surfaces. This effect adds a degree of numerical instability to the calculations, and the method of minimising the squares of residuals failed to provide satisfactory solutions to this example.

However, this study is for a system of 10 layers and so the problem does not arise. One thermodynamic property which can be obtained without any difficulty is the average internal energy for the internal layers. In the absence of surfaces the internal energy per particle is simply:-

$$U/N\epsilon = -z\bar{P}_2/2. \qquad 6.8$$

For a system of L layers each of n particles, the internal energy per molecule is given by:-

$$\frac{U}{nL\epsilon} = -\frac{1}{2}\sum_{i=1}^{L} 4\bar{P}_2{}^{i\,2} - \frac{1}{2}\sum_{i=1}^{L} (\bar{P}_2{}^{i}\bar{P}_2{}^{i-1} + \bar{P}_2{}^{i}\bar{P}_2{}^{i+1}) \qquad 6.9$$

where $\bar{P}_2{}^{i}$ for i=0 and i=L+1 corresponds to the order parameter of the surfaces and in this case equals 1.0. This

result is obtained from the expression for the singlet orientational energy given by equation 6.5, where the energy of a molecule in the i^{th} layer depends not only on the order parameter of the four molecules in the same layer, but also on the order of the neighbouring molecule in the (i+1) and (i-1) layers.

A very similar although slightly more complex theory has also been developed by Schröder (1977) where an expansion based on anisotropic dispersion forces is used. In this case the properties depend also on the direction of surface alignment since the potential energy is a function of the orientation of the intermolecular vector. However, since the simulation in this Chapter used only a simple $P_2(\cos\beta)$ type interaction, this theory will not be discussed further.

6.3 Continuum theory and the Freedericksz transition

In Chapter 1, the basic theoretical predictions of continuum theory were given for the Freederickz transition. In general, the deformation of the director in the centre of the cell, θ_m, from the direction of surface alignment as a function of the magnetic flux density, B, assuming the geometry in Figure 1.5 a) is:-

$$\frac{Bd}{2}\left(\frac{\Delta\chi}{K_{11}}\right)^{1/2} = \int_0^{\pi/2}\left(\frac{1 + K\sin^2\theta_m\sin^2\lambda}{1 - \sin^2\theta_m\sin^2\lambda}\right)^{1/2} d\lambda \qquad 6.10$$

here d is the distance between the surfaces, $\Delta\chi$ is the anisotropic diamagnetic susceptibility, K_{11} is the splay elastic constant (Frank, 1958) and K is defined as:-

$$K = \frac{K_{33}}{K_{11}} - 1, \qquad 6.11$$

where K_{33} is the bend elastic constant. The quantity $\sin\lambda$ is the value of $\sin\theta/\sin\theta_m$. As $\theta_m \rightarrow 0$, the

critical field, B_c, is reached and equation 6.10 reduces to:-

$$k_{11} = \left(\frac{B_c d}{\pi}\right)^2 \Delta\chi \qquad 6.12$$

However, from the nature of the pair potential used in the Lebwohl Lasher model, the properties in our model system are independent of the orientation of the intermolecular vector with respect to surface alignment and so the critical field is also independent of the direction of the surface molecules. This means that all three elastic constants are equal, i.e. $K_{11} = K_{22} = K_{33}$. Equation 6.10 now simplifies to the complete elliptic integral of the first kind:-

$$\frac{Bd}{2}\left(\frac{\Delta\chi}{K}\right)^{1/2} = \int_0^{\pi/2} \frac{1}{\left(1 - \sin^2\theta_m \sin^2\lambda\right)^{1/2}} d\lambda \qquad 6.13$$

Thus substitution of equation 6.12 gives:-

$$\frac{B}{B_c} = \frac{2}{\pi} \int_0^{\pi/2} \frac{1}{\left(1 - 1\sin^2\theta_m \sin^2\lambda\right)^{1/2}} d\lambda \qquad 6.14$$

Knowing several values of θm for various experimental fields will therefore yield the critical field from which can be calculated the elastic constant.

6.4 Computational Details

For ease of reference, the simulation to observe the effect of surface forces shall be called system A, while the Freedericksz transition simulation shall be called system B. The two systems were identical in every respect except that in system B a magnetic field interaction was applied orthogonal to the direction of surface alignment. (equation 6.2). In each case the systems consisted of a 10x10xL particle lattice, with L equal to 10 in system A, but only equal to 8 in the slightly more complex system B. Here, L is the number of layers parallel to the xy plane, not including the fixed surface layers. In the majority of the

calculations the molecules in the surface were fixed to lie parallel with the z-direction, although as we shall verify, the direction of surface alignment is unimportant for the simple $P_2(\cos\beta)$ potential.

The particles between the fixed surfaces (in the bulk) were selected randomly using a random number generated uniformly in the range 1 to N, where N is the number of movable particles. The molecular orientations were stored using their respective direction cosines and so a new orientation was generated using the algorithm proposed by Barker and Watts (1969). This involves performing a rotation of a controlled maximum random amount about a laboratory axis selected at random. Thus the rotation, γ, was generated using:-

$$\gamma = \xi\Delta \qquad 6.15$$

Here ξ is a uniform number generated in the range of +1 to -1 and Δ is an input parameter used to control the maximum rotation in order to obtain an acceptance-rejection ratio of approximately 1.0. This algorithm has the advantage that excellent control of the acceptance-rejection ratio can be obtained regardless of the director orientation (c.f Chapter 5).

As the inhomogeneous properties of the system were required the orientational properties were not only calculated with respect to the bulk of the system, but also within each layer. The average order parameter for each layer was evaluated by setting up and diagonalising a Q-tensor (see Chapter 2) at the end of every cycle in the production stage of the simulation, although the director orientation was calculated by a slightly different route. The Q-tensor itself was averaged over the entire production stage and then diagonalsed, from which the eigenvector corresponding to the largest eigenvalue gives the average director orientation. This slightly different method of

averaging was employed to remove the difficulty of averaging the polar angle, θ, the angle the director makes with the laboratory z-axis, which is positive for all orientations of the director. In principle it would be correct to average θ, provided it was close or equal to $\pi/2$, but when the director fluctuates about the z direction, θ is always positive resulting in its overestimation. Averaging the Q-tensor over the entire production run, simply gives the average director over all configurations and therefore in this constained system correctly gives the average director orientation. In an unconstrained system however, this technique would fail since the director would be able to fluctuate freely, and the tensor would therefore vanish.

This averaged Q-tensor also provides a measure of the director fluctuations since in a system in which the director does not fluctuate, the order parameter calculated from the averaged Q-tensor ($\bar{P}_2(\bar{Q})$) will be identical to that calculated from the Q-tensor diagonalised at the end of each cycle and averaged. Conversly, $\bar{P}_2(\bar{Q})$ will be less than $\bar{P}_2$ in systems in which the director does fluctuate. In addition, for some of the simulations of system B, a further method of averaging was employed. In this case to evaluate the director orientation in the i^{th} layer, the Q-tensor was averaged over the i-1, i and i+1 layers. This therefore gives statistically better results, and as we shall see, it gives almost identical results to those obtained from averaging the i^{th} layer Q-tensor only.

The starting configuration for the initial equilibration stage for both systems was taken to be a completely ordered state with the molecules parallel to the z-axis and the starting configuration for subsequent runs was taken from the configuration at the end of a production run at a similar temperature in system A and a similar temperature or external field in system B. Typical equilibration and production stages each consisted of 10 thousand cycles although in some cases (e.g. for weak

external fields) this figure was substantially higher. Explicit details of all the starting configurations, lengths of equilibration and production stages are given in Tables 6.1 and 6.2 for systems A and B respectively.

The only thermodynamic quantity calculated throughout the simulations was the average of the total internal energy, and includes the contribution from all pairs of particles within the bulk of the system (not the surface layers). Since transition properties were not required, the heat capacity was not evaluated.

6.5 Results and Discussion

The two systems will be discussed individually.

6.6 System A

The most important orientational quantities evaluated were the second rank order parameter, $\bar{P}_2$ calculated within each layer and the director orientation. The variation of $\bar{P}_2$ as a function of layer number, at different temperatures is plotted as the points in Figure 6.2. To within statistical uncertainty the values of $\bar{P}_2$ are symmetrical about the central two layers, so in each case the average values of the pair of results have been plotted. The fixed surface layers are labelled with numbers 0 and 11. The profile of the order parameter is exactly as we would expect, with the order parameter decaying from unity at the surfaces to a limiting value towards the centre of the sample. One interesting feature is the shape of the profiles, since at relatively low temperatures (eg $T^* = 1.0$) and at high temperatures ($T^* = 1.6$) the order parameter is approximately constant throughout the central 8 layers, whereas for moderate temperatures (eg $T^* = 1.4$) the order parameter varies through the whole sample.

The same results are plotted as the solid squares and circles in Figure 6.3 but now as a function of the reduced temperature, T^*. For clarity only $\bar{P}_2$ for the central and

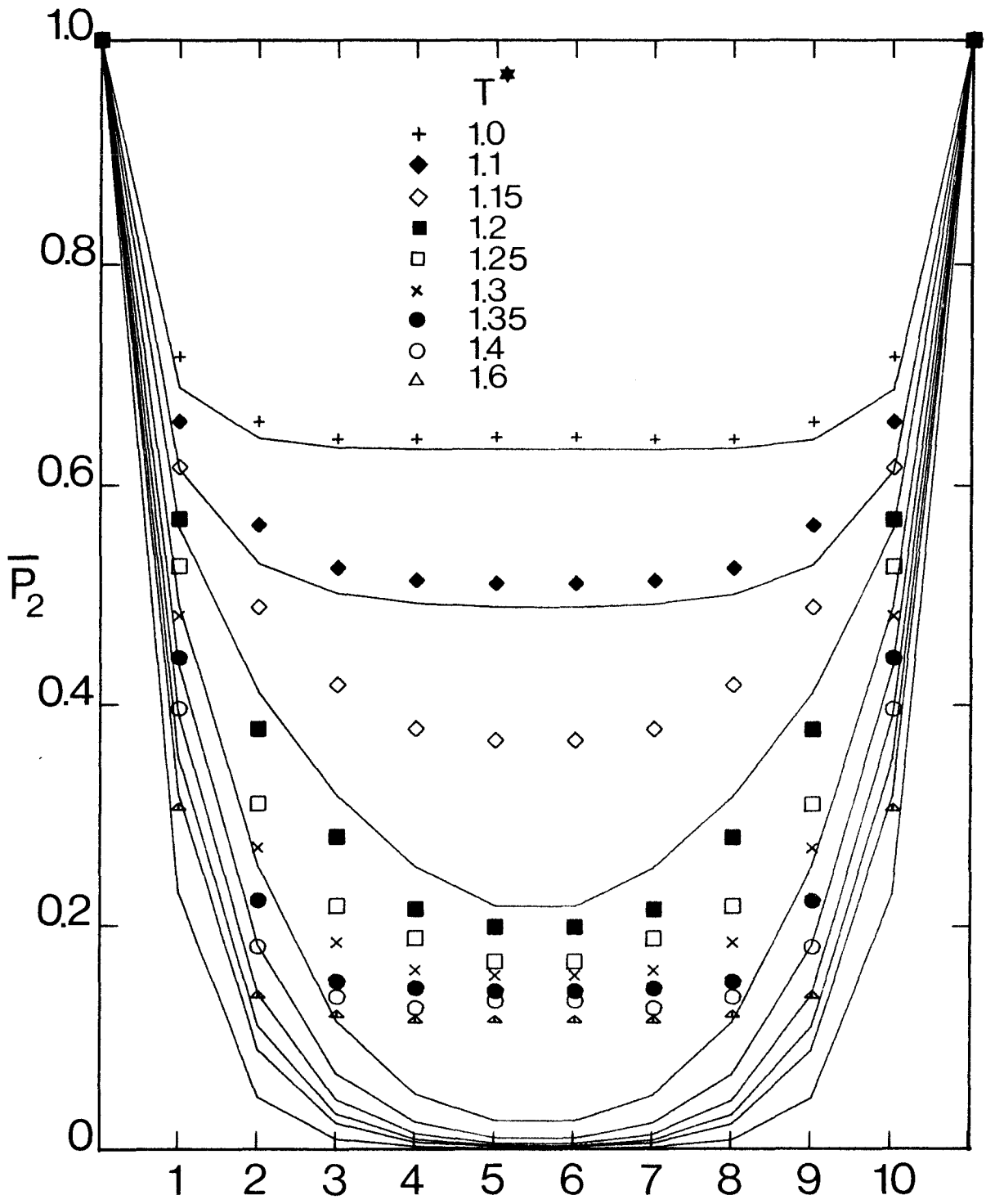

Fig 6.2 The variation of the orientational order parameter, $\bar{P}_2$, as a function of position in the system for the 9 temperatures studied in system A. The surface layers are numbered 0 and 11. The molecular field predictions are shown as the lines scaled to the same transition temperature in the absence of any surfaces.

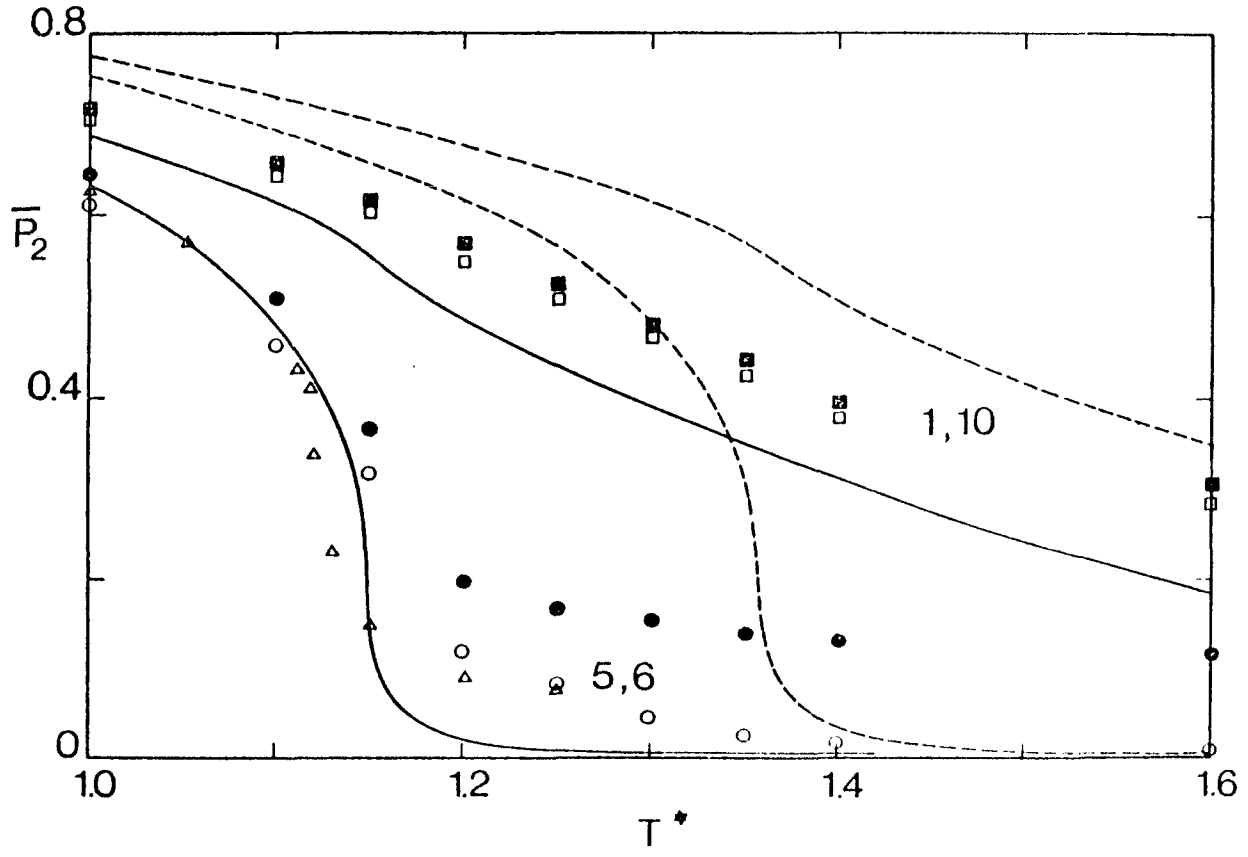

Fig 6.3 The temperature dependence of the orientational order parameter, $\bar{P}_2$, calculated in the layers adjacent to the surfaces[2] (solid squares) and in the central two layers (solid circles). The open squares and open circles are $\bar{P}_2(\bar{Q})$, i.e. the order parameter calculated from the averaged Q-tensor. The dashed and solid curves are the molecular field predictions calculated at the same reduced temperature, and scaled to the same transition temperature in the absence of surfaces, respectively. The open triangles are results for the Lebwohl-Lasher model in the abs-ence of surface forces (Zannoni, 1979).

layers adjacent to the surfaces have been plotted. At high temperatures the order parameter in the central layers appears to be tending to a limiting value of about 0.1, as opposed to an isotropic value of zero. This effect is expected when we realise that the order parameter measured in each layer is an average order of only 100 molecules, and as we have seen in Chapter 3, in order to achieve a completely disordered isotropic phase extremely large systems have to be used. The results for these calculations are listed in Table 6.3.

The order parameters $\bar{P}_2(\bar{Q})$ calculated from the Q-tensor averaged over the production stage of the calculation are also plotted in Figure 6.3, in this case as the open squares and circles for layers 1 and 10, and 5 and 6 respectively. Here we see that $\bar{P}_2(\bar{Q})$ is always slightly less than the corresponding value calculated from the unaveraged Q-tensor, although significantly less in the central layers at high temperatures, where instead of tending to a limiting value of about 0.1, $\bar{P}_2(\bar{Q})$ tends to zero. This is in accord with our expectations, since director fluctuations will always make $\bar{P}_2(\bar{Q})$ less than $\bar{P}_2$, and at high temperatures, away from the surfaces, these fluctuations will be at a maximum. An increase in director fluctuations, infers a weakening of the ability of the surfaces to pin the director. Indeed, as observed in Table 6.4 this is what we find, where the cosines of the average director orientation with respect to the surface alignment are listed. At low temperatures and close to the surfaces, the director pinning is at a maximum, while the effect decreases with increasing temperature and away from the surfaces. In order to observe the quantitative effect of surfaces on the order parameter throughout the system, results obtained for the Lebwohl-Lasher model without surfaces have been plotted on Figure 6.3 as the open triangles (Zannoni, 1979). These results are for a system of 1000 particles and are again in accord with our

expectations. At low temperatures in the unconstrained system the order parameter is slightly less than the central value in this simulation, thus indicating the apparently very small effect caused by the surfaces in those central layers. At higher temperatures the unconstrained system undergoes a phase transition as can be seen by the fairly rapid change in the orientational order, whereas in the layered system the rate of change in $\bar{P}_2$ is very much smaller and a higher degree of long range order exists at higher temperatures.

To investigate the effect of the direction of surface pinning, calculations at $T^* = 1.2$ and $T^* = 1.4$ were also carried out with the molecules in the surface aligned parallel with the x direction. Clearly from Table 6.3 at $T^* = 1.2$ where a similar calculation was performed with normal molecular alignment, both sets of results agree perfectly and the values of $\bar{P}_2$ at $T^* = 1.4$ are clearly consistent with values calculated at $T^* = 1.6$ at $T^* = 1.35$, thus confirming that the direction of surface alignment has no effect on this system in which the molecules interact via this simple P_2 potential.

Finally, in Figure 6.4 we plot the internal energy as a function of temperature, as the solid squares. The energy is the average energy per particle within the bulk of the system. Therefore contributions arising from pair interactions between fixed particles within the surface layers have been ignored, although average interactions between the surface molecules and the molecules in the first layer are included. To within experimental error the curve is continuous throughout the temperature range studied, thus indicating that the system remains in an ordered state.

With a knowlege of our findings in the previous chapter, this is exactly as we would expect, since the surfaces could in principle be replaced by an inhomogeneous magnetic field varying thoughout the sample. With perfect order in the surface layers, the effective field in the

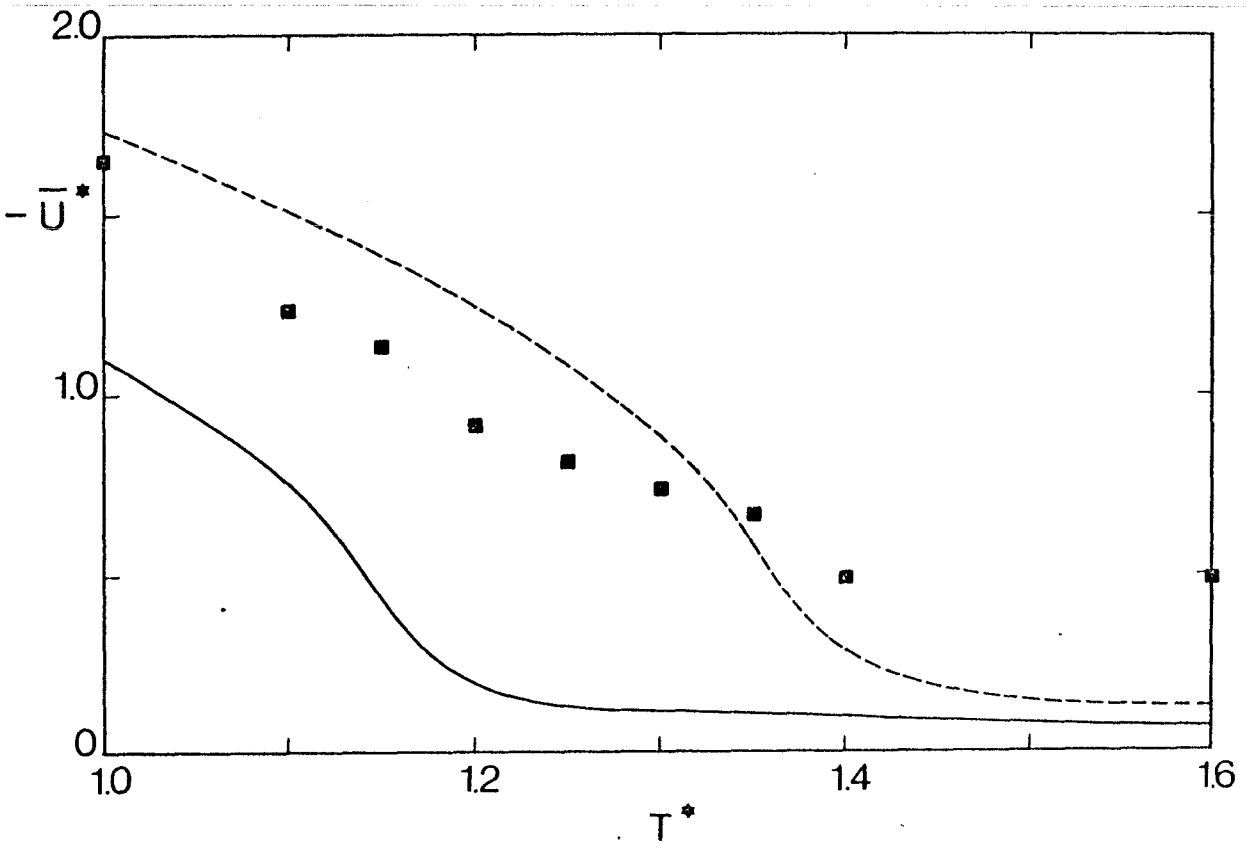

Fig 6.4 The temperature dependence of the average internal energy, (The errors are given in Table 6.3) together with the molecular field predictions calculated at the same reduced temperature (dashed curve) and scaled to the same transition temperatures (solid curve) in the absence of surfaces.

first layer will be of unit strength, a value well in excess of the predicted critical field.

The identical system has also been studied by Bagmet (1982) using the method of molecular dynamics, and in all cases to within experimental error identical results are obtained for the properties calculated. For simplicity these results have not been plotted.

6.7 Comparison with molecular field theory

The predictions of the molecular field theory are shown in Figures 6.2 and 6.3 as solid lines. In Figure 6.2 the lines serve only as a guide to the eye, since solutions are only obtained at integer layer numbers. Firstly comparing the order parameter profiles in Figure 6.2, in making the comparison, to allow for the known failure in molecular field theory to overestimate the nematic-isotropic phase transition temperature, the theoretical predictions have been evaluated scaled to the same transition temperature in the absence of surface forces. So a molecular field theory transition temperature of $kT/\varepsilon=1.321$ and a simulation transition temperature of $T^*=1.145$ (Humphries, 1979) have been used. As we would expect the agreement at low temperatures is excellent (e.g. at $T^*=1.0$) although much worse at temperatures higher than $T^* = 1.1$, where a combination of two effects contribute to give such poor agreement. Firstly and probably the major contribution to the deviation is the finite size effect arising in the simulation and mentioned earlier, since each layer has only 100 molecules. Secondly, and only a small effect, is the failure of the molecular field theory to predict accurately the order parameter at the transition in the absence of any surface forces. This error would undoubtably arise in a system with surfaces, although its effect will be very small since it will actually enhance the order parameter profiles, cancelling with the finite size effect.

The same effect is observed in Figure 6.3 where the order parameters for the central and layers adjacent to the surfaces are plotted. The dashed curve is the molecular field prediction without any scaling and is clearly in complete disagreement with the simulated data. However, the solid curves are the molecular field predictions scaled to the transition temperature in the absence of surface forces and again the agreement at low temperatures is good although finite size effects are probably responsible for the very poor agreement in the high temperature region.

Another of the failings in molecular field theory is the underestimation of the short range order parameter. In the previous chapter we observed that without any scaling, the internal energy, which is related to the short range order parameter, was in quite good agreement with simulation. This was attributed to the cancellation of two errors, the over estimation of the transition temperature and the underestimation of the short range order. This effect is also seen in Figure 6.4 where the dashed curve is the molecular field prediction of the internal energy, calculated using equation 6.9. The agreement is reasonably good, although much better than the curve scaled to the same transition temperature in the absence of surfaces, as shown by the solid curve. In this case the curve is more positive (n.b. negative ordinate scale) by almost a constant amount, emphasising the theory's underestimation of the short range order parameter by an almost constant amount.

To conclude this section, we have seen the effect of surfaces on the Lebwohl-Lasher model and observe very similar properties to those seen in Chapter 5 for system C. When compared with the predictions of the molecular field theory, very similar failures to those seen previously (c.f Chapters 3,5) occur, in particular the theory's underestimation of the short range order resulting in incorrect predictions to the internal energy, and an overestimation of the long range order.

6.8 System B

The most important orientational property calculated for this system was the director orientation, θ, with respect to the direction of surface alignment as a function of the external field, χ. From the dependence of θ on χ information related to the elastic constants can be evaluated. This dependence is shown in Figure 6.5 as the symbols at the four reduced temperatures studied, $T^* = 0.9$, 1.0, 1.08 and 1.2. For clarity the errors associated with each point have not been plotted since they are difficult to quantify when calculated from the Q-tensor. However, a reasonable estimate would be $\pm 5^0$ at the layers adjacent to the surface, rising to $\pm 10^0$ in the central region. The behaviour is characteristic of what we would expect, with very weak distortions occuring at low fields of less than about $\chi = 0.10$, which increase to a saturation limit of $\theta = 90^0$ at large fields of about $\chi = 0.30$. One feature is the observation that extremely high fields (i.e. beyond the range used in this study) are required to rotate the director in layers adjacent to the surfaces to give a completely saturated sample. For certain simulations of this system (i.e. $T^* = 0.9, \chi = 0.17$, $T^* = 1.0, \chi = 0.12$, $T^* = 1.08, \chi = 0.16$, $T^* = 1.20, \chi = 0.08$) the deformation throughout the sample was obtained from the averaged Q-tensor combined with the tensors from adjacent layers to give the director orientation averaged over three layers. This therefore should give statistically better results since now 300 particles are involved in the director evaluation. The results for this calculation are shown as the open triangles on the plots in Figure 6.5 and to within the experimental error they are identical to those obtained from the Q-tensor of each layer alone.

Figure 6.6 shows a cross section of the graphs in Figure 6.5 with the deformation in the centre of the sample, θ_m, plotted as a function of the applied external field

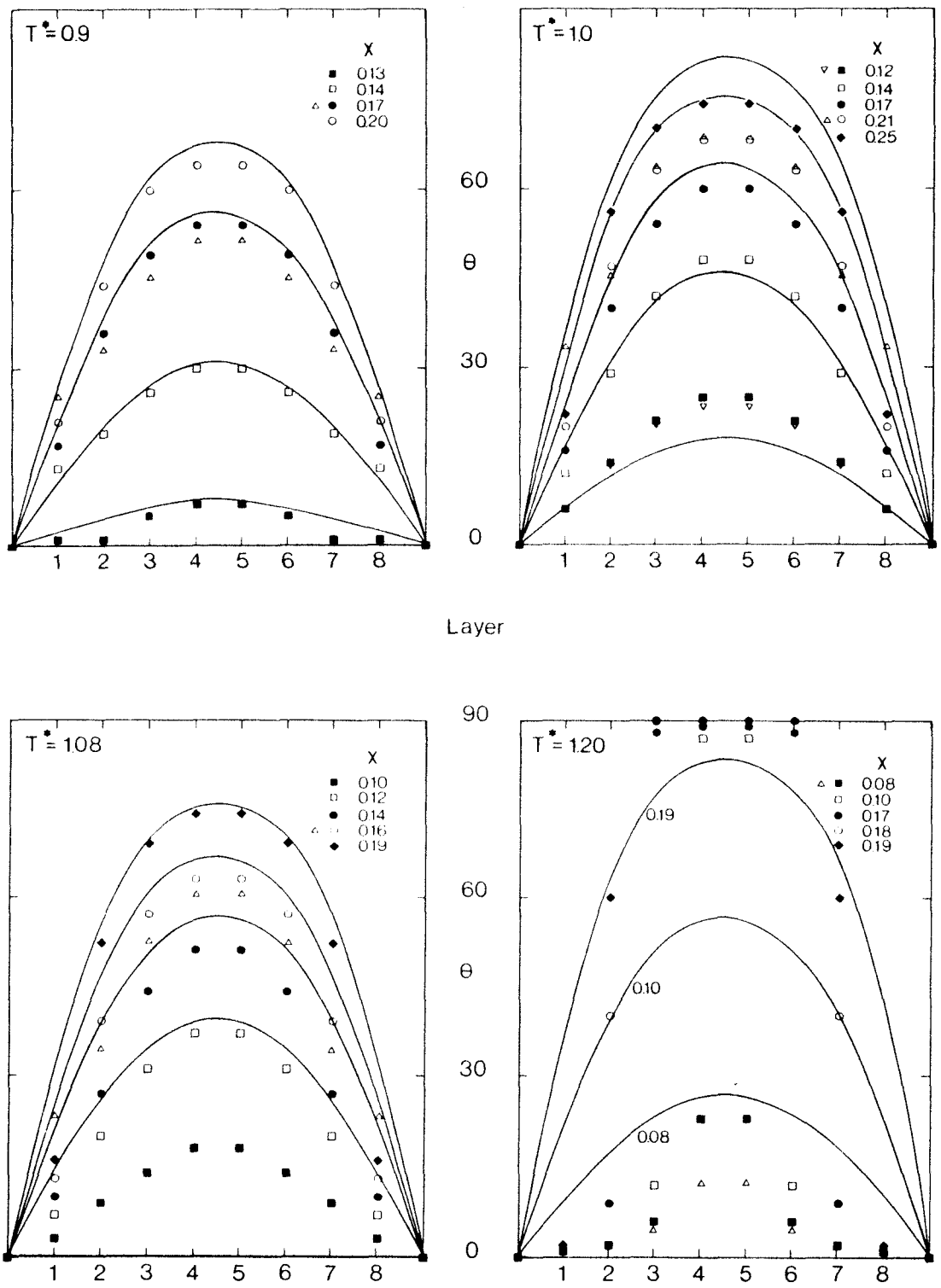

Fig 6.5 The variation of the orientation of the director with respect to the surface alignment for system B for the four temperatures studied at selected external field strengths. The open triangles correspond to results obtained from averaging the Q-tensor with the tensors of neighbouring layers. The curves are the predictions of continuum theory based on the critical fields evaluated and listed in Figure 6.6.

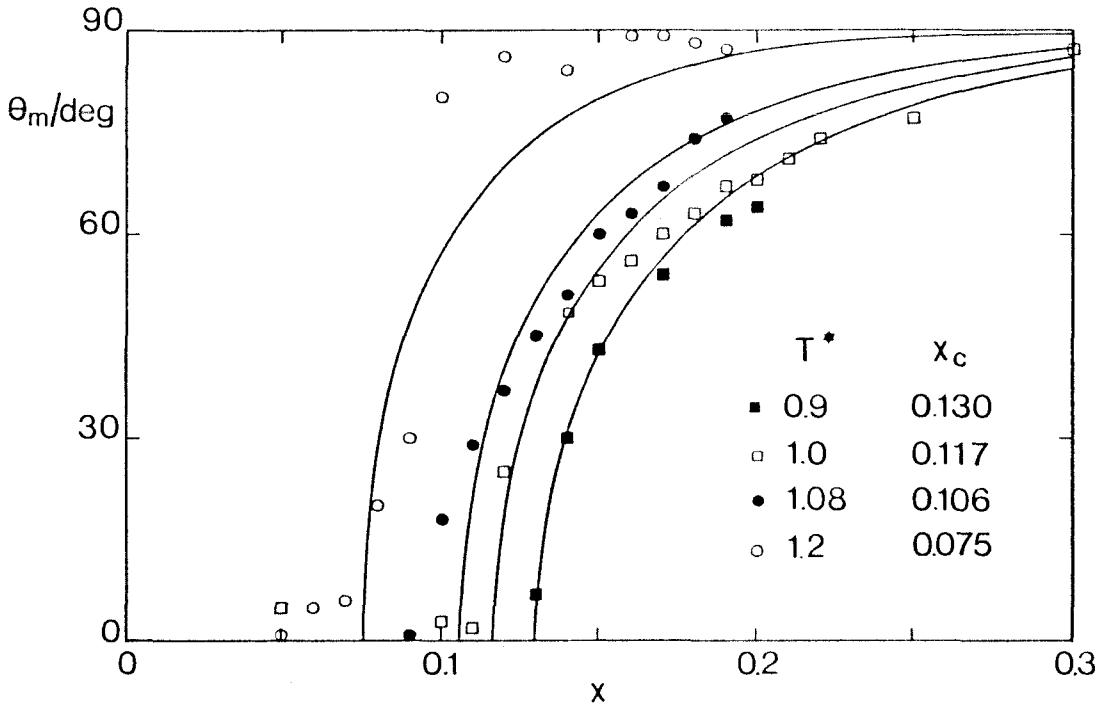

Fig 6.6 The variation of the maximum director orientation with respect to the direction of surface alignment, θ_m, as a function of the applied external field, χ. The curves are the best fits obtained using equation 6.14 with the optimum values of the critical field χ_c listed.

for the four temperatures studied. Again, for clarity the errors have not been shown although the errors associated with θ_m, for θ_m less than 30^0 are probably $\pm 10^0$, decaying to $\pm 5^0$ for θ_m greater than about 75^0. These results are also listed in Table 6.5. The behaviour observed is very encouraging, being almost identical to the form predicted from measurements of bulk anisotropic properties in classical experiments of the Freedericzs transition. In other words below a critical field, no deformation throughout the sample occurs, although above it the deformation approaches its limiting value with increasing external field.

Finally the order parameters calculated throughout the sample at the four temperatures studied and at selected external field strengths are plotted in Figure 6.7. The lines joining the points serve only as a guide to the eye. Errors in this case are estimated to be about ± 0.01 for $\bar{P}_2$ greater than about 0.50 and less than 0.23 and about ± 0.02 for intermediate values. At low external field strengths the behaviour is exactly as we would predict, with the order parameter dropping from 1.0 at the surfaces to a temperature controlled limiting value in the centre. However at higher field strengths in the region where the director reorientates through a large angle, the external field begins to enhance the order as shown by the maxima in the curves in the central layers. Thus on increasing the field orthogonal to the director, the overall order in the system gradually declines, until at a critical point, the director reorientates and the long range orientational order increases. This effect is only observed in the central layers, as close to the surface, the molecules experience a large field created by the surfaces, and a cancelling orthogonal force caused by the applied external field, thus close to the surfaces (i.e. in the second and seventh layers) the particles experience weak destabalising forces

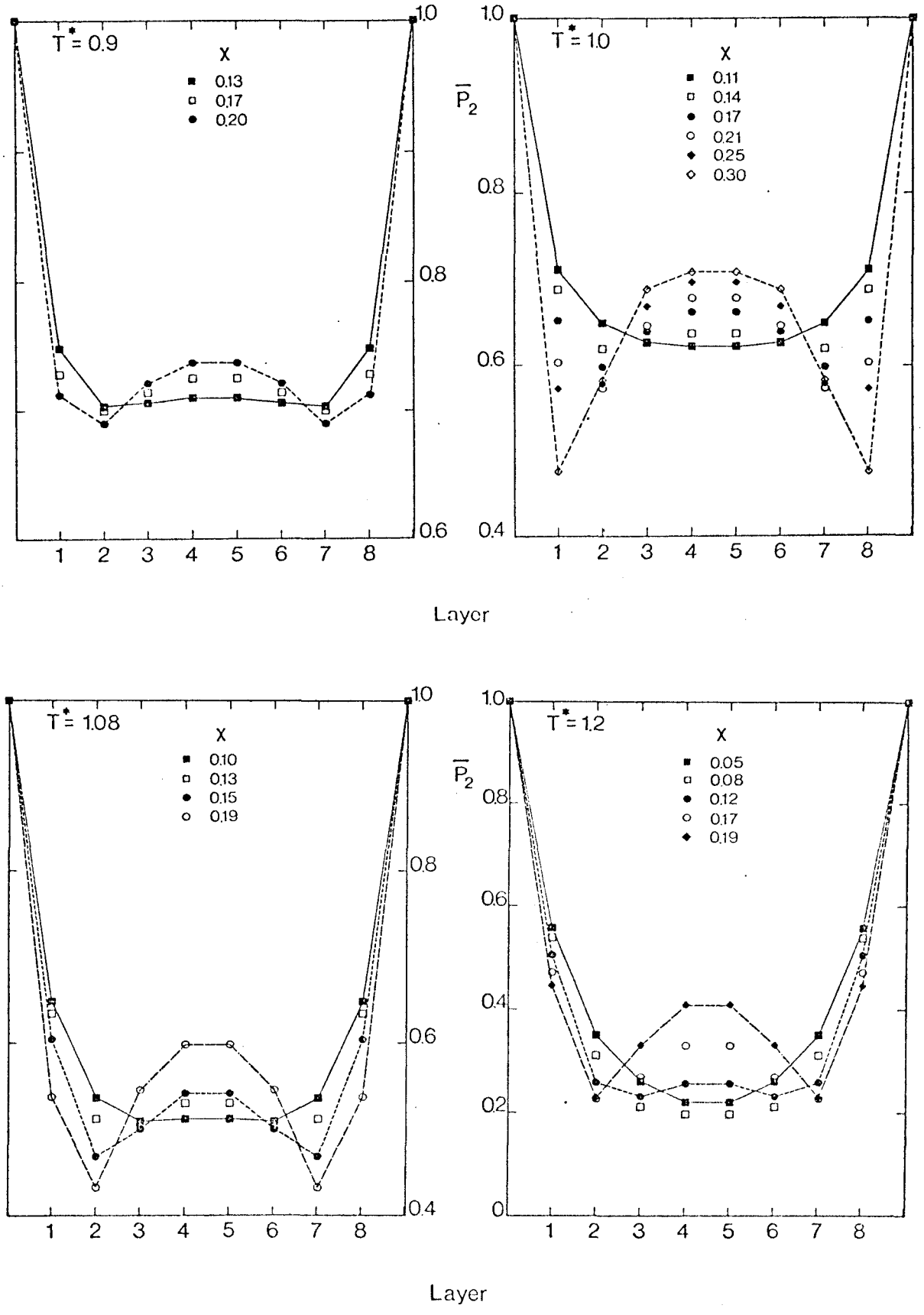

Fig 6.7 The variation of the long range orientational order throughout the samples at the four temperatures studied and at selected field strengths. The lines serve only as a guide to the eye.

as reflected in the minima in the order parameters in this region.

This effect is in contrast with that observed experimentally, where it is impossible to detect any significant variation of the order parameter throughout the sample. However this is only due to technical reasons, since there will probably be a few layers of molecules adjacent to the surfaces experiencing this effect. Also the fact that $\bar{P}_2$ does vary throughout the sample means that strictly speaking the elastic constant will also vary throughout the sample, so any attempt to obtain the constant from a bulk property will yield an average value.

6.9 Comparison with theory

We have seen from section 6.3 how the elasticity of this simple system relates to the deformation under the influence of an applied external field. In principle the value of the elastic constant, K, can be determined directly from the values of the estimated critical fields in Figure 6.6. However a more accurate method is to use more of the available information, in this case the shape of the deformation above the critical field. This deformation is given by equation 6.14. Using a minimisation procedure (NAG routine E04JBF), the best fit to this equation was obtained by minimising the sum of the squares of residuals of $\theta_m - \theta_m^{calc}$, where θ_m^{calc} is the theoretical prediction based on the known value of the applied field, as a function of the ratio of B/B_c which in this case is identical with $(\chi/\chi_c)^{1/2}$. The values of the critical field χ_c obtained in this way are given in Figure 6.6 together with curves representing the best fits to the experimental data. At the three lower temperatures, the best fits obtained agree reasonably well with the simulated data, although at the high temperature of $T^*=1.2$ it is poor. This failing at higher temperatures can easily be explained in view of the approximations used in the derivation of equation 6.14. One

of the most severe of which is the assumption that the long range orientational order is constant throughout the sample. Clearly, as we have seen in in Figure 6.7 this is untrue, with the biggest variations occuring at $T^*=1.2$. Furthermore, in an unconstrained system, this temperature actually corresponds to the isotropic phase.

In principle the values for the critical field can be evaluated from the way in which the director varies throughout the whole sample, since:-

$$\frac{x}{d} = \frac{1}{\pi}\left(\frac{\chi}{\chi_c}\right)^{1/2} \int_0^{\psi} \frac{1}{(\sin^2\theta_m - \sin^2\psi)^{1/2}} d\psi \qquad 6.16$$

where x/d is the relative distance through the cell and ψ is the orientation of the director at a distance x (Chandrasekhar, 1977). However, attempts to obtain an optimised fit to this equation failed, although its predictions based on the critical fields evaluated from the maximum deformation, θ_m, were evaluated. The curves in Figure 6.5 show the theoretical predictions based on the previously determined critical fields, calculated at the same experimental field and in most cases very good agreement is obtained, thus again confirming the application of continuum theory to our simple system. As we saw previously the poorest agreement is found at the higher temperatures where the order parameter varies most throughout the sample and where in the absence of constraints the system would be isotropic.

Theory can also predict the variation of the elastic constants with the order parameter or temperature. However, before attempting any comparison the elastic constants must be evaluated from the values obtained for the critical fields.

In a real experiment, an elastic constant is evaluated using the relationship:-

$$K = (B_c d/\pi)^2 \Delta\chi/\mu_0 \qquad 6.17$$

Where μ_0 is the magnetic constant or permeability of free space and $\Delta\chi$ is the anisotropy in the diamagnetic susceptibility, which can also be written as:-

$$\Delta\chi = \Delta\chi' \bar{P}_2 \qquad 6.18$$

where now $\Delta\chi'$ is the anistropy in the diamagnetic susceptibility for a perfectly ordered system or a single crystal. The parameter $\Delta\chi'$ can be linked to χ used in the simulation, since experimentally the total magnetic energy of a single crystal is:-

$$U^{mag}/V = -1/2\ \mu_0^{-1} \Delta\chi' B^2, \qquad 6.19$$

and in the simulation for a perfectly ordered system:-

$$U^{mag} = -N\chi\varepsilon. \qquad 6.20$$

Therefore

$$N\chi\varepsilon = 1/2\mu_0^{-1} \Delta\chi' B^2 V, \qquad 6.21$$

so defining a number density, $N/V=a$ and a scaled distance unit, $d^*=d/a$ allows us to write equation 6.17 as:-

$$K^* = 2\pi^{-2}\ a^{-1}\ \chi_c \varepsilon d^* \bar{P}_2, \qquad 6.22$$

thus providing us with a reduced elastic constant K^* ($= K/\varepsilon a^{-1}$) equal to:-

$$K^* = 2(d^*/\pi)^2 \chi_c \bar{P}_2. \qquad 6.23$$

Using a reduced distance between surface layers equal to 8, the values for K^* were calculated, and are:- 1.20,

0.94, 0.71 and 0.19 at the four temperature studied of T^*=0.90, 1.00, 1.08 and 1.20 respectively. The values for $\bar{P}_2$ in equation 6.23 were estimated from Figure 6.7 to be the limiting values in the central layers at the critical field and are 0.71, 0.62, 0.52 and 0.20 respectively. Alternatively, $\bar{P}_2$ can also be taken from an unconstrained system, however, to within experimental error, the values for $\bar{P}_2$ are identical to those given above (Zannoni, 1979), (with the exception of T^*=1.20, where a value of $\bar{P}_2$=0.08 is reported), and were therefore not be used to evaluate K^*.

The values of K^* can now be compared with theory. Firstly with the predictions of continuum theory. This states (de Jeu, 1980) that K^* is proportional to the square of the second rank order parameter, which for the three lower temperatures is approximately observed, since the ratio of $K^*/\bar{P}_2^2$ is 2.37, 2.45, 2.64 and 4.86 for T^*=0.90, 1.00, 1.08 and 1.20 respectively. The failure at T^*=1.20 is expected in view of the previous observation that at this high temperature the order parameter varies most throughout the sample, in contrast with the assumption in continuum theory that is constant.

A theory has also been proposed by Priest (1972) based on a molecular field treatment of a lattice model. According to this, the elastic constants are predicted to be:-

$$K_{11} = K_{22} = (3/4v_o)\bar{P}_2^2 \sum_i A(r_{oi})x_{oi}^2 \qquad 6.24$$

$$K_{33} = (3/2v_o)\bar{P}_2^2 \sum_i A(r_{oi})z_{oi}^2 \qquad 6.25$$

Here $A(r_{oi})$ is an interaction strength parameter, with r_{oi} being the intermolecular vector between the reference and the i^{th} molecule. z_{oi} is the projection of the vector r_{oi} onto the director axis, x_{oi} is the projection onto an axis orthogonal to the director and v_o is the molecular volume. The fact that $K_{11} \neq K_{33}$ is a consequence of the anisotropy

in the spatial pair distribution function. However, for a simple cubic lattice this anisotropy does not occur, since:-

$$\sum_i A(r_{oi}) z_{oi}^2 = 2\epsilon a^2 \qquad 6.26$$

and

$$\sum_i A(r_{oi}) x_{oi}^2 = 4\epsilon a^2, \qquad 6.27$$

where a is the lattice spacing. This results in equal elastic constants with

$$K = (3/v_o)\bar{P}_2^2 \epsilon a^2$$

For a simple cubic lattice, the total volume is Na^3, giving a molecular volume, v_o equal to a^3. Hence:-

$$K = 3\bar{P}_2^2 a^{-1}\epsilon, \qquad 6.28$$

or

$$K^* = 3\bar{P}_2^2. \qquad 6.29$$

Thus like continuum theory, K is also predicted to be proportional to $\bar{P}_2^2$ but now we can test the constant of proportionality. The ratio of $K^*/3\bar{P}_2^2$ is found to be 0.79, 0.82, 0.88 and 1.62 for T^* equal to 0.90, 1.00, 1.08 and 1.20 respectively in contrast with the theoretical prediction of unity. So again, reasonable agreement is found at low temperatures although it progressively gets worse with increasing temperatures.

Finally these elastic constants can be compared with a continuum theory based on disorder rather than order proposed by Faber (1977). In this case it is assumed that the nematic is a continuum with a fully disordered ground state, and it is shown that:-

$$\ln(1/\bar{P}_2) = \left(\frac{3k}{2\pi^2}\frac{T}{K}\right)\left(\frac{6\pi^2 N}{V}\right)^{1/3} \qquad 6.30$$

where K is 'the mean stiffness constant', which in the limit that $K_{11}=K_{22}=K_{33}$ reduces to the K defined earlier in this section. In terms of a reduced elastic constant equation 6.30 becomes:-

$$\ln(1/\bar{P}_2)K^*/T^* = 0.592 \qquad 6.31$$

Thus we now have a relationship between the reduced elastic constant, order parameter, and temperature. Using the values for these as given previously, the left hand side of equation 6.31 is 0.46, 0.45, 0.43 and 0.25 for the temperatures studied of $T^* = 0.90$, 1.00, 1.08 and 1.20 respectively. Although these values do not agree exactly with the theoretical prediction of 0.592, they are none the less fairly constant (with the exception of $T^* = 1.20$).

A summary of the previous three theoretical comparisons are given in Table 6.6.

To conclude the comparison of the elastic constants with the long range order and temperature, in all three cases, reasonable agreement with the predictions of theory has been observed, especially at the 'well behaved' temperatures studied at $T^* = 0.90$, 1.00 and 1.08. However at the high temperature study of $T^* = 1.20$, which in the absence of surfaces is actually isotropic, the long range order parameter is seen to vary widely throughout the sample, thus invalidating a serious comparison with theory. It should also be noted that any form of accurate comparison with the predictions of a theory is very difficult with only four experimental points. Therefore, in order to test more fully these predictions, a much more comprehensive set of simulations should be undertaken over a much wider temperature range. Indeed it is for this reason that the numerical values quoted in this final section have not been

specified with error limits, since there are numerous factors which could seriously effect their values, for example, the errors in the values of $\bar{P}_2$ and χ_c which could be quite large, have been ignored, and therefore it should be appreciated that the comparison should be treated qualitatively rather than quantitatively. However, these preliminary calculations have clearly demonstrated the ability of the simple modified Lebwohl-Lasher model to simulate the Freederickzs transition, and furthermore, has shown that to a certain extent the predictions of continuum theory can also be applied to this lattice system.

Chapter 7

Simulation of the S_E to S_B phase transition

7.1 Introduction

Many organic compounds exhibit liquid crystalline phases in addition to the normal liquid and crystal phases. We have seen in Chapter 1 how these liquid crystalline phases could be further classified into various states, in particular the nematic phase, the cholesteric phase and a host of smectic phases. A few compounds on going from the crystalline phase exhibit a smectic E followed by a smectic B phase with increasing temperature. For example the ester,

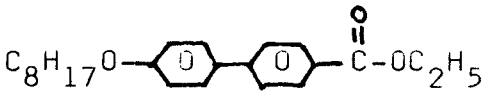

and various compounds of the form:-

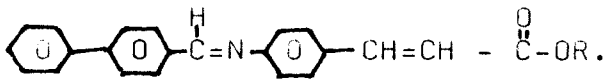

To date only a few of these latter cinnamate esters have been found to produce Smectic E and Smectic B phases, for example those given in Table 7.1, whose transitional properties are tabulated in Table 7.2.

Detailed structual analysis of ordered systems is normally carried out by X-ray or neutron diffraction and indeed recent work has given us much detailed information concerning the molecular structures of the smectic E and B phases. The earliest work was performed by Doucet *et al*, (1975) on PPBAC using X-ray diffraction on single and polydomain samples. Their conclusions were that the molecules in both phases tended to lie with their long axes perpendicular to the layers and within each layer the molecules were sited on a triangular network. In the lower temperature smectic E phase they observed that within layers the short molecular axis of molecules formed herring bone

packing extending over long distances, while in the smectic B phase they found rotational disorder about the long molecular axes. (See Figures 1.3b and 1.4). This result for the smectic B phases has been verified by Richards, Leadbetter and Frost (1978) using incoherent, quasi-elastic neutron scattering, where they find rotation about the long molecular axis on a time scale of 10^{-10}s. In addition their X-ray work suggested that the molecules were tilted with respect to the layer normal by about 6^0. Incoherent neutron scattering from the S_E phase has provided information (Leadbetter, Richards and Carlile, 1976) related to the rotational motion of the molecules, which are found to rotate (reorient) though an angle π about the long molecular axis. The precise nature of this rotation is uncertain, it could be due to parts of the molecule reorientating, e.g. some of the phenyl rings, or the whole molecule. Further detailed X-ray diffraction work (Leadbetter et al, 1979) on the S_E phase of IBPBAC has revealed that the molecules lie on a distorted triangular lattice and that the structure is probably a bi-layer with the alkyl chains of the molecules present in the inter layer region. In the S_B phase the layer structure is truly hexagonal (i.e. the molecules occur on a regular triangular lattice), although the molecules are tilted by about 6^0. This work has also disclosed that correlations of the hexagonal network between layers greater than two layer separations are negligible.

A few chemical compounds exhibit smectic B phases as their lowest temperature mesophase. In particular TBBA (terephthalylidene-bis-4-n-butylaniline) has a smectic B phase between 113°C and 144°C, and its structure has been examined in some detail using X-ray diffraction. (Doucet et al, 1974) The analysis shows that the molecules do lie on a triangular lattice within each layer, although they are tilted by up to 30^0 with respect to the layer normal, and within each layer molecules tend to form moderately ordered domains of 'herring bone' structure. The relatively large

tilt angle is rather disturbing so perhaps this phase is not actually a S_B phase anyway, and it has recently been suggested that this tilted S_B phase should be classified as a smectic H phase. This work does none the less re-emphasise the fact that within each layer, the molecular centres form a regular triangular network and there is long range rotational disorder about the long molecular axes.

The precise stucture of the smectic E and B phases is still to be established although we can draw some conclusions. In the smectic B phase, the molecules within each layer lie on a triangular network with the long molecular axes almost parallel to the layer normal. There is a high degree of long range rotational disorder about the molecular axes although there is some evidence to suggest this disorder can be attributed to short range 'herring bone' order within disordered domains. In the S_E phase however, the molecular centres lie on a slightly distorted triangular network where they are parallel to the layer normal. The molecules also exhibit a high degree of long range orientational order, reflected in the additional 'herring bone' structure which extends over large distances. We shall therefore, justifiably assume that in both the smectic B and E phases, the molecules lie on a triangular network, with their long molecular axis perpendicular to the layer.

In the next section we develop a pair potential based on this type of molecular structure using a multipole-multipole expansion. The computational details for the simulation of the model system and results are then discussed in the following two sections. A comparison of experimental scattering patterns of the smectic E and B phases is then made with patterns produced by the optical masking technique, and finally various results are compared with predictions based on a mean field theory.

7.2 The pair Potential

In section 7.1 a few examples of molecules exhibiting $S_E \rightarrow S_B$ phase transitions were given. Generally these molecules consist of a large rigid core comprised of two or three bulky aromatic rings, with a smaller flexible alkyl region. As a first approximation in describing the pair potential, we assume the molecules to be rigid. This allows us to use the equation given in Chapter 1 for the exact pair interaction between non flexible molecules of arbitrary shape. We shall use the laboratory coordinate system for a pair of molecules as shown in Figure 7.1 Our starting point is then (Stone, 1978):-

$$U_{ij} = \sum_{LL'Jkk'} u^{kk'}_{LL'J}(r) S^{kk'}_{LL'J}(\Omega) \qquad 7.1$$

where the scalar function is :-

$$S^{kk'}_{LL'J} = (i)^{L-L'-J} \sum_{mmM} \begin{pmatrix} L & L' & J \\ m & m & M \end{pmatrix} D^{L}_{mk}(\Omega_1) D^{L'}_{mk'}(\Omega_2) \times C_{JM}(\theta\phi) \qquad 7.2$$

The term in parenthesis is the Wigner 3-j symbol, $D^{L}_{mk}(\Omega)$ is the usual Wigner rotation matrix, and Ω_1, Ω_2 describe the orientations of molecules respectively, (see Fig 7.1) in a laboratory frame. $C_{JM}(\theta,\phi)$ is a modified spherical harmonic where θ and ϕ define the orientation of the intermolecular vector again in some laboratory frame. This equation is invariant to any change in the laboratory frame of reference.

From X-ray evidence of the S_E phase we shall assume that the centres of mass for the molecules lie on a 2 dimensional hexagonal network, and the principle molecular axes lie perpendicular to the layers, parallel to our laboratory z-axis. Since X-ray scattering has shown that interlayer correlations are small, we shall also assume that

interactions between layers are negligible. Hence we need only consider interactions between molecules within each layer. We know that the Wigner rotation matrices in equation 7.2 can be written as:-

$$D^{L}_{mk}(\Omega) = e^{-im\alpha} d^{L}_{mk}(\beta) e^{-ik\gamma} \quad 7.3$$

In the laboratory coordinate system (Figure 7.1) $\alpha=\beta=0$, and so equation 7.3 simplifies to (Zannoni, 1979):-

$$D^{L}_{mk}(0,0,\gamma) = \delta_{mk} e^{-ik\gamma} \quad 7.4$$

Here δ_{mk} is the kroneker delta and equals zero unless m=k. Equation 7.2 now becomes:-

$$S^{kk'}_{LL'J} = i^{L-L'-J} \sum_{mmM} \begin{pmatrix} LL'J \\ m m M \end{pmatrix} \delta_{mk} \delta_{m'k'} e^{-k\gamma i} e^{-k'\gamma j} C_{Jm}(\theta\phi) \quad 7.5$$

At this point we shall assume that the molecules have a mirror plane perpendicular to their principle molecular axis, hence k,k' ,m,m' , L and L' must all be even since the ends of the molecules are now indistinguishable. L can therefore take any even value between zero and infinity. The zero term however, gives rise to an orientational independent term only. In order to reduce the infinite number of parameters which would occur, a restriction of L=2 is imposed. Indeed if we assume that the molecular separation is relatively large, then higher rank terms can be ignored, since they are extremely short ranged. So we shall only deal with second rank contributions. J can therefore adopt any even value between +4 and -4.

Looking firstly at the angular terms, θ in the spherical harmonic is $\pi/2$ from our choice of axis system, hence only three types of angular terms remain, the first

being dependent only on γ_1, and γ_2 and the other two, functions of γ_1, γ_2 and ϕ_r the angle of the intermolecular vector. Our potential is now of the form:-

$$U_{ij} = a\cos 2(\theta_1 - \theta_j) + b(\cos 2(\theta_i - \phi_r) + \cos 2(\theta_j - \phi_r)) + c\cos 2(\theta_i + \theta_j - 2\phi_r) \quad 7.6$$

Where ϕ_r can be identified with ϕ in equation 7.5. The constants a, b and c are related to the expansion coefficients and will be discussed later.

In our model we are going to restrict the molecules to lie on a triangular network. The consequence of this is that the middle term vanishes when the total interaction energy is evaluated (see Appendix 5) leaving only the first and third terms in the pair potential to be considered further.

Our only unknowns now are the expansion coefficients a and c. We know that the smectic E phase has a very long range herring bone structure and it is also well known that quadrupolar interactions give this kind of structure (for example O'Shea and Klein, 1979) so we shall justifiably use a multipolar expansion to evaluate the values of the coefficients a and c. For multipolar forces J becomes restricted to equal $L+L'$ only, and the relevant expansion coefficients can be written as (Gubbins et al, 1981):-

$$u^{kk'}_{LL'J}(r) = \frac{1}{4\pi\varepsilon_o} \sum (-)^{L+L'} \left[\frac{(2L + 2L' + 1)!}{(2L)!\ (2L')!}\right] r^{-L-L'-1} \times \hat{Q}_{LN} \hat{Q}'_{LK} \quad 7.7$$

where ε_o is the permittivity of free space and the tensors $\hat{Q}_{Lk}$ describe the components of the multipolar moments in our laboratory frame.

The first term in the pair potential (Equation 7.6) arises from the expansion with J=4, 2 or 0 (although since we are dealing with multipole interactions $J=L+L'$, so J=4) and with M=0. Hence $m+m'=0$ giving k=2 and $k'=-2$ and vice versa. Thus the components of the multipole moments take the

form $\hat{Q}_{2-2}$ $\hat{Q}_{22}$ and $\hat{Q}_{22}\hat{Q}_{2-2}$. Adopting a similar route for the third term, the components are $\hat{Q}_{22}$ $\hat{Q}_{22}$ and $\hat{Q}_{2-2}$ $\hat{Q}_{2-2}$. Since our molecules have a mirror plane orthogonal to the molecular symmetry axis $\hat{Q}_{22}$ has to equal the component $\hat{Q}_{2-2}$, and so the multipolar components for the first and third terms in our expansion are identical and can be factored out. Therefore the only terms that contribute to the ratio of a and c in equation 7.6 are these from the 3-j symbol and the coefficient of the modified spherical harmonic. The 3-j symbols are related to the Clebsh-Gordan coefficients (which are tabulated in Appendix 6) by:-

$$\begin{pmatrix} L & L' & J \\ m & m' & M \end{pmatrix} = (-1)^{L-L'-M} \frac{1}{(2J+1)^{1/2}} C(LL'J;mm') \qquad 7.8$$

We are now in a position to calculate the ratio of a to c. The first term arises with J=4, M=0 and with m= ± 2 m'=∓ 2, and the third with J=4, M=± 4 and with m=± 2, m' =± 2. The ratio of a to c is therefore:-

$$\frac{C(224;\pm 2 \quad \pm 2) \quad X_{4+4}}{C(224;\pm 2 \quad \mp 2) \quad X_{40}} = \frac{35}{3} \qquad 7.9$$

where $X_{4\pm 4}$ and X_{40} are the coefficients of their respective modified spherical harmonics. Substituting this ratio in equation 7.6 gives an effective pair potential of:-

$$U_{ij} = \frac{\xi}{r^5} \left(\cos 2(\theta_i - \theta_j) + \frac{35}{3}\cos 2(\theta_i - \theta_j - 2\phi_r)\right) \qquad 7.10$$

ξ contains the components of the quadrupole moments for the molecules. The distance dependence of this potential (r^{-5}) is sufficiently short ranged allowing us to restrict our interest to nearest neighbour interactions only. Thus we can replace ξ/r^5 with some arbitrary interaction parameter, ε. Our effective pair potential for nearest neighbour molecules

interacting on a triangular lattice via multipolar (in this case quadrupolar) forces now becomes:-

$$U_{ij} = \varepsilon(\cos 2(\theta_i - \theta_j) + \frac{35}{3}\cos 2(\theta_i + \theta_j - 2\phi_r)) \qquad 7.11$$

At this point is worth looking at the functional form of this potential. On a triangular lattice there are six intermolecular vectors, ϕ_{r1}, ϕ_{r2}.....ϕ_{r6}. We shall give these explicit values of 0, $\pi/3$, $2\pi/3$.....$5\pi/3$., respectively. The quantity U_{ij}/ε can now be calculated as a function of θ_i and θ_j for specific values of ϕ_{rij}. Before doing this, however, the symmetry of the second rank potential is such that we need only consider three values of ϕ_{rij}, 0, $\pi/3$ and $2\pi/3$. In Figure 7.3a U_{ij}/ε is plotted as a function of θ_i and θ_j for $\phi_{rij} = 0$. For simplicity Figure 7.3b shows the contour plot for the same energy surface and clearly indicates where the minima occur in the potential. The equal minima are at $\theta_i = 0^0$, $\theta_j = 90^0$ and at $\theta_i = 90^0$, $\theta_j = 0^0$. For the intermolecular vector at $\pi/3$ and $2\pi/3$ exactly the same surface is observed, but with the coordinates of the x and y axes rotated through an angle ϕ_r. So in all three cases the most stable configuration between a pair of molecules is with one of the molecules perpendicular and the other exactly parallel with the intermolecular vector. However, for a collection of molecules interacting with their centres of mass restricted to lie on a triangular lattice, it is impossible to arrange the system with all pairs of molecules adopting this configuration, since a molecule cannot be parallel or perpendicular to all intermolecular vectors at any one time. As a consequence the minimum energy, zero temperature configuration is a compromise between competing configurations. Using a computational minimisation procedure (NAG routine E02CCF), this ground state configuration can be evaluated.

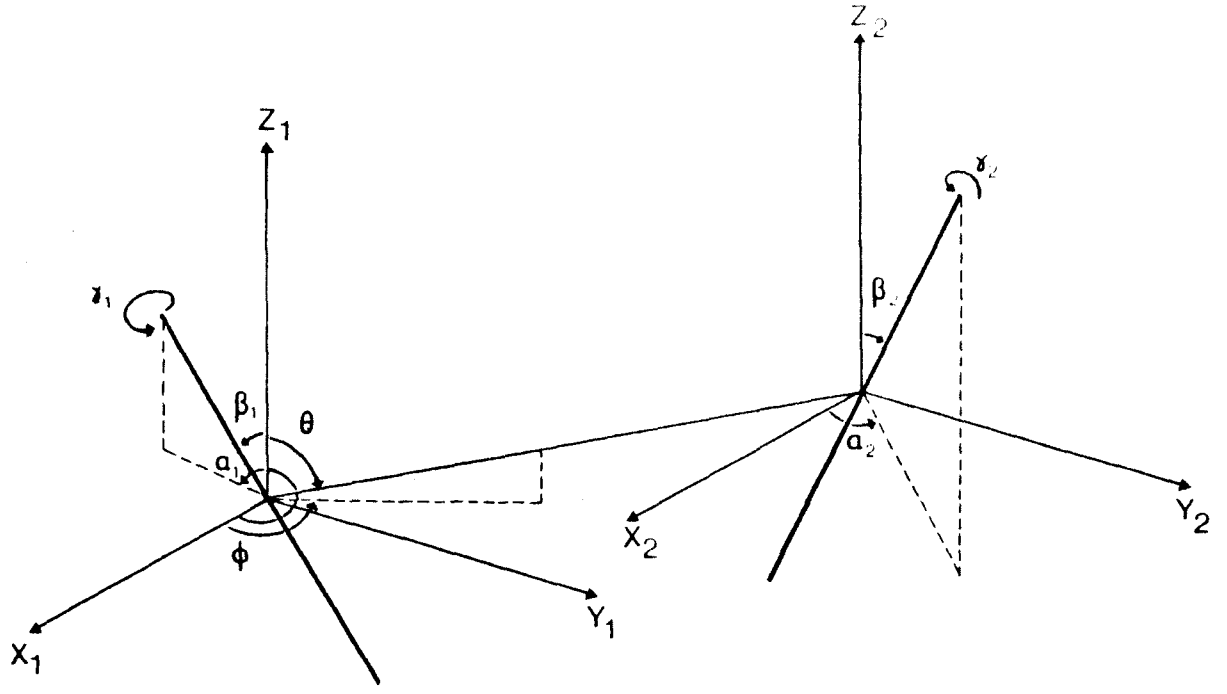

Fig 7.1 The coordinate system used to define the orientations of two molecules of arbitory shape.

Fig 7.2 Diagram representing part of the ground state herringbone configuration, used as the starting configuration in the simulation. θ is the angle between the short molecular symmetry axis and the laboratory x direction. The two dashed lines represent the two glide planes present in this structure. Throughout the text of this chapter, the glide plane refers to that parallel with the x-axis. The labels A and B represent the two sub lattices present (see section 7.6).

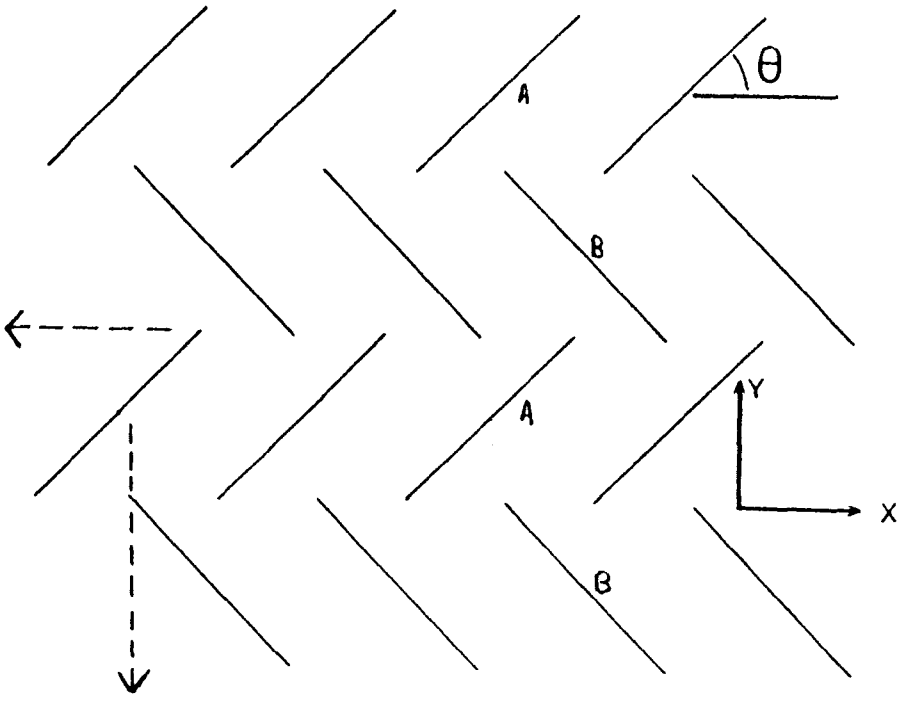

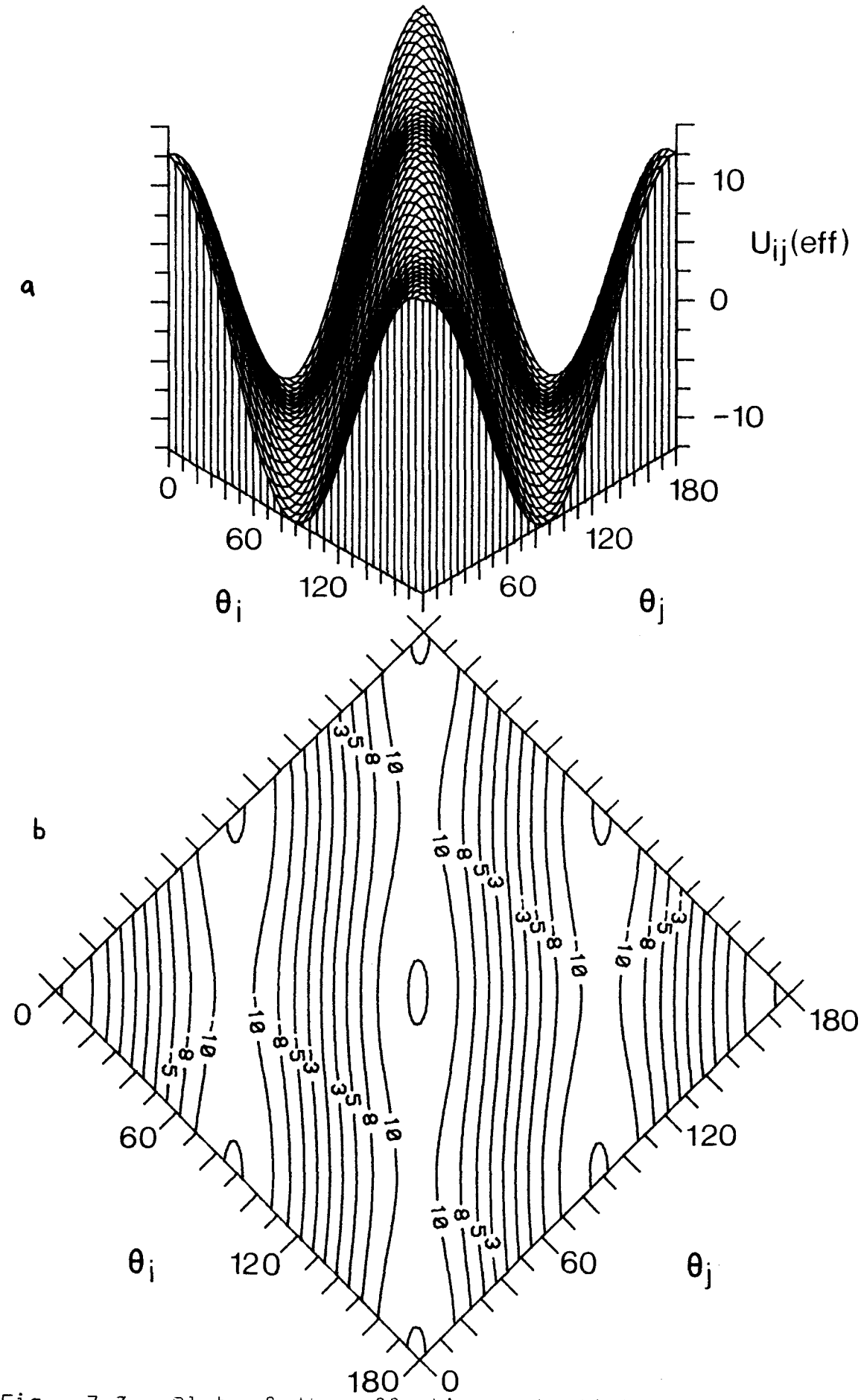

Fig 7.3 Plot of the effective potential energy surface as defined by equation 7.11 as a function of the two angular variables θ_i and θ_j with $\phi_r=0$. Fig 7.3a shows the surface, whilst 7.3b represents a contour plot of 7.3a.

Obviously one is restricted to the number of variables in a computational minimisation, so a small system of 16 molecules was set up and the ground state configuration calculated. The resulting stable configuration is shown in Figure 7.2. This organisation is exactly what we would expect, since the derivation of the pair potential was based on quadrupolar interactions which has a 'herring bone' ground state structure (O'Shea and Klein, 1979, Fuselier et al, 1978). The short range structure consists of two pairs of molecules parallel with each other, and at 45^0 to the intermolecular vector, and four pairs at right angles to each other and at the same time at 15^0 and 135^0 to the intermolecular vector. This results in the internal energy per particle, $\bar{U}/N\epsilon = -24.33$ in the ground state.

7.3 Computational Details

This study consisted of a triangular lattice of 24 x 24 molecules (i.e. N = 576). The simulation was performed using the standard Monte Carlo procedure (Rosenbluth et al, 1953) developed for studying liquids. The system was given normal two dimensional periodic boundary conditions as defined in Chapter 2.

The particles interacted with each other via the potential developed in the previous section (Eq 7.11). Where ϵ is a positive constant for molecules i and j when they are nearest neighbours, but zero otherwise. Thus each molecule interacted with its six nearest neighbours only. Throughout the simulation the particles were selected randomly by generating a random number uniformly between 1 and N^2 where in this case N=24. The particle selected was given a new orientation as defined by:-

$$\theta_{new} = \theta_{old} + \Delta(\xi-(1/2)) \qquad 7.12$$

where ξ is a random number generated uniformly in the range

0 to 1.0 and Δ is the permitted maximum displacement, controlled to govern the acceptance rejection ratio. The value of the angle θ was forced to lie in the range $0<\theta<2\pi$, by subtracting or adding 2π to prevent θ from going to very excessive values. The orientation of each molecule was stored as θ as defined in Fig 7.2.

For each temperature studied the total run was divided into two parts, firstly, an equilibration stage of typically 1000 cycles, where one cycle is N attempted moves, in which only the internal energy was output. Secondly a much longer production run of typically 4000 - 8000 cycles during which time averages of the required properties were calculated. The starting configuration for the first temperature studied, $T^* = 1.0$ where:-

$$T^* = kT/\varepsilon \qquad 7.13$$

was taken to be a perfect 'herring bone' with its glide plane, as defined in Figure 7.2 along the x laboratory axis. In principle any starting configuration could have been used, but since the zero temperature configuration has three degenerate states, each with the 'herring bone' axis along each of the three respective intermolecular vectors, problems would have arisen in reaching an equilibrium configuration. In the case of the starting configuration being totally random, i.e. a state at infinite temperature then as the system was allowed to cool, local 'herring bone' domains would form along arbitrary intermolecular vectors. It would then take a very long equilibration run to get all the domains to align along some unique intermolecular vector. An example of such a 'locked' state is given in Figure 7.4. This behaviour has been studied (Safran (1981)) for p-fold degenerate states in d dimensional systems. It was postulated that the domain sizes equilibrate as a logarithmic function of time for our 2 dimensional, 3 fold degenerate system, implying that the domains in our system

will never in fact reach the stable state with all the domains along one degenerate intermolecular vector. Because of this effect each run was started from the final production run of a lower temperature calculation which was an evolution from the initial starting configuration of a perfect herringbone ground state. The explicit details of the lengths of equilibration and production runs and starting configurations are summarised in Table 7.3. Also given in Table 7.3 are the optimum values for the maximum displacement. The final configurations of the production runs have been drawn for several temperatures and are shown in Figure 7.5.

Throughout the production run, several properties were calculated, of these the most significant thermodynamic property being the average of the internal energy, defined as:-

$$\bar{U}^* = \bar{U}/N\epsilon \qquad 7.14$$

Where $\bar{U}/N\epsilon$ is the average interaction between a pair of molecules in the system given by equation 7.11. One other thermodynamic result obtainable from the fluctuations in the internal energy is the heat capacity at constant volume given by:-

$$C_V^* = \left[\overline{U^{*2}} - \bar{U}^{*2} \right] / T^{*2} \qquad 7.15$$

The results for $\bar{U}^*$ are plotted in Figure 7.6 as a function of T^* as solid squares, and in addition are listed in Table 7.4. The heat capacity at constant volume can also be expressed as:-

$$C_V = (\partial \bar{U}^* / \partial T^*)_V \qquad 7.16$$

Using a cubic spline interpotating routine (CERN library routine E209) the heat capacity was evaluated by evaluating the derivative of the internal energy with respect to temperature, T^*. These results are also plotted on Figure 7.6 and tabulated in Table 7.4, together with those calculated using equation 7.15.

During the production stage several orientational properties were calculated, in particular various pair correlation functions and order parameters. The total pair correlation functions of rank 2 and 4 were calculated, defined by:-

$$F_2(r) = \langle \cos 2(\theta_i - \theta_j) \rangle_{r_{ij}} \qquad 7.17$$

$$F_4(r) = \langle \cos 4(\theta_i - \theta_j) \rangle_{r_{ij}} \qquad 7.18$$

These are analagous to the pair correlation functions $G_2(r)$ and $G_4(r)$ for three dimensional systems encountered in Chapters 3 and 4. Here $(\theta_i - \theta_j)$ is the difference in orientation between molecules i and j at a separation of r_{ij}. For most temperatures these correlation functions were obtained by averaging at the end of every cycle the final 4000 cycles of the production run, over all pairs of molecules in the system, up to a maximum separation distance of 10a, where a is the nearest neighbour separation. This cut-off was imposed because of the periodic boundary conditions, as contributions to the functions would have been counted twice for $r > 3xL/4$ where, as before L is the cell dimension. The results for these correlation functions are plotted in Figure 7.7 and listed in Table 7.5a and 7.5b. They will be discussed in detail in the next section.

Another pair correlation calculated was the function:-

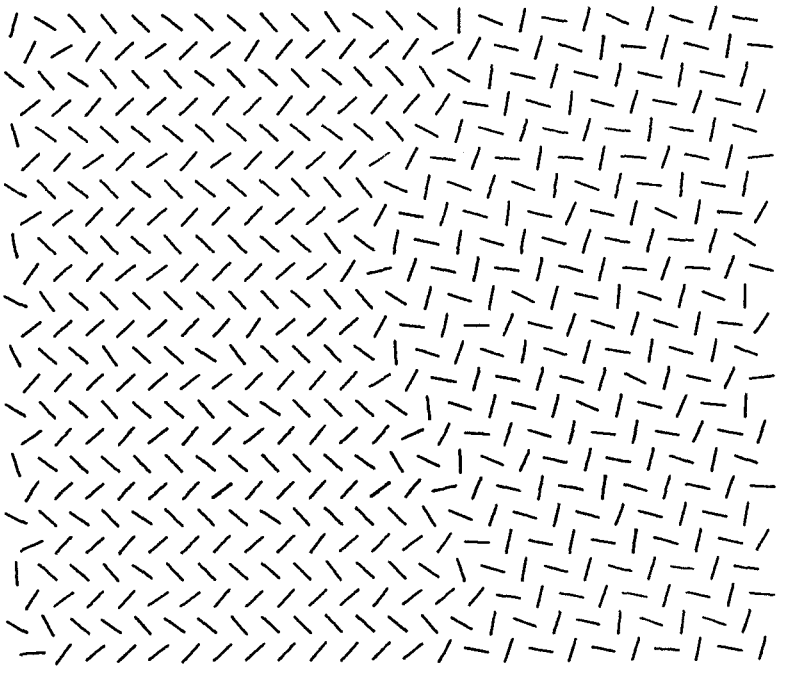

Fig 7.4 A 'locked' state which was started originally from a totally disordered state and allowed to cool at $T^*=1.0$.

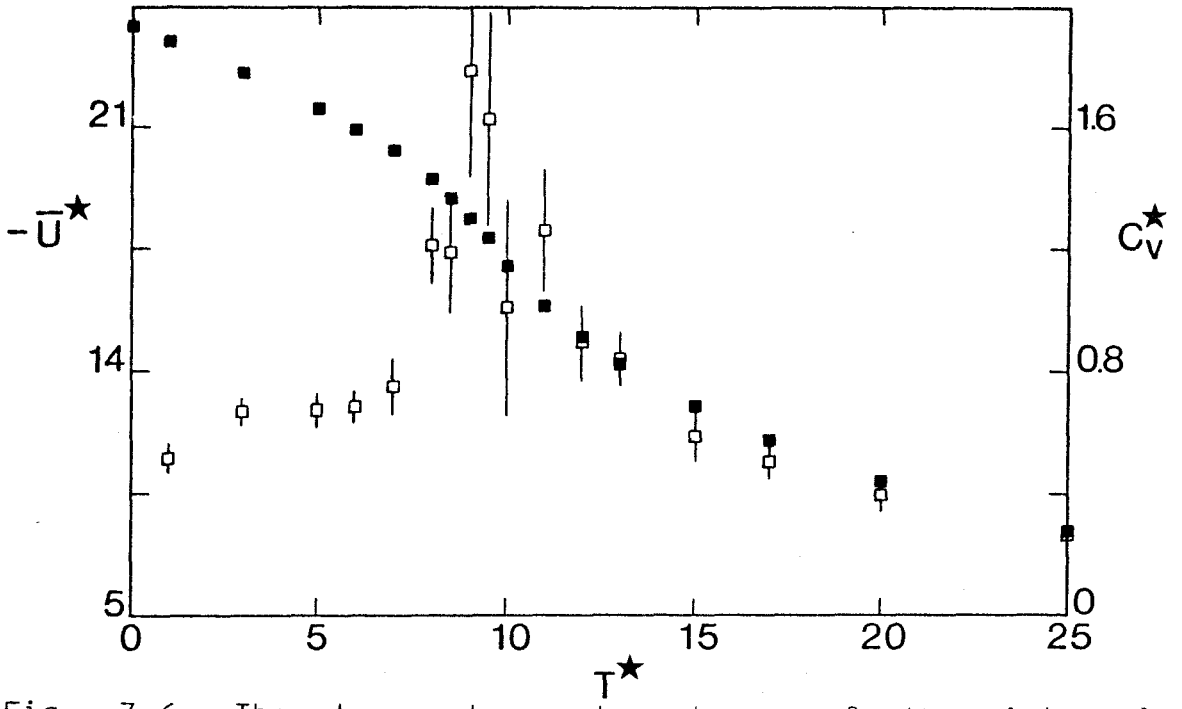

Fig 7.6 The temperature dependence of the internal energy as shown by the solid symbols and heat capacity at constant volume, C_v^* as calculated by spline fitting and differentiating the internal energy data (open squares).

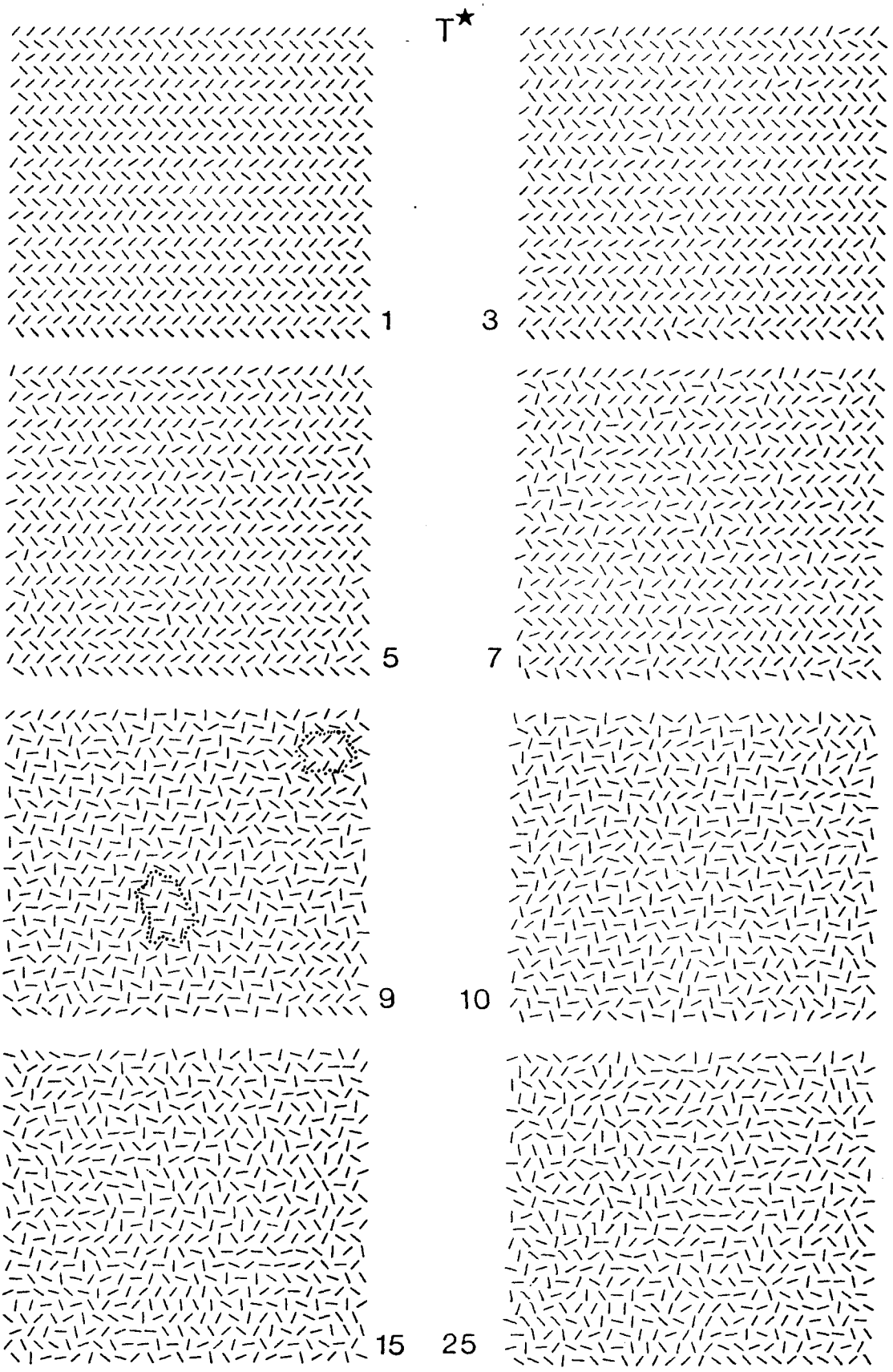

Fig 7.5 Eight typical configurations taken at the end of their respective production stages at the temperatures indicated. The dotted lines at $T^*=9.0$ indicate two highly ordered domains, with their herring bone structure along different lattice vectors.

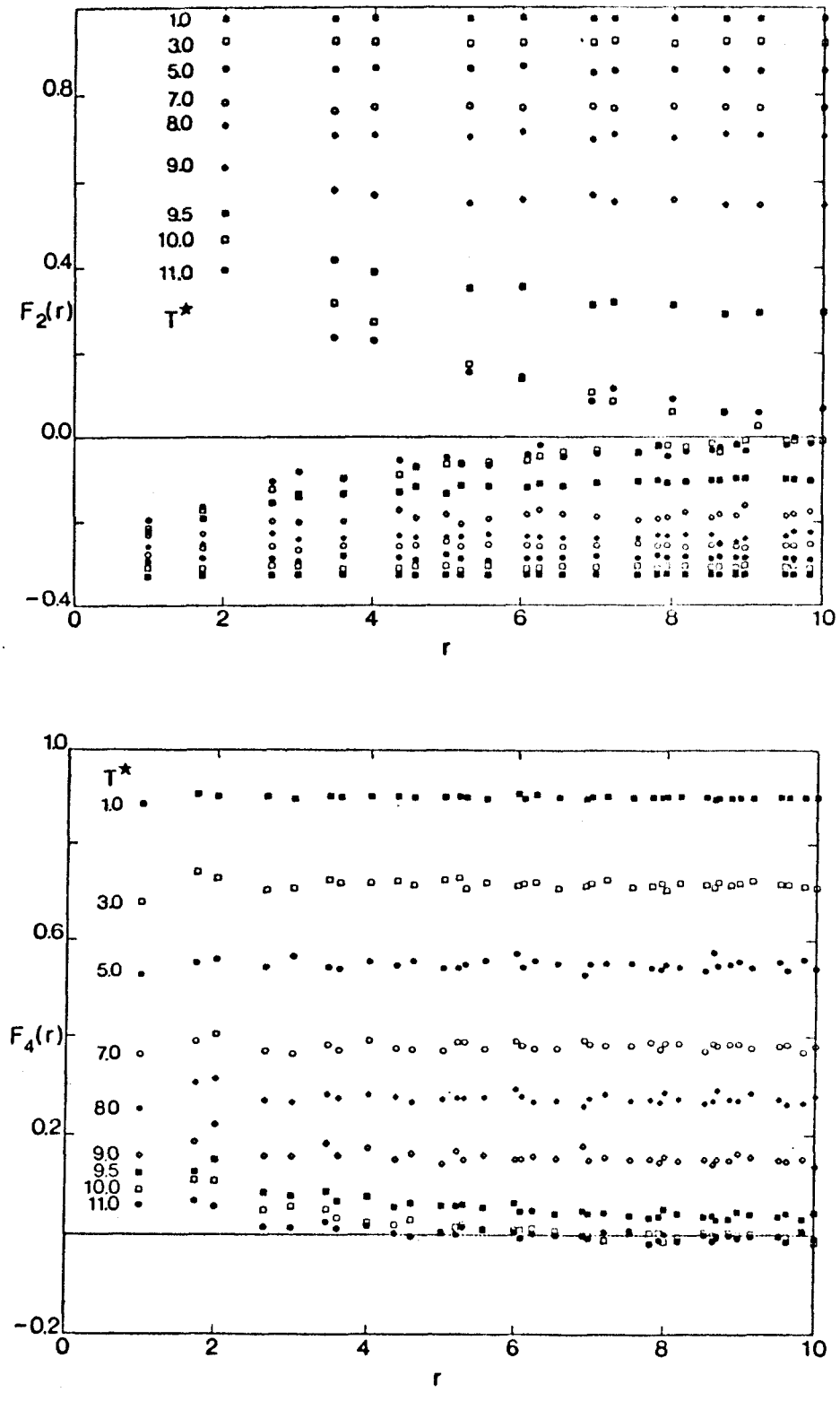

Fig 7.7 The angular distribution functions $F_2(r)$ and $F_4(r)$ as a function of intermolecular separation, r, at various temperatures studied.

$$E_2(\phi_{imv})r_{ij} = \langle\cos 2(\theta_i - \theta_j)\rangle\, r_{ij} \qquad 7.19$$

where again r_{ij} is the intermolecular separation, but r_{ij} was restricted such that it was parallel to the six unique intermolecular vectors defined by ϕ_{imv}. This property was calculated at the end of every cycle and averaged over the entire production stage of the calculation. This results in three separate pair correlation functions, with r_{ij} parallel to the 0, $\pi/3$ and $2\pi/3$ intermolecular vectors, i.e. $E_2(0)$, $E_2(\pi/3)$ and $E_2(2\pi/3)$ respectively, since the pair correlation functions for the 0, π; $\pi/3$, $4\pi/3$; and $2\pi/3$, $5\pi/3$ intermolecular vectors will be obviously equal. In addition, with the herring bone glide plane parallel to the 0 intermolecular vector, $E_2(\pi/3)$ and $E_2(2\pi/3)$ will be also similar. The results for $E_2(0)$ and the average of $E_2(\pi/3)$ and $E_2(2\pi/3)$ are plotted in Figure 7.8 and listed in Tables 7.5a and 7.6b respectively.

We can now discuss what order parameters could be calcualted for this particular system. What we require is an order parameter which will distinguish between the long range 'herring bone'order in the S_E phase and the rotational disorder in the S_B phase. In a perfect S_E phase with one domain, i.e. with a 'herring bone' structure with the glide planes along some unique vector, the structure can be described as arising from two sub-lattice structures, for example in Figure 7.2 the two sub-lattices are labelled A and B. Unfortunately there is no easy way of distinguishing between these two sub lattices in the simulation, otherwise order parameters of the form $\langle\cos 2\,\theta_i\rangle$ or $\langle\cos 2(\theta_1 - \phi_r)$ could readily be calculated. In the case of the first order parameter, it will equal +1 or -1 depending on the choice of sublattice and similarly for more general case $\langle\cos 2(\theta_i - \phi_r)\rangle$. The easiest way round this problem is to calculate a higher rank order parameter, for example $\langle\cos 4$

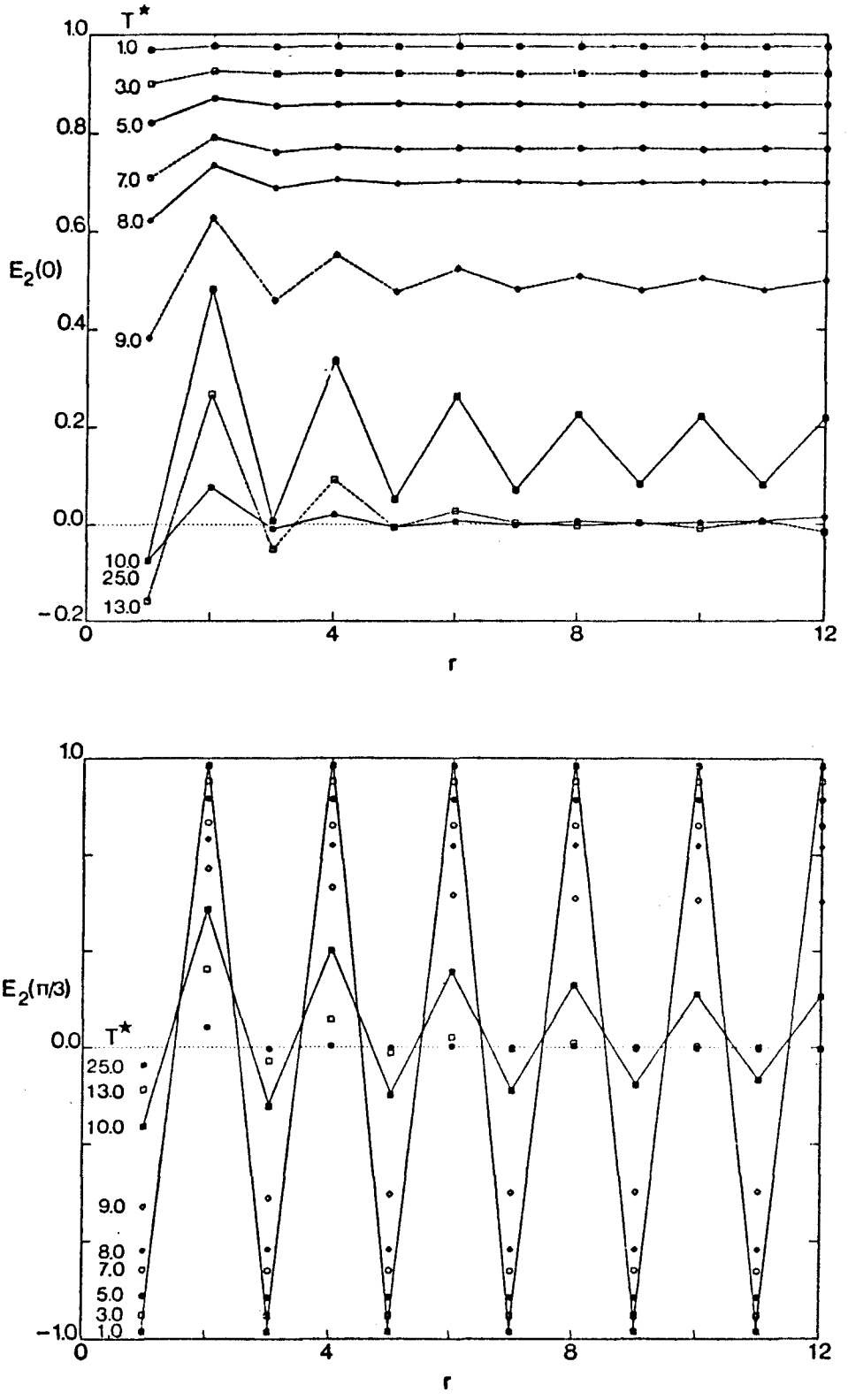

Fig 7.8 The angular distribution functions $E_2(\phi_r)$ evaluated at $\phi_r=0$ and $\phi_r=\pi/3$ as a function of intermolecular separation r, at various temperatures. The lines serve only as a guide to the eye.

$\theta_i>$ or more explicitly $<\cos 4(\theta_i - \phi_r)>$ giving order parameters with respect to the lattice vectors. In this case for ϕ_r parallel to the herring bone glide plane, all order parameters, regardless of sub lattices will be similar, and likewise for ϕ_r equal to π or $2\pi/3$. This set of order parameters will be denoted $\bar{C}_4(0)$, $\bar{C}(\pi/3)$ and $\bar{C}_4(2\pi/3)$. It can be seen from observation of Figure 7.2 of a perfect herring bone configuration that $\bar{C}_4(0)$ will equal +1 and $\bar{C}_4(\pi/3)$ and $\bar{C}_4(2\pi/3)$ will both equal -1/2. These order parameters were calculated by averaging over the entire system at the end of every cycle in the production run. As a check against the herringbone rotating (remember the initial simulation was started from a perfect herring bone with the glide planes parallel to the $\phi_r = 0$ direction) or domains setting in near the transition, which undoubtably does happen, a fourth order parameter was evaluated denoted as $\bar{C}_4(\max)$ and defined as the maximum of $\bar{C}_4(0)$, $\bar{C}_4(\pi/3)$ and $\bar{C}_4(2\pi/3)$. This maximum value was taken at the end of each cycle for the value of $\bar{C}_4(0)$, $\bar{C}_4(\pi/3)$ or $\bar{C}_4(2\pi/3)$ averaged over that cycle only, and averaged over the total production phase. These results are plotted in Figures 7.9 and listed in Table 7.7

7.4 Discussion of Results

The most useful thermodynamic property calculated in this simulation was the internal energy as defined in equation 7.11. The results obtained for $\bar{U}^*$ are plotted as a function of the reduced temperature T^* in Figure 7.6. The variation of the internal energy clearly shows a slight change of slope in the region of $T^* = 9.0$ to $T^* = 11.0$ which is confirmed by the heat capacity calculated from spline fitting the internal energy, which shows a divergence in this region. This behaviour suggests a second order phase transition occuring at $T^* = 9.3 \pm 0.4$, the location of the maximum in the heat capacity.

The presence of a transition is further confirmed from

observation of the low and high temperature configurational plots in Figure 7.5. Also plotted on Figure 7.6 is the specific heat calculated from the energy fluctuations as given by equation 7.15. However, the agreement between the heat capacity calculated this way is poor compared with that obtained from spline fitting the internal energy. This is probably due to taking sub averages over too smaller intervals during which time the energy fluctuations are relatively small. Indeed in Chapter 3 we saw excellent agreement in the values for $\bar{C}_v^*$ calculated by both methods.

It has recently been suggested (Mouritsen and Berlinsky, 1982) in a study of nitrogen adsorbed on graphite, using a very similar pair potential (without the $\cos 2(\theta_i - \theta_j)$ term) that a first order transition at $T^* = 9.04$ does in fact occur. However, in order to observe a sharp discontinous transition in the internal energy they had to employ very large sample sizes (up to 10000 molecules), although obviously the term omitted in their pair potential would give the system different transition properties. In fact their value for the entropy of transition ($\Delta S/R \sim 0.01$) is so small that it could be interpretated as not being of first order, but possibly second also. This problem of determining the order of transition, especially in systems which would appear to be very dependent on size, and in which degenerate states can occur, has always been worrying (Landau and Swendsen, 1981) particularly in simulations using the Ising model in which particles can occur in two states only (e.g. up or down) or more generally in the q-state Potts model (a generalisation of the Ising model). Indeed, computer simulation of a three dimensional, three state Potts model with renormalisation group theory calculations yields a continuous transition, although it is arguably first order when simulated using the Monte-Carlo technique (Knak-Jensen and Mouritsen, 1979).

What can be concluded, however, is that we do observe a transition between a rotationally ordered and disordered phase, which is second order or higher.

This order-disorder transition is further emphasised in the plots of the order parameters $\bar{C}_4(0)$, $\bar{C}_4(2\pi/3)$, $\bar{C}_4(2\pi/_3)$ and $\bar{C}_4(\text{Max})$ as a function of T^* as shown in Figures 7.9 and Table 7.7. At low temperatures, as we would expect the system is highly ordered, with this order decreasing with increasing temperature, until it is negligible at high temperatures. The existence of a transition is clearly shown, and from the plot we can say that it occurs within the range of $T^* = 9.0$ to 10.0, confirming our result obtained previously from thermodynamic considerations.

It is worth noting that the ordering is essentially continuous through the transition, which again could be due to the finite size of the system, or more probably due to the high order of the transition. The behavior of the $\bar{C}_4(\pi/3,\ 2\pi/3)$ order parameter (plotted as the open circles) is exactly as expected, and within the experimental error on the points this order parameter is exactly -(1/2) times the value of $\bar{C}_4(0)$. At low temperatures the value of $\bar{C}_4(\text{max})$ is identical with $\bar{C}_4(0)$, although close to the transition its value does become slightly greater, indicating locally ordered domains forming with the herring bone glide plane aligned along some other inter-molecular vector. This is apparent in the configuration plots, (Fig. 7.5) where for example, at $T^* = 9.0$ the dotted line indicates two of these relatively highly ordered domains.

We now turn our attention to the total pair correlation functions $F_L(r)$ as defined in equations 7.17 and 7.18. However, before discussing the results it is worth considering what we should expect for a perfect herring bone structure on a triangular lattice. Examination of such a system gives different values of $F_2(r)$ depending on the value of r. In some of the coordination shells all the

particles are parallel with the reference, so $F_2(r) = 1$, whilst in other shells, two molecules are parallel, and four orthogonal to the reference molecule, giving $F_2(r) = -1/3$. In contrast the value of $F_4(r)$ is always one regardless of the coordination shell. This behaviour is confirmed by what we observe. Figure 7.7 shows the results for $F_2(r)$ as a function of r, obtained by averaging over all pairs of molecules up to a maximum distance of $r < 10$ lattice vector units. Each set of data points represent averages over typically 4000 cycles and even 8000 cycles for $T^*=9.5$ (1000 cylces for $T^*=1.0$). Above the transition at $T^*=9.3 \pm 0.04$, we would expect all long range correlations to vanish, whilst remain finite in the S_E phase. However, even at $T^*=11.0$, these correlations decrease slowly with increasing r, and only disappear totally at the extremities of the cut off. This relatively high long range order is probably related to the fact that the transition is of high order and will be discussed further later. The fourth rank correlation again indicates exactly what we would expect, with correlations existing over long distances in the S_E phase, and decreasing with temperature, until all long range order is destroyed completely above the transition temperature. This behaviour is in contrast with the second rank function, but could be a consequence of the fact that $F_4(r) < F_2(r)$ for any given temperature. One other very interesting feature is a slight maximum in the correlation function at about r=2, being more pronounced near the transition. This again will be discussed later. As we have seen in other pair correlation functions (in Chapters 3 and 4), the long range limiting value is simply the square of the corresponding order parameter (Zannoni, 1979). Therefore, for example, taking the positive limits in the pair correlation function $F_2(r_{ij})$, will yield an order parameter for the average of $\cos 2\theta$ which otherwise would not be calculable, since it would average to zero with the inclusion of the negative correlations. Similarly taking this negative limit, multiplying it by

-(1/2) and taking the square root will give the same order parameter. The results for this order parameter, together with $\overline{\cos 4\theta}$ where the bar denotes an average, obtained from the limiting values of $F_4(r_{ij})$ are plotted as a function of T^* in Figure 7.10 and tabulated in Table 7.8. As expected the plots clearly show a transition from an orientationally ordered to a disordered phase in the region of $T^* = 9.0$ to $T^* = 10.0$.

However, these two total pair correlations functions tell us nothing of the ordering in the system with respect to the lattice axes, so we now turn to the pair correlation functions defined by equation 7.19 i.e.

$$E_2(0) = \langle \cos 2(\theta_i - \theta_j)(r_{ij}) \rangle \quad , \phi_{r_{ij}} = 0 \qquad 7.20$$

$$E_2(\pi/3) = \langle \cos 2(\theta_i - \theta_j)(r_{ij}) \rangle \quad , \phi_{r_{ij}} = \pi/3 \qquad 7.21$$

$$E_2(2\pi/3) = \langle \cos 2(\theta_i - \theta_j)(r_{ij}) \rangle \quad , \phi_{r_{ij}} = 2\pi/3 \qquad 7.22$$

In this case the correlations are for pairs of molecules along given lattice vectors, where r_{ij} is again the distance in lattice vector units between molecules i and j, hence r_{ij} can adopt integer values only. Thus for a perfect herring bone structure, all the molecules along the vector parallel to the glide plane will be parallel to each other and so the pair correlations will all equal 1.0 for all r_{ij}. However, for the intermolecular vectors at $\pi/3$ and $2\pi/3$ to the glide plane the molecules will alternate between being parallel and orthogonal, so for odd values of r, it will equal -1 while for even values +1. At low temperatures this is exactly what is observed. The results for $E_2(0)$ and the

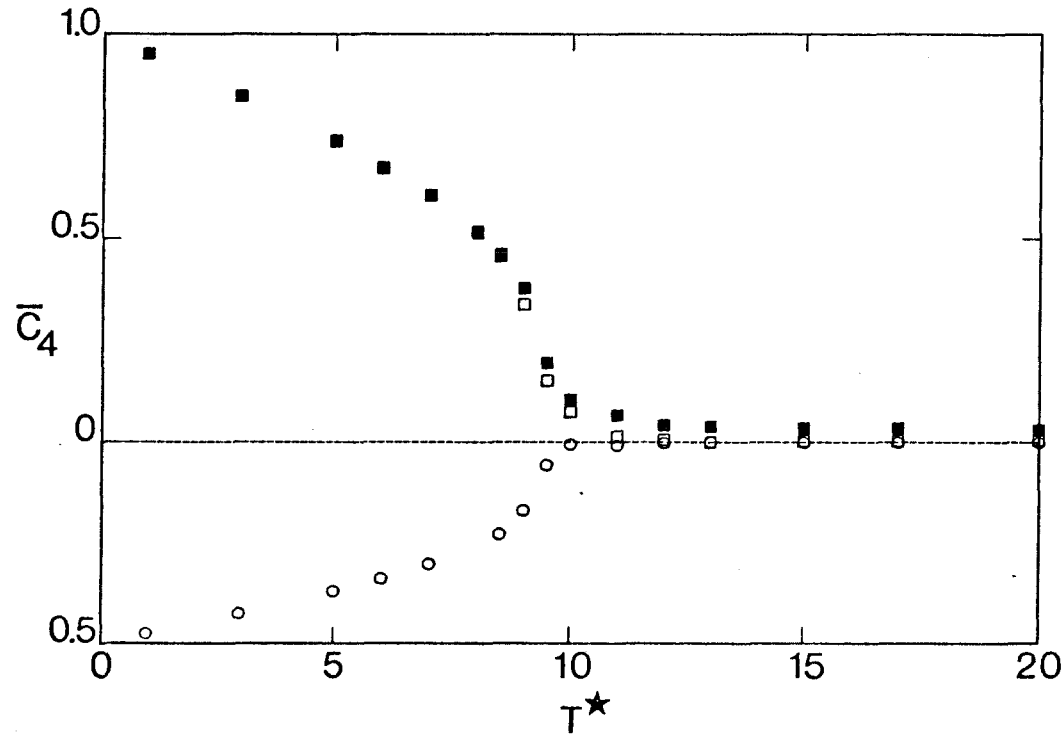

Fig 7.9 The reduced temperature dependence of the order parameter $\bar{C}_4$. Here the solid squares represent $\bar{C}_4(0)$, the open circles the average of $\bar{C}_4(\pi/3)$ and $\bar{C}_4(2\pi/3)$, and the open squares $\bar{C}_4$ (max).

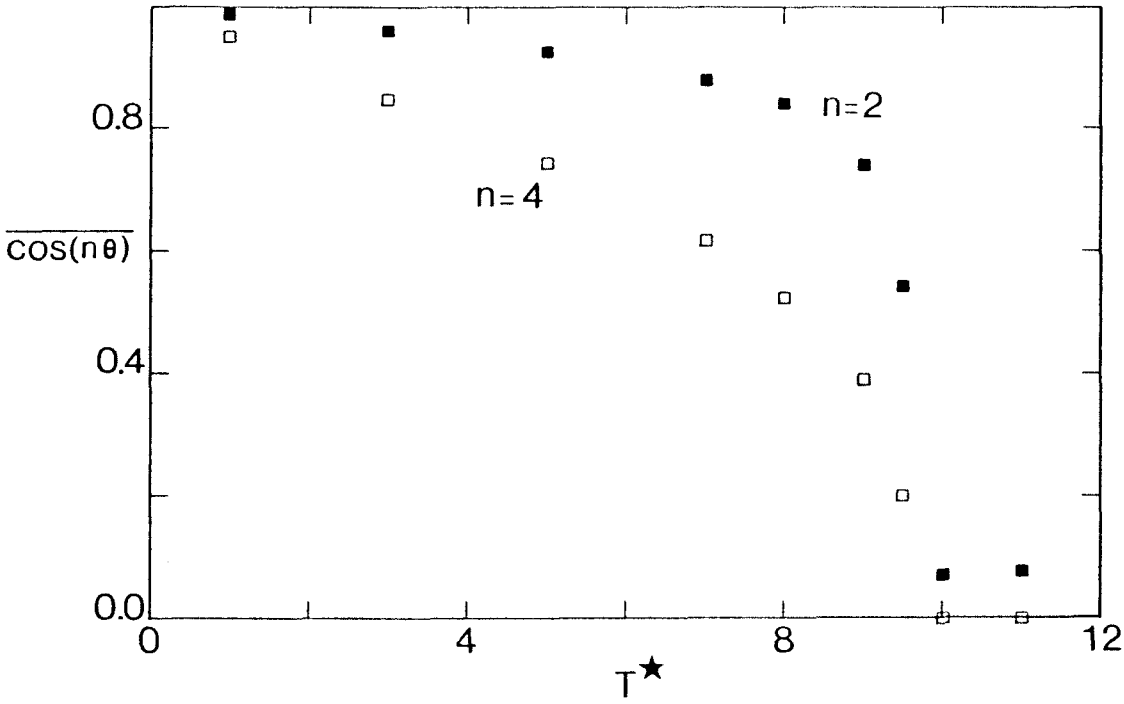

Fig 7.10 The reduced temperature dependence for the order parameters $\cos(n\theta)$ for n=2 and n=4 calculated from the limiting values of the distribution function $F_2(r)$ and $F_4(r)$ respectively.

average of $E_2(\pi/3)$ and $E_2(2\pi/3)$ obtained from the simulation are plotted in Figure 7.8 as a function of r_{ij} at different temperatures. (The lines serve only as a guide to the eye). At low temperatures the functions are well behaved, in that the angular correlations are long range, and they decrease with increasing temperature. However, close to the transition an alternating effect is observed, with even r values being larger than odd values. This is due entirely to the fact that close to the transition local domains start to occur, and so the correlations $E_2(0)$,$E_2(\pi/3)$ and $E_2(2\pi/3)$ no longer become unique. What we see therefore, is an average of these three functions. For even r_{ij} the correlations are always positive and equal, but for odd r_{ij}, $E_2(\pi/3)$ and $E_2(2\pi/3)$ adopt negative values, resulting in a reduction in the value of $E_2(0)$. This effect is especially noticable for r_{ij}=1, when the correlation goes negative through the transition. This alternating effect therefore, is a measure of domain growth in the system. One other interesting feature is the slight maximum again at r_{ij}=2 and in neighbouring shells, similar to the effect seen in $F_2(r_{ij})$. Again in the S_B phase quite large correlations at short r_{ij} are present which decrease only slowly on going to higher temperatures.

In addition order parameters can be obtained from the limiting values of $E_2(0)$ and $E_2(\pi/3)$, which should be similar to those evaluated from the limits of the complete pair correlation functions. Indeed within limits of experimental error this is what is observed, and the results for the average of the positive limiting values for $E_2(0)$ are also given in Table 7.8.

We can now consider the observation of increased correlations at a lattice distance of about r_{ij}=2. This behaviour is seen in the plots of the fourth rank total pair correlation function $F_4(r_{ij})$ in Figure 7.7 and in the plots of $E_2(0)$ in Figure 7.8. Indeed, if $E_2(\pi/3)$ (Figure 7.8) were plotted such that the correlations were all positive, then

this effect would also be observed. Another phenomena linked to this, is that the correlations in the first shell are slighly smaller than the limiting values. One explanation for this effect, is due to the nature of the pair potential. If we turn back to equation 7.11 the potential consists of two terms, the more dominant being the latter. At extremely low temperatures we know that the ground state configuration for the potential in equation 7.11 is a herring bone structure. However, at the end of section 7.2 we saw where this ground state configuration occured on the potential energy surface, with two of the pair configurations on the sides of a relatively steep ridge (see Figure 7.3). What may occur at temperatures close to the transition, is that these pairs of molecules tend to fall further into the potential well, so going to more perpendicular type nearest neighbours structures, resulting in a decrease in the nearest neighbour pair correlations. This in turn means that pairs of molecules at a distance of two inter molecular units will have increased parallel correlations, showing up in the pair correlation functions. This effect will be small compared with, at low temperatures, the dominant herring bone structure, and at high temperatures the complete rotational disorder, hence, it is only just apparent close to the transition.

In the Introduction to this Chapter it was mentioned that X-ray analysis work on TBBA (Doucet, Levelut and Lambert, 1974) revealed that the S_B phase could consist of small domains of ordered herring bone structure. If indeed this were the case then our calculated correlation functions verify it, since in all the second rank functions, short range order does extend well into the smectic B phase.

7.5 Optical Masking

The greatest difficulty in X-ray diffraction is the determination of structural information from very complex scattering patterns. The most common method for this

analysis is to calculate scattering patterns from proposed crystal structures. The calculated patterns are then compared with experimental patterns, necessary refinements made to the proposed structure and the whole process repeated until satisfactory agreement of patterns is observed.

An alternative, much simpler technique, although not as accurate, is that of optical masking. The interatomic distances in crystal structures are such that they will diffract X-ray radiation by fulfilling the Bragg scattering law. However, if the interatomic distances are increased then eventually optical radiation can be used for scattering. This is the basic principle behind optical masking. Normally a photographic negative is made with transparent holes suitably produced such that the locations and diameter of the holes represent the positions and sizes of the atoms in a proposed structure. Obviously the negative represents a projection of the three dimensional structure onto a two dimensional plane, corresponding to diffraction of X-rays from a particular crystalline face. Using monochromatic light directed through the mask, a diffraction pattern is produced and normally recorded on photographic plates. This methoo therefore removes the problem of having to numerically calculate scattering patterns.

Using three configurations taken from the simulation at reduced temperatures, of 1.0, 8.0, and 17.0 corresponding to highly ordered, weakly ordered and highly disordered systems, scattering patterns were obtained using these configurations as optical masks. The configurations and respective scattering patterns are shown in Figure 7.11. This corresponds to scattering produced with the incident radiation perpendicular to the layers.

Before comparing the patterns with experiment it is worth while calculating what kind of pattern we would expect from such a system. First of all, the rotationally disordered S_B phase. The only symmetry element present in

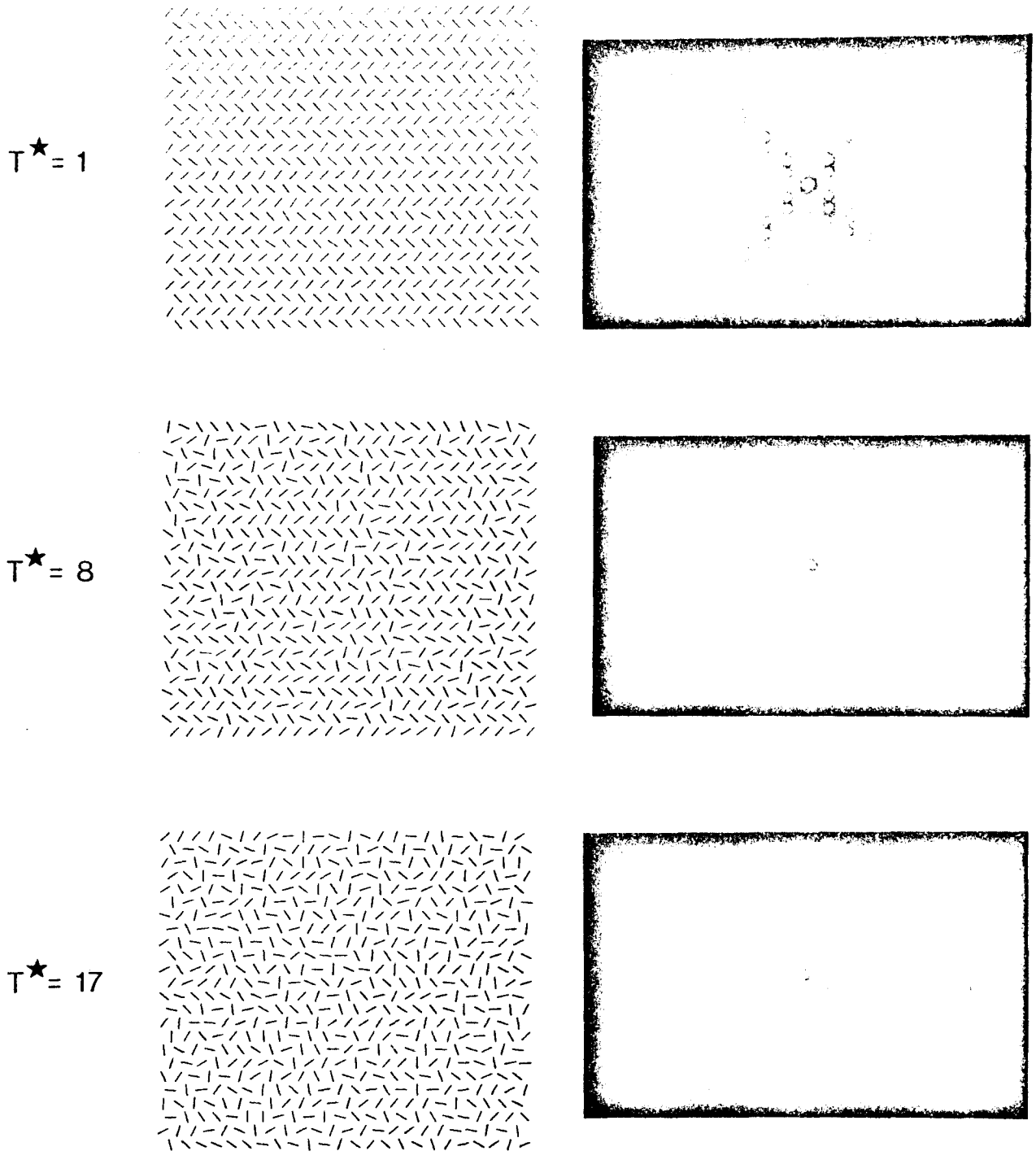

Fig 7.11 Configurations taken at three different temperatures with their respective scattering patterns obtained using the technique of optical masking.

such a phase is the six fold translational symmetry. The unit cell for such a system is shown in Figure 7.12a. This is the smallest repeating unit possible in order to build up a triangular network. The next problem is to calculate the reciprocal lattice structure. If our real lattice is defined as having non-orthogonal axes a and b, then in reciprocal space these will be a^* and b^*. Using the notation of Muller, indices labelling various planes in the real lattice can be defined. The set of planes in the real lattice whose indices are h and k, intercept the a and b axes at a/h and b/k respectively. Various planes are shown in Figure 7.12a. The perpendicular distances of these planes from the origin are denoted d_{hk}. The reciprocal lattice is then formed with vectors along d_{hk} whose length is inversely proportional to the length of d_{hk} in real space. This gives an infinite array of points labled (h,k) in reciprocal space. Figure 7.12b shows part of the reciprocal lattice of the unit cell structure in Figure 7.12a which can be compared directly with experiment, since scattering patterns are simply representations of the reciprocal lattice. Thus for our S_B configuration we would expect a scattering pattern identical with the reciprocal lattice structure in Figure 7.12b. This is indeed exactly what we do observe in the bottom scattering pattern in Figure 7.11. In addition to the regular array of spots, close to the central six spots, are diffuse scattering regions, the presence of which will be discussed later.

Adopting a similar procedure we can calculate the reciprocal lattice structure for the unit cell defining the low temperature S_E phase. Now the unit cell is twice as large (Figure 7.13a) giving a closer packed reciprocal lattice (Figure 7.13b). Thus, at this point we would expect the reciprocal lattice to consist of an array of points with half the separation along the a^* direction to that in the S_B phase. However, additional symmetry in the S_E phase dictates that certain spots on the reciprocal lattice are absent. In particular, it has two glide planes (equivalent to a mirror

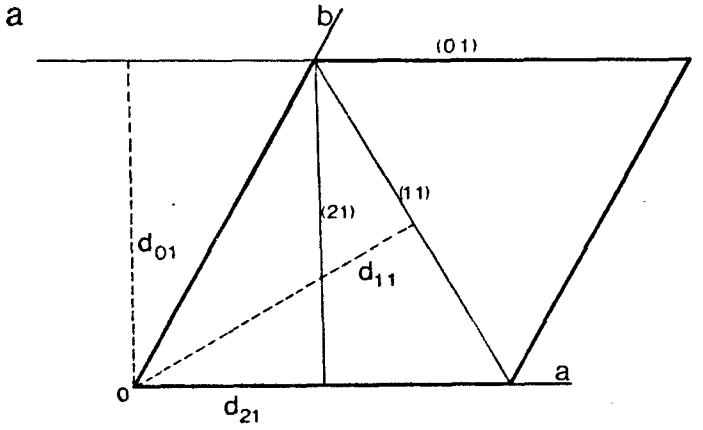

Fig 7.12

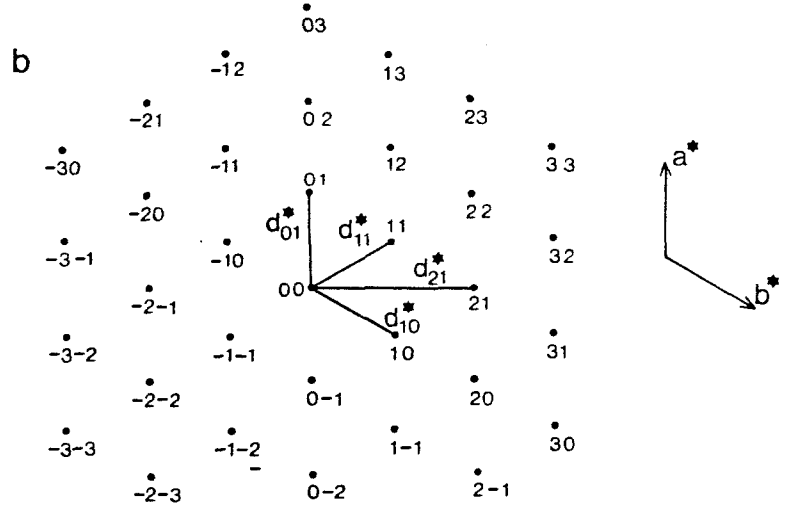

The unit cell (7.12a) representing the S_B phase, together with a part of its reciprocal lattice (7.12b)

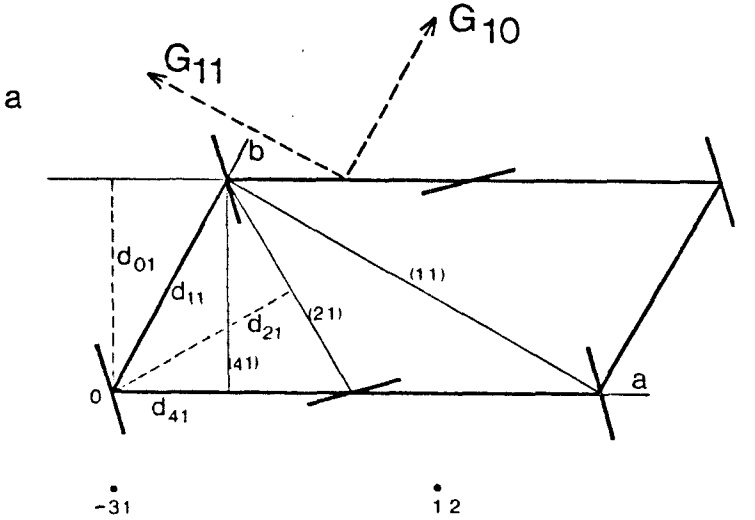

Fig 7.13

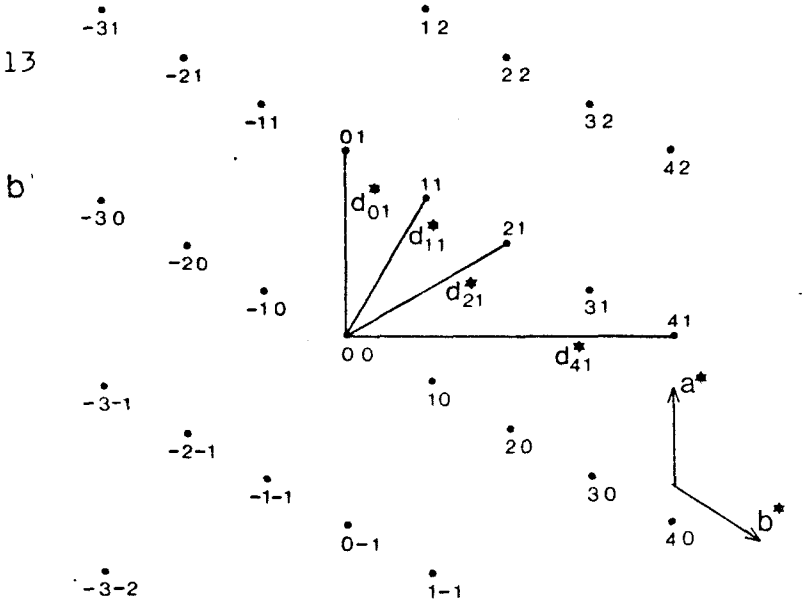

The unit cell (7.13a) representing the S_E phase, together with a part of its reciprocal lattice (7.13b)

plane after translation along that plane) marked as the dashed lines in Figure 7.13a parallel to the (10) and (11) planes. This results in alternate absences in diffraction spots along these two directions on the reciprocal lattice. This pattern, together with these systematic absences are seen in the optical diffraction pattern at the top of Figure 7.11 for the configuration at $T^*=1.0$. The total diffraction pattern expected for the S_E and S_B phases is shown in Figure 7.14. The solid squares represent the pattern that the S_B phase only would give and the solid circles the additional spots arising from the reduced symmetry of the S_E phase. The alternate absences along the (10) and (11) directions are shown as the open circles. It should be noted that the labelling of spots is consistent with the unit cell for the S_E phase only. (For the S_B unit cell, the a^* labels would be divided by two).

We can now comment on the cause of the diffuse regions around the central six spots in the S_B phase. This is due to the high short ranged order which we also saw in the previous section in the pair correlation functions. This local herring bone order will exist along all three lattice vectors. The most significant difference between the scattering patterns in the S_B and S_E phases close to the origin are the presence of the eight spots labelled (32), (31), (1-1), (-12), (-3 -2), (-3 -1) (-11) and (12). Therefore with very local herring bone order present in the S_B phase, along all three lattice vectors, a weak average scattering will be formed, observable as the blurred regions in the bottom scattering pattern in Figure 7.11.

So far no mention has been made of the striking cross pattern in the two scattering patterns of the S_E phase. In deriving our scattering pattern in Figure 7.14 all that was assumed was the shape of the unit cell, being twice the size of that in the S_B phase. This is because in the S_E phase the additional order allows us to distinguish between the two orientations of the molecules. Thus superimposed on the

Fig 7.14 The diffraction pattern expected for the S_E and S_B phases. The solid squares are those from the S_B structure, and the additional spots (solid circles) are those arising from the additional symmetry in the S_E phase. The open circles are the systematic absences occurring because of the two glide planes in the S_E structure.

scattering described earlier will be a pattern attributed to the order with respect to the two orientations in which the molecules lie. This results in the dominant 'cross' pattern being present at both temperatures in the S_E phase. For example, if the optical diffraction pattern had been obtained from a mask in which all the lines were parallel and randomly distributed, then the resulting diffraction pattern would consist of a series of lines orthogonal to the direction of the lines in the mask, which would decrease in intensity on going from the centre of the pattern. Hence, for two sets of lines at right angles to each other on a mask, the pattern would consist of a series of orthogonal lines decreasing in intensity from the origin giving a 'cross' like diffraction pattern. Thus the pattern for the low temperature S_E phases actually consist of two superimposable patterns, a series of spots resulting from the structural unit cell, together with a 'cross' caused by the actual shape and orientation of the lines representing the molecules.

A comparison with real X-ray scattering patterns can now be made. The resolution of such patterns is normally only sufficient to resolve the first few spots only. X-ray scattering from TBBA (terephthalylidene-bis-4-n-butylaniline) (Doucet et al, 1975; Doucet, 1979) in its S_B phase reveals the six central spots and in addition the diffuse regions mentioned above. In the S_E phase of PBAPC (Leadbeater et al, 1979, Doucet et al, 1975) the six central spots are observed, together with the next closest four. So although X-ray diffraction does not allow the complete resolution one would wish for, the patterns obtained are very consistent with our optical masking patterns produced from configurations taken from the simulation. Actually slightly better resolution is obtained in scattering from nitrogen molecules physisorbed on graphite (Diehl, Toney and Fain, 1982) using low energy electron diffraction. In this case the long molecular axes of the nitrogen molecules form

a herring bone structure at temperatures less than about 30K, similar to the S_E phase.

7.6 Comparison with molecular field theory

In many of the preceding Chapters, wherever possible, the results obtained from the computer simulations have been compared, often quite successfully, with the predictions of molecular field theories. Therefore, for completeness a similar comparison will be made here. To date, the only theories available for the description of order in the smectic E and B phases are those developed by Meger and Jay, 1975, 1976. Basically they have performed both a molecular field treatment and a theory based on the Landau expansion of the free energy at the transition. In both cases they assume an intermolecular pair potential exactly identical to that used in this Chapter.

The molecular field treatment simply derives the average potential of a molecule in the system, resulting from the interactions between pairs of molecules in both sub lattices. Thus for example, a molecule in sub-lattice, a (see Figure 7.2), experiences an average interaction from two other molecules in the same sublattice, together with four in sublattice b. A full description of this treatment can be found in the above references. The most significant prediction is that of the S_E and S_B transition temperature. It is evaluated to be:-

$$kT/\varepsilon = 24.33$$

Thus when compared with the result of the simulation it is actually overestimated by 160%. This overestimation by theory is common, as we have seen in previous chapters. Furthermore, a 50% over prediction by molecular field theory was observed in the simulation of a two dimensional nematic. (Denham et al, 1980).

To conclude this chapter therefore, the use of a very simple model with a relatively simple pair potential based on quadrupolar interactions, has allowed a fairly detailed investigation of some of the orientational properties associated with the smectic-B to smectic-E phase transition, properties which are unavailable by other means. Furthermore, the application of the technique of optical masking has to a certain extent, demonstrated the validity of such of simple tool to give diffraction patterns which would otherwise only be obtainable by X-ray or neutron scattering.

Table 1.1

A table of a few liquid crystal molecules and their mesophases. The transitions are in degrees centigrade.

Cholesteryl benzoate	$C \overset{153}{\rightleftharpoons} Ch \overset{182}{\rightleftharpoons} I$
4,4-dimethoxyazoxybenzene (PAA)	$C \overset{118}{\rightleftharpoons} N \overset{136}{\rightleftharpoons} I$
4, 4-di-n-heptyloxyazoxybenzene (HOAB)	$C \overset{74}{\rightleftharpoons} S_C \overset{95}{\rightleftharpoons} N \overset{124}{\rightleftharpoons} I$
terephthalylidene-bis-(4-n-butylaniline)	$C \overset{113}{\rightleftharpoons} S_B \overset{114}{\rightleftharpoons} S \overset{172}{\rightleftharpoons} S_A \overset{199}{\rightleftharpoons} N \overset{235}{\rightleftharpoons} I$
2-(4-n-pentylphenybeuzylidene-p-amino n-pentyl cinnamate) (PBAPC)	$C \overset{92}{\rightleftharpoons} S_E \overset{101.5}{\rightleftharpoons} S_B \overset{168}{\rightleftharpoons} S_A \overset{204}{\rightleftharpoons} I$
2-(4-n-pentylphenyl)-5-(4-n-pentyloxyphengl) pyrimidine (PPP)	$C \overset{79}{\rightleftharpoons} S_G \overset{103}{\rightleftharpoons} S_F \overset{114}{\rightleftharpoons} S_C \overset{144}{\rightleftharpoons} S_A \overset{210}{\rightleftharpoons} I$

Abbreviations

C - crystalline
N - nematic
I - Isotropic
S - smectic

Table 3.1 Transition properties

	T_{NI}	$\bar{P}_2^{NI}$	$\triangle S/R$	$\bar{u}_2^*$	$T_{NI}/\bar{u}_2^*$
I	1.127±0.003	0.27±0.02	0.06±0.01	6	0.1878±0.0005
II	2.43 ±0.03	0.31±0.03	0.04±0.02	12	0.203 ±0.003
III	1.54 ±0.02	0.35±0.03	0.06±0.03	7.796	0.198 ±0.003
IV	3.06 ±0.05	0.24±0.56	0.10±0.07	14.31	0.214 ±0.003
Lebwohl & Lasher (1972)	1.124±0.006	0.38±0.01	0.10	6	0.187 ±0.001
Jansen et al. (1977)	1.119±0.001	0.33±0.04	0.09±0.01	6	0.186 ±0.001
Meirovitch (1977)	1.111±0.004	0.27±0.02	0.11±0.04	6	1.852 ±0.001
Maier Saupe	-	0.429	0.417	-	0.2202
Two site cluster z=6	1.160	0.382	0.282	-	0.193
z=12 (Sheng & Wojtowicz 1976)	-	0.408	0.361	-	0.207

Table 3.2 Properties evaluated from the pair correlation functions $G_2(r_{ij})$ and $G_4(r_{ij})$ for Model IV

T^*	$-\bar{U}^*$		$\bar{P}_4$	
	direct	via $G_2(r_{ij})$	$G_4(r_{ij})$	predicted[1]
1.250	5.79±0.01	5.77	0.671	0.673±0.005
1.750	5.09±0.01	5.11	0.527	0.536±0.004
2.250	4.26±0.03	4.22	0.387	0.399±0.006
2.500	3.66±0.02	3.56	0.303	0.320±0.005
2.875	2.36±0.05	2.22	0.145	0.154±0.013
3.000	1.48±0.09	1.40	0.063	0.062±0.006
3.125	0.87±0.05	0.90	0.024	0.018±0.006
3.750	0.572±0.008	0.528	0.000	0.004±0.001

[1] Maier-Saupe prediction of $\bar{P}_4$. The errors arise from the uncertainty in $\bar{P}_2$ leading to an uncertainty in $\bar{u}_2$.

Table 3.3

The coefficient a in the singlet orientational distribution function and its dependence on $\bar{P}_2$ for Model I.

T*	$\bar{P}_2$	a	$aT^*/\bar{P}_2$
1.000	0.625	3.154	5.047
1.020	0.604	3.054	5.056
1.042	0.577	2.917	5.055
1.064	0.544	2.777	5.068
1.087	0.485	2.435	5.021
1.111	0.398	1.996	5.015
1.124	0.311	1.573	5.051

Table 4.1 Computational details

T*	Starting T*	Number of Cycles:-		
		Equilibration	Production	Written to magnetic tape
1.5	2.0	1000	2500	1500
1.75	1.5	500	2000	-
2.0	2.5	1000	1500	1250
2.25	2.0	1000	1500	1500
2.4	2.25	1000	1500	-
2.5	0.0[1]	2000	2500	2500
2.6	2.5	2500	2500	2500
2.65	2.25	1500	2500	1500
2.7	2.5	1000	6250	4000
2.75	2.0	2500	5000	-
2.8	2.7	1750	2000	-
3.0	2.5	1000	2000	-
3.25	1.5	500	2000	-
3.5	2.5	1000	2000	-
4.0	2.5	1000	1000	1000

Total averages obtained by averaging sub averages each of 50 cycles.

[1] All aligned antiferroelectric configuration.

Table 4.2 Thermodynamic Results

T*	$-\bar{U}_{DISP}$	$-\bar{U}_{DIP}$	$-\bar{U}_{TOT}$	Cv (Spline)	Cv (fluctuations)
1.5	4.637±0.023	3.891±0.006	8.528±0.029	1.48±0.20	0.92 ±0.49
1.75	4.356±0.044	3.817±0.014	8.173±0.058	1.29±0.30	0.89 ±0.54
2.0	4.097±0.058	3.747±0.020	7.844±0.078	1.58±0.50	-
2.25	3.747±0.062	3.598±0.047	7.345±0.109	2.32±0.60	1.14 ±0.64
2.4	3.459±0.086	3.480±0.056	6.939±0.142	3.32±0.90	1.58 ±1.14
2.5	3.264±0.086	3.331±0.075	6.595±0.161	3.10±1.10	-
2.6	3.212±0.097	3.050±0.103	6.262±0.200	4.57±2.00	1.47 ±0.99
2.65	2.819±0.162	3.039±0.147	5.858±0.309	10.87±4.50	1.54 ±1.26
2.7	2.292±0.364	2.600±0.256	4.892±0.620	21.64±8.00	1.39 ±1.04
2.75	1.930±0.455	2.394±0.258	4.324±0.713	16.52±6.50	1.38 ±0.88
2.8	1.269±0.094	2.012±0.055	3.281±0.149	8.94±4.00	0.96 ±0.38
3.0	1.089±0.055	1.873±0.037	2.962±0.092	3.10±2.00	0.92 ±0.37
3.25	0.969±0.034	1.731±0.031	2.700±0.065	1.47±0.50	0.85 ±0.41
3.5	0.872±0.031	1.619±0.031	2.491±0.062	0.55±0.30	0.61 ±0.21
4.0	0.725±0.022	1.442±0.027	2.167±0.049	0.75±0.10	-

Table 4.3 Second Rank Orientational Order Parameters

T*	$\bar{P}_2$ (a)	$\bar{P}_2$ (b)	$\bar{P}_2$ (c)	$\bar{P}_2$ (d)2
1.5	0.852±0.004	0.851±0.007	0.851	0.851±0.001
1.75[1]	0.817±0.007			
2.0	0.785±0.009	0.785±0.014	0.785	0.784±0.001
2.25	0.740±0.011	0.739±0.016	0.739	0.738±0.001
2.4[1]	0.696±0.015			
2.5	0.669±0.016	0.669±0.022	0.669	0.668±0.001
2.6	0.637±0.019	0.638±0.026	0.637	0.636±0.002
2.65	0.595±0.031	0.582±0.037	0.582	0.581±0.004
2.7	0.481±0.108	0.451±0.121	0.449	0.463±0.004
2.75[1]	0.358±0.178			
2.8[1]	0.077±0.053			
3.0[1]	0.056±0.032			
3.25[1]	0.040±0.023			
3.5[1]	0.034±0.018			
4.0	0.023±0.013	0.044±0.017		0.000±0.032

a) Calculated by averaging the Q-tensor over 50 cycle macrosteps.
b) Calculated by averaging $\bar{P}_2$ from diagonalised Q-tensor at end of each cycle.
c) Calculated with respect to the laboratory z-axis.
d) Calculated from limiting the value of the pair correlation function, $G_2(r_{ij})$.

1 Configurational history not written to magnetic tape during these production runs.

2 These errors are only associated with locating the long range limiting value, not from the uncertainty in the values themselves.

Table 4.4 Other Order Parameters

T*	$P_1^{(a)}$	$P_4^{(a)}$	$P_4^{(b,d)}$	$P_4^{(c)}$
1.5	0.000	0.587	0.587±0.001	0.588
2.0	-0.001	0.455	0.455±0.001	0.467
2.25	-0.008	0.383	0.382±0.001	0.397
2.5	0.012	0.296	0.293±0.004	0.311
2.6	0.000	0.264	0.263±0.003	0.278
2.65	0.001	0.222	0.221±0.005	0.234
2.7	-0.008	0.154	0.161±0.003	0.132
4.0	-	-	0.000±0.032	-

a) Calculated with respect to the laboratory z-axis.
b) Calculated from the limit of the pair correlation function ($G_4(r_{ij})$.
c) Mean Field prediction at same value of ϵ.
d) Errors are associated in the uncertainty in locating the limiting value of $G_4(r_{ij})$ only.

Table 4.5 Singlet Distribution results

T*	a	b	$\bar{P}_2/T^*$
1.5	5.746×10^{-4}	6.898	0.5673
2.0	0.925×10^{-4}	4.812	0.3925
2.25	2.322×10^{-4}	4.080	0.3284
2.5	5.608×10^{-4}	3.344	0.2676
2.6	7.398×10^{-4}	3.101	0.2454
2.65	10.657×10^{-4}	2.765	0.2196
2.7	19.111×10^{-4}	2.175	0.1670

Table 4.6 First rank pair correlation functions

a) Total normalised $G_1(r)$

r^2/T^*	1.5	2.0	2.25	2.5	2.6	2.65	2.7	4.0
1	0.906	0.858	0.774	0.645	0.561	0.396	0.021	0.030
2	0.909	0.864	0.801	0.705	0.657	0.546	0.333	0.063
3	0.901	0.850	0.786	0.666	0.606	0.474	0.171	0.000
4	0.903	0.853	0.793	0.690	0.634	0.511	0.236	0.032
5	0.900	0.849	0.786	0.678	0.612	0.480	0.207	0.009
6	0.897	0.846	0.783	0.663	0.597	0.453	0.084	0.000
8	0.898	0.846	0.782	0.667	0.603	0.465	0.126	0.000
9	0.897	0.846	0.780	0.660	0.588	0.464	0.078	0.006
10	0.900	0.846	0.783	0.672	0.612	0.483	0.210	0.003
11	0.898	0.845	0.781	0.667	0.597	0.457	0.117	0.002
12	0.898	0.845	0.781	0.667	0.597	0.459	0.104	0.001
13	0.897	0.846	0.780	0.663	0.588	0.438	0.054	0.001
14	0.897	0.846	0.780	0.666	0.600	0.459	0.117	0.005

b) Unnormalised $G_1^{\perp}(r)$

r^2/T^*	1.5	2.0	2.25	2.5	2.6	2.65	2.7	4.0
1	-0.891	-0.836	-0.768	-0.660	-0.600	-0.474	-0.212	-
2	0.891	0.837	0.769	0.654	0.583	0.446	0.143	-
4	0.903	0.853	0.790	0.678	0.615	0.482	0.158	-
5	-0.899	-0.846	-0.781	-0.667	-0.600	-0.458	-0.124	-
8	0.898	0.846	0.782	0.668	0.604	0.461	0.106	-
9	-0.896	-0.843	-0.777	-0.660	-0.590	-0.447	-0.089	-
10	0.897	0.846	0.778	0.664	0.593	0.446	0.092	-
13	-0.897	-0.845	-0.779	-0.664	-0.597	-0.449	-0.091	-

c Unnormalised $G_1^{\parallel}(r)$

r^2/T^*	1.5	2.0	2.25	2.6	2.65	2.7	4.0
1	0.876	0.813	0.761	0.673	0.637	0.554	0.403
4	0.903	0.854	0.798	0.713	0.673	0.568	0.392
9	0.897	0.843	0.783	0.688	0.643	0.523	0.334

Table 4.7 Second rank pair correlation functions

a) Total $G_2(r)$

r^2/T^*	1.5	2.0	2.25	2.5	2.6	2.65	2.7	4.0
1	0.700	0.582	0.510	0.415	0.378	0.320	0.224	0.020
2	0.723	0.616	0.547	0.449	0.409	0.347	0.235	0.012
3	0.732	0.626	0.558	0.464	0.422	0.359	0.239	0.007
4	0.737	0.632	0.566	0.473	0.433	0.369	0.252	0.015
5	0.722	0.613	0.543	0.444	0.403	0.338	0.220	0.002
6	0.722	0.613	0.544	0.444	0.403	0.337	0.217	0.001
8	0.726	0.618	0.550	0.452	0.411	0.346	0.222	0.002
9	0.724	0.616	0.545	0.445	0.404	0.338	0.216	0.001
10	0.724	0.617	0.546	0.447	0.407	0.340	0.218	0.001
11	0.725	0.616	0.549	0.450	0.408	0.343	0.218	0.001
12	0.725	0.614	0.548	0.448	0.407	0.342	0.216	0.000
13	0.723	0.615	0.545	0.445	0.404	0.337	0.215	0.001
14	0.724	0.616	0.545	0.447	0.406	0.338	0.214	0.000

b) $G_2^{\perp}(r)$

r^2/T^*	1.5	2.0	2.25	2.5	2.6	2.65	2.7	4.0
1	0.709	0.597	0.526	0.431	0.393	0.334	0.235	-
2	0.709	0.597	0.525	0.423	0.383	0.319	0.211	-
4	0.737	0.632	0.567	0.473	0.432	0.367	0.245	-
5	0.726	0.618	0.548	0.450	0.409	0.344	0.221	-
8	0.726	0.617	0.550	0.452	0.410	0.345	0.218	-
9	0.721	0.611	0.541	0.440	0.399	0.334	0.213	-
10	0.722	0.616	0.543	0.444	0.403	0.335	0.213	-
13	0.724	0.615	0.545	0.445	0.404	0.337	0.213	-

c) $G_2^{\parallel}(r)$

$r^2/ *$	1.5	2.0	2.25	2.5	2.6	2.65	2.7	4.0
1	0.674	0.551	0.479	0.381	0.345	0.291	0.214	-
4	0.736	0.634	0.564	0.473	0.434	0.374	0.238	-
9	0.723	0.611	0.543	0.442	0.401	0.337	0.221	-

Table 4.8 Fourth rank pair correlation functions

a) Total $G_4(r)$

r^2/T^*	1.5	2.0	2.25	2.5	2.6	2.65	2.7	4.0
1	0.310	0.179	0.125	0.077	0.062	0.047	0.028	0.000
2	0.345	0.209	0.149	0.091	0.073	0.054	0.031	0.001
3	0.358	0.219	0.157	0.097	0.078	0.057	0.032	0.000
4	0.365	0.226	0.165	0.104	0.085	0.063	0.036	0.000
5	0.342	0.205	0.144	0.086	0.069	0.049	0.027	0.000
6	0.342	0.204	0.145	0.086	0.068	0.049	0.026	0.000
8	0.348	0.209	0.150	0.091	0.073	0.052	0.028	0.001
9	0.344	0.207	0.145	0.087	0.069	0.049	0.026	0.000
10	0.345	0.208	0.147	0.089	0.071	0.050	0.027	0.001
11	0.347	0.207	0.149	0.089	0.070	0.051	0.027	0.000
12	0.346	0.207	0.148	0.088	0.070	0.051	0.027	0.000
13	0.344	0.206	0.146	0.086	0.069	0.048	0.026	0.000
14	0.345	0.207	0.146	0.087	0.069	0.049	0.026	0.000

r^2/T^*	1.5	2.0	2.25	2.5	2.6	2.65	2.7	4.0
1	0.327	0.194	0.137	0.086	0.070	0.053	0.032	-
2	0.321	0.189	0.130	0.075	0.059	0.043	0.025	-
4	0.365	0.225	0.165	0.103	0.085	0.062	0.034	-
5	0.348	0.209	0.148	0.090	0.072	0.051	0.028	-
8	0.347	0.208	0.149	0.090	0.072	0.051	0.027	-
9	0.339	0.203	0.143	0.084	0.067	0.048	0.025	-
10	0.342	0.207	0.144	0.085	0.068	0.048	0.026	-
13	0.344	0.206	0.147	0.087	0.068	0.047	0.026	-

r^2/T^*	1.5	2.0	2.25	2.5	2.6	2.65	2.7	4.0
1	0.276	0.151	0.102	0.061	0.048	0.035	0.022	-
4	0.365	0.228	0.164	0.107	0.085	0.066	0.040	-
9	0.343	0.212	0.143	0.086	0.066	0.049	0.027	-

Table 5.1

System A

N = 1000

$T^* = 1.0$

χ	$\bar{P}_2$	$\bar{P}_2$field	$-\bar{U}^*$
0.03	0.637±0.004	0.616±0.012	1.631±0.009
0.04	0.640±0.006	0.618±0.008	1.643±0.009
0.05	0.643±0.011	0.633±0.012	1.668±0.013
0.06	0.652±0.007	0.635±0.013	1.684±0.013
0.07	0.656±0.006	0.639±0.011	1.698±0.014
0.08	0.658±0.005	0.647±0.008	1.714±0.012
0.09	0.660±0.007	0.651±0.006	1.723±0.006
0.10	0.666±0.012	0.658±0.009	1.734±0.019
0.20	0.686±0.010	0.686±0.014	1.884±0.010
0.30	0.708±0.003	0.707±0.003	1.991±0.014
0.40	0.727±0.002	0.726±0.003	2.121±0.012
0.80	0.773±0.005	0.772±0.006	2.604±0.008

Table 5.2

System B

$N = 8000$

$T^* = 1.0$

χ	$\bar{P}_2$	$\bar{P}_2$(field)	$\bar{U}^*$
0	0.606±0.008	-	1.582±0.012
0.001	0.609±0.004	0.482±0.080	1.589±0.004
0.0025	0.610±0.003	0.453±0.075	1.591±0.003
0.005	0.611±0.004	0.569±0.011	1.596±0.005
0.006	0.614±0.005	0.612±0.010	1.598±0.005
0.010	0.617±0.008	0.613±0.009	1.606±0.005
0.025	0.622±0.004	0.616±0.004	1.627±0.002
0.050	0.635±0.008	0.632±0.008	1.663±0.005
0.100	0.657±0.005	0.657±0.005	1.741±0.010

Table 5.3

System C

T^*	$\bar{P}_2(Q)$	$-\bar{U}^*$	$C^*_{V(spline)}$
1.0	0.686±0.010	1.884±0.010	2.73
1.05	0.653±0.010	1.747±0.014	2.77
1.1	0.607±0.005	1.604±0.011	3.00
1.2	0.499±0.011	1.283±0.011	3.25
1.25	0.435±0.022	1.111±0.020	3.88
1.3	0.332±0.033	0.911±0.024	3.54
1.35	0.256±0.040	0.773±0.016	2.22
1.4	0.210±0.023	0.676±0.016	1.66
1.6	0.108±0.009	0.493±0.008	0.50
1.8	0.078±0.002	0.409±0.005	0.39
2.5	0.044±0.001	0.270±0.004	0.05

Table 5.4

Singlet distribution function results

	System A	System B
T^*	1.1146	1.0
χ	0.1	0.05
N	1000	8000
$\bar{P}_2$	0.52	0.611
Number of cycles averaged over:-	1000	1000
Fit to equation 5.25:-		
a	2.21±0.05	2.69±0.05
Z	484 ±75	794 ±100
Fit to equation 5.27:-		
a_2	2.70±0.06	3.43±0.06
a_4	-0.16±0.02	-0.27±0.02
Z	220 ±5	205 ±50

Table 6.1

Computational Details for System A

T^*	starting config. temperature	Number of cycles		direction of surface molecules
		Length of equilibration	Length of production	
1.0	1.1	10,000	10,000	z
1.1	1.6	10,000	10,000	z
1.15	1.0	5,000	5,000	z
1.2	1.6	10,000	10,000	z
1.2	1.4	5,000	5,000	x
1.25	1.15	5,000	5,000	z
1.3	1.15	5,000	5,000	z
1.35	1.15	5,000	5,000	z
1.4	0.0‡	11,000	5,000	x
1.6	0.0‡	10,000	10,000	z

‡ all aligned configuration parallel to z laboratory axis.

Table 6.2

Computational details for System B.

T^*	0.90			1.00			1.08			1.20		
χ	A	B	C	A	B	C	A	B	C	A	B	C
0.05	-	-	-	-	-	-	-	-	-	0.0	20	10
0.06	-	-	-	-	-	-	-	-	-	0.05	20	10
0.07	-	-	-	-	-	-	-	-	-	0.05	20	10
0.08	-	-	-	-	-	-	-	-	-	0.05	20	10
0.09	-	-	-	-	-	-	0.0	10	10	0.14	20	10
0.10	-	-	-	0.0	12	10	0.15	20	20	0.09	20	10
0.11	-	-	-	0.25	20	10	0.10	10	20	-	-	-
0.12	-	-	-	0.11	20	10	0.15	20	20	0.16	20	10
0.13	0.14	10	10	-	-	-	0.12	10	20	-	-	-
0.14	0.15	10	10	0.11	10	10	0.12	20	20	0.18	10	20
0.15	0.0	20	20	0.14	10	10	0.12	30	20	-	-	-
0.16	-	-	-	0.11	10	10	0.15	20	20	0.14	10	20
0.17	*	10	20	0.16	10	10	0.16	20	20	0.16	10	20
0.18	-	-	-	0.11	8	10	0.17	20	20	0.16	10	20
0.19	0.2	10	20	0.18	14	10	0.18	10	20	0.18	10	20
0.20	*	10	20	0.10	5	20	-	-	-	-	-	-
0.21	-	-	-	0.20	14	10	-	-	-	-	-	-
0.22	-	-	-	0.18	10	10	-	-	-	-	-	-
0.25	-	-	-	0.20	12	10	-	-	-	-	-	-
0.30	-	-	-	0.25	8	20	-	-	-	-	-	-

A starting configuration :-field value is given.
B length of equilibration (thousand cycles)
C length of production (thousand cycles)

* from $T^*=1.0, \chi=0.20$ configuration.

Table 6.3

Simulated properties of system A

P_2 calculated from Q-tensor diagonalised at end of each cycle in production stage.

layer	T^* 1.0	1.1	1.15	1.2	1.2^b	1.25	1.3	1.35	1.4^b	1.6
1	0.715	0.657	0.618	0.575	0.570	0.530	0.471	0.446	0.387	0.308
2	0.653	0.563	0.500	0.387	0.384	0.311	0.257	0.219	0.171	0.138
3	0.641	0.526	0.428	0.271	0.284	0.228	0.174	0.146	0.132	0.120
4	0.643	0.518	0.386	0.219	0.232	0.198	0.154	0.140	0.127	0.116
5	0.644	0.514	0.373	0.196	0.198	0.172	0.153	0.140	0.133	0.116
6	0.645	0.506	0.362	0.198	0.201	0.164	0.157	0.143	0.129	0.117
7	0.642	0.508	0.370	0.223	0.219	0.181	0.167	0.148	0.125	0.115
8	0.643	0.522	0.408	0.281	0.276	0.208	0.196	0.155	0.141	0.121
9	0.663	0.564	0.478	0.386	0.372	0.309	0.283	0.226	0.191	0.137
10	0.718	0.656	0.614	0.569	0.568	0.523	0.491	0.441	0.405	0.305

$P_2(Q)$ calculated from averaged Q-tensor.

LAYER	T^* 1.0	1.1	1.15	1.2	1.2[b]	1.25	1.3	1.35	1.4[b]	1.6
1	0.706	0.645	0.607	0.564	0.560	0.517	0.459	0.432	0.374	0.290
2	0.634	0.539	0.482	0.365	0.363	0.280	0.225	0.180	0.133	0.076
3	0.612	0.490	0.400	0.236	0.241	0.162	0.113	0.078	0.045	0.019
4	0.612	0.472	0.352	0.166	0.164	0.117	0.056	0.054	0.023	0.006
5	0.613	0.465	0.330	0.129	0.115	0.092	0.044	0.037	0.017	0.009
6	0.615	0.459	0.310	0.123	0.127	0.082	0.054	0.017	0.019	0.009
7	0.613	0.473	0.326	0.160	0.166	0.102	0.076	0.039	0.021	0.012
8	0.617	0.494	0.376	0.234	0.231	0.150	0.142	0.081	0.066	0.027
9	0.643	0.542	0.457	0.357	0.346	0.278	0.251	0.192	0.153	0.080
10	0.708	0.645	0.604	0.555	0.546	0.509	0.480	0.428	0.391	0.289
overall average	0.637	0.522	0.424	0.288	0.285	0.227	0.189	0.153	0.101	0.078
$-U^*$	1.651	1.235	1.136	0.918	0.913	0.814	0.738	0.668	0.491	0.490
error	0.040	0.041	0.057	0.053	0.051	0.052	0.047	0.038	0.037	0.032

b Surface alignment along x direction.

Table 6.4

Director orientation for system A

The direction cosines between the director and the surface alignment.

Layer \ T^*	1.0	1.1	1.15	1.2	1.2[b]	1.25	1.3	1.35	1.4[b]	1.6
0[a]	1.000	1.000	1.000	1.000	1.000	1.000	1.000	1.000	1.000	1.000
1	1.000	1.000	1.000	1.000	1.000	1.000	1.000	1.000	1.000	1.000
2	0.999	1.000	1.000	0.999	1.000	0.999	0.999	1.000	1.000	0.996
3	0.997	0.998	0.999	0.998	0.999	0.993	0.999	0.997	0.983	0.968
4	0.996	0.997	0.999	0.994	0.999	0.987	0.998	0.985	0.956	0.890
5	0.996	0.996	0.999	0.989	0.999	0.980	0.990	0.966	0.880	0.862
6	0.997	0.996	0.999	0.988	0.991	0.979	0.965	0.989	0.760	0.758
7	0.997	0.995	0.999	0.992	0.992	0.985	0.988	0.994	0.922	0.733
8	0.999	0.996	1.000	0.996	0.995	0.999	0.999	0.986	0.999	0.982
9	1.000	0.998	1.000	0.999	0.999	1.000	1.000	0.998	1.000	0.999
10	1.000	1.000	1.000	1.000	1.000	1.000	1.000	1.000	1.000	1.000
11[a]	1.000	1.000	1.000	1.000	1.000	1.000	1.000	1.000	1.000	1.000

[a] Layers 0 and 11 correspond to the surfaces.

[b] Surface alignment is along x direction.

Table 6.5

A table of the maximum director deformations (degrees) obtained at the temperatures studied and at various external fields.

x T*	0.90	1.00	1.08	1.20
0.05	-	-	-	1
0.06	-	-	-	5
0.07	-	-	-	6
0.08	-	-	-	20
0.09	-	-	1	30
0.10	-	3	18	87
0.11	-	2	29	-
0.12	-	25	37	86
0.13	7	-	45	-
0.14	30	44	51	84
0.15	43	53	60	-
0.16	-	56	63	89
0.17	54	60	67	89
0.18	-	63	74	88
0.19	62	67	77	87
0.20	64	68	-	-
0.21	-	71	-	-
0.22	-	74	-	-
0.25	-	77	-	-
0.30	-	87	-	-

Table 6.6

Elastic properties system B

T^*	$\bar{P}_2$	K^*	$K^*/\bar{P}_2^2$	$K^*/3\bar{P}_2^2$	$\ln(1/\bar{P}_2)\frac{K^*}{T^*}$
0.90	0.71	1.20	2.37	0.79	0.46
1.00	0.62	0.94	2.45	0.82	0.45
1.08	0.52	0.71	2.64	0.88	0.43
1.20	0.20	0.19	4.86	1.62	0.25

Table 7.1

Some cinnimate esters giving rise to Smectic E and B mesophases.

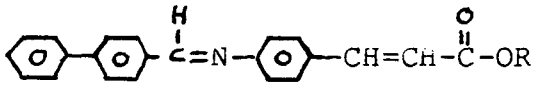

R	name	initials
$CH_2CH_2CH_2CH$	n-butyl 4(4' phenyl-benzylidineamino)cinnamate	BPBAC
$CH_2CH(CH_3)_2$	iso-butyl 4(4' phenyl-benzylidineamino) cinnamate	IBPBAC
$CH_2CH_2CH_2CH_2CH_3$	n-pentyl 4(4' phenyl-benzylidineamino) cinnamate	PPBAC

Table 7.2

Transition properties of a few 4(4' phenyl benzylidineamino) cinnamates

BPBAC (Richardson et al., 1978)

$$\text{Crystal} \overset{77^\circ C}{\rightleftharpoons} S_E \overset{108^\circ C}{\rightleftharpoons} S_B \overset{172^\circ C}{\rightleftharpoons} S_A \overset{208^\circ C}{\rightleftharpoons} \text{Isotropic}$$

IBPBAC (Richards et al., 1978)

$$\text{Crystal} \overset{86^\circ C}{\rightleftharpoons} S_E \overset{114^\circ C}{\rightleftharpoons} S_B \overset{162^\circ C}{\rightleftharpoons} S_A \overset{206^\circ C}{\rightleftharpoons} N \overset{214^\circ C}{\rightleftharpoons} \text{Isotropic}$$

PPBAC (Doucet, 1979)

$$\text{Crystal} \overset{92^\circ C}{\rightleftharpoons} S_E \overset{101.5^\circ C}{\rightleftharpoons} S_B \overset{168^\circ C}{\rightleftharpoons} S_A \overset{204^\circ C}{\rightleftharpoons} \text{Isotropic.}$$

Table 7.3

Computation details

T^*	Starting config. temperatures	Equilibration cycles ($x10^3$)	Production cycles ($x10^3$)	$\triangle$ (radians)
1.0	0[1]	1.0	6.0	1.0
3.0	1.0	1.0	4.0	1.0
5.0	3.0	1.0	4.0	1.0
6.0	5.0	1.0	1.0	1.1
7.0	5.0	1.25	8.0	1.25
8.0	3.0	1.0	8.0	1.25
8.5	7.0	1.0	3.0	1.4
9.0	3.0	1.25	8.0	1.5
9.5	3.0	2.0	8.0	1.5
10.0	3.0	1.0	11.0	1.6
11.0	7.0	1.0	9.0	1.75
12.0	7.0	1.0	4.0	1.90
13.0	9.0	1.0	4.0	2.1
15.0	11.0	1.25	3.5	2.5
17.0	13.0	1.25	4.0	2.8
20.0	17.0	1.50	4.0	3.5
25.0	15.0	1.0	3.0	3.5
30.0	25.0	1.0	3.0	4.0

[1] Perfect "herring bone"

Table 7.4

Thermodynamic Properties

T^*	$-\bar{U}^*$	C_V^* (fluctuations)	C_V^* (spline)
0.0	24.33	-	-
1.0	23.82±0.01	0.65±0.03	0.51±0.04
3.0	22.77±0.01	0.71±0.05	0.54±0.04
5.0	21.59±0.04	0.70±0.04	0.67±0.05
6.0	20.90±0.04	0.75±0.03	0.68±0.05
7.0	20.21±0.05	0.79±0.04	0.75±0.09
8.0	19.27±0.11	0.73±0.07	1.21±0.12
8.5	18.64±0.12	0.76±0.06	1.19±0.20
9.0	17.98±0.37	0.80±0.04	1.78±0.35
9.5	16.98±0.25	0.71±0.02	1.63±0.35
10.0	16.43±0.24	0.76±0.03	1.01±0.35
11.0	15.12±0.16	0.72±0.09	1.26±0.20
12.0	14.12±0.16	0.76±0.05	0.90±0.13
13.0	13.22±0.14	0.76±0.04	0.84±0.10
15.0	11.85±0.07	0.76±0.04	0.59±0.08
17.0	10.76±0.04	0.75±0.03	0.51±0.05
20.0	9.41±0.05	0.63±0.08	0.40±0.04
25.0	7.77±0.04	0.52±0.09	0.26±0.04
30.0	6.64±0.04	0.47±0.087	0.19±0.03

Table 7.5a $F_2(r)$

r \ T^*	1.0	3.0	5.0	8.0	9.0	9.5	10.0	11.0	7.0
1.0	0.885	0.678	0.528	0.252	0.159	0.124	0.090	0.060	0.363
1.732	0.906	0.741	0.553	0.304	0.186	0.126	0.109	0.068	0.390
2.0	0.901	0.728	0.560	0.312	0.221	0.151	0.108	0.057	0.404
2.646	0.901	0.703	0.544	0.269	0.158	0.085	0.050	0.016	0.370
3.0	0.896	0.707	0.566	0.265	0.157	0.078	0.057	0.014	0.364
3.464	0.902	0.725	0.544	0.281	0.183	0.087	0.051	0.026	0.383
3.606	0.901	0.719	0.541	0.274	0.159	0.068	0.034	0.013	0.372
4.0	0.902	0.719	0.556	0.281	0.174	0.077	0.025	0.018	0.392
4.359	0.902	0.723	0.548	0.276	0.151	0.056	0.020	0.003	0.376
4.583	0.900	0.715	0.557	0.266	0.163	0.064	0.030	-0.003	0.374
5.0	0.901	0.726	0.543	0.272	0.143	0.059	0.004	0.007	0.371
5.196	0.902	0.730	0.543	0.274	0.168	0.058	0.016	0.001	0.389
5.291	0.900	0.707	0.550	0.274	0.151	0.061	0.021	0.016	0.389
5.568	0.897	0.720	0.558	0.276	0.160	0.055	0.011	0.013	0.375
6.0	0.908	0.714	0.573	0.292	0.152	0.065	0.011	0.006	0.391
6.083	0.898	0.718	0.545	0.278	0.153	0.048	0.011	-0.006	0.382
6.245	0.906	0.721	0.558	0.267	0.158	0.049	0.014	0.003	0.376
6.557	0.900	0.708	0.552	0.269	0.154	0.043	0.009	0.000	0.376
6.929	0.897	0.713	0.529	0.259	0.179	0.049	0.000	-0.001	0.939
7.0	0.901	0.718	0.551	0.273	0.150	0.043	-0.001	-0.007	0.384
7.211	0.902	0.726	0.553	0.282	0.156	0.045	-0.010	0.007	0.382
7.550	0.900	0.711	0.553	0.270	0.151	0.039	0.005	0.010	0.382
7.810	0.901	0.713	0.544	0.272	0.153	0.035	0.005	-0.016	0.389
7.937	0.901	0.719	0.541	0.267	0.147	0.038	0.006	-0.009	0.375
8.0	0.901	0.704	0.550	0.286	0.158	0.053	-0.012	0.003	0.387
8.185	0.902	0.719	0.545	0.273	0.149	0.043	-0.004	-0.012	0.386
8.544	0.901	0.716	0.538	0.264	0.152	0.037	0.005	0.000	0.371
8.660	0.896	0.710	0.576	0.269	0.142	0.039	0.000	-0.012	0.386
8.718	0.899	0.721	0.548	0.290	0.152	0.031	-0.002	-0.006	0.382
8.888	0.899	0.715	0.551	0.272	0.150	0.032	0.005	-0.001	0.385
9.0	0.900	0.719	0.557	0.270	0.164	0.047	0.001	-0.006	0.386
9.165	0.899	0.724	0.544	0.284	0.156	0.041	0.002	-0.003	0.377
9.539	0.901	0.717	0.556	0.272	0.150	0.037	-0.002	-0.003	0.381
9.644	0.900	0.716	0.539	0.262	0.148	0.043	-0.003	-0.013	0.384
9.849	0.900	0.712	0.561	0.265	0.153	0.032	0.009	0.007	0.369
10.0	0.900	0.709	0.542	0.278	0.138	0.045	-0.014	-0.007	0.381
Ncycles	1000	1000	1000	4000	4000	8000	4000	4000	4000

Table 7.5b $F_4(r)$

r \ T^*	1.0	3.0	5.0	8.0	9.0	9.5	10.0	11.0	7.0	Z(r)
1.0	-0.328	-0.308	-0.292	-0.259	-0.232	-0.222	-0.215	-0.195	-0.277	6
1.732	-0.326	-0.309	-0.285	-0.253	-0.228	-0.192	-0.172	-0.163	-0.262	6
2	0.974	0.923	0.860	0.730	0.634	0.527	0.466	0.395	0.783	6
2.646	-0.325	-0.303	-0.286	-0.228	-0.199	-0.154	-0.123	-0.104	-0.258	12
3	-0.324	-0.305	-0.292	-0.212	-0.201	-0.140	-0.134	-0.081	-0.267	6
3.464	0.974	0.923	0.858	0.707	0.581	0.419	0.318	0.237	0.764	6
3.606	-0.323	-0.311	-0.280	-0.239	-0.198	-0.133	-0.096	-0.097	-0.257	12
4	0.975	0.921	0.861	0.708	0.569	0.390	0.273	0.230	0.772	6
4.359	-0.325	-0.309	-0.284	-0.233	-0.172	-0.129	-0.088	-0.054	-0.258	12
4.583	-0.325	-0.304	-0.289	-0.237	-0.190	-0.116	-0.069	-0.067	-0.256	12
5	-0.325	-0.304	-0.277	-0.236	-0.182	-0.132	-0.063	-0.047	-0.247	6
5.196	-0.325	-0.315	-0.287	-0.236	-0.202	-0.113	-0.062	-0.064	-0.259	6
5.291	0.974	0.917	0.860	0.703	0.550	0.352	0.174	0.155	0.774	12
5.568	-0.325	-0.304	-0.291	-0.230	-0.193	-0.115	-0.058	-0.066	-0.254	12
6	0.976	0.919	0.866	0.715	0.559	0.355	0.140	0.145	0.771	6
6.083	-0.324	-0.310	-0.286	-0.235	-0.182	-0.117	-0.054	-0.040	-0.256	12
6.245	-0.325	-0.309	-0.287	-0.237	-0.172	-0.109	-0.045	-0.019	-0.259	12
6.557	-0.325	-0.305	-0.284	-0.239	-0.181	-0.115	-0.034	-0.046	-0.260	12
6.928	0.973	0.919	0.850	0.697	0.569	0.313	0.107	0.086	0.776	6
7	-0.325	-0.307	-0.281	-0.240	-0.188	-0.107	-0.031	-0.039	-0.257	18
7.211	0.974	0.923	0.855	0.709	0.553	0.319	0.086	0.116	0.769	12
7.550	-0.325	-0.304	-0.285	-0.239	-0.196	-0.103	-0.035	-0.034	-0.252	12
7.810	-0.325	-0.309	-0.279	-0.232	-0.193	-0.101	-0.021	-0.017	-0.257	12
7.937	0.323	-0.305	-0.285	-0.235	-0.190	-0.107	-0.020	-0.045	-0.257	12
8(	0.974	0.916	0.857	0.701	0.558	0.313	0.060	0.091	0.773	6
8.185	-0.325	-0.305	-0.282	-0.232	-0.177	-0.105	-0.023	-0.034	-0.261	12
8.544	-0.324	-0.307	-0.287	-0.231	-0.190	-0.101	-0.014	-0.030	-0.256	12
8.660	-0.325	-0.306	-0.282	-0.250	-0.182	-0.101	-0.035	-0.023	-0.253	6
8.718	0.974	0.922	0.857	0.710	0.547	0.291	0.060	0.058	0.772	12
8.888	-0.325	-0.308	-0.284	-0.248	-0.185	-0.096	-0.017	-0.015	-0.259	12
9	-0.324	-0.303	-0.285	-0.241	-0.161	-0.096	-0.008	-0.032	-0.263	6
9.165	0.974	0.922	0.854	0.707	0.546	0.295	0.027	0.059	0.770	12
9.539	-0.325	-0.307	-0.286	-0.235	-0.186	-0.096	-0.010	-0.018	-0.257	24
9.644	-0.325	-0.304	-0.287	-0.224	-0.182	-0.098	-0.008	0.000	-0.257	12
9.849	-0.325	-0.310	-0.289	-0.225	-0.175	-0.102	-0.003	-0.014	-0.253	12
10	0.974	0.918	0.855	0.705	0.545	0.296	-0.008	0.068	0.771	6
Ncycles	1000	1000	1000	4000	4000	8000	4000	4000	4000	

z(r) is the coordination number

Table 7.6

$E_2(0)r$

r	T^* 1.0	3.0	5.0	7.0	8.0	9.0	10.0	11.0	12.0	13.0	15.0	17.0	20.0	25.0
1	0.968	0.900	0.821	0.709	0.621	0.382	-0.075	-0.120	-0.171	-0.158	-0.122	-0.111	-0.081	-0.076
2	0.976	0.926	0.871	0.791	0.734	0.627	0.482	0.418	0.319	0.268	0.204	0.154	0.109	0.077
3	0.974	0.920	0.855	0.761	0.688	0.459	0.008	-0.034	-0.064	-0.050	-0.031	-0.020	-0.010	-0.008
4	0.975	0.921	0.858	0.771	0.705	0.551	0.336	0.271	0.140	0.092	0.052	0.031	0.020	0.020
5	0.975	0.921	0.860	0.767	0.697	0.477	0.052	-0.004	-0.019	-0.005	-0.008	-0.005	-0.001	-0.005
6	0.975	0.921	0.858	0.769	0.702	0.524	0.264	0.214	0.065	0.028	0.006	0.004	0.006	0.007
7	0.975	0.920	0.859	0.768	0.700	0.482	0.071	0.009	0.005	0.004	0.001	-0.001	-0.010	-0.001
8	0.975	0.921	0.858	0.769	0.698	0.509	0.227	0.185	0.033	-0.002	-0.007	-0.002	-0.002	-0.008
9	0.975	0.920	0.858	0.767	0.699	0.480	0.083	0.020	0.013	0.004	0.011	-0.003	-0.009	0.002
10	0.975	0.921	0.858	0.769	0.700	0.500	0.222	0.176	0.015	-0.008	-0.013	0.003	-0.007	0.004
11	0.975	0.921	0.858	0.768	0.700	0.481	0.082	0.023	0.019	0.007	0.002	-0.006	0.009	0.008
12	0.975	0.921	0.858	0.768	0.699	0.500	0.219	0.180	0.015	-0.016	-0.013	-0.003	-0.011	0.015

Table 7.6b

$E_2(\pi/3, 2\pi/3)r$

r	T^* 1.0	3.0	5.0	7.0	8.0	9.0	10.0	11.0	12.0	13.0	15.0	17.0	20.0	25.0
1	-0.973	-0.916	-0.851	-0.764	-0.699	-0.549	-0.273	-0.226	-0.175	-0.146	-0.130	-0.108	-0.089	-0.061
2	0.975	0.921	0.860	0.778	0.719	0.618	0.475	0.420	0.321	0.269	0.201	0.154	0.101	0.068
3	-0.975	-0.920	-0.858	-0.768	-0.697	-0.520	-0.204	-0.146	-0.074	-0.047	-0.033	-0.021	-0.008	-0.006
4	0.975	0.921	0.859	0.768	0.698	0.552	0.334	0.266	0.141	0.097	0.054	0.032	0.013	0.005
5	-0.975	-0.921	-0.858	-0.768	-0.697	-0.508	-0.167	-0.112	-0.041	-0.019	-0.006	-0.004	-0.001	-0.003
6	0.975	0.921	0.858	0.769	0.696	0.526	0.261	0.208	0.070	0.033	0.020	0.003	-0.003	0.003
7	-0.975	-0.921	-0.858	-0.769	-0.697	-0.502	-0.150	-0.097	-0.027	-0.005	-0.002	-0.002	-0.001	-0.002
8	0.975	0.922	0.858	0.769	0.698	0.515	0.216	0.180	0.037	0.014	0.006	-0.005	0.000	0.004
9	-0.975	-0.921	-0.859	-0.767	-0.696	-0.499	-0.130	-0.092	-0.024	-0.002	0.000	-0.002	-0.003	-0.006
10	0.975	0.921	0.858	0.768	0.696	0.508	0.185	0.167	0.021	0.003	0.000	0.002	0.005	-0.004
11	-0.975	-0.921	-0.858	-0.769	-0.696	-0.497	-0.112	-0.090	-0.024	0.001	0.001	-0.000	-0.002	-0.005
12	0.975	0.921	0.858	0.768	0.693	0.504	0.117	0.164	0.013	-0.004	0.001	-0.003	0.004	-0.005

Table 7.7

The order parameters $\bar{C}4(0)$, $\bar{C}4(\pi/3)$ and $\bar{C}4^{(max)}$

T^*	$C_4(0)$	$C_4(\pi/3)$	$C_4(max)$
1.0	0.950±0.001	-0.475±0.001	0.950±0.003
3.0	0.848±0.002	-0.424±0.002	0.848±0.010
5.0	0.739±0.004	-0.369±0.002	0.737±0.017
6.0	0.674±0.005	-0.337±0.003	0.671±0.024
7.0	0.605±0.009	-0.302±0.002	0.604±0.027
8.0	0.517±0.012	-0.257±0.006	0.513±0.044
8.5	0.456±0.020	-0.228±0.011	0.461±0.049
9.0	0.338±0.112	-0.169±0.052	0.378±0.067
9.5	0.151±0.163	-0.057±0.124	0.195±0.126
10.0	0.073±0.074	-0.006±0.007	0.103±0.049
11 0	0.013±0.062	-0.008±0.064	0.065±0.035
12.0	0.005±0.010	-0.003±0.010	0.041±0.023
13.0	0.000±0.006	-0.000±0.011	0.038±0.022
15.0	0.003±0.002	-0.001±0.002	0.034±0.019
17.0	0.003±0.002	-0.001±0.004	0.034±0.019
20.0	0.005±0.007	-0.001±0.004	0.030±0.016

Table 7.8

$\langle \cos 2(\theta_i - \theta_j) \rangle$ and $\langle \cos 4(\theta_i - \theta_j) \rangle$

T^*	$+\lim F_2(r)$	$\lim F_4(r)$	$\langle \cos 2\theta \rangle$	$\langle \cos 4\theta \rangle$
1.0	0.974	0.900	0.987	0.949
3.0	0.920	0.715	0.959	0.846
5.0	0.855	0.551	0.925	0.742
7.0	0.771	0.381	0.878	0.617
8.0	0.706	0.274	0.840	0.523
9.0	0.546	0.151	0.739	0.389
9.5	0.294	0.040	0.542	0.200
10.0	0.005	0.000	0.071	0.000
11.0	0.006	0.000	0.077	0.000

	$\lim E_2(0)$
1.0	0.975
3.0	0.921
5.0	0.858
7.0	0.768
8.0	0.698
9.0	0.504
10.0	0.200
11.0	0.160
12.0	0.013
13.0	0.005
15.0	0.003
17.0	0.003
20.0	0.002
25.0	0.001

References

Abramowitz, M., Stegun, I.A.; 1965, Handbook of Mathematical functions, Dover Publications, New York.

Adams, D.J.; 1982, Private Communication.

Adams, D.J.; McDonald, I.R. 1976, Molec. Phys., 32, 931.

Aneva, N., Petrov, A.G., Sokerov, S., Stoglov, V,; 1980, Molec. Crystals liq. Crystals, 60, 1.

Bagmet, A.D.; 1982, Private Communcation.

Barker, J.A., Watts, R.O.; 1969, Chem. Phys. Lett., 3, 144.

Ben-Abraham, S.I.; 1976, Phys. Rev., A14, 1251.

Ben-Reuven, A., Gershon, N.D.; 1969, J.Chem. Phys. 51, 893.

de Boer, J.; 1942, Physica, 9, 363.

Buckingham, A.D.; 1967, Disc. Fara. Soc., 43 205.

Bunning, J.D., Faber, T.E., Sherrell, P.L.; 1981. J. Phys (Orsay, Fr), 42, 1175.

Chandrasekhar, S.; 1977, Liquid Crystals, Cambridge University Press.

Chandrasekhar, S, Madhusudana, N.V.; 1971, Acta Crystallogr., A27, 303.

Chandrasekhar, S., Shashidhar, R., Tara, N.; 1970, Molec. Crystals liq. Crystals, 10, 337.

Chang, T.S.; 1937, Proc. Cam. Phil. Soc., 33, 524.

Cotter, M.A.; 1977, Molec. Crystals liq. Crystals, 39, 173.

Coveyou, R.R., MacPherson. R.D.; 1967, J. Assoc. Comp. Mach., 14, 100.

Dafermos, C.M.; 1968, SIAM J. Appl. Math., 16, 1305.

Denham, J.Y., Humphries, R.L., Luckhurst, G.R.; 1977, Molec. Crystals liq. Crystals Lett., 41, 67.

Denham, J.Y., Luckhurst, G.R., Zannoni, C., Lewis, J.W.; 1980, Molec. Crystals liq. Crystals, 60, 185.

Deuling, H.J.; 1972, Molec. Crystals, liq. Crystals, 19, 123.

Deuling, H.J.; 1974a, Molec. Crystals, liq. Crystals, 26, 281.

Deuling, H.J.; 1974b, Molec. Crystals, liq. Crystals, 26, 281.

Deuling, H.J., Buka, A., Janassy, I.; 1976, J. Physique, 37, 965.

Deuling, H.J., Gabay, M., Guyon, E., Pieranski, P.; 1975, J. Physique, 36 689.

Deuling, H.J., Guyon, E., Pieranski, P.; 1975, Sol. State Comm., 15, 277.

Diele, R.F. Brand, P., Sackmann, T.; 1972, Molec. Crystals liq. Crystals, 17, 163.

Diele, R.F. Toney, M.F., Fain, S.C.; 1982, Phys. Rev. Lett., 48, 177.

Doucet, J.; 1979, The Molecular Physics of Liquid Crystals, edited by G.R. Luckhurst and G.W. Gray (Academic Press), Chap 14.

Doucet, J., Levelut, A.M., Lambert, M.; 1974, Molec. Crystals liq. Crystals, 24 317.

Doucet, J., Levelut, A.M., Lambert, M., Liebert, L., Strzelecki, L.; 1975, J. Phys (Paris), Colloq., 36,13.

Dunmur, D.A., Miller, W.H.; 1980, Molec Crystals liq. Crystals, 60, 281.

Dunmur, D.A., Miller, W.H.; 1982, Chem. Phys. Lett., 86, 353.

Durand, G., Leger, L., Roadelez, R., Veyssie, M.; 1969, Phys. Rev. Lett., 22, 227.

Emsley, J.W., Lindon, J.J.; 1975, N.M.R. using Liquid Crystal Solvents, Pergammon Press.

Ericksen, J.L.; 1960, Arch. Rational Mech. Anal., 4, 231.

Ericksen, J.L.; 1961, Trans. Soc. Rhed., 5, 23.

Ewald, P.P.; 1921, Ann. der Physik, 64, 253.

Faber, T.E.; 1977, Proc. R. Soc. Lond., A353, 247.

Faber, T.E.; 1980, Proc. R. Soc. Lond., A370, 509.
Flapper, S.D.P., Vertogen, G., Leenhouts, F.; 1981, J. Phys. (Orsay, Fr.) 42, 1647.
Frank, F.C.; 1958, Disc. Fara. Soc., 25, 19.
Fraser, C.; 1978, J. Phys. A, 11, 1439.
Freedericksz, V., Tsvetkov, V.; 1934, Phys. Z. Sov. Un., 6, 490.
Freedericksz, V., Zolina, V.; 1933, Trans. Fara. Soc., 29, 919.
Fuselier, C.R., Gillis, N.S., Raich, J.C.; 1978, Sol. State Comm., 25, 747.
de Gennes, P.G.; 1969, Phys. Lett., A30, 454.
de Gennes, P.G.; 1974, The Physics of Liquid Crystals, Clarendon Press.
Goodman, L.A.; 1973, J. Vac. Sci. Tech., 10, 804.
Gray, G.W.; 1979, The Molecular Physics of Liquid Crystals, edited by G.R. Luckhurst and G.W. Gray (Academic Press), Chap 12.
Gray, G.W., Winsor, P.A.; 1974, Liquid Crystals and Plastic Crystals, Wiley (New York) Volumes I and II.
Gruler, H.; 1973, Z. Naturforsch, 28A, 474.
Gruler, H.; 1974, J. Chem. Phys., 61, 5408.
Gruler, H.; 1975, Z. Naturforsch, 30A, 230.
Gruler, H., Meier, G.; 1972, Molec. Crystals liq. Crystals, 16, 299.
Gruler, H., Meier, G.; 1973, Molec. Crystals liq. Crystals, 23, 261.
Gruler, H., Scheffer, T. J., Meier, G.; 1972, Z. Naturforsch, 27A, 966.
Gubbins, K.E. Gray, C.G., Machado, J.R.S.; 1981, Molec. Phys., 42, 817.
Haller, I.; 1972, J. Chem. Phys., 57, 1400.
Hansen, J.P. McDonald, I.R.; 1976, Theory of Simple Liquids, Academic Press.

Hervet, F., Volino, A.J., Dianoux, R.E. Leckner, T.; 1975, Phys. Rev. Lett., 34, 451.

Hirschfelder, J.O., Curtiss, C.F., Bird, R.B.; 1964, Molecular Theory of Gases and Liquids, John Wiley (New York), Second edition.

Horn. R.G., Faber, T.E.; 1979, Proc. R. Soc. Lond., A368, 199.

Humphries, R.L.; 1982, Unpublished results.

Humphries, R.L., James, P.G., Luckhurst, G.R.; 1972, J. Chem. Soc. Fara. Trans. II., 68, 1031.

Humphries, R.L., Luckhurst, G.R.; 1972, Chem. Phys. Lett., 17, 514.

Humphries, R.L., Luckhurst, G.R., Romano, S.; 1981, Molec. Phys., 42, 1205.

Jansen, H.J.F., Vertogen, G., Ypma, J.G.J.; 1977, Molec. Crystals liq. Crystals, 38, 87.

de Jeu, W.H.; 1980, Physical properties of Liquid Crystalline materials, Gordon and Breach.

de Jeu, W.H. Classen, W.A.P.; 1977, J. Chem. Phys. 67, 3705.

de Jeu, W.H. Classen, W.A.P., Spruigt, A.M.J.; 1976, Molec. Crystals liq. Crystals, 37, 269.

Karat, P.P., Madhusudana, N.V.; 1976, Molec Crystals liq. Crystals, 36, 51.

Karat, P.P., Madhusudana, N.V.; 1977, Molec. Crystals liq. Crystals, 40, 239.

Karat, P.P., Madhusudana, N.V.; 1977, Molec. Crystals liq. Crystals, 42, 1067.

Karat, P.P., Madhusudana, N.V.; 1979, Molec. Crystals liq. Crystals, 55, 119.

Kelker, H.; 1973, Molec. Crystals liq. Crystals, 21, 1.

Keyes, P.H., Shane, J.R.; 1979, Phys. Rev. Lett., 42, 722.

Kirkwood, J.G.; 1939, J. Chem. Phys. 7, 911.

Knak-Jensen, S.J., Mouritsen, O.G.; 1979, Phys. Rev. Lett., 43, 1736.

Kohin, B.C.; 1960, J. Chem. Phys., 33, 882.

Kornfeld, H.; 1924, Z. Phys., 22, 27.
Krieger, T.J. James, H.M.; 1954, J. Chem. Phys., 22, 796.
Kventzel, G.F., Katriel, J.; 1982, Molec. Crystals liq. Crystals, 84, 93.
Landau, D.P., Swendsen, R.H.; 1981, Phys. Rev. Lett., 46, 1437.
Lasher, G.; 1972, Phys. Rev., A5, 1350.
Leadbetter, A.J., Frost, J., Goughan, J.P., Mazid, M.A.; 1979, J. Phys. (Orsay, Fr., C3, 185.
Leadbetter, A.J., Mazid, M.A., Malik, K.M.A.; 1980, Molec. Crystals liq. Crytals, 61, 39.
Leadbetter, A.J., Norris, E.K.; 1979, Molec. Phys., 38, 669.
Leadbetter, A.J. Richardson, R.M., Carlile, C.J.; 1976, J. Phys. (Paris), C3, 65.
Lebowitz, J.L., Percus, J.K., Verlet, L.; 1967, Phys. Rev., 153, 250.
Lebwohl, P.A., Lasher, G.; 1972, Phys. Rev., A6, 426.
Lebwohl, P.A., Lasher, G.; 1973, Phys. Rev., A7, 2222.
Leger, L.; 1973, Phys. Lett., A44, 535.
Lehmann, O.; 1900, Verhandl d. Deutschen. Phys. Ges., 16, 1.
Lekkerkerker, H.N.W., Debruyne, J., Van der Haegen, R., Luyckx, R.; 1978, Physica (Utrecht), 94A, 465.
Leslie, F.M.; 1966, Quart, J. Mech. Appl. Math., 19, 357.
Leslie, F.M.; 1968, Arch. Rational Mech. Anal., 28, 265.
Lobisch, W.; 1872, Ber., 5, 513.
London, F.; 1930, Z. Physik, 63, 245.
London, F.; 1930, Z. Physik, Chem. B., 11, 221.
Luckhurst, G.R.; 1972, Phys. Bulletin, 23, 279.
Luckhurst, G.R.; 1979, The Molecular Physics of Liquid Crystals, edited by G.R. Luckhurst and G.W. Gray (Academic Press), Chap. 4.
Luckhurst, G.R., Romano, S.; 1980, Molec. Phys., 40, 129.

Luckhurst, G.R., Romano, S.; 1980, Proc. R. Soc. London, A373, 111.

Luckhurst, G.R., Romano, S., Simpson, P.; 1982, Chem. Phys, 73, 337.

Luckhurst, G.R., Simpson, P.; 1982, Molec. Phys. 47, 251.

Luckhurst, G.R., Simpson, P.; 1983, Chem. Phys. Lett., 95, 149.

Luckhurst, G.R. , Simpson, P., Zannoni, C.; 1981, Chem. Phys. Lett,, 78, 429.

Luckhurst, G.R., Zannoni, C.; 1977, Nature, 267, 412.

Luckhurst, G.R., Zannoni, C., Nordio, P.C., Segre, U.; 1975, Molec. Phys., 30, 1345.

Madusuadana, N.V., Chandrasekhar, S.; 1975, Pramana Suppl., 1, 57.

Maier, W., Saupe, A.; 1958, Z. Naturforsch, 13A, 564.

Maier, W., Saupe, A.; 1959, Z. Naturforsch, 14A, 882.

Maier, W., Saupe, A.; 1960, Z. Naturforsch, 15A, 287.

Malraison, B., Poggi, Y., Guyon, E.; 1980, Phys. Rev., A21, 1012.

Margenau, H., Kestner, N.R.; 1969, Theory of Intermolecular Forces, Pergamon Press.

Martire, D.E.; 1969, The Molecular Physics of Liquid Crystals, edited by G.R. Luckhurst and G.W. Gray (Academic Press), Chap. 10.

Maze, C.; 1978, Molec. Crystals liq. Crystals, 48, 273.

Maze, C., Johnson, D.L.; 1975, Bull. Am. Phys. Soc., 20, 886.

Maze, C., Johnson, D.L.; 1976, Molec. Crystals liq Crystals, 33, 213.

McColl, J.R., Shih, C.S.; 1972, Phys. Rev. Lett, 29, 85.

McDonald, I.R., Singer, K.; 1970, Quart. Rev., 238.

Meirovitch, H.; 1977, Chem. Phys., 21, 251.

Metropolis, N., Rosenbluth, A.W. Rosenbluth, M.N., Teller, E.; 1953, J. Chem. Phys., 21, 1087.

Meyer, R.J.; 1975, Phys. Rev., A12, 1066.

Meyer, R.J.; 1976, Phys. Rev., A13, 1613.

Miller, W.H.; 1979, Ph.D. Thesis, University of Sheffield.

Motooka, T., Fukuhara, A.; 1979, J. Appl. Phys., 50, 6907.

Motooka, T., Fukuhara, A., Suzuki, K.; 1979, Appl. Phys. Lett., 34, 305.

Mouritsen, O.G., Berlinsky, A.J.; 1982, Phys. Rev. Lett., 48, 181.

Nehring, J., Saupe, A.; 1971, J. Chem. Phys., 54, 337.

Oseen, C.W.; 1933, Trans. Fara. Soc., 29, 883.

O'Shea, S.F., Klein, M.L.; 1979, Chem. Phys. Lett., 66, 381.

Pincus, P.; 1970, J. Appl. Phys., 41, 974.

Pindak, R., Monoton, D.E. Davey, S.G. Goodby, J.W.; 1981, Phys. Rev. Lett., 46, 1135.

Planar, M., Phillips, W.D.; 1968, J. Am. Chem. Soc., 90, 3880.

Planer, P.; 1861, Ann., 118, 25.

Poggi, Y., Filippini, J.C.; 1977, Phys. Rev. Lett., 39, 150.

Poniewierski, A., Stecki, J.; 1979, Molec. Phys., 38, 1931.

Pople, J.A.; 1954, Proc. R. Soc., 221A, 498.

Priest, R.G.; 1972, Molec. Crystals liq. Crystals, 17m 129.

Priest, R.G.; 1973, Phys. Rev., A7, 720.

Priestly, E.B., Wojtowicz, P.J., Sheng, P.; 1974, Introduction to Liquid Crystals, Plenum, New York.

Rao, N.V.S., Kishore, R.P., Ray, T.F.S., Avadhanlu, M.N., Nurty, C.R.K.; 1976, Molec. Crystals liq. Crystals, 36, 65.

Reinitzer, F.; 1888, Mouatsh. Chem, 9, 421.

Richardson, R.M., Leadbetter, A.J., Frost, J.C.; 1978, Ann. Phys. 3, 177.

Romano, S.; 1982, Private Communication.

Rose, M.E.; 1957, Elementary Theory of Angular Momentum, Wiley.

Rosenblatt, C.; 1982. Phys. Rev., A25, 1239.

Rosenbluth, M.N., Rosenbluth, A.W.; 1954, J. Chem. Phys., 22, 881.

Safran, S.A.; 1981, Phys. Rev. Lett., 46, 1581.

Saupe, A.; 1960, Z. Naturforsch, 15a, 810.

Schad, H., Baur, G., Meier, G.; 1978, Appl. Phys., 17, 177.

Schad, H., Baur, G., Meier, G.; 1979. J. Chem. Phys., 70, 2770.

Schroder, H.; 1977, J. Chem. Phys., 67, 16.

Shanks, I. A.; 1982, Contemp. Phys., 23, 65.

Sheng, P., Wojtowicz, P.J.; 1976, Phys. Rev., A14, 1883.

Stinson, T.W. Litster, J.W.; 1970, Phys. Rev. Lett., 25, 503.

Stone, A.J.; 1978, Molec. Phys., 36, 241.

Stone, A.J.; 1979, The Molecular Physics of Liquid Crystals, edited by G.R. Luckhurst and G.W. Gray (Academic Press), Chap. 2.

Straley, J.P.; 1974, Phys. Rev., A10, 1881.

Symposium 1931, Z. Krist.; 79, 1.

Symposium 1933, Trans. Fara. Soc., 29, 881.

Symposium 1958, Disc. Fara. Soc., 25, 1.

Taylor, T.R., Arora, S.L., Ferguson, J.L.; 1970, Phys. Rev. Lett., 25, 722.

Tildesley, D.J.; 1982, Lecture Notes, University of Southampton.

Tough, R.J.A., Raynes, E.P.; 1979, Molec. Crystals liq. Crystals, 56, 19.

Tsylalo, A.L., Bagmet, A.D.; 1976, Russ. J. Phys. Chem., 50, 439.

Tsylalo, A.L., Bagmet, A.D.; 1978, Molec. Crystals liq. Crystals, 46, 111.

Uchida, T., Takahashi, Y.; 1981, Molec. Crystals liq. Crystals, 72, 133.

Valleau, J.P., Whittington, S.G.; 1980, Statistical Mechanics, part A, Edited by B.J. Berne, Plenum press., Chap. 4.

Van der Haegen, R., Debrugyne, J., Kuyckx, R., Lekkerkerker, H.N.W.; 1980, J. Chem. Phys., 73, 2469.

Vieillard-Baron, J.; 1972, J. Chem. Phys. 56, 4729.

Vieillard-Baron, J.; 1974, Molec. Phys., 28, 809.

de Vries, A., Ekachai, A., Spielberg, N.; 1979, J. Physique, 40, C3, 147.

Wojtowicz, P.J., Sheng, P.; 1974, Phys. Lett., 48A, 235.

Zannoni, C.; 1979, The Molecular Physics of Liquid Crystals, edited by G.R. Luckhurst and G.W. Gray (Academic Press), Chap. 3 and Chap 9.

Zannoni, C., Guerra, M.; 1981, Molec. Phys., 44, 849.

Zocher, H.; 1933, Trans. Fara. Soc., 29, 945.

Appendix 1

Properties of Wigner Rotation matrices and related functions

A complete account of the properties and definition of Wigner rotation matrices is given by Rose (1957). The following relations are those that have been used in this thesis.

1) Orthogonality.

$$\int d\alpha \sin\beta d\beta d\gamma D^{L*}_{mn}(\alpha\beta\gamma) D^{L'}_{m',n'}(\alpha\beta\gamma) = [8\pi^2/(2L+1)]\,\delta_{mm'}\,\delta_{nn'}\,\delta_{LL'}$$

2) Closure.

$$D^{L}_{mn},(\alpha\beta\gamma) = \sum_{n} D^{L}_{mn}(\alpha_1\beta_1\gamma_1)\, D^{L}_{nm},(\alpha_2\beta_2\gamma_2)$$

where $(\alpha\beta\gamma)$ is the resultant of rotation $(\alpha_1\beta_1\gamma_1)$ and $(\alpha_2\beta_2\gamma_2)$

3) Symmetry

$$D^{L*}_{mn}(\alpha\beta\gamma) = (-)^{m-n} D^{L}_{-m-n}(\alpha\beta\gamma)$$

$$= D^{L}_{nm}(-\alpha,-\beta,-\gamma)$$

4) Special cases

$$D^{L}_{mo}(\alpha\beta 0) = [4\pi/(2L+1)]^{1/2} Y^{*}_{Lm}(\beta\alpha)$$

where $Y_{Lm}(\beta\alpha)$ is a spherical harmonic

$$D^{L}_{oo}(0\beta 0) = P_L(\cos\beta)$$

where $P_L(\cos\beta)$ is a Legendre polynomial

5) Spherical Harmonic addition theorem.

$$P_L(\cos\theta) = \frac{4\pi}{2L+1} \sum_p Y^*_{Lp}(\theta_1\phi_1)\, Y_{Lp}(\theta_2\phi_2)$$

where $\cos\theta = \cos\theta_1\cos\theta_2 + \sin\theta_1\sin\theta_2\cos(\phi_1-\phi_2)$

6) Modified spherical harmonics

$$C_{Lm}(\beta\alpha) = \left[\frac{4\pi}{(2L+1)}\right]^{1/2} Y_{Lm}(\beta\alpha)$$

Appendix 2

Scalar Functions

The scalar functions $S^{oo}_{LL',J}$ for small values of L L' and J in terms of unit vectors $\hat{z}_1$, $\hat{z}_2$, $\hat{R}$, the vectors describing the orientation of the long molecular axes and the inter molecular vector. (Stone, 1979).

$$S_{000} = 1$$

$$\sqrt{3}\ S_{110} = -\hat{z}_1.\hat{z}_2$$

$$\sqrt{3}\ S_{101} = -\hat{z}_1.\hat{R}$$

$$\sqrt{3}\ S_{011} = +\hat{z}_2.\hat{R}$$

$$\sqrt{30}\ S_{112} = \hat{z}_1.\hat{z}_2 - 3(\hat{z}_1.\hat{R})(\hat{z}_2.\hat{R})$$

$$\sqrt{30}\ S_{121} = \hat{z}_1.\hat{R} - 3(\hat{z}_1.\hat{z}_2)(\hat{z}_2.\hat{R})$$

$$\sqrt{30}\ S_{211} = -\hat{z}_2.\hat{R} + 3(\hat{z}_1.\hat{z}_2)(\hat{z}_1.\hat{R})$$

$$2\sqrt{5}\ S_{220} = 3(\hat{z}_1.\hat{z}_2)^2 - 1$$

$$\sqrt{70}\ S_{222} = 2 - 3(\hat{z}_1.\hat{R})^2 - 3(\hat{z}_1.\hat{z}_2)^2 + 9(\hat{z}_1.\hat{R})(\hat{z}_2.\hat{R})(\hat{z}_1.\hat{z}_2)$$

$$4\sqrt{70}\ S_{224} = 1 - 5(\hat{z}_1.\hat{R})^2 + 2(\hat{z}_1.\hat{z}_2)^2 - 5(\hat{z}_2.\hat{R})^2 - 20(\hat{z}_1.\hat{z}_2)(\hat{z}_1.\hat{R})(\hat{z}_2.\hat{R}) + 35(\hat{z}_1.\hat{R})^2(\hat{z}_2.R)^2$$

Also given $S_{L_1L_2J}$, $S_{L_1JL_2}$ may be obtained by replacing $\hat{z}_2$ by $\hat{R}$ and vice versa.

$S_{JL_2L_1}$ may be obtained by replacing $\hat{z}_1$ by $-\hat{R}$ and vice versa.

$S_{L_2L_1J}$ may be obtained by replacing $\hat{z}_1$ by $-\hat{z}_1$ and vice versa

Appendix 3

Random number generation

In any Monte-Carlo simulation, the generation of random numbers is always required. Although called random, they are actually pseudo random in that they follow a predefined periodic sequence. The usual method of generating such a sequence of numbers uniformly distributed in the range $0>\xi>1$ is via the recursive equation.

$$N_i = a \times N_{i-1} \text{mod}(b) \qquad \text{A3.1}$$

where mod is a function returning the remainder of N/b. The i^{th} pseudo random number, ξ_i, is then defined as

$$\xi_i = N_i/b \qquad \text{A3.2}$$

Here a and b are constants suitably chosen to give statistically random and uncorrelated numbers. Usually b is taken to be 2^n where n is the computer word length, thus avoiding the necessity for the mod function as ignored overflow will perform the same task. The constant a is normally chosen to be sufficiently large, and using Fourier Analysis on such problems, it has been shown (Coveyou and MacPherson, 1967) that the binary representation of a should contain a significant number of ones, and at the same time, not a close multiple of b or $\sqrt{b}$. For example, the Numerical Algorithms Group (NAG) routine sets a equal to 13^{13} (Routine G05CAF), although other values could safely be used.

Appendix 4

Simple and Face centre, cubic lattices

Some properties of simple cubic and face centre cubic lattices.

Unit cell

simple cubic

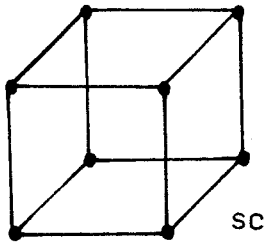

sc

face centre cubic

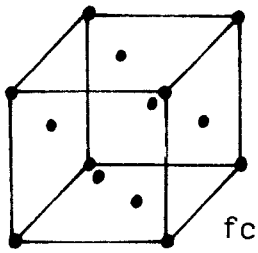

fcc

	simple cubic	face centre cubic
number of molecules per unit cell	1	4
unit cell repeating distance	a	a

intermolecular seperation and coordination number for coordination shell number:

	simple cubic		face centre cubic	
1	a	: 6	a/√2	: 12
2	√2a	: 12	√a	: 6
3	√3a	: 8	√(3/2)a	: 24
4	√2a	: 6	√2 a	: 12
5	√5a	: 24	√(5/2)a	: 24
6	√6a	: 24	√3 a	: 8
7	√8a	: 12	√(7/2)a	: 48
8	√3a	: 30	√4 a	: 6
9	√10a	: 24	√(9/2)a	: 36
10	√11a	: 24	√5 a	: 24

Appendix 5

Proof that the middle term vanishes in the pair potential used in Chapter 7

To prove that the J=4, M=±2 term in the quadrupole-quadrupole pair potential for nearest neighbours summed over all molecules is zero on a triangular lattice. We can express the term as:-

$$E_{ij} = \cos 2(\theta_i - \phi_{rij}) + \cos 2(\theta_j - \phi_{rij})$$

The total energy contribution is then

$$E_{tot} = \frac{1}{2} \sum_i \sum_j E_{ij}$$

$$= \frac{1}{2} \sum_{i=1} \sum_{j=1} (\cos 2(\theta_i - \phi_{rij}) + \cos 2(\theta_j - \phi_{rij}))$$

The factor of (1/2) arises because the double summation counts all pairs of molecules twice. This can be broken down to:-

$$E_{tot} = \frac{1}{2} \sum_{i=1} \sum_{j \neq 1} \cos 2(\theta_i - \phi_{rij})$$

$$+ \frac{1}{2} \sum_{i=1} \sum_{j=1} \cos 2(\theta_j - \phi_{rij})$$

Here both terms are zero unless i and j are neighbouring molecules.

The summation:- $\sum_{j=1}^{6} \cos 2(\theta - \phi_r)$

$$= \cos 2\theta\cos 0 - \sin 2\theta\sin 0$$
$$+ \cos 2\theta\cos \pi/3 - \sin 2\theta\sin \pi/3$$
$$+ \cos 2\theta\cos 2\pi/3 - \sin 2\theta\sin 2\pi/3$$
$$+ \cos 2\theta\cos \pi - \sin 2\theta\sin \pi$$
$$+ \cos 2\theta\cos 2\pi/3 - \sin 2\theta\sin 4\pi/3$$
$$+ \cos 2\theta\cos 5\pi/3 - \sin 2\theta\sin 5\pi/3$$

$$= 0$$

since the six intermolecular vectors are at 0, $\pi/3$, $2\pi/3$, π, $4\pi/3$, $5\pi/3$ respectively. This term also vanishes regardless of the choice of the laboratory frame of reference.

Appendix 6 A few non-zero Clebsch Gordan Coefficents

j_1	j_2	J	m_1	m_2	$C(j_1 j_2 J; m_1 m_2)$
0	0	0	0	0	+1
0	1	1	0	0	+1
0	1	1	0	1	+1
0	2	2	0	0	+1
0	2	2	0	1	+1
0	2	2	0	2	+1
1	1	0	1	-1	$+1/\sqrt{3}$
1	1	0	0	0	$-1/\sqrt{3}$
1	1	1	0	1	$-1/\sqrt{2}$
1	1	1	0	-1	$+1/\sqrt{2}$
1	1	1	1	0	$+1/\sqrt{2}$
1	1	2	0	0	$+2/\sqrt{6}$
1	1	2	0	1	$+1/\sqrt{2}$
1	1	2	1	-1	$+1/\sqrt{6}$
1	1	2	1	0	$+1/\sqrt{2}$
1	1	2	1	1	+1
1	2	1	0	0	$-2/\sqrt{10}$
1	2	1	0	1	$-\sqrt{3}/\sqrt{10}$
1	2	1	1	-2	$+\sqrt{3}/\sqrt{5}$
1	2	1	1	-1	$+\sqrt{3}/\sqrt{10}$
1	2	1	1	0	$+1/\sqrt{10}$
1	2	2	0	1	$-1/\sqrt{6}$
1	2	2	0	2	$-2/\sqrt{6}$
1	2	2	1	-2	$+1/\sqrt{3}$
1	2	2	1	-1	$+1/\sqrt{2}$
1	2	2	1	0	$+1/\sqrt{2}$
1	2	2	1	1	$+1/\sqrt{3}$
2	2	0	0	0	$+1/\sqrt{5}$
2	2	0	1	-1	$-1/\sqrt{5}$
2	2	0	2	-2	$+1/\sqrt{5}$
2	2	1	0	1	$+\sqrt{3}/\sqrt{10}$

j_1	j_2	J	m_1	m_2	$C(j_1 j_2 J; m_1 m_2)$
2	2	1	1	-2	$+1/\sqrt{5}$
2	2	1	1	-2	$-1/\sqrt{10}$
2	2	1	1	-1	$-\sqrt{3}/\sqrt{10}$
2	2	1	1	0	$+2/\sqrt{10}$
2	2	1	2	-2	$+2/\sqrt{10}$
2	2	1	2	-1	$+1/\sqrt{5}$
2	2	2	0	0	$-2/\sqrt{7}$
2	2	2	0	1	$-1/\sqrt{14}$
2	2	2	0	2	$+2/\sqrt{7}$
2	2	2	1	-2	$+\sqrt{3}/\sqrt{7}$
2	2	2	1	-1	$+1/\sqrt{14}$
2	2	2	1	0	$-1/\sqrt{14}$
2	2	2	1	1	$-\sqrt{3}/\sqrt{7}$
2	2	2	2	-2	$+\sqrt{2}/\sqrt{7}$
2	2	2	2	-1	$+\sqrt{3}/\sqrt{7}$
2	2	2	2	0	$+\sqrt{2}/\sqrt{7}$
2	2	4	0	0	$+6/\sqrt{70}$
2	2	4	0	1	$+\sqrt{3}/\sqrt{7}$
2	2	4	0	2	$+3/\sqrt{42}$
2	2	4	1	-2	$+1/\sqrt{14}$
2	2	4	1	-1	$+4/\sqrt{70}$
2	2	4	1	0	$+\sqrt{3}/\sqrt{7}$
2	2	4	1	1	$+2/\sqrt{7}$
2	2	4	1	2	$+1/\sqrt{2}$
2	2	4	2	-2	$+1/\sqrt{70}$
2	2	4	2	-1	$+1/\sqrt{14}$
2	2	4	2	0	$+3/\sqrt{42}$
2	2	4	2	1	$+1/\sqrt{2}$
2	2	4	2	2	+1

Recursive Relations:-

$$C(j_1 j_2 J; m_1 m_2) = (-1)^{j_1+j_2-J} C(j_2 j_1 J; m_2 m_1)$$

$$C(j_1 j_2 J; m_1 m_2) = (-1)^{j_1+j_2-J} C(j_1 j_2 J; m_2 m_1)$$

Appendix 7

The first six even Legendre Polynomials

$$P_0(x) = 1$$
$$P_2(x) = (3x^2-1)/2$$
$$P_4(x) = (35x^4-30x^2+3)/8$$
$$P_6(x) = (231x^6-315x^4+105x^2-5)/16$$
$$P_8(x) = (6435x^8-12012x^6+6930x^4 -1260x^2+35)/128$$
$$P_{10}(x) = (46189x^{10}-109395x^8+90090x^6 -30030x^4+3465x^2-63)/256$$